Dayal, Austin Robinson
Ph.D.   *15 march 1991*

The University of Sydney

Copyright in relation to this thesis*

This thesis has been
accepted for the award
of the degree in the
Faculty of Engineering

SF_6 ARC SPECTROSCOPY

by

A.R. DAYAL, B.Sc., B.E.

A thesis submitted for examination towards the degree of

Doctor of Philosophy
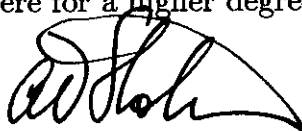
School of Electrical Engineering
The University of Sydney
July 18, 1990

Declaration of Originality

All the experimental work reported here has been carried out solely by the author and has not been submitted elsewhere for a higher degree.

A.R. Dayal

Acknowledgements

Contents

List of Figures

List of Tables

List of Symbols

A - Aperture
A_{nm} — Transition probability
ASA - Standard specifying speed of the photographic material
$C(\nu)$ — Continuum emission coefficient
D - Photographic density
d_0 — Constant
d - Distance measured from reference position d_0
DIN - Standard specifying speed of the photographic material
E - Electric field strength
E - Incident radiation on the photographic plate (section B.1)
E_n — Excitation potential of level n
eV - Electron volt
f - Focal length
F_e — Electrical form factor
g_n — Statistical weight of level n
H–D - Hunter & Driffield curve (graph between photographic density and incident radiation on the plate)
I - Current
I - Relative line intensity (section A.3)
I - Image position (section 3.5)
I_0 — Relative line intensity of the control argon line (section A.3)
I_{nm} — Line intensity emitted by trasitions between the n and m states
$I(\nu)$ — Continuum intensity (per unit frequency interval)
K - Kelvin
k - Thermal conductivity
L - Lens
LTE - Local thermal equilibrium
M - Mirror
MS - Make switch
N_I — Unionised nitrogen atom
N_{II} — Singly ionised nitrogen atom
N_n — Population density in level n
N_e — Population density of electrons
N_i — Population density of ions
P_e — Electrical power input to the arc
P_u — Radiated power from the arc
Q - Partition function
R - Arc radius
R - Resistor (section 3.3)

RP - Reference plane
r - Radial position
SG - Spark gap
T - Transmittance (Section B.1)
T - Temperature
TD - Time delay pulse generator
T_s- Shutter opening time
u - Net radiation emission
u_t- Transparent radiation
uv - Ultra-violet
x - Normalised radial position
Y - Arc conductance
Z - Distance (section 3.5)
$\lambda-$ Wavelength of the line
$\nu-$ Continuum emission frequency
$\Delta E-$ Lowering of the ionisation potential
$\Delta\lambda-$ Full half-width of the line
$\sigma-$ Electrical conductivity
$\kappa-$ Planck function

Chapter 1

INTRODUCTION

Use of sulfur hexafluoride (SF_6) gas as a quenching medium in high interrupting capacity circuit breakers has been widespread for the last twenty years due to its excellent insulating and quenching properties [23]. SF_6 circuit breakers are capable of interrupting up to 100 kA at 200 kV. But more research is necessary to improve the current and voltage specifications. In order to understand the quenching processes better, the problems of turbulent flow, energy transport and the electrode phenomena associated with them must be fully investigated.

The scope of this thesis is limited to an investigation of the energy transport mechanism. To get a deeper insight and for making proper estimates of quantitative energy transfer, it is necessary to know the transport properties for the temperature range of 5,000K to 30,000K and for pressures of up to 20 atmospheres.

Various theoretical estimates of the SF_6 transport properties have been made by Frie, Frost, Liebermann, Lowke, and Dienemann [22,24,41,17], for the required temperature and pressure ranges. But the experimental determinations of the transport properties by Motchmann, Hertz, Wittle, Airey and Dienemann are scanty [50,34,48,3,18]. All the work that has been done is at atmospheric pressure and there is no experimental evaluation of these properties at higher pressures, except for the experimental determination of electrical conductivity by Dienemann at 2 atmospheres pressure. This lack of experimental investigation can be attributed to the difficulties that are associated with such investigations. Whatever the reason, it is very important to determine experimentally the transport properties of SF_6, because the experimental measurements are the only means which provide real information regarding the processes involved inside an actual arc. It also provides a means by which the theoretical estimates can be verified, especially in regions of temperature and pressure where the accuracy of the approximations used in the calculation appear to be questionable.

In these experiments spectrographic studies of SF_6 arcs have been conducted in order to determine the transport properties at temperatures and pressures typical of gas blast switching arcs.

To establish the validity and the accuracy of the entire experimental procedure, measurements were also made on nitrogen and argon arcs and the results were compared with other experiments. Temperature profiles and E–I characteristic of argon arcs were used to calculate transport properties using Devoto and Mukherjee's 'trial function' method of evaluating electrical conductivity and Ter Horst and Pflanz's 'form factor' method of evaluating thermal conductivity. These results were compared with other standard experimental results of Yos, Morris, Rudis and Cram [40,47,14]. This comparison established the credibility of the methods used for calculating transport properties.

After having thus established the accuracy of the experimental procedures and calculating methods for the evaluation of transport properties, experiments were conducted for SF_6 arcs at 1, 4 and 8 atmospheres pressure.

The electrical conductivity has been calculated using Devoto and Mukherjee's method [16], involving the use of a 'trial function' containing several adjustable parameters. The advantage of this method is, that it requires measurements only at a few currents and furthermore, there is no necessity to commence the measurements at low currents in order to construct the curve for $\sigma(t)$ at high temperatures, as a continuation of low temperature values.

Thermal conductivity is the most important parameter of energy transport in arcs, and it has been evaluated using the 'form factor' technique of Ter Horst and Pflanz [68]. The method has the basic advantage that it evaluates thermal conductivity quite accurately without being too complicated. Unlike the concept of zero-arc radius it does not need measurements at a number of arc radii. It has been shown by Pflanz and Ter Horst [55], that this method can be used to determine thermal conductivity for very high current arcs where radiation plays an important part in the energy transport within the arc column, without introducing serious errors.

The net radiation emission has been calculated by solving the energy balance equation. As all the other terms of the equation are known at this point, the net radiation emission can be determined as a last unknown function.

The layout of the thesis is as follows. The remaining part of this chapter gives a review of the research work that has been done for the evaluation of transport properties of SF_6 and argon arcs. Chapter two gives the details of the theory of the calculating methods used for evaluating temperature profiles and transport properties. Description of equipment and the experimental set-up is given in chapter three. Chapter four outlines the experimental procedures adopted for recording spectrum and E–I characteristic of the arcs. A brief description of the software developed for data acquisition and reduction is given in chapter five. Results are presented in chapter six and discussed in chapter seven. Chapter eight gives the summary and conclusion of the thesis.

A brief report of the preliminary investigation of the SF_6 arcs is given in appendix A. This early work was aimed at quantifying the use of spectroscopy for impurity determination in SF_6. Details of the photographic process for recording the spectrum is given in appendix B, Plasma composition tables for nitrogen, argon and SF_6 are given in appendix C, and listings of all the programmes are in appendix D.

1.1 Review of the Literature

Over the years, a number of investigators have evaluated the transport properties of high temperature arcs burning in different gases. This section outlines some of the research work carried out in this field, with special emphasis on SF_6 and argon arcs.

Most of the available information on transport properties of gases at high temperatures has been generated by theoretical calculations. Ordinary experimental techniques for measuring electrical and thermal conductivity become infeasable at temperatures above 2,000K. Some data have been obtained from shock tube measurements of heat transfer in the reflected shock region [30,54], on the shock tube walls [32], and at stagnation point [6]. However, none of these techniques have yielded transport properties for gases at temperatures where thermal ionization is significant.

A steady-state wall-confined arc, popularly known as a cascade arc arrangement was first developed by Maecker [43]. Using this arrangement, he calculated thermal conductivity of nitrogen for temperatures of up to 15,000K [42,45].

Olsen [53], reported evaluation of electrical conductivity of argon for temperatures of up to 23,000K, using free burning arc measurements. Analytical calculations of argon plasma composition and measured transition probabilities of a few selected argon atomic and ionic lines were also published.

Knopp, Liebermann, Bade and Yos [39], improved upon Maecker's thermal conductivity result of nitrogen by including analytical values for the ultraviolet continuum and line radiation.

Emmons [19], conducted experiments on the cascade arc configuration and measured the E-I characteristic, the radiation heat transfer, the continuum and line intensity, to calculate transport properties of argon for temperatures of up to 23,000K.

Grier [27], and Devoto [15], published theoretical estimates of the electrical conductivity of hydrogen for temperatures of up to 26,000K at atmospheric pressure.

Motschmann [49], and Behringer, Kollmar and Mentel [11], measured the thermal conductivity of hydrogen for the temperature range below 12,000K.

The first theoretical estimates of electrical and thermal conductivity of SF_6 were given by Frie [22]. In his computation of particle density, Frie took demixing effect into consideration. These calculations were based upon standard analytical methods of computation.

Motschmann [50], gave the first experimental estimates of transport properties of SF_6. Experiments were conducted on 5 mm diameter cascade arcs. Temperature profiles were determined by absolute line intensity measurements of F_I, S_I and S_{II} lines at 624.0, 469.5 and 545.4 nm. Demixing effects were considered in these calculations. Results were found to be in good agreement with the then existing theoretical results of Frie.

Morris, Rudis and Yos [47], used wall stabilised electric arcs to evaluate experimentally the thermal conductivity of nitrogen, argon and hydrogen at 0.5, 1 and 2 atmospheres pressure for temperatures of up to 14,000K. Electrical conductivity was reported to have good agreement with theory. Thermal conductivity of nitrogen and argon were also in good agreement with theory when energy transfer by vacuum ultra-violet radiation was included in the energy transport calculations.

Bauder and Devoto [9] and Bauder [8], investigated argon arcs at high pressures of up to 150 atmospheres. The E–I characteristics and the temperature profiles of argon were published for the first time at such high pressures.

Bauder and Maecker [10], calculated the electrical and thermal conductivity of nitrogen and hydrogen at atmospheric pressure for temperatures of up to 26,000K, and

electrical conductivity of argon at 50 atmospheres pressure.

Hertz, Motschmann and Wittel [34], did further experimental investigation of SF_6 arcs in which non-stationary arcs were also studied. These studies indicated that the good quenching capability of SF_6 was due to energy transport mechanisms taking place below 10,000K. Below 8,000K, the conductance decay in nitrogen was much slower than in SF_6. Further, these measurements indicated that the fast conductance decay in SF_6 was not caused by electron attachement but was due to the energy transport mechanism.

Asinovsky, Kirillin, Pakhomov and Shabashov [5], published the results of experimental investigation carried out in the USSR since 1960, on argon, nitrogen and carbon-dioxide cascade arcs for the temperature range of 7,000 to 16,000K. The results included electrical and thermal conductivity and total radiation of the above mentioned gases.

Frost and Liebermann [24], published the most comprehensive theoretical estimates of SF_6 transport properties for the temperature range of 1,000 to 40,000K and pressure range of 1 to 16 atmospheres. Their values for the thermal conductivity at atmospheric pressure were lower by a factor of three than the earlier theoretical values of Frie [22].

Ernst, Kopainsky and Maecker [20], carried out intensive experimental investigation of steady cascade nitrogen arcs with tube diameters of 2, 3 and 5 mm at atmospheric pressure to gain insight into the radiative energy transport for temperatures of up to 27,000K. Measurements were made of the E–I characteristic, the total emitted radiation and the temperature distribution profiles. Electrical conductivity and transparent emission were evaluated. The thermal conductivity and the radiative energy balance as the difference between total emission and absorption per unit volume were determined by introducing the concept of a zero arc radius.

Liebermann and Lowke [41], calculated analytically the net radiation emission coefficient of SF_6 at 1 and 10 atmospheres pressure for different arc radii, and for temperatures of up to 35,000K. The E–I characteristics and the arc centre temperatures were also published, for 1 and 10 atmospheres pressure.

Shayler and Fang [65], studied the radiation transport mechanism within wall stabilized nitrogen arcs at 1 and 10 atmospheres pressure. These studies showed that the calculated radiative arc loss accounted for a significant fraction of the electrical power input. It was found that the losses at wavelengths less than 200 nm were most important over a wide range of conditions.

Dienemann [17], calculated material properties for temperatures between 1,000 and 20,000K and pressures of up to 100 atmospheres. These theoretical calculations were made using an advanced physical model which takes into account the electrostatic interaction of the charged particles. Dienemann, Hinz and Freyer [18], also determined experimentally the electrical conductivity by approximating the arc profile to a rectangular shape for temperatures of up to 20,000K and for the pressure range of 40 to 200 kPa.

Chapter 2

THEORY

2.1 Determination of the Arc Temperature

The temperature of hot plasma can not be measured with thermocouples and other immersion pyrometers. A radiation pyrometer measures temperatures without physical contact with the hot body and its temperature measuring range is, in principle, unlimited. The spectroscopic method employs a measurement of optical radiation in the wavelength range of 200 nm in the ultraviolet region to 25 micron in the infrared [69]. Measurement of radiation is done in terms of the blackening of a photographic plate or by means of a transducer (photo-electrical) which converts radiant energy into an electric signal. Transducers can measure radiation at all wave lengths whereas photographic detection is limited to the ultra-violet, visible and near infrared radiation. In a spectrometer method of plasma pyrometry, the temperature-indicating parameter is an explicit function of the radiation mechanism. The temperature determination may depend upon the measurement of a single line radiation or of several lines.

2.1.1 Absolute Intensity Method

The measurement of the absolute line or the continuum intensity in a plasma in local thermal equilibrium can be used to determine its temperature. The necessary conditions for the intensity measurements are.

- Plasma should be azimuthally symmetric in order to calculate the radial distribution of the intensity from the recorded lateral line radiance using the Abel transform.

- The measured line or continuum intensity should be free from any overlapping by the neighbouring lines.

- Negligible self absorption.

Cascade arcs, described in section 3.2, provide such plasma conditions in which radial distribution of intensities can be calculated by the Abel inversion.

Absolute Intensity of a Single Line

The integrated line intensity of a spectral line is given as [69],

$$I_{nm} = \frac{C}{4\pi} N_n A_{nm} h\nu_{nm} \qquad W/m^3 - steradian, \qquad (2.1)$$

$$N_n = N \frac{g_n}{Q} e^{-E_n/kT} \qquad particles/m^3, \qquad (2.2)$$

where

I_{nm} = integrated line intensity

C = constant

N_n = number density of ions in state n.

A_{nm} = transition probability

h = Planck's constant

ν_{nm} = wavenumber of the line

N = number density of ions in all states

g_n = statistical weight of level n

E_n = energy of the upper state

k = constant

T = temperature

Q = partition function.

$$I_{nm} = \frac{hc}{4\pi} l N \frac{g_n A_{nm}}{Q \lambda_{nm}} e^{-E_n/kT}, \qquad (2.3)$$

for λ expressed in nm,

$$I_{nm} = 1.582 \times 10^{-17} \frac{g_n A_{nm}}{Q \lambda_{nm}} N e^{-E_n/kT} \qquad W/m^3 - steradian, \qquad (2.4)$$

where

c = velocity of light

l = distance of the ray path inside the plasma

λ_{nm} = wavelength of the line.

To calculate temperatures from equation 2.4 one does not solve the equation explicitly. Instead a relationship is prepared between intensity and temperature from the known plasma composition and values of $g_n, A_{nm}, Q, \lambda_{nm}$ and E_n. The measured radial intensity is then compared with the intensity versus temperature graph to determine the plasma temperature.

Absolute Continuum Intensity

The continuous spectra are produced by radiative transitions of free electrons to other free states, bremstrahlung, or between free and bound states (recombination). The radiated intensity for the continuum is given as [26],

$$I(\nu) = [C_{ff1}(\nu) + C_{fb1}(\nu)] \frac{N_e N_i}{T^{1/2}} + [C_{ff2}(\nu) + C_{fb2}(\nu)] \frac{N_e N_{2i}}{T^{1/2}} + --, \qquad (2.5)$$

where constants $C(\nu)$ are a function of wavelength, but not of the population density or temperature in the wavelength range covered here. Since second ionization is not significant, $C = C_{ff1} + C_{fb1}$.

$$I(\nu) = C(\nu) \frac{N_e N_i}{T^{1/2}}, \qquad (2.6)$$

where

N_e = electron density

6

N_i = ion density of the first ionization

N_{2i} = ion density of the second ionization.

From the known temperature distribution of the arc, the value of $C(\nu)$ can be calculated. Since $C(\nu)$ is independent of temperature and pressure, the same value can be used to calculate temperatures at other pressures if the continuum intensity is known.

2.1.2 Fowler and Milne Method

If the temperature of the plasma extends higher than the normal temperature for which the line intensity is a maximum, then the radial distribution of measured line intensity has an off-axis maximum. For such intensity distributions the temperature can be calculated from the normalized intensities rather than absolute measurements. This is known as the Fowler and Milne method [21] and is applicable under the following conditions:

- The temperature should be a maximum on the axis of the arc and must decrease monotonically with increasing radius.

- The temperature profile must include temperatures both higher than and lower than the normal temperature above which the intensity decreases with increasing temperature.

- The arc should not bifurcate or spiral within the channel.

In the calculated intensity–temperature graph, the intensities are normalised with the maximum intensity. The temperature at maximum intensity of unity being the normal temperature. The measured radial distributions of intensities are also normalised in the same way with maximum off-axis intensity and made equal to unity.

To calculate the temperature of the arc the normalised measured radial intensities from r_{max} to the point where the intensity has a maximum (unity), are compared with the normalised calculated intensities to the left of the normal temperature. The measured intensities from the maximum point up to the arc axis are compared with the calculated intensities to the right of the normal temperature.

This method has the advantage of using relative intensities and is equally accurate on both sides of the normal temperature at which the intensity is maximum.

2.2 Electron Density from Hα Line Profile

The electrons and ions present in the plasma create an intermolecular electric field of statistically changing magnitude and direction. The intensity of this micro-field can easily reach up to 100 to 10,000 kV/m [36]. The hydrogen atoms present in the plasma subjected to this field experience splitting of the energy levels, which shows up as Stark broadening in the radiated line intensity profile. It is essentially proportional to the two thirds power of the electron density. Therefore the electron density can be written as,

$$N_e = C(N_e, T)\Delta\lambda_s^{3/2} \qquad cm^{-3}, \qquad (2.7)$$

where $\Delta\lambda_s$ is the full half-width and the coefficient $C(N_e, T)$ is only a weak function of the electron density(N_e) and temperature (T). In table 6.6 values of $C(N_e, T)$ are

7

listed for different N_e and T. From the given values of the coefficient $C(N_e, T)$, full half-widths are calculated at different temperature and pressure. Graphs between full half-widths and electron densities are then prepared for different pressures. The electron densities can be evaluated from the measured full half-widths of H_α and the lines using the $\Delta\lambda_s$ versus N_e graphs. The uncertainty in the calculation of N_e from the line profile is estimated at 10% [26].

2.3 Transport Properties as a Function of Temperature and Pressure

There are various methods for determining transport properties, namely electrical and thermal conductivities, and net radiation emission of high-temperature plasma from experimental measurements.

There are two basic measurements required for the evaluation of the transport properties. First, the temperature of the plasma as a function of arc radius. Second, the current and the electric field of the arc. In some cases, transparent radiation is also measured. In this experiment, the method employed for calculating transport properties required only the measurements of temperature profiles of the arc and the E–I characteristics.

The energy balance of a volume element of an azimuthally symmetric arc column without convection or radiation absorption can be written in the form of the Elenbaas Heller equation [67]:

$$\sigma E^2 + \frac{1}{r}\frac{d}{dr}\left[rk\frac{dT}{dr}\right] - u = 0, \qquad (2.8)$$

with boundary conditions

$$\left(\frac{dT}{dr}\right)_r = 0 \qquad T_{wall} = constant, \qquad (2.9)$$

where
   σ = electrical conductivity
   E = electric field
   k = thermal conductivity
   u = net radiation emission
   T = arc temperature
   r = arc radius.

The entire energy transport within the arc column depends upon these three parameters; namely, electrical conductivity, σ, thermal conductivity, k, and net radiation emission, u. In this section, three methods which have been used to evaluate these three energy transport parameter (σ, k and u), have been described.

2.3.1 Electrical Conductivity Using the 'Trial Function' Technique of Devoto and Mukherjee

For the evaluation of electrical conductivity, Ohm's law is integrated over the cross section of the arc column:

$$I = 2\pi E \int_0^R \sigma(r)\, r\, dr, \qquad (2.10)$$

where

I = arc current

E = arc field

r = arc radius

R = arc radius at the wall.

Substituting $x = (r/R)^2$ and $Ta(I)$ and Tw as the arc temperatures at the axis and the wall respectively,

$$\frac{I}{\pi R^2 E(I)} = \int_{Tw}^{Ta(I)} \frac{\sigma}{T} \left[-\frac{\delta x}{\delta T} \right] dT. \qquad (2.11)$$

This equation can be rewritten with the aid of an integration by parts as,

$$\frac{I}{\pi R^2 E(I)} = \int_{Tw}^{Ta(I)} \frac{d\sigma}{dT} x\, dT. \qquad (2.12)$$

In this integral equation, all the variables; E, I, x, Ta and Tw, are known in the form of measured data. To solve for σ, a 'trial function' consisting of three parameters A, B and C is substituted into equation 2.12, and adjusted until the computed value of the arc conductance is in good agreement with the measured value. The 'trial function', involving polynomial, exponential and logarithmic terms is given by Devoto and Mukherjee [16], describing $\sigma(T)$ as,

$$\sigma(T) = A\, T^{-B} e^{-C/T}. \qquad (2.13)$$

The Gauss-Seidel method can be used to calculate the values of parameters A, B and C in the following manner.

At three current values for which temperature profiles are known, values of the arc conductance can be calculated from the measured E–I characteristic.

$$\text{Arc conductance}, Y = I/\pi R^2 E \qquad S/m. \qquad (2.14)$$

Integrand 2.12 is calculated for each of the three currents, since the values of radial positions x and the corresponding temperatures (T) are known from the measured temperature profiles, $d\sigma/dT$ is evaluated by differentiating equation 2.13 and substituting initial trial values of A, B and C.

$$\frac{d\sigma}{dT} = -AB\, e^{-C/T} T^{-(B+1)} + \frac{AC}{T^2} T^{-B} e^{-C/T} \qquad (2.15)$$

$$Y_1 = f_1(A, B, C) \quad (Y_1 \text{ at current } I_l) \qquad (2.16)$$

$$Y_1 + A_1 = A_1 + f_1(A, B, C) \qquad (2.17)$$

$$or \quad A_1 = -Y_1 + A + f_1(A, B, C). \qquad (2.18)$$

For the next current I_2 the value of the integrand is calculated using the updated value of A.

$$B_1 = -Y_2 + B + f_2(A_1, B, C). \tag{2.19}$$

Similarly for the third value of the current I_3 the value of the integrand is calculated using the updated values of A and B.

$$C_1 = -Y_3 + C + f_3(A_1, B_1, C). \tag{2.20}$$

In general form, the values of the parameters A, B and C for $(i+1)$th iteration can be written as,

$$A_{i+1} = -Y_1 + A_i + f_1(A_i, B_i, C_i) \tag{2.21}$$

$$B_{i+1} = -Y_2 + B_i + f_2(A_{i+1}, B_i, C_i) \tag{2.22}$$

$$C_{i+1} = -Y_3 + C_i + f_3(A_{i+1}, B_{i+1}, C). \tag{2.23}$$

Calculation is continued and the values of A, B and C are updated until the solution relaxes.

2.3.2 Thermal Conductivity Using the 'Form Factor' Technique

From the energy balance equation of an azimuthally symmetric arc, an expression can be derived which gives the thermal conductivity as a product of a parameter called the 'form factor' [68] and the derivative of electrical power input with respect to the arc centre temperature. The form factor is a measure of the radial distribution of the electrical conductivity. The energy balance equation can be written as,

$$\sigma E^2 = -\frac{1}{r}\frac{d}{dr}\left[rk\frac{dT}{dr}\right]. \tag{2.24}$$

If $\sigma = \sigma_0 f(r)$, integrating equation 2.24 once and using the boundary condition $dT/dr = 0$ at $r = 0$ and replacing the variable r with t gives

$$\frac{\sigma_0 E^2}{r} \int_0^r t f(t) dt = -\left[k\frac{dT}{dr}\right]. \tag{2.25}$$

Changing the variable r with s and integrating the equation 2.25 a second time

$$\sigma_0 E^2 \int_0^r \frac{ds}{s} \int_0^s t f(t) dt = -\int_0^r \left[k\frac{dT}{ds}\right]. \tag{2.26}$$

With the changed limits,
$r = R, T = T_w = 0$ (wall temperature),
$r = 0, T = T_a$ (arc centre temperature),

$$\sigma_0 E^2 \int_0^R \frac{ds}{s} \int_0^s t f(t) dt = -\int_0^{T_a} k dt. \tag{2.27}$$

Changing the order of integration and performing inner integration, yields,

$$\sigma_0 E^2 \int_0^R t f(t) \ln\frac{R}{t} dt = \int_0^{T_a} k dt. \tag{2.28}$$

10

The electrical power input P_{el} is given by,

$$P_{el} = 2\pi \int_0^R \sigma E^2 t dt. \qquad (2.29)$$

$$or \quad P_{el} = 2\pi \sigma_0 E^2 \int_0^R tf(t) dt \qquad \{\sigma = \sigma_0 f(r)\}. \qquad (2.30)$$

Substituting values $\sigma_0 E^2$ into the equation 2.28 and changing the variable t by r,

$$P_{el} \frac{\int_0^R rf(r) \ln\frac{R}{r} dr}{2\pi \int_0^R rf(r) dr} = \int_0^{T_a} k dT, \qquad (2.31)$$

and differentiating equation 2.31 with respect to the arc centre temperature,

$$\frac{d}{dT_a}(P_{el} F_{el}) = k(T_a), \qquad (2.32)$$

which gives the value of the form factor,

$$2\pi F_{el} = \frac{\int_0^R rf(r) \ln\frac{R}{r} dr}{\int_0^R rf(r) dr}. \qquad (2.33)$$

Until now, it has been assumed that radiation is negligible. In order to take radiation into account, in the form of a radiation emission, u, it is assumed that u will be given by a radial distribution, $u = u_0 g(r)$. Therefore the energy balance equation can be rewritten as,

$$\sigma_0 f(r) E^2 - u_0 g(r) = -\frac{1}{r}\frac{d}{dr}\left[rk\frac{dT}{dr}\right], \qquad (2.34)$$

and the total radiation power is given by,

$$P_u = 2\pi u_0 \int_0^R rg(r) dr. \qquad (2.35)$$

Proceeding in the same way as for the electrical form factor the solution yields,

$$P_{el} \frac{\int_0^R rf(r) \ln\frac{R}{r} dr}{2\pi \int_0^R rf(r) dr} - P_u \frac{\int_0^R rg(r) \ln\frac{R}{r} dr}{2\pi \int_0^R rg(r) dr} = \int_0^{T_a} k dt \qquad (2.36)$$

$$2\pi F_u = \frac{\int_0^R rg(r) \ln\frac{R}{r} dr}{\int_0^R rg(r) dr}. \qquad (2.37)$$

Differentiating equation 2.36 once with respect to T_a, the value of k is obtained in terms of both the form factors,

$$k(T_a) = \frac{d}{dT_a}(P_e F_e - P_u F_u). \qquad (2.38)$$

Pflanz and Ter Horst have shown [55] that for a wide range of profiles $F_e \simeq F_u \simeq F$. The numerical value of F can be approximated by $2\pi F = 0.5$ for very flat profiles without any appreciable error in the evaluation of k. The thermal conductivity can be written as,

$$k(T_a) = F\frac{d}{dT_a}(P_e - P_u). \qquad (2.39)$$

2.3.3 Net Radiation Emission

The energy balance equation 2.8 can be solved to evaluate the net radiation emission, u, once $\sigma(T)$ and $k(T)$ are known.

$$u(T) = \sigma(T)E^2 + \frac{1}{r}\frac{d}{dr}\left[rk(T)\frac{dT}{dr}\right] \qquad (2.40)$$

$$or \quad u(T) = \sigma(T)E^2 + k(T)\left[\frac{d^2T}{dr^2} + \frac{1}{r}\frac{dT}{dr}\right], \qquad (2.41)$$

where

$$\frac{d^2T}{dr^2} = \left[\frac{T^{i+1} - 2T^i + T^{i-1}}{\Delta r^2}\right] \qquad (2.42)$$

$$\frac{1}{r}\frac{dT}{dr} = \frac{1}{r\,\Delta r}\left[\frac{T^{i-1} - T^{i+1}}{2}\right]. \qquad (2.43)$$

From the measured temperature profile at a current and corresponding electric field, equation 2.41 yields the value of the net radiation emission.

2.4 SF$_6$ Emission Data Calculations (Continuum Coefficient of Emission and Transition Probability)

The spectroscopic measurements of the SF$_6$ arc temperatures are mostly done using absolute and relative line intensity, continuum emission coefficient and line broadening parameters. All the parameters required for these calculations are available from theoretical calculations [26,71,70] except for the continuum coefficents of emission. There have been a few experimental evaluations of the absolute and the relative transition probabilities of some of the selected fluorine and sulfur lines [12,38,51,61,62,7], used by the absolute and the relative intensity method for temperature measurement. In this work, experimental evaluation of the continuum coefficients of emission and the absolute transition probabilities at a few selected wavelengths have been made.

Continuum Coefficient of Emission

As described earlier in section 2.1.1(b), the value of the emission coefficient $C(\nu)$ can be determined from the known temperature distribution and the continuum intensity distribution using equation 2.6. Since the value of $C(\nu)$ does not depend upon the pressure, its value can be calculated from the available data at any pressure at which the radial distribution of the continuum intensity and temperature is accurately known.

Transition Probabilities

The Coulomb approximation method in conjunction with the assumption of LS coupling has been the main source of the transition probabilities of sulfur and fluorine lines [71,70]. The only experimental data which are available are from shock tube measurements [12], life time measurements of the resonance level by the beam foil technique [38] and wall-stabilised arc experiments [51,61,62,7]. In this work, wall-stabilised arcs run with pure

12

SF$_6$ have been used to determine absolute transition probabilities of the selected F$_I$, S$_I$ and S$_{II}$ lines.

The absolute transition probability, A$_{nm}$, in sec^{-1}, of a spectral line may be regarded as the proportionality constant which relates its absolute intensity, I$_\lambda$, to a theoretical function [53,52],

$$F_\lambda(T) = 1.582 \times 10^{-17} \frac{g_n N}{Q \lambda_{nm}} e^{-E_n/kT} \quad W/m^3 - st - sec, \quad (2.44)$$

where λ is in nm and N is in particles/m^3. A value of $F_\lambda(T)$ can be completely determined for any given line using calculated particle densities. Transition probability can be determined if the relation between I$_\lambda(T)$ and $F_\lambda(T)$ is known. At the higher temperatures at which radial distribution of the intensity has an off-axis maximum this can be achieved using the Fowler and Milne method. Because the maximum of the measured I$_\lambda$ and the calculated F_λ occur at the same temperature, the normal temperature and the transition probability are simply the ratio of the two maximums, provided the self-absorption is negligible.

$$A_{nm} = \frac{I_{\lambda(max)}}{F_{\lambda(max)}} \quad sec^{-1} \quad (2.45)$$

This method is applicable for the atomic and the ionic lines. But it cannot be used for those cases where the temperature does not exceed the normal temperature for the species under consideration. This is more likely to happen for the ionic lines whose normal temperatures are quite high. The transition probability can then be calculated from the ratio of the ionic line and the atomic line intensity whose transition probability is known [53].

$$\frac{A_2}{A_1} = \frac{I_{\lambda 2} Q_2 \lambda_2 g_1 N_1}{I_{\lambda 1} Q_1 \lambda_1 g_2 N_2} e^{(E_2 - E_1)/kT}, \quad (2.46)$$

where the suffix 1 and 2 refer to atomic and ionic lines respectively and the temperature is determined from the atomic line intensity.

For the self-absorbed lines, the maximum of I$_\lambda$ is reduced and therefore a correction is necessary for the accurate evaluation of the transition probability. Under LTE conditions the self absorption coefficient, $\kappa_\lambda(T)$, is given by [52],

$$\kappa_\lambda(T) = \frac{g_m A_{nm} \lambda}{8\pi c g_n \Delta \lambda_s} \frac{N}{Q}(T) \left[1 - e^{-hc/\lambda kT}\right] e^{-E_n/kT}, \quad (2.47)$$

where full half-width is equal to $\Delta \lambda_s$.

Since the absolute value of the absorption depends on the transition probability to be evaluated, this expression can be used only to give the relative temperature dependence. If the radial temperature distribution can be accurately measured by means of a line which is not self absorbed, a normalised radial distribution of absorption coefficient can be obtained for the line in question. This can then be used to compute the correct distribution of I_λ. Olsen [52] has shown that, since for a plasma in LTE the absorption coefficient peaks at the same position on the temperature scale as the radiation emission I_λ, and the zonal path length for the integrated radiation increases as the point of observation is moved to the edge of the plasma, it can be expected that the measured line intensities would be affected less on the arc axis than at the normal temperature or off-axis peak. Olsen's results have indicated that for the self-absorbed lines the measured on-axis minimum value can be used without any absorption correction for the evaluation of the absolute transition probabilities.

13

In the SF_6 plasma, diffusive demixing of the gaseous species causes depletion of sulfur near the arc axis [22,44]. The ratio of the fluorine to sulfur concentration, [F]/[S], has been found to be greater than 6, in qualitative agreement with theoretical predictions [22]. This can cause error in the computation of F_λ. Schulz-Gulde has shown [62], that with proper corrections for the demixing, wall stabilised arcs can be used to determine absolute transition probabilities.

Chapter 3

EQUIPMENT AND EXPERIMENTAL SET-UP

3.1   Pressure Vessel and Gas Recovery System

All the cascade arc experiments were conducted in a pressure vessel which had been originally constructed for double-nozzle-flow switching-arc studies. The cascade stack was placed inside the pressure vessel and the arc was observed from the side through one of the 18-cm-diameter windows, shown in figure 3.1. The working pressure rating of the vessel was 25 kPa and the voltage rating was 100 kV. It had two large glass windows from which the arc could be observed. Gas could be admitted through an inlet at the bottom of the vessel and evacuated by two dump cylinders mounted at the top of the vessel.

A gas recovery system for SF_6, based on a cryogenic principle was used for recovering the gas from the pressure vessel. The pumping speed of the system was much higher in comparison to other, conventional systems. The size of the recovery rig was quite small, since it did not use compressors or refrigerating machinery. It was capable of recovering gas down to very low pressures (5 kPa).

The other useful features were the ability to completely remove non-condensable gases, such as air, down to concentrations of tens of ppm. Under some conditions, it was also possible to remove water, oil and other condensable impurities, even if present in massive proportions, to less than 10 ppm in a single pass through the system, and independently of the separate filtration and adsorption module.

3.2   Cascade Arc and Ignitor System

An azimuthally symmetrical arc was generated using a cascade assembly originally designed by Schmidt-Harms [60], figures 3.2 and 3.3. The cascade assembly consisted of thirty, half-millimetre-thick copper plates, C, stacked together with insulating rings, E, between the plates, fastened at all four corners by 5-millimetre threaded perspex rods, B. The distance between the plates was 1.75-millimetres. At each end of the stack there were two, 2-millimetre thick, copper plates, A, to secure the whole assembly. There were two specially designed 2-millimetre plates, H, at the centre of the stack. A circular portion was cut from each side of the plate to allow for a larger solid angle for viewing the arc. Four holes of different sizes (3, 4, 5 and 6 mm) drilled into each plate were aligned on a common pitch circle diameter. With this arrangement, an arc channel of a certain diameter could be selected by simply rotating the stack about the pitch circle.

15
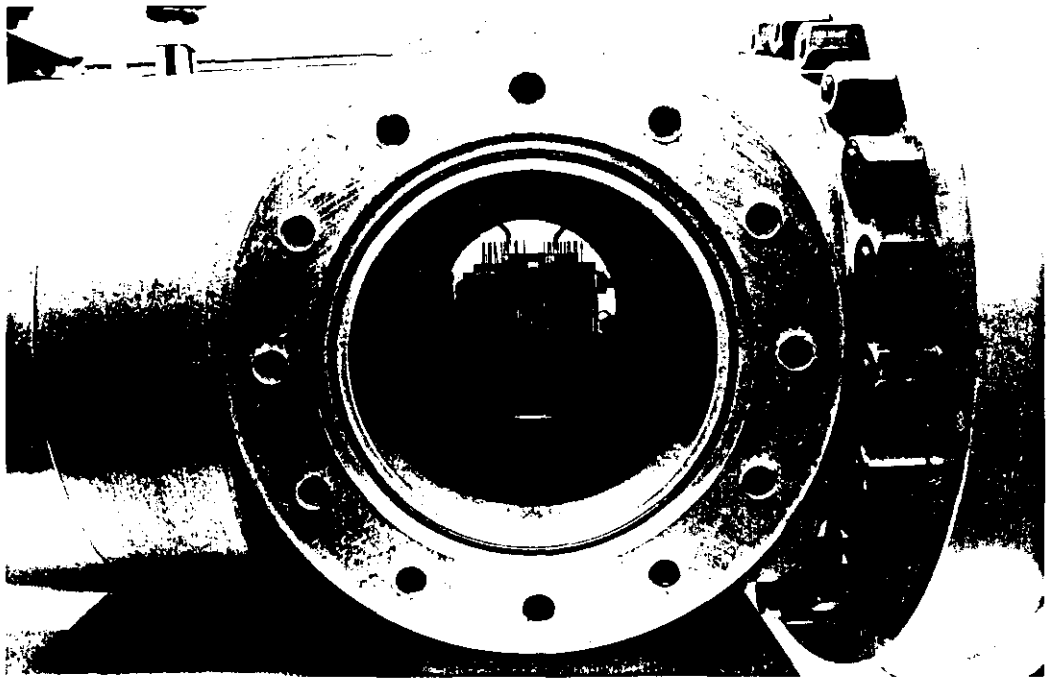
Figure 3.1: The pressure vessel with the cascade assembly installed inside.

The stack was able to withstand brief exposure to arc temperatures of up to 22,500K at the centre of the arc without melting. The maximum thermal loading that could be tolerated by the cascade stack was about 20 kW/cm^2 when the arc was run in a pulsed mode. For higher currents, the maximum duration for the pulse was kept to twenty milliseconds, which allowed arcs of up to 550-amperes.

The arc was initiated by a separate ignitor capable of striking a clean pilot arc repetitively without having to open the pressure vessel [60]. A cross section of the ignitor is shown in figure 3.4. A sliding spring steel rod of 1.8-mm diameter was firmly connected to the disc 1.5-mm thick and 40 mm in diameter, which travelled freely in a nylon guide along the arc axis, as shown in figure 3.3. There were holes at the far end of the tube to permit the reloading of the ignitor rod by injecting compressed gas. The tube had a number of holes, 10 mm in diameter, to allow the gas compressed by the disc, to escape and to reduce the drag force on the disc. The entire kinetic energy of the disc was absorbed by the bounce-free cushion fixed at the far end of the tube.

The cushion was made of foam rubber and had a steel washer sandwiched between the foam. The steel washer had the same weight as the ignitor rod and during impact its entire momentum was transferred to the washer. The foam rubber was quite inelastic which prevented the ignitor from rebounding.

The driving coil was placed at the end towards the cascade stack. For optimum performance, the coil must be as flat as possible. There were three layers of the coil of 100 turns of 0.5-mm enameled copper wire, vacuum impregnated with epoxy. The coil surface was insulated from the aluminium disc by a thin sheet of mica to prevent flashover.

16

The power was supplied to the driving coil from a 30 microfarad capacitor, charged to 1 - 2.5 kV and discharged through a spark gap. The inductance of the circuit was very low and allowed efficient conversion of the energy stored in the capacitor to the magnetic field of the coil. The eddy currents induced in the disc generated the force which drove the ignitor rod and the disc. The force depended upon the disc thickness, amplitude of magnetic field and the annular area near the disc circumference where the force was concentrated. The thickness of the disc did not influence the acceleration of the ignitor. The load mass that the disc drove did have a marked effect on the velocity that the ignitor attained.

3.3 Electrical Set-up

There were two parts of the entire electrical setup. The first part consisted of the high current power supply, the resistors, the spark gaps, the current shunt and the voltage dividers, which supplied the required amount of power for a specified duration, shown in figure 3.5. The supply busbar was connected to the high voltage electrode through a make switch, MS, in series with resistors, R and R_g, and the low voltage electrode was connected to the supply ground through a current shunt. The spark gap, SG1 was connected across the resistor, R_g and the spark gap, SG2 across the cascade electrodes. The spark gap, SG1 short circuited the resistor, R_g at time, T1 and SG2 short circuited the arcing electrodes at time, T3. The sixth cascade plate on either side of the centre of the stack were connected to voltage dividers having division ratio of 1/1000. The value of R_g was selected such that the low current was enough to maintain a pilot arc for about 25 ms. The resistor, R was kept to a maximum possible value depending upon the main arcing current requirements in order to have large time constant. This allowed the drop in arcing current to be kept below 10% during the time in which the spectrum was recorded, shown in figures 3.6 and 3.7.

The second part of the electrical set-up consisted of all the measuring instruments together with the controlling devices, shown in figure 3.8. One Nicolet digital oscilloscope was connected across the two cascade plates to measure the arcing voltage and the other was connected to the current shunt and to the photo-multiplier for measuring arcing current and the shutter opening time respectively. The Tektronix-465 oscilloscope was connected to the Nicolets, the spark gaps, the uniblitz shutter and the ignitor through time-delay generators. This oscilloscope was used to send the triggering pulse to the driving mechanism of different units. There were three time-delay pulse generators, TD1, TD2 and TD3. The delay generator, TD1 was connected to the spark gap, SG1, TD2 to the shutter and TD3 to the second spark gap, SG2, shown in figure 3.8.

The triggering pulse from the Tektronix oscilloscope was sent directly to the two Nicolets and the ignitor driving mechanism as soon as the make switch, MS was closed. The spark gap was triggered after a delay of T1 ms through the time-delay generator, TD1, and main arcing current was applied. The shutter received the triggering pulse after a time-delay of T2 ms through the time-delay generator, TD2, and the shutter was opened for the time duration of Ts ms. The spark gap, SG2, was triggered after T3 ms through TD3 and the arcing current was chopped to zero. To avoid interference from unwanted stray signals, all the Nicolets and Tektronix oscilloscopes including the time-delay pulse generators were kept inside a screened room and were linked with various equipments outside the room through optical fibre.

17

3.4 Spectrograph

The Steinheil Universal spectrograph, model GH, was used in these experiments. It had three prisms supported on a base plate which held the prisms in an accurately vertical position. On one side of the base plate there were four mounting pads by which the collimator was attached. On the other side there were two more mounting pads by which the telescope arm and the camera were attached.

The slit plate carrying the slit and the shutter was attached to the collimator by means of three screws. The shutter, Copal-No.1, placed behind the slit worked with a cable release mechanism and could be used for time exposures of 25 ms to 1 second. The collimator tube was adjusted parallel to the base plate. The far end of the tube carried the slit head and the other end supported the collimator lens mount and its focusing mechanism. The prisms could be set at different positions as given by the data sheet for recording a particular region of the spectrum on the camera plate.

The inclination of the plate with respect to the optical axis was also adjustable. The tilting axis coincided with the centre of the plate. Therefore, in order to focus the entire range of the spectrum, the centre line was first brought into sharp focus by adjusting the distance between the lens and the plate and then the inclination of the plate was adjusted to bring both ends of the spectrum into focus. For accurate focusing, a series of spectra was photographed at different positions around the best focusing point located by eye observation by changing both the distance and the inclination of the camera plate. A careful examination of these photographs determined the best position.

3.5 Spectrum Imaging

The optical set-up for imaging the arc on the entrance slit of the spectrograph was required to meet four objectives to ensure the recording of good quality spectra. These were,

1. Good spatial resolution of the spectrum lines along the arc diameter for the entire range of the spectrum, 400 - 800 nm.

2. Large field of view (10 mm) to image arcs of up to 8 mm diameter on the entrance slit.

3. Three-times-magnification of the arc image at the attenuator wheel position.

4. To image the arc and the standard lamp filament through the same optical set-up with minimum rearrangement.

A ray tracing method was used in which the gaussian optics were represented by a matrix [28]. The entire optical set-up was reduced to a series of matrices. For example, a lens having a focal length of f_1 and f_2, shown in figure 3.9, can be represented by a matrix of the form,

$$(FP_1 - FP_2) = \begin{bmatrix} 0 & f_1 \\ -1/f_2 & 0 \end{bmatrix},$$

,

connecting the two focal planes,

where $f_1 = r_2/r_1\prime$ and $f_2 = -r_1/r_2\prime$.

18

The matrix establishing the connection between reference plane RP_1, located at a distance of Z_1 to the left of the focal plane FP_1 and RP_2 located at a distance of Z_2 to the right of FP_2, is obtained by multiplying this matrix from the left by,

$$\begin{bmatrix} 1 & Z_2 \\ 0 & 1 \end{bmatrix},$$

and from the right by,

$$\begin{bmatrix} 1 & Z_1 \\ 0 & 1 \end{bmatrix}.$$

Thus the two reference planes RP_1 and RP_2 are connected by the resultant matrix,

$$A_{12} = \begin{bmatrix} 1 & Z_2 \\ 0 & 1 \end{bmatrix} \times \begin{bmatrix} 0 & f_1 \\ -1/f_2 & 0 \end{bmatrix} \times \begin{bmatrix} 1 & Z_1 \\ 0 & 1 \end{bmatrix}$$

or

$$A_{12} = -\frac{1}{f_2} \begin{bmatrix} Z_2 & Z_1 Z_2 - f_1 \\ 1 & Z_2 \end{bmatrix},$$

therefore $A_{12} = f_1/f_2 = n_1/n_2$.

By setting the upper right element of the matrix to zero, the object-plane magnification can be obtained,

$Z_1/Z_2 = f_1/f_2$,

from which lateral magnification can be obtained,

$m = -Z_2/f_2 = -f_1/Z_1$.

The other important consideration that could be estimated by this method, is the effect of the aperture which not only limits the amount of light passing through the system, but also influences the maximum field of view of the arc column. This was done by projecting the aperture into the space to the left or to the right of the optical system, shown in figure 3.10. If a light ray, originating from P, intersects the image of the obstructing part of the aperture, A, it must also intersect A, and is therefore, not transmitted through the entire optical system.

By the help of this simple mathematical representation of the optical system it was possible to calculate proper image-to-object ratios at the two intermediate positions I_1 and I_2 and at the entrance slit of the spectrograph. By projecting various apertures of the lenses it was possible to optimise the lens locations for best field of view of the arc area and maximize the overall aperture, subject to the above constraints. A programme written for the VAX-11/780 by Schmidt-Harms, based upon the above method, was used for computing the lens positions.

3.6   Spectrum Plate Scanner

The photographed spectrum lines on the plates were scanned by a modified CarlZeiss-Jena rapid photometer (serial number 270804), shown in figure 3.11. It has been modified to provide automatic scanning of the plates under the full control of an HP 9836 computer. The instrument has a robust body which stands on three legs used for leveling. A carriage, which holds the plate, was capable of movements in both X and Y directions. The two stepping motors, having 400 steps per revolution, were mounted

to control both the movements. They provided 10-micron steps in the X direction (wavelength) and 70-micron steps in Y direction (arc cross-section). For coarse scanning, the step size could be doubled by sending two pulses instead of one to the stepping motors.

The light source, a 10-volt, 50-watt bulb, was supplied from a constant current source to provide steady illumination to the plate. The main scanner slit could be adjusted for width and height, depending upon the step size in the X and Y directions. The light falling on the photo cell was controlled by a step and a wedge filter positioned at the back of the main slit.

To bring the entire plate into sharp focus, the carriage was provided with leveling screws which could tilt the carriage over the long and the short side of the plate. The carriage could also be rotated in its own plane to ensure the spectra were parallel to the carriage travel in the X direction. The voltage output from the photocell was amplified and the analog output was digitised by an A-to-D converter, which was collected by the computer, and then stored on floppy disks.

A − Brass end plate (50 x 50 x 2)

B − Perspex rod (5 ⌀ x 85)

C − Copper plates (50 x 50 x 0·5)

D − Holes for perspex rod

E − Teflon washers

F − Arc channel diameter (3-6⌀)

G − Nuts to hold the plates

H − Central plates

(All dimensions in millimetres)
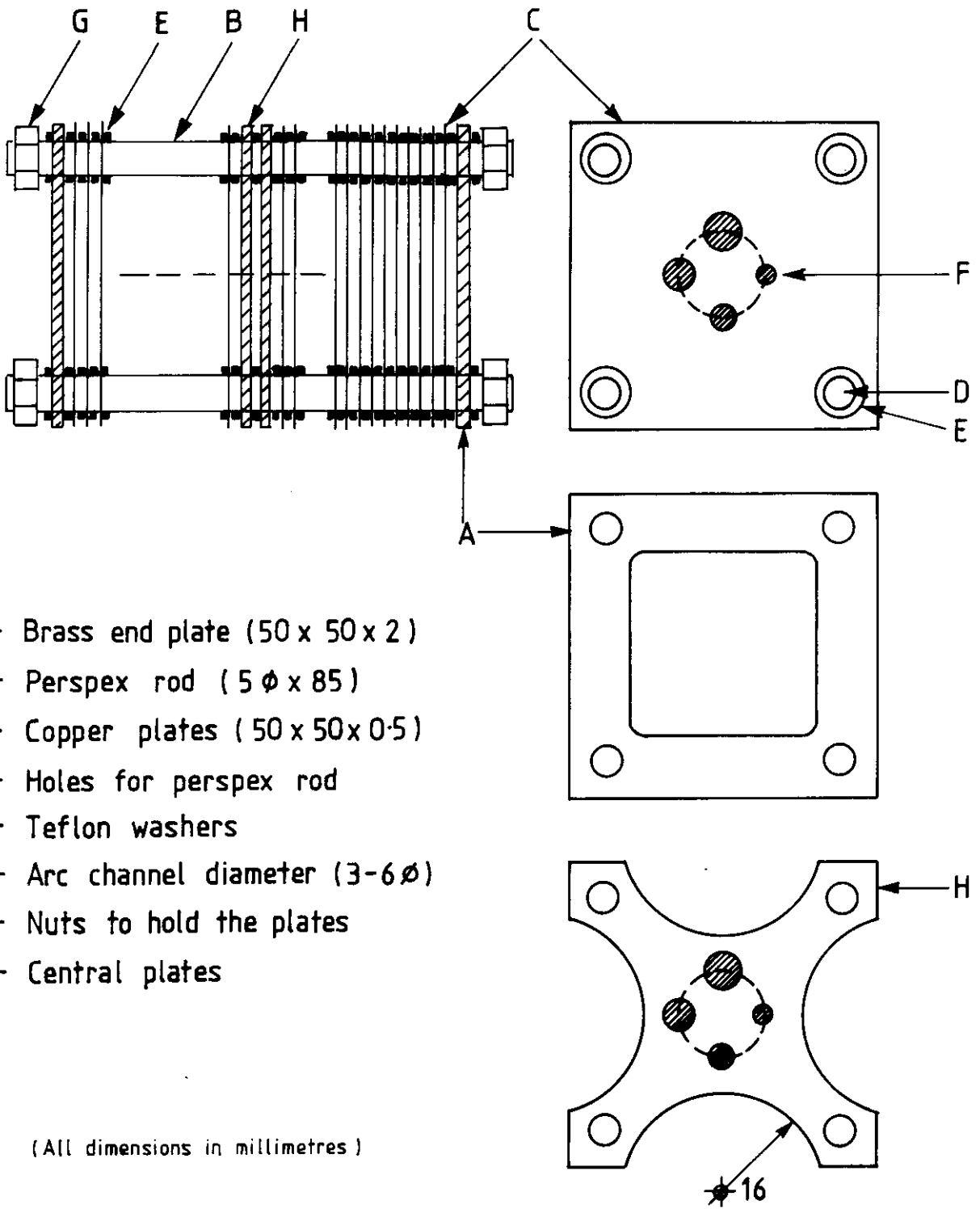
Figure 3.2: The cascade stack assembly.

21
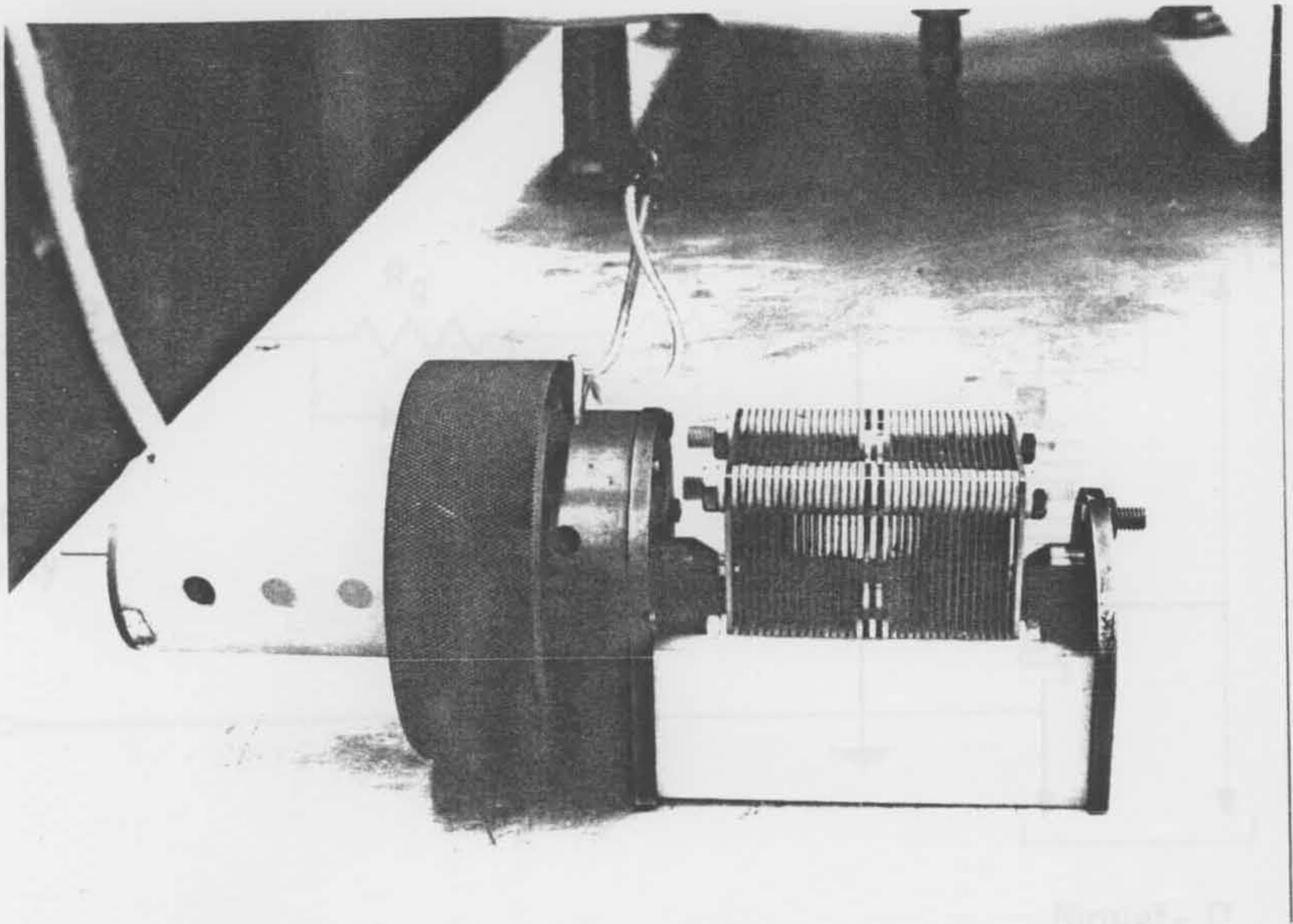
Figure 3.3: The ignitor and the cascade stack assembly.

Cascade stack

Perspex end plate

10mm Φ holes spaced
90° apart in azimuth

PTFE
guide

Al. disc 40mm Φ

Steel collett

Gas admission
for re-loading

Drive coil

nylon guide tube
41 mm Φ

Bounce-free cushion with
momentum transfer washer

Elconite electrodes

1·8mm Φ spring steel
rod
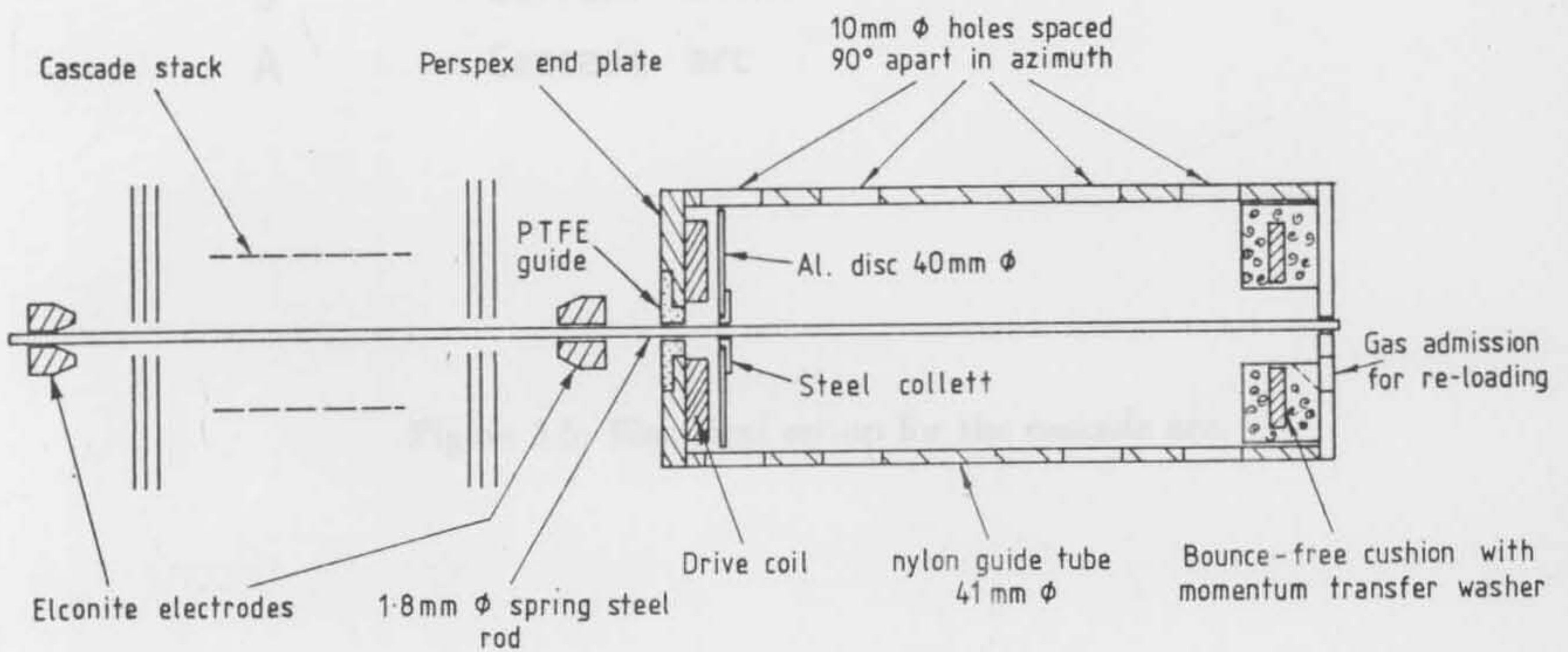
Figure 3.4: Cross-sectional view of the ignitor and the cascade stack.
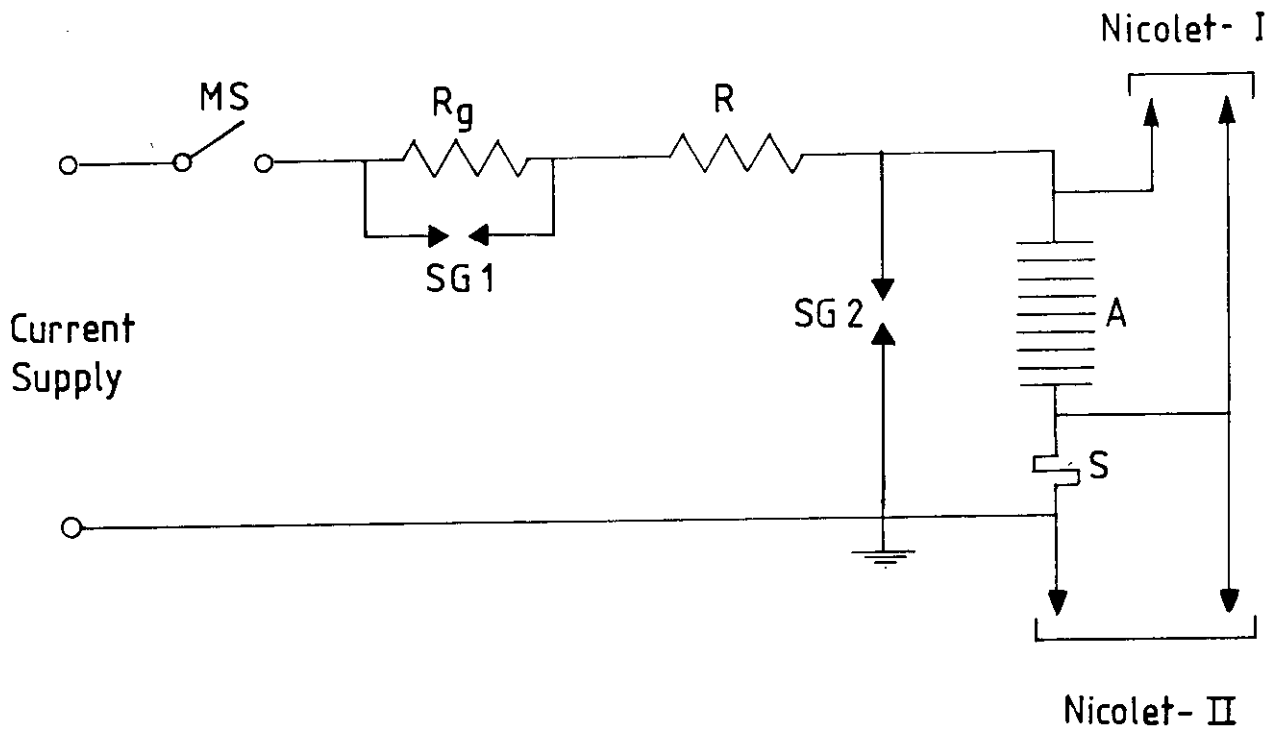
MS   – Make switch

R_g, R   – Resistors

SG1, SG2 – Spark gaps

S   – Current shunt

A   – Cascade arc

Figure 3.5: Electrical set-up for the cascade arc.
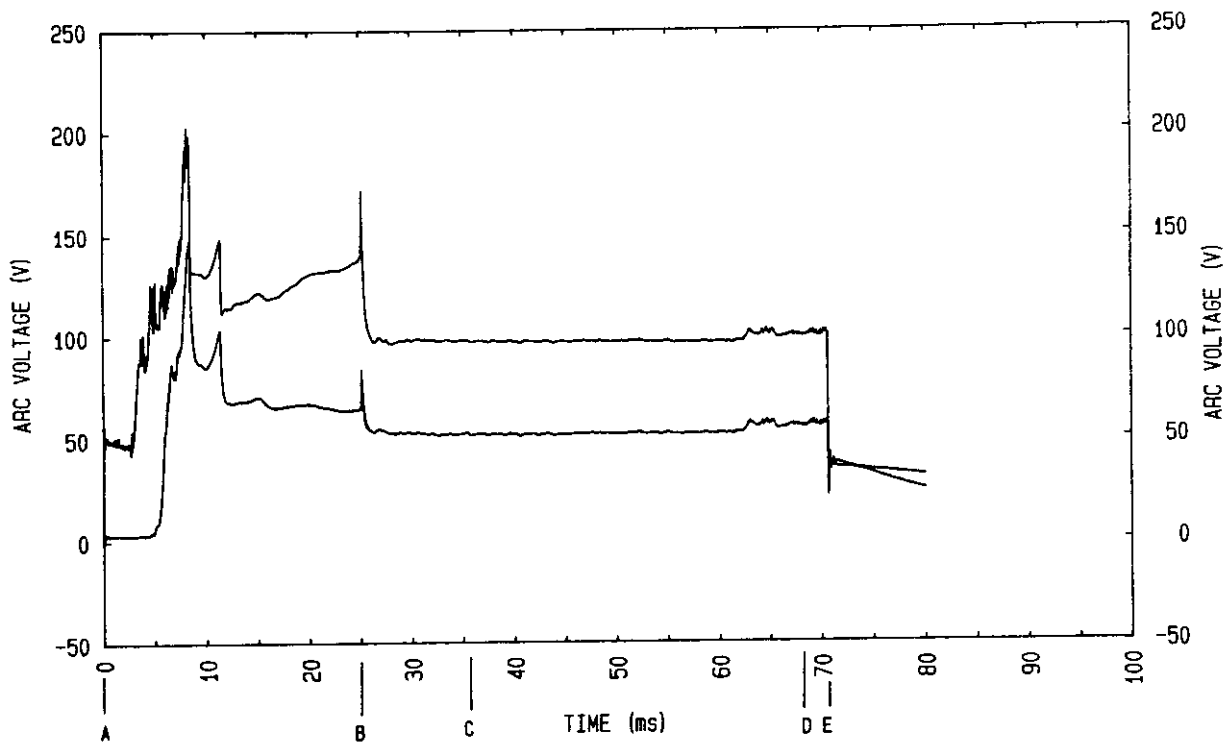
Figure 3.6: Arc voltage waveforms measured at two cascade plates.
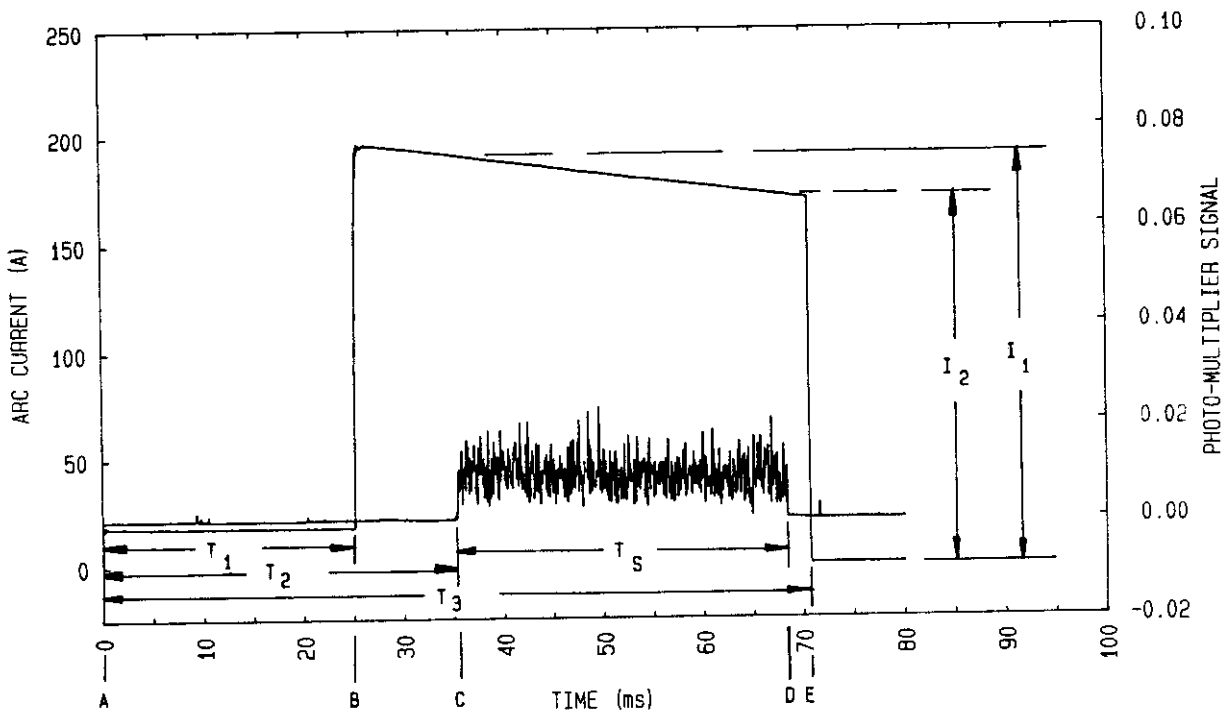
I1, I2   Arc Currents at Time C and D
C, D   Shutter Opening and Closing Times
B - E   Main Arcing Current Duration

Figure 3.7: Arc current and exposure time waveforms.

24
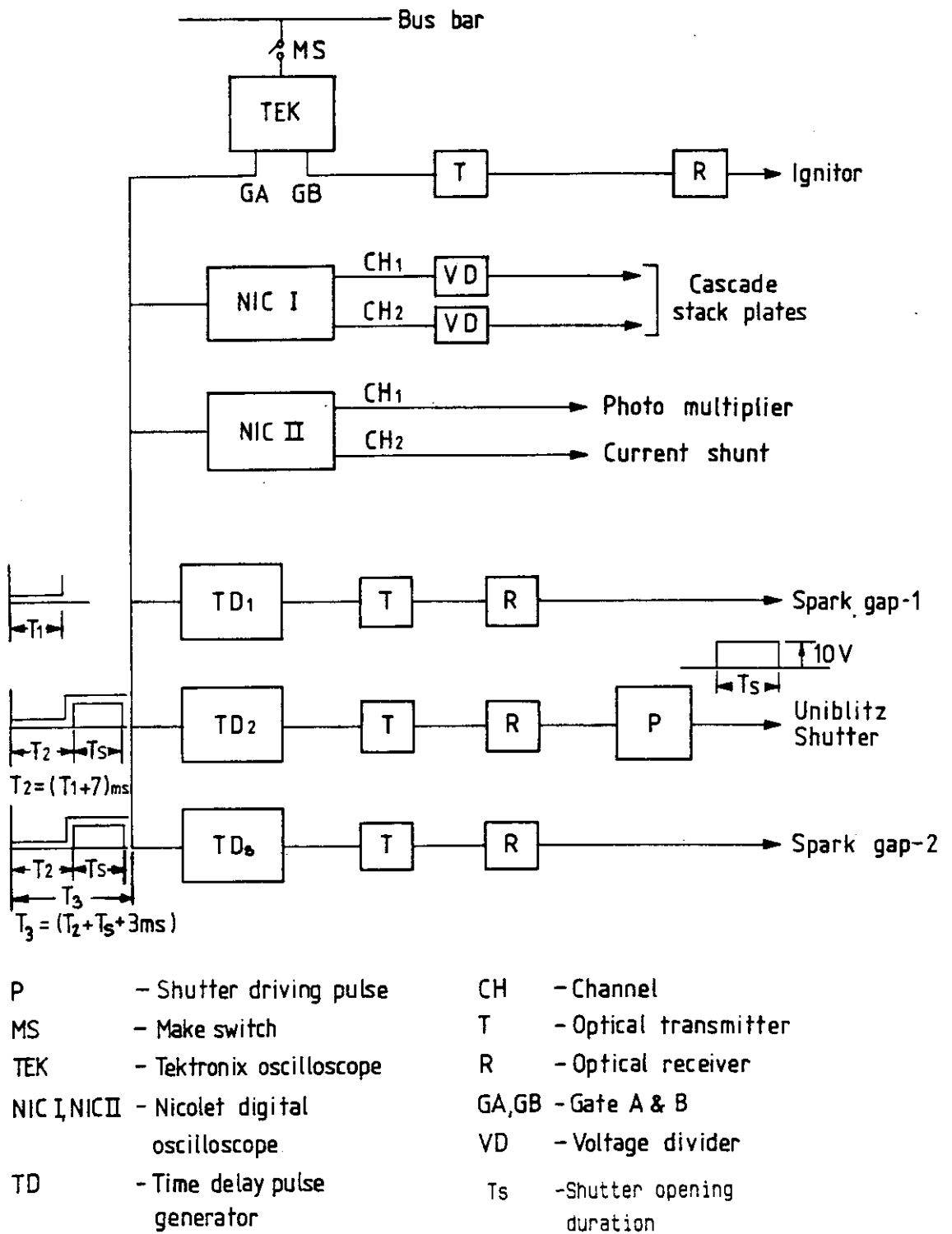
Figure 3.8: Schematic connection diagram of the recording instruments.

P — Shutter driving pulse
MS — Make switch
TEK — Tektronix oscilloscope
NIC I, NIC II — Nicolet digital oscilloscope
TD — Time delay pulse generator

CH — Channel
T — Optical transmitter
R — Optical receiver
GA, GB — Gate A & B
VD — Voltage divider
Ts — Shutter opening duration
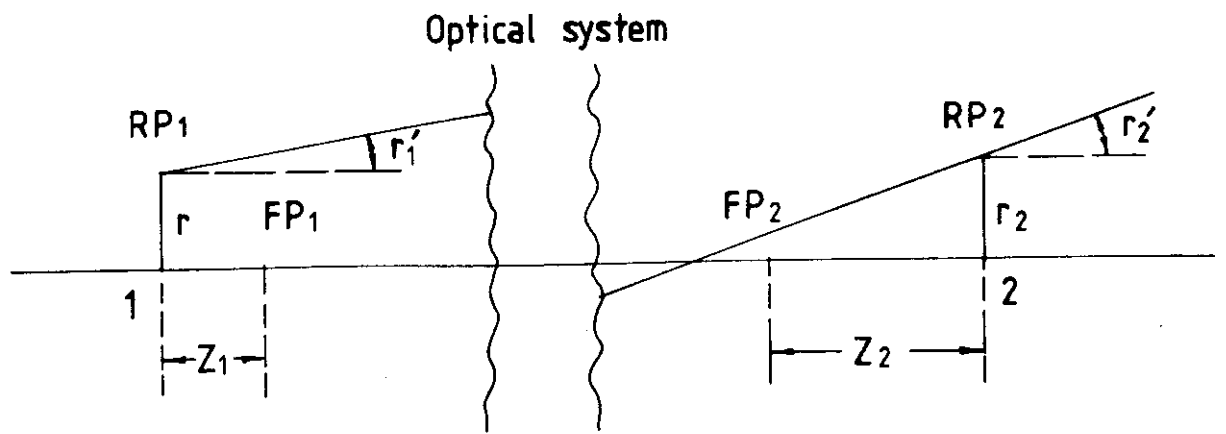
Figure 3.9: Image object relationship between two reference planes RP1 and RP2.
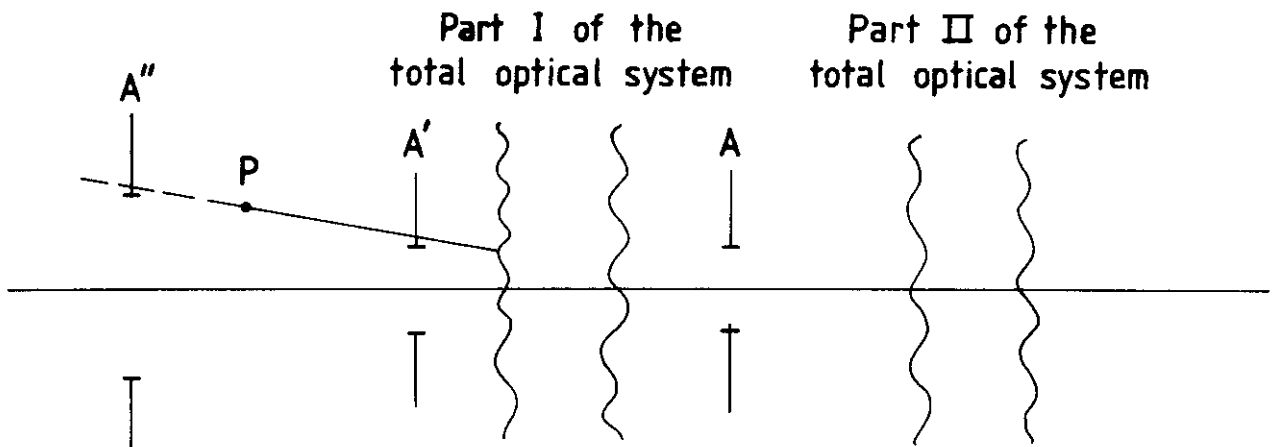
Figure 3.10: Effect of an aperture on the field of view.

Chapter 4

EXPERIMENTAL PROCEDURE

4.1 Set... of the Opt...

Figure 3.11: The plate scanner.

Chapter 4

EXPERIMENTAL PROCEDURE

4.1 Set-up of the Optics

The procedure for recording spectra of high spatial resolution on a photographic plate is described in this section. A helium-neon laser beam was used to align the entire optical train with the spectrograph optic axis. The laser beam was trained at the exit plane of the spectrograph at the position corresponding to its wavelength, 632.8 nm. The angle and the height of the beam were adjusted so that the it emerged horizontally from the centre of the entrance slit. The optical bench on which all the lenses and the mirrors were placed was aligned with the laser beam and clamped firmly to a heavy adjustable table.

At the far end, another optical bench was fixed at right angles to this and, at the intersection, a front-polished mirror was placed which could be rotated through ninety degrees. The two stops which restrict the angular movement of the mirror were so positioned that the mirror was always at forty five degrees to the optical axis, shown in figures 4.1 and 4.2. Therefore, the light could be received by the spectrograph from either side by rotating the mirror. On one side the cascade arc assembly, placed inside the pressure vessel, was positioned so that the laser beam was reflected from the mirror to the centre of the cascade stack. On the opposite side, a standard lamp was placed at exactly the same distance from the mirror as that of the cascade stack.

The focusing and alignment of the lenses was done very carefully in two stages. In the first stage, lenses were placed in their pre-calculated positions, starting with the lens L_4 and adjusted for x, y and z coordinates such that the laser beam remained focused at the centre of the arc. Then the mirror was rotated by ninety degrees and the horn lamp was adjusted for the x, y and z coordinates such that the laser beam was focused at the centre of the filament. This ensured that all the lenses were properly aligned with the optical axis of the spectrograph.

In the second stage, lenses were moved along the optical axis to focus the arc and the horn lamp filament on the entrance slit of the spectrograph. At the same time, the correct image-object ratio was achieved by placing a pattern transparency having one line per millimetre at the arc axis. It was illuminated by a bright light in the background and its image was brought in to sharp focus at I_1 position, by adjusting lens L_1, shown in figure 4.1. The lens L_2 was then adjusted to obtain a sharp image at I_2 with three-times magnification. This magnification was necessary in order that the largest step of the attenuator wheel was illuminated by the central five millimetre section of the horn lamp filament. This ensured that the light from the standard horn lamp passed exactly through the same optical path as that of the five-millimetre diameter arc. The lens L_3
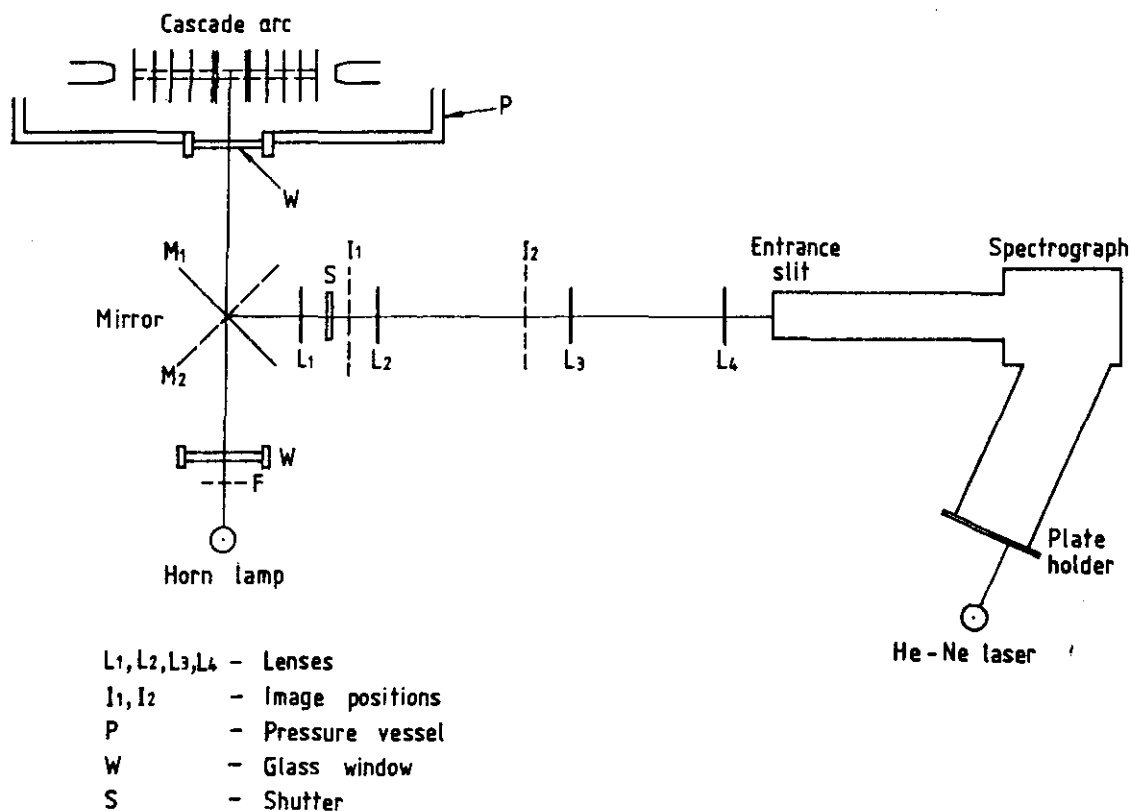
Figure 4.1: Optical arrangement for the cascade arc.

was placed at the pre-calculated position and lens L_4 was moved to focus the pattern image at the entrance slit. Minor adjustments were made to L_3 and L_4 positions, in order to obtain 1:1 image ratio at the entrance slit.

When the spectrum was observed by the eyepiece at the exit plane of the spectrograph it was found that the pattern was not in focus in the entire visible range. This distortion was due to chromatic aberration of the lenses. It was especially pronounced in the red end of the spectrum. To focus the spectrum in the range of interest and to have the correct resolution, a fine pattern having six lines per millimetre was placed at the axis of the cascade arc and the lens L_4 was moved to bring the horizontal lines in the spectrum to a sharp focus in the wavelength range of interest. For the near infra-red range of the spectrum where the eye is not sensitive, a series of spectra were photographed for different positions of the lens L_4 at an interval of 2.5 mm, and the position of the lens was marked on the optical bench at which best spatial resolution was obtained in the wavelength range of interest.

4.2 Spectrum Recording

Once the optics were set up, the cascade stack was placed between the electrodes and the image of the cascade central limiting plates was adjusted by means of lens L_4 so that it centered on the entrance slit of the spectrograph.

Electrical connections were made to the cascade limiting plates to measure the arc voltage drop and the viewing glass window was closed. The pressure vessel and the dump cylinders were evacuated to about 2 torr pressure and the entire system was

29
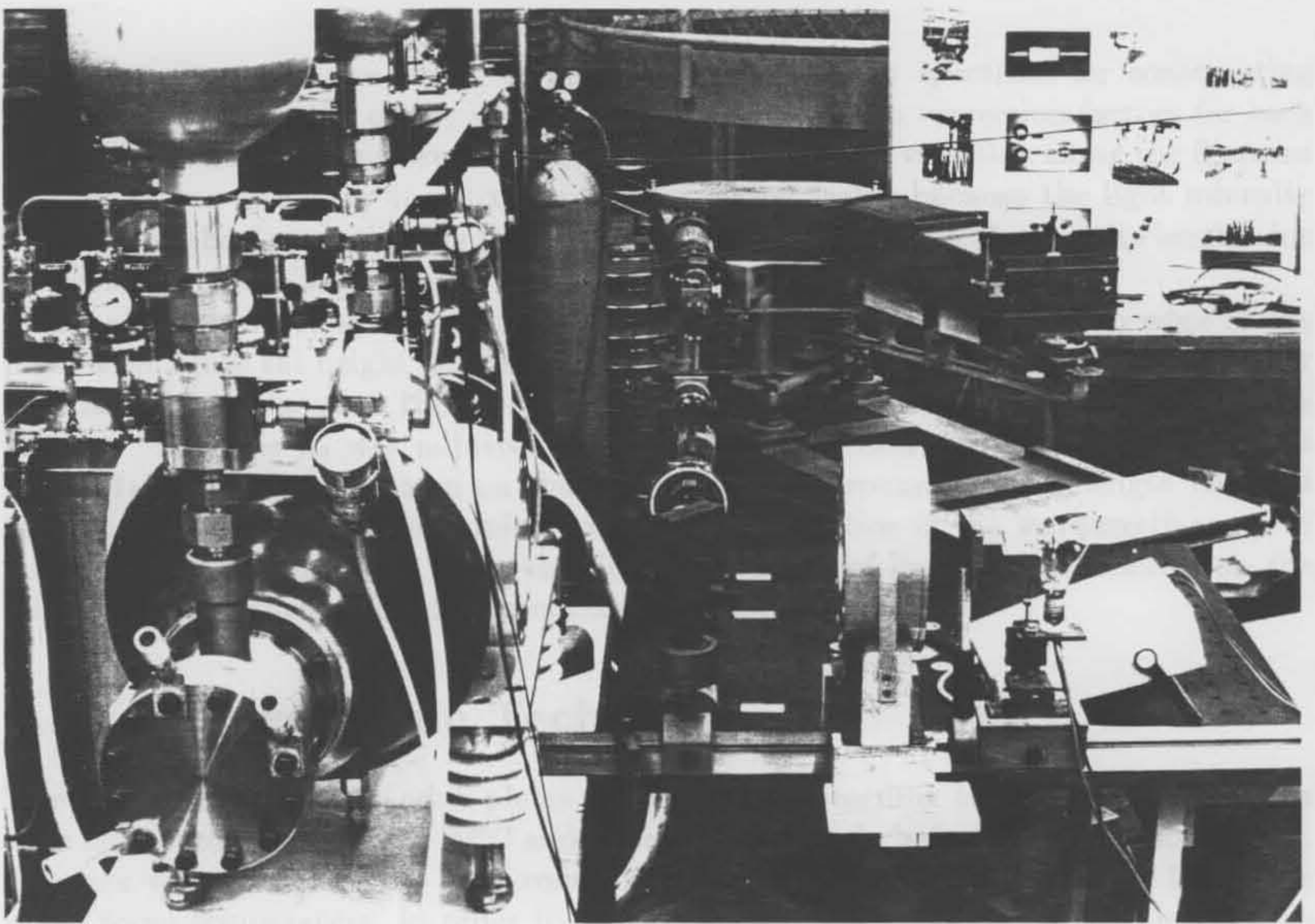
Figure 4.2: The optical set-up for imaging the cascade arc and the standard lamp exposures (pressure vessel on the left, standard lamp on the right and the optical train in the centre).

twice flushed with the test gas and then filled to the required pressure.

Six spectra were recorded on each plate and for each pressure two plates were made giving a total of twelve spectra between 50 and 550 amperes. Besides the arc spectra a reference spectrum from a Hg–Cd lamp was recorded on each plate. This was used to identify the lines. A He–Ne laser line was also recorded on each spectrum, to provide a reference point from which the position of all the test arc spectrum lines could be measured.

To record the intensity reference spectrum the mirror was rotated by ninety degrees to position M_2, shown in figures 4.1 and 4.2. This allowed the light from the horn lamp to fall on to the entrance slit . A spare glass window was placed in front of the horn lamp to compensate for the light absorbed by the pressure vessel's window. The horn lamp was run at a fixed current of 12.251 amperes which was set precisely by measuring the voltage across a standard shunt resistance. For the lamp E-242 the shunt voltage drop was 0.03104 volts. Before taking an exposure, the lamp was run at the fixed current for about 10 minutes in order to stabilize the filament temperature . The filament of the lamp was adjusted again to ensure that it was vertical and its image was parallel to the slit. By fine horizontal movement given to the lamp, the filament was focused such that the entrance slit was in its centre.

The attenuator wheel was then placed at the I_2 position, shown in figures 4.1 and 4.2, and run at a speed of 3600 rpm. By viewing the spectrum through the eye piece at the exit plane of the spectrograph, the wheel was adjusted in order to bring the stepped intensity calibration spectrum to a sharp focus in the wavelength range of interest. The photographic plate was placed in the camera back and was exposed at two different

positions. One with the wheel, to get a stepped intensity spectrum for constructing the H–D curve and the other, without the wheel, to obtain correction factors for each step of the calibration spectrum caused by the temperature variation along the filament length. It was necessary to calculate this correction factor because the light intensity radiated by the filament of the horn lamp changed by up to 1.5 % along its length due to the temperature variation.

Finally, one more spectrum of a fine pattern was recorded at the top edge of the plate with 3-mm slit height and 500-micron slit width. The pattern, having six lines per millimetre, was placed at the cascade arc axis and was illuminated by a bright source of light. The lens L_4 was adjusted, as described in section 4.1, to sharply focus the horizontal lines of the pattern on the spectrum plate around the wavelength range of interest. This helped in maintaining good spatial resolution in the wavelength range of interest. At the same time, by measuring the number of lines per millimetere on the plate, the arc diameter could be accurately calculated.

4.3 Photographic Technique

The I-N and III-F type Kodak plates were used for recording the spectra. The plates were kept in a freezer below -20°C and were taken out only before they were to be used. The box was opened in the dark room after the temperature of the plates had come up to room temperature, in order to avoid moisture condensation on the plates. The plate was then transferred to the camera-back plate-holder and was pushed to the left and then down so that it fitted perfectly to the bottom left hand corner of the plate holder. This was necessary as the size varied slightly from plate to plate. To have the spectra parallel to one side of the plate helped in orienting the plate on the plate scanner holder for proper scanning. The plate holder containing the plate was placed in the camera back of the spectrograph and left for half an hour to allow the plate to come to the laboratory temperature. The plate was then exposed to record various spectra. To allow for the latent images of all the spectra to come to the same state, as described in appendix B, the plate was developed after four or five hours from the last spectrum recording. The plate development procedure had a considerable influence on the quality of recorded spectrum. Therefore rigid control was exercised in four areas while developing the plates.

1. Type and quality of developer

   The developer D-19 was used throughout all the development work. Fresh stocks of solution were made following the manufacturer's instructions precisely. After developing a plate the unused left-over solution was discarded.

2. Development temperature

   The dark room temperature was maintained at 22°C. At this room temperature the developer stabilized at around 20°C after it was allowed to stand in the developing tray for 15 or 20 minutes. This procedure was followed in the absence of a water bath for controlling the temperature of the developer. A slight fluctuation in developer temperature did not affect the intensity measurements because each plate was individually calibrated. Therefore, any variation between different plates did not matter.

31

3. Development time

   The development time of two minutes was selected for the entire work according to the Kodak hand book [1] as the soft development was better suited for Abel inversion process.

4. Mode and degree of agitation

   The way in which the developer or the plate is agitated and the degree to which it is agitated is very important in quantitative spectrography. There are various ways by which it can be performed. Tray rocking, plate shaking, mechanically rotating rocker, gaseous-burst and brushing are some of the usual techniques [31]. Rocking techniques are not satisfactory due to Aberhard's effect described in appendix B. Gaseous-burst for which usually nitrogen is used is better than rocking but the bubbles leave track marks on the plate emulsion. Due to the above mentioned reasons, a brushing technique was used for the development of the plates. This is the only method which effectively replenishes the developer layer close to the plate emulsion to reduce Aberhard's effect.

The plates were brushed softly along their entire length in both directions and then in the perpendicular direction. The process was repeated after every fifteen seconds as continuous brushing caused damage to the emulsion. A very soft camel hair brush was used as a hard brush also caused damage to the emulsion of the plate.

After the development was complete, plates were quickly removed from the developer and placed in a stop bath for one minute. The plates were then placed in the fixer for twenty minutes and rocked gently from time to time. The plates were then thoroughly washed in cold water for a few minutes. This entire procedure of development was done in complete darkness. After washing the plates, the light was turned on and the plates were placed in the photoflow solution in order to wash the surface. This helped in removing the marks left by the water droplets. The plates were then left to dry at room temperature for a couple of hours.

4.4 Arc Voltage and Current Measurement

There are two functions of the electrical system; one, to provide power for initiating and running of the cascade arc; two, to measure the arc voltage and the current. Electrical connections were made, as described in section 3.3. The working of the entire system was tested by substituting a resistor for the arc. This was done to safeguard the ignitor system and the cascade stack against accidental damage due to malfunctioning. After removing all the snags from the system, the resistance was replaced by the cascade arc assembly. Then at least one more trial run was conducted, without recording the spectrum, in order to check the working of the ignitor and the shutter.

The arcing current was supplied by a high-current capacitor bank. By selecting an appropriate value of resistor, R and current supply voltage, the decay of current during the arcing was limited to five percent. The capacitor bank was charged to a pre-calculated voltage. The make switch, MS, was closed to apply the voltage across the electrodes; at the same time a Tektronix-465 oscilloscope sent a gate-pulse through an optical link to the ignitor triggering unit which activated the ignitor. The ignitor rod moved from the anode to the cathode drawing a small pilot arc of about ten amperes limited by resistors, R_g and R. At atmospheric pressure, the pilot arc of ten amperes was sustained easily for about thirty milliseconds. The main arc was ignited after twenty

five milliseconds. But in SF_6 at higher pressures of 4 and 8 atmospheres pressure the pilot arcing current had to be doubled to maintain the arcing for thirty milliseconds duration. A period of twenty five milliseconds was necessary to allow the ignitor rod to withdraw fully from the anode to the cathode. When the main arc was ignited the rod was safely inside the hollow cathode, to avoid damage.

The first spark gap, SG_1 was fired at time, B, by sending a pulse from the screened room through an optical link to the spark-gap triggering mechanism, shown in figure 3.5. This short circuited the ignitor resistance, R_g, reducing the circuit resistance to R. The value of R varied from 60 ohms for small current (50 amperes) to 10 Ω for the highest current (550 amperes). Finally, a gate-pulse from the Tektronix-465 oscilloscope triggered the second spark gap, SG_2 after a time delay depending upon the selected time of exposure for the spectrum recording. This shorted the cascade arc, chopping the arcing current to zero at time E; figure 3.7. At each current level, a suitable value of resistance R was selected, so that the decay of current between time C and D was about five percent. C and D being the shutter opening and closing times respectively. Average value of the current was used for the E–I characteristic.

Two Nicolet digital oscilloscopes were used for the measurement of the arc current, voltage and the spectrum exposure time. The first Nicolet measured the voltages at the two cascade stack plates, acting as probes in contact with the plasma. The two plates were 2.65 cm apart and were symmetrically placed about the centre of the stack. Both the Nicolets were triggered by a pulse from the gate A of the Tektronix-465 oscilloscope as the make switch, MS, closed. This provided continuous measurement of the arc voltage at two points along the arc length. To determine the arc field, the average voltage was calculated between time C and D, as shown in figure 3.6, and was divided by the distance between the two plates.

The second Nicolet recorded arc current by measuring voltage output of the current shunt in one channel and the exposure time of the spectrum in the other channel by recording the signal from a photomultiplier. The current shunt was connected as shown in figure 3.5, and was rated to give a voltage output of 190 amperes per volt. By measuring the voltage across this shunt, a complete record of the arcing current from the time the make switch was closed was obtained.

To monitor the shutter performance, the reflected light from the spectrograph prism was collected by an optic fibre, which was then measured using a photomultiplier. The output of the photomultiplier was recorded on channel B of the second Nicolet. The shutter opened at time C when a pulse from a pulse delay generator triggered a pulse of ten volts of duration T_s. The delay pulse was adjusted so that the shutter opened seven milliseconds after the main arcing current was established. This allowed sufficient time for the arc to reach a steady state, because theoretical calculations have shown that the arc stabilizes in 1 to 2 ms. The shutter was kept open as long as the ten-volt pulse lasted. The Uniblitz shutter took two milliseconds to open and four milliseconds to close, due to inertia. Any variation in the shutter opening did not cause any error since for each shot, the light input to the spectrograph was measured. The time at which the shutter closed was so adjusted that it was two or three milliseconds before the arc collapsed at time E. Therefore, the exposure time, T_s, was kept within the steady state arcing period.

For the intensity reference spectrum taken from the standard horn lamp, a Copal-number-1 shutter, mounted on the spectrograph, was used. Its opening duration was also measured by the Nicolet in the same way as for the Uniblitz shutter. The ratio of the two exposure times for the arc spectrum and for the reference spectrum gave

the value of the factor by which the standard lamp intensity was multiplied. The slit width for the arc spectrum was kept between 30 and 50 microns and for the reference spectrum, 750 microns. The ratio of these two slit widths gave the value of the second factor by which standard lamp intensity was to be multiplied for calculating the line intensities from the H–D curve.

4.5 Data Acquisition by the Plate Scanner

The plate scanner is an automated micro-densitometer working fully under the control of a HP-9836 computer. The hardware was designed by Armstrong [4] and also the software for the data acquisition. It can collect data at the rate of fifteen hundred bits per minute. The data are in the form of voltage output of a logarithmic amplifier proportioned to the transmittance of the spectrum plate being scanned. The full scale reading of 255 counts corresponded to the maximum transmittance 100 %.

The current signal received from the photo-cell of the densitometer was amplified by a current amplifier and fed to the operational amplifier of gain 100. The output of this was fed to the 757N log-ratio amplifier. The log output was digitised by an A to D converter and stored by the HP-9836 on the disks.

By following a standard procedure of adjustments, the output of the log amplifier was set to give the minimum output of nine counts for the maximum photographic density. To achieve this, the dc offset of the operational amplifier was set at zero both for linear and log output. Then the dc offset of the log-ratio amplifier was also set at zero.

The log amplifier was then set to give the same ratio output for low as well as high signals. This ensured that the output of the log amplifier was 4.15 volts for all of the four decades. Therefore, the percentage error was limited to ±0.5 % of full scale for the high density as well as for the low density of the plate.

The plate was placed on the scanner carriage, emulsion facing upwards and pressed down firmly by two magnetic strips along both the sides, as shown in figure 3.11. Two pairs of spring loaded pins on two sides and two fixed stops on the opposite sides provided support for the plate so that it did not slip side-ways. Next the plate was levelled and brought into the focus over the entire spectrum length by the help of two levelling screws at the bottom of the carriage. At the same time the plate was rotated by a shifting mechanism about a pivot in order to make the plate parallel to the travel of the carriage.

The plate was first scanned to identify the lines of the spectrum. The scanner carriage was positioned so that the image of the He–Ne laser reference line was centered on the entrance slit of the scanner. Both the stepping motors were then locked in this position and brought under the control of the HP-9836 computer. The data acquisitioning programme was run and information such as the distance of X-shift, Y-shift, number of points to be scanned, fine scan or coarse scan, were entered from the key board. The computer then took over the scanner and scanned the spectrum on the plate from one end to the other and collected 8192 samples of information in six minutes. The data were then stored on floppy disk for analysis.

Once the lines were identified, a selection was made for one, two or three lines which were well isolated and were optically thin. These lines were then scanned in a particular fashion so as to collect line profiles at various positions of the arc diameter. Each scan in the X-direction consisted of sixty samples of data points each spaced by ten microns.

A total number of a hundred scans were used to cover the entire line and each scan

was spaced by a distance of seventy microns in the Y-direction. This picked up six thousand samples of information (60x100 mesh) from the area covering the spectrum line. Information about each of the hundred scans was first entered into the computer, for example, X-shift, and Y-shift, number of points to be scanned. The scanner was then locked into position at the He-Ne laser reference line from which all the X-shifts and the Y-shifts were measured to locate the line to be scanned. The computer then scanned the line and stored all the data information on the floppy disc for data reduction work.

For the absolute intensity calculation, two more scans were done. One, for the standard horn lamp intensity reference spectrum and two for the filament temperature variation spectrum.

Chapter 5

SOFTWARE FOR THE DATA ACQUISITION AND REDUCTION

Programme development for data acquisition and reduction has been an important part of this project. The data from the photographic plates were gathered by the scanner (a modified Carl Zeiss Jena rapid photometer) described in section 4.5 . At present, data collection from the plates is done at a much faster speed as compared to the previous manual process. The software for the data acquisition developed by Armstrong has made it possible to make substantial progress in the spectrographic work. Typically it took six minutes to scan and store the entire length (16 cm) of the spectrum (400 to 800 nm) and 2.5 minutes to identify and compute the wavelengths and the densities of all the lines. Whereas manually it took 5 to 6 hours to scan the spectrum and much longer to record and key in the data for the computation. It was almost an impossible task to do manual scanning of the entire line profile.

Data reduction programmes for the entire computational work have been developed by the author. It consists of line identification, relative intensity calculations, temperature profiles and transport properties evaluations. In this section, a brief description of the working of these programmes is given.

5.1   Data Acquisition Programme 'PLTSCN'

The programme 'PLTSCN' has five major sections. Input (data), disking, playback, output and plot. This programme is capable of controlling the plate scanner for the collection of the data and storing it on floppy disks. The data can then be displayed on the Nicolet digital oscilloscope or plotted.

1. Input

   This section controls the plate scanner movements according to the information keyed in to the computer. The scanner can be made to do both the coarse and the fine scanning, for which the step sizes are 20 and 10 microns respectively.

2. Disk

   This part of the programme stores the collected data after checking its size and the format.

36

3. Playback

This enables the stored data to be called back in to the computer memory for display and analysis by other programmes.

4. Output

The collected data is prepared by this section for the display on the Nicolet screen. For this purpose the raw data are converted into a special format which has scaling bits attached to the data so that it can be displayed on the Nicolet screen.

5. Plot

This is the largest and the most powerful section of the programme. Any portion of the collected data can be plotted on the monitor screen or on the plotter to any specified enlargement size. It is also capable of printing the data listing and the slope (derivative) of the stored waveform. In the normal mode it plots the entire data on A3 or A4 paper size. In the expansion mode it plots a specified section of the data to a desired enlargement size.

5.2 Data Reduction Programmes

The entire calculation of this work was done on the Hewlett Packard computer (HP-9836). There were a number of programmes written for this purpose in Hewlett Packard language (HPL). These programmes are listed in the appendix D. Each programme performed a special operation on the collected data to calculate the required parameters. In this section, the main features of these programmes are described.

5.2.1 Spectrum Line Identification

1. Continuum

All the points of the scanned spectrum data are screened and continuum points are isolated. A polynomial is fitted to these points to assess the continuum level at each point in the spectrum (lines 21 – 43 in appendix D).

2. Line positions

The entire data are once again screened to locate possible line positions. From among these, only those points which are above a certain density level from the background continuum are isolated as potentially useful line positions (lines 44 – 55).

3. Wavelength calculation

From the three known wavelengths of Hg–Cd lines and their positions measured from the He–Ne reference as the unknown spectrum lines, the values of three constants are calculated. Using Hartmann's equation A.1, given in appendix A, the wavelengths of all the isolated points and their relative intensities are evaluated (lines 56 - 77).

4. Subroutine 'CONST'

This subroutine calculates the three parameters λ_0, d_0 and c of the Hartmann's equation A.1 from the given input of three line positions and their wavelengths.

5.2.2 Temperature Profiles

Temperatures have been calculated by three different methods.

1. Absolute line intensity

2. Absolute continuum intensity

3. H_α line profile

Absolute Line Intensity Programme 'TEMPFI'

There are different versions of this programme such as, 'TEMPFI', 'TEMPNII', 'TEM-PARI' etc. The suffix to TEMP indicates the spectrum lines by which the programme calculates temperature profiles. The basic structure of these programmes is the same except for some spectroscopic data. As an example here, one of them, 'TEMPFI', listed in appendix D, is described.

1. Collect

   The first section of the programme subroutine 'Collect' is common to all the programmes. Its function is to collect all the files containing the data from the eight scans of the intensity reference spectrum (lines 3 - 28). The short section following the subroutine, plays back in sequence a specified number of files which are to be reduced (lines 32 - 36).

2. Data-set

   A set of data specifying line position, dispersion curve constants, wavelength, statistical weight, transition probability, upper energy level of the excited states etc., are built into the programme (lines 40 - 69)

3. Continua

   In this part, the continuum density on either side of a line is calculated. This is stored in the variable r80 and is subtracted from the calculated line density (lines 72 - 88)

4. Line density

   The profile of the line is isolated from the continuum and its density is stored in an array A (lines 90 - 99)

5. H–D curve

   This section calculates densities of the eight steps of the intensity reference spectrum and stores it in an array R. These values are corrected for the filament temperature variation along its length. The normalizing factor stored in an array Q, is calculated using the evaluated densities at different positions, from the standard lamp exposure without the attenuation wheel (lines 101 - 131).

   From the spectral radiance data (array M) of the standard lamp, the radiative power is calculated at a line wave length, which enables the programme to calculate the intensity received by the plate at each of the eight attenuated intensity steps and it is stored in an array Q. The H–D curve is evaluated by fitting a fifth order polynomial to the previously calculated densities and corresponding values of the eight intensity steps (lines 132 - 172).

38

6. Integrated line intensity

   Using the H–D curve, which is in the form of a set of polynomial constants, (array Z), line densities are converted into intensities and integrated over the entire line profile. This process is repeated for the line profile recorded at different positions of the arc diameter. These integrated line intensities are stored in an array F[4,*] (lines 181 - 188)

   Spatially resolved line intensities are converted into radially distributed intensities (array F[5,*]) by the subroutine 'Abel' described later in this section.

7. Temperature - Intensity (T–I) curve

   This section of the programme calculates the intensity radiated by a line at a temperature from the known plasma composition. For the temperature range of 5,000 to 30,000K, with an increment step of 100K, particle density and lowering of the ionization potential is determined by the subroutine 'TABD'. And subroutine 'TABP' evaluates the value of the partition function. Spatially distributed intensities of a line are calculated from the known particle density, partition function and other spectroscopic data. These calculated intensities are stored in an array T (lines 206 - 234)

8. Temperature profile

   This section converts the measured line intensities into temperatures using the calculated T–I curve. It is performed in two different ways. The intensity profile is first of all tested for an off-axis maximum. If the test result is true, the intensities are normalized with the off-axis maximum intensity and stored in array F[5,*]. (lines 235 - 262)

   If the test does not find an off-axis maximum, then the measured intensities are compared with the calculated intensities and the corresponding temperature is calculated using the T–I curve (lines 264 - 275). In the case of an off-axis maximum, the normalized measured intensities are compared with the normalized calculated intensities on both sides of the normal temperature at which intensity is a maximum. Calculated temperature profile is stored in array F[6,*] (lines 278 - 299). The programme then loads another file from the disk into the computer memory, containing data from a different spectrum, and calculates the temperature profile. Each temperature profile is centered and stored in blocks in array F[1,*], and are finally stored in a separate file on the disk, (lines 300 - 306).

9. Subroutine 'TABD'

   This contains particle density data of plasma from 5,000 to 30,000K in mole fractions, calculated by the NASA programme as modified by Kovitya [25,40]. It evaluates the population density of all the species, at a given temperature, in particles per cubic meter (lines 325 - 389).

10. Subroutine 'TABP'

    This contains the partition function table as a function of temperature and lowering of the ionization potential. It evaluates the partition function at a temperature and at a calculated lowering of the ionization potential (lines 391 - 453)

11. Subroutine 'POLYFIT'

This fits a polynomial of a specified order to a set of data points, using the least squares error method, and returns the polynomial constants in an array Z (lines 456 - 476).

12. Subroutine 'ABEL'

This subroutine converts the lateral intensities of a line into radially distributed line intensities. The subroutine prepares the lateral intensity profile of the line for Abel inversion. It balances the number of points on each side of the maximum and then averages the intensity on either side of the centre. (lines 477 - 535)

This programme is based upon inversion of the Abel integral by means of the orthogonal polynomial developed by Minerbo and Levy [46]. It was adapted for the HP-9836 from a programme written by Schmidt-Harms for the VAX-11/780. The lateral line intensities $K(x)$ across the cylindrical section of the arc are sampled discretely at $n+1$ points $X(n)$, such that $X(0) = 0$ and $X(n) = R$, where R is the arc radius.

Using the recurrence relation from the theory of linear spaces, a triangular family of polynomials of mth order is erected over an arbitrary net. By an appropriate change of variables each polynomial is explicitly inverted. Using these properties of the polynomials $P(m)$, a unique least squares decomposition of $K(n)$ into the set $P(m)$ is followed by an inversion yielding the least squares fit to the radial intensity distribution $E(r)$. This entire process is accomplished by a sequence of matrix multiplications. For a polynomial fit of degree K, the radial intensity distribution is given by the inversion equation $-E = N \times K$. Where $K(n)$ is the lateral intensity distribution and N is the $(n+1) \times (n+1)$ transform matrix given by $-N = U \times rmC \times S$. The matrices U, C and S are separately evaluated.

13. Matrices U, C and S

A uniform net for interval (0,R) is set up. Using the recurrence relation, and by changing the variable from $R(n)$ to $O(n)$, the matrix U is evaluated. Another change of variables is performed from $X(n)$ to $V(n)$ and values of alpha and beta are calculated yielding matrix C, column by column. The first two rows are first assigned, then recursively the 0th column of S is calculated. Using the full recurrence relation, columns 1 to K are calculated (lines 538 - 626).

14. Transform matrix N

From the calculated matrices U, C and S, the transform matrix is evaluated by a sequence of multiplications $-N = U \times C \times S$. Radial distribution of the intensity is determined by simply multiplying the column matrix K with the transform matrix N (lines 627 - 642)

Absolute Continuum Intensity Programme 'TEMPC'

There are only minor differences between this and the absolute line intensity programme. These are described as follows.

1. Integrated continuum intensity

To calculate density of the continuum at a point, an average of ten points on either side is taken to eliminate the effect of noise. These continuum densities at different points along the arc diameter are converted into lateral intensities using

the H–D curve; these are then transformed by Abel inversion to give the radial distribution of intensities (lines 40 - 86).

For constructing the intensity versus temperature (T–I) curve, electron density is calculated using the subroutine 'Tabd'. The intensity at a pressure as a function of temperature is calculated by equation 2.6, section 2.1.1 (lines 203 - 247). The rest of the temperature calculation procedure is the same as that for the programme 'TEMPFI'.

H_α Line Profile Programme 'STARK'

This programme calculates electron density of the arc from the measured full half width of the Stark broadened H_α line profile. The first part of the programme up to line 60 is similar to previous programmes.

1. Line profile

   Data of the line profile are isolated from the background continuum and an approximate half-width point is located and stored in the variable r130. Its value is updated until the centre of the line is reached. This helps in specifying the position from which the spatially resolved lateral line intensities are to be unfolded by the Abel transform to obtain radially distributed intensities, and stored in array T (lines 63 - 169). All the intensity points from each line profile related to the same wave length are collected together to form spatially resolved lateral intensity profiles in array F[4,*].

2. Abel inverted line profile

   Spatially resolved lateral intensity profiles are then converted into radially distributed intensities and stored in array F[5,*] (lines 170 - 182). Data are regrouped and rewritten over the un-transformed line profiles in array T (lines 183 to 192). Finally, after data smoothing, these Abel inverted line profiles yield full half widths at each radial position of the arc. The electron density is calculated from the N_e - $\Delta\lambda_s$ curves (lines 193 - 232).

3. Temperature calculation

   The temperature versus electron density curve has been prepared from known plasma composition tables 'Tabd' and arc temperatures are calculated by comparing the measured electron densities (lines 235 - 255).

5.2.3   Transport Properties

There were three programmes to calculate transport properties. Programme 'SIGMA' was used to calculate the electrical conductivity, using E–I characteristics and temperature profiles. The thermal conductivity calculations were done in two parts. In the first part, form factors were calculated and in the second the thermal conductivity was evaluated using form factors and the electrical power input as a function of the arc centre temperature, (P_e - T_0), curves and radiated power from the arc as a function of arc centre temperature, (P_u - T_0), curves. The net radiation emission estimates were made using temperature profiles and calculated values of the electrical and thermal conductivities and power input.

Programme 'SIGMA'

1. Input data

   Input data to the programme is a set of three selected temperature profiles and three corresponding values of arc current, electric field and arc radius, and the initial trial values of the constants A, B and C (lines 1 - 16).

2. Parameters A, B and C

   This section calculates the constants A, B and C iteratively, using the Gauss-Seidel numerical technique, as described in section 2.3.1 (lines 18 - 43).

3. Subroutine 'Integrand'

   This subroutine calculates the value of the integrand, which is the estimated value of the arc conductance calculated from the measured temperature profiles and updated values of the parameters A, B and C (lines 45 - 61). The printout subroutine calculates electrical conductivities from the updated values of parameters A, B and C and (lines 65 - 70).

Programme 'THERMAL'

Programmes 'THERMAL' and 'NETRAD' work together, since the thermal conductivities are recalculated from the estimates of the radiation losses. At the same time, radiation losses are calculated from the known values of thermal conductivities. Therefore, in the programme listings given in the appendix D, both programmes have been listed together.

An approximate estimate of the thermal conductivity is made by differentiating the P_e - T_0 curve. From these values of k, thermal power loss by conduction is calculated at each radial position and stored in array X. The electrical power input at each radial position is calculated from the known electrical conductivities and stored in array B. The difference of the two yields the radiation loss at a radial position. Therefore, from the known electrical conductivity and net radiation emission distribution, the two form factors F_e and F_u are calculated (lines 454 - 520). At the same time the value of the total radiated power P_u from the arc is also calculated.

From these calculated values of P_u as a function of the arc centre temperature and measured values of P_e, the thermal conductivity is calculated. First, a curve is fitted to the known values of P_e and P_u and the slope is calculated at different radial positions for both the curves. Since both F_e and F_u are known, thermal condutivity is now calculated, using equation 2.38.

Programme 'NETRAD'

The first part of the programme from line 1 to 454 is the temperature profile calculation as described in section 5.2.2.

Solving the energy balance equation

A suitable polynomial is fitted to the measured temperature profile and the number of points is increased by five times for better accuracy in differentiating temperature profile, and stored in array F[1,*]. (lines 457 - 469). The thermal loss by conduction is calculated by evaluating the term -

$$k \left[\frac{d^2T}{dr^2} + \frac{dT}{r \, dr} \right]. \tag{5.1}$$

Since large errors can be introduced in the double differentiation of the temperature profile, both forward and backward differences are taken giving at i^{th} radial position -

$$\frac{d^2T}{dr^2} = \frac{T^{i+1} - 2T^i + T^{i-1}}{\Delta r^2}. \tag{5.2}$$

The calculated value of thermal conduction loss is stored in array X.

Electrical power input at each radial position is calculated from the known electrical field and the electrical conductivity at each radial position and stored in array B.

Difference of the two gives the value of the net radiation at each radial position and is stored in an array V (lines 470 - 481). Since the temperature is known at each radial position, the net radiation is related with the temperature to obtain $u(T)$.

Chapter 6

RESULTS

6.1 Nitrogen, Argon and SF$_6$ Spectra

Emission spectra of nitrogen, argon and sulfur hexafluoride (SF$_6$) were recorded on Kodak III-F and I-N type photographic plates, shown in figures 6.1 to 6.6. All the lines of a spectrum were identified using Hartmann's equation A.1 described in section A.3 of appendix A.

For the purpose of evaluating the temperature of nitrogen and argon arcs, the well isolated and optically thin N$_{II}$ line at 504.5 nm and Ar$_I$ line at 696.5 nm were selected. The nitrogen and argon spectra are shown in figures 6.1, 6.2 and figures 6.3, 6.4 respectively.

The SF$_6$ spectrum, shown in figures 6.5, 6.6, was of special interest in these experiments, mainly for its practical application to gas blast switching arcs, and particularly because very little experimental work has been done in this area. The spectrum could be divided into two distinct regions. One, the 400 to 550 nm range, consisted of about forty singly ionised S$_{II}$ lines with a single atomic S$_I$ line at 469.5 nm. The other, the 600 to 800 nm range, was populated by about twenty five atomic F$_I$ lines. There was only one exception to this distinct division between sulfur and fluorine lines. At arc temperatures above 20,000K the F$_{II}$ line at 444.7 nm appeared in the spectrum range otherwise exclusively populated by S$_{II}$ lines.

Three optically thin and well isolated F$_I$ lines at 641.4, 670.8 and 720.2 nm, and one S$_{II}$ line at 545.4 nm, were selected for the measurement of SF$_6$ plasma temperature. At higher pressures, the continuum at 600.4 nm and H$_\alpha$ line profile were also used for measuring the arc temperature. This was done in order to check the absolute line intensity measurements for self-absorption at higher pressures.

6.1.1 SF$_6$ Emission Data Calculations (Continuum Coefficient and Transition Probability)

These calculations have been done to provide a set of useful data in the form of continuum coefficients of emission, C(ν), and transition probabilities, A, of a few optically thin lines. This provided additional information for temperature measurements and an in-house data standard which could be used in further investigation of SF$_6$ arcs.

Continuum Coefficients of Emission

At five selected wavelengths continuum coefficients were calculated. Selection of the wavelengths at which continuum was to be measured depended upon two things. One

No.	Wavelength (nm)	$C(\nu)$ W-m^{-3}-K$^{-1/2}$-st^{-1}	Error %
1	472.3	6.34×10^{-42}	± 39
2	573.3	13.33×10^{-42}	± 13
3	600.4	16.50×10^{-42}	± 11
4	621.0	6.92×10^{-42}	± 52
5	666.6	10.10×10^{-42}	± 22

Table 6.1: Continuum coefficients of emission $C(\nu)$ at selected wavelengths in SF$_6$.

is that there should be no interference from the neighbouring lines, especially at higher pressures when the lines get broadened. The other is that the intensity of the continuum should be sufficient so that it could be measured accurately. Based upon these considerations five points were selected. These were located at 472.3, 573.3, 600.4, 621.0 and 666.6 nm wavelengths. The width of the continuum band ranged from 5 to 9 nm.

To calculate the coefficient, $C(\nu)$, at different wavelengths, the radial distribution of the continuum radiation emission was measured at the required wavelength by scanning the spectrum in the same way as was done for the line intensity measurements. The radial distribution of emission was converted into temperature dependent radiation emission, using the measured temperature profiles. Plasma composition was calculated by the updated NASA programme [25,40]. An average value of the coefficient $C(\nu)$, was evaluated from these known parameters for temperatures ranging from 16,000 to 22,500K. The results are presented in table 6.1.

Using these values of the continuum emission coefficients, the radiation emission intensity was calculated at 4 and 8 atmospheres pressure from the known plasma composition. As a cross check, these calculated values were compared with the measured continuum intensities at these pressures. Results are shown in figures 6.7 and 6.8.

Transition Probabilities

Transition probabilities of six optically thin lines have been calculated. Selected lines were unionised F$_I$ lines at 720.2, 670.8, 641.4 and 623.9 nm, one S$_I$ line at 469.5, and one S$_{II}$ line at 545.4 nm.

Transition probabilities have been calculated using Olsen's method [53,52], as described in section 2.4. The value of F_λ, was calculated from the known plasma composition, which included the demixing effect as given by Frie [22]. I_{max} was determined from the measured radial distribution of intensity for the line under consideration where the normal temperature has been reached. The ratio of I_{max} and F_{max} gave the transition probability of the particular line. This method was used for the evaluation of transition probability for all the selected F$_I$, S$_I$ and S$_{II}$ lines, because the normal temperature at which intensity is maximum has been reached for all the above mentioned species of fluorine and sulfur. Results are presented in table 6.2.

No.	Transition	Wavelength (nm)	A_{nm} (10^{-8} sec^{-1})			Error %
			(A)	(B)	(C)	
1	$3s^2P$ - $3p^2P^0$	720.2	.055	.050	.072	±35
2	$3s^4P$ - $3p^4D^0$	670.8	.016	.006	.024	±37
3	$3s^4P$ - $3p^4S^0$	641.4	.065	.054	.090	±38
4	$3s^4P$ - $3p^4S^0$	623.9	.110	.129	.290	±34
5	$4s^5S^0$ - $5p^5P$	469.5	.0062	.0067	.0074	±39
6	$4s^4P$ - $4p^4D^0$	545.4	.740	.710	.780	±32

(A)   This experiment
(B)   Schulz-Gulde
(C)   Wiese

Table 6.2: Transition probabilities of F_I, S_I and S_{II} lines.

6.2   Nitrogen and Argon Arc Temperature Profiles

Nitrogen Arcs

Temperature measurements of nitrogen arcs were primarily carried out to compare the present results with those of Maecker [45,20], which are well proven standard results. This confirmed the experimental procedures and gave confidence for further spectroscopic diagnostic work on Ar and SF$_6$ arcs. The nitrogen arc of 5-mm diameter was run from 175.7 to 370.6 amperes current at atmospheric pressure. The spatial distribution of absolute intensity for the N$_{II}$ line at 504.5 nm, measured from the side-on arc was converted into a radial distribution using the Abel transform. The radial distribution was then compared with the calculated intensity - temperature curves, shown in figure 6.9, to obtain the temperature profile of the arc. The line intensity as a function of temperature was calculated from the nitrogen plasma composition, computed by a programme originally developed at NASA [25], and is given in table C.1. The NASA programme has been modified by Kovitya [40] to calculate particle densities for the higher temperature range of up to 30,000K. The programme uses minimisation of the Gibb's free energy of the chemical mixture. In calculating the partition function the Debye shielding effect was taken into account. Maximum lowering of the ionisation potential was found to be 0.02 eV. The maximum radiated power was 4.59 W/cc, at 29,300 K, as shown in figure 6.9. Nitrogen arc temperature profiles are shown in figure 6.10. The results agree well with those of Maecker [45,20], although profiles do not extend to the same limits of radius as given by Maecker. This happened due to the lower exposure time used for recording the spectra because of which spectral lines did not extend to the full outer limit of the arc boundary.

Argon Arcs

The wall stabilised 5-mm diameter argon arcs have been investigated at 1 and 8 atmospheres pressure. High-pressure work on argon was done especially, so that some of the present high-pressure measurements could be compared with the other experimental work done at high pressure [28]. Various Ar$_I$ atomic lines and continua have been used for argon plasma temperature measurement. The most commonly used Ar$_I$ lines are at 425.9, 641.6, 693.2, 696.5, 751.5 and 763.5 nm [30,31,32]. Continua at 553.5,

782.5, 482.5, 428.8 nm have also been used [52,66], for measuring temperatures of up to 20,000 K. In this experiment, the Ar_I line at 696.5 nm has been used for temperature measurements, due to its low self absorption. Intensity-temperature graphs, shown in figure 6.11, were constructed using plasma composition at 1 and 8 atmospheres pressure, as computed by the modified NASA programme [25,40], and are given in tables C.2 and C.3. Debye's shielding effect was also considered in calculating partition functions. Tables C.2 and C.3 show the lowering of ionisation potential at different temperatures. Figure 6.11 shows intensity versus temperature graphs at 1 and 8 atmospheres pressure. Figure 6.12 shows temperature profiles of argon arcs for currents of up to 485 amperes at atmospheric pressure and figure 6.13 shows the temperature profiles of argon arcs for currents of up to 438 amperes at 8 atmospheres pressure.

E–I Characteristics of Nitrogen and Argon Arcs

The E–I characteristic of nitrogen at 1 atmosphere pressure, shown in figure 6.14, compared well with Kopainsky and Maecker [20]. The E–I characteristics of argon at 1 and 8 atmospheres pressure are shown in figure 6.15. The characteristic at 1 atmosphere pressure compared well with Maecker [45] and at 8 atmospheres the characteristic was in good agreement with interpolated values derived from the high-pressure experimental results of Bauder [8]. The arc centre temperature as a function of electrical power input for argon at 1 and 8 atmospheres pressure is shown in figure 6.16.

6.3 Transport Properties of Argon at 1 and 8 Atmospheres Pressure

Transport properties of argon were determined for two important reasons. One, to test the validity of the calculation methods adopted in this experiment for the evaluation of transport properties described in section 2.3. Two, because the enormous amount of work done on argon provided well established results with which confident comparison could be made.

Electrical Conductivity of Argon at 1 and 8 Atmospheres Pressure

Electrical conductivity calculations were based upon Devoto and Mukherjee's method [16] of 'trial function', described in section 2.3.1. At atmospheric pressure, the initial values for the constants A, B and C taken from the literature [16], were 7.00×10^{12}, 2.20 and 6.00×10^4 respectively. Final values of the constants at atmospheric pressure were taken as the initial values for 8 atmospheres pressure calculations. Initial and final values of the constants A, B and C, and calculated and measured values of arc conductances are listed in table 6.3. Figure 6.17 shows electrical conductivity of argon at 1 and 8 atmospheres pressures, as determined in this experiment and the theoretical estimates of Yos and Kovitya [73,40].

Thermal Conductivity of Argon at 1 and 8 Atmospheres Pressure

Experimental evaluation of thermal conductivity, k, as a function of temperature has been done using the 'form factor' technique [68], details of which are given in section 2.3.2.

47

Pressure (atmospheres)	Parameters A, B and C		Arc conductance		Current (amperes)	Error %
	Initial	Final	Measured (S/cm)	Calculated (S/cm)		
1	A–7.00×10^{12}	7.06×10^{12}	42.57	41.53	71	2.4
	B–2.20	2.22	85.34	84.17	312	1.4
	C–6.00×10^{4}	5.90×10^{4}	94.62	98.21	382	3.8
8	A–7.06×10^{12}	7.10×10^{12}	16.86	16.58	48	1.7
	B–2.22	2.18	45.72	45.83	190	0.2
	C–5.90×10^{4}	6.40×10^{4}	75.46	74.18	438	1.7

Table 6.3: Parameters A, B and C for argon.

Thermal conductivity of argon was calculated at 1 and 8 atmospheres pressure using the actual values of the 'form factor', calculated from the measured temperature profiles. Electrical and radiated power, P_{el} and P_u, as a function of arc centre temperature are shown in figure 6.18. Variation of 'form factor' with the arc temperature at 1 and 8 atmospheres pressure is shown in figure 6.19. Values of 'form factor' fluctuated between 0.65 and 0.5. Once P_{el}, P_u, $2\pi F_{el}$ and $2\pi F_u$ were known, the thermal conductivity could be calculated, using equation 2.38. Figure 6.20 shows thermal conductivity of argon at 1 and 8 atmospheres pressure, as measured in this experiment and the theoretical estimates of Yos and Kovitya [47,40].

Net Radiation Emission of Argon at 1 and 8 Atmospheres Pressure

In this experiment, the net emission coefficient of radiation, u, has been calculated by solving the energy balance equation 2.40, details of which are given in section 2.3.3. Figure 6.21 shows the estimated value of the net radiation emission. Experimental results were in good agreement with the theoretical predictions of Cram [14], but were at variance with the theoretical estimates of Yos [47].

6.4 SF$_6$ Temperature Profiles at 1, 4 and 8 Atmospheres Pressure

Measurements of the radial temperature distribution of wall stabilised SF$_6$ arcs have been carried out to evaluate energy transport properties. Temperature measurements were done on 3 mm and 5 mm diameter arcs. Evaluation of the transport properties was done primarily using 5 mm arc measurements, because more data were collected on 5 mm arcs. Values calculated from 3 mm arc measurements were used to provide support for the main results obtained from 5 mm arcs. Temperature measurements were crucial for the determination of transport properties. Lower temperatures were estimated from the absolute line intensity measurements. At higher temperatures (above 18,000K), the intensity distribution had an off-axis maximum, and therefore, the Fowler and Milne method was used for calculating the temperatures. The plasma composition given in tables C.4 to C.9, was computed by the updated NASA programme [25,40]. The demixing effect was not considered in these calculations. Other emission data were taken from Wiese [71,70]. Transition probabilities were taken from Wiese, instead of the new values determined in this experiment, in order to keep the same emission data standard as has been used in the other evaluations [50,24,41,22], with which these results were

compared. Figures 6.22 and 6.23 show the calculated line intensity versus temperature curves for F_I lines at 641.4 and 720.2 nm. Linear interpolation for calculating particle densities for intermediate temperatures produced ripples in the above curves. To remove these ripples, a curve smoothing technique was used. A single polynomial could not be fitted to the entire temperature range of 5,000 to 30,000K, since the particle densities varied over several orders of magnitude. Therefore, the temperatures were split up into three or four segments of suitable range depending upon the accuracy with which curves could be fitted. A least-squares-error method of curve fitting was used to fit polynomials of up to fourth order.

SF_6 Temperature Profiles at Atmospheric Pressure

The measured range of the temperature for 5 mm diameter SF_6 arcs extends up to 22,500K. Initially, two F_I lines at 641.4 and 720.2 nm were used to calculate some of the temperature profiles. Figure 6.24 shows good agreement between the temperatures calculated for 99, 180 and 359 amperes arcs using both of these lines. For the subsequent experimental work, the F_I line at 720.2 nm alone was used for measuring the temperature profiles. For currents of up to 250 amperes, it was necessary to use the absolute line intensity method. However, above this current the radial intensity distribution had an off-axis maximum, permitting the use of the Fowler and Milne method. Figures 6.25 and 6.26 show temperature profiles for 5 mm and 3 mm diameter SF_6 arcs at atmospheric pressure.

Theoretical estimates of the temperature by Liebermann and Lowke [41] were higher by up to 15% for higher currents; figure 6.32. At the same time, the results compare well with the experimental results of Schulz-Gulde [63]. The estimated error in the measurement of absolute intensities was ±5%.

SF_6 Temperature Profiles at 4 and 8 Atmospheres Pressure

Temperature measurements have been made on 3 mm and 5 mm arcs for pressures of up to 8 atmospheres. The measured absolute continuum intensity at 600.4 nm for the 5 mm arc was also used for the temperature profile determination at higher pressures. This was primarily done because the measured temperatures at higher pressures were lower by as much as 15% than the theory predictions [41]. This pointed to the possibility of error caused by self-absorption of the line intensity.

The SF_6 arc centre temperature, as a function of current shown in figure 6.32, indicated a large reduction in the arc temperature at a current as the pressure increased. Table 6.4 illustrates the variation in the SF_6 arc centre temperature.

The choice of continuum at 600.4 nm was made for two reasons. One, because it was well isolated from the interference of overlapping lines, especially at higher pressures when lines became broadened. Two, because the spectrograph was set for the best spatial resolution at the red end of the spectrum.

The value of emission constant, $C(\nu)$, which is independent of temperature and pressure, was calculated from absolute continuum intensity and temperatures measured by line intensities at the atmospheric pressure. From the known plasma composition, given in tables C.4 to C.9, the continuum intensity-temperature graphs were constructed for the relevant pressures. The value of the emission constant $C(\nu)$, was found to be 16.5×10^{-42} W-k$^{1/2}$-m^3-ster^{-1}. Intensity versus temperature graphs for the continuum at 600.4 nm at different pressures are shown in figure 6.27. Temperatures calculated using the absolute continuum intensity were found to be within ±1% of the temperatures

Arc Current (amperes)	Pressure (atmospheres)	Arc centre temperature (K)
	1	16,000
150	4	11,750
	8	11,500
	1	20,500
400	4	14,000
	8	12,700

Table 6.4: Arc centre temperature as a function of pressure at two selected currents.

Arc Current (amperes)	Arc centre temperature 'T$_0$'			Pressure (atmospheres)
	F$_I$ 720.2 nm (K)	Continuum 600.4 nm (K)	H$_\alpha$ 656.3 nm (K)	
180	11,940	12,050	11,500	
305	12,700	12,890	13,180	4
430	14,730	14,900	14,850	
125	11,200	11,100	11,270	
261	12,250	12,000	12,320	8
365	12,800	12,650	13,000	

Table 6.5: Arc temperature measured using continuum, F$_I$ and H$_\alpha$ line.

measured using the absolute line intensity. The main source of error in the temperatures measured using the continuum was introduced by the poor accuracy of the H-D curve at lower densities. For good line resolution, spectra were recorded with the spectrograph entrance slit-width at 30 to 60 microns. Due to this reason, the continuum density level in the recorded spectra was low. This could not be avoided as the experiment was geared for line intensity measurements. The error introduced by the H-D curve in continuum intensity measurements was up to 5%.

For 4 and 8 atmospheres pressure, temperatures were also calculated for the 5 mm arc from the measured full half-width of the H$_\alpha$ line profiles. These results are presented in table 6.5. Values of the coefficient C(N$_e$,T) were taken from Griem [26], and are given in table 6.6. However, for the evaluation of transport properties, the temperatures measured by absolute line intensities have been used. Figures 6.28, 6.29, 6.30 and 6.31 show temperature profiles measured using absolute intensities at 4 and 8 atmospheres pressures for 5 and 3 mm diameter arcs.

Temperature (K)	Electron density (cm^{-3})		
	10^{16}	10^{17}	10^{18}
10,000	6.16×10^{15}	3.61×10^{15}	3.23×10^{15}
20,000	7.13×10^{15}	3.88×10^{15}	2.79×10^{15}
40,000	4.22×10^{16}	6.01×10^{15}	2.67×10^{15}

Table 6.6: Coefficient $C(N_e, T)$ in $\text{Å}^{-3/2}$ - cm^{-3} for electron density evaluation from full half-width of H$_\alpha$ line.

Theoretical Calculations of SF$_6$ Arc Temperature Profiles at 1, 4 and 8 Atmospheres Pressure

Temperature measurements were one of the most important factors in these experiments. The accuracy with which transport properties were calculated depended largely upon the temperature measurements. In the preceeding section two experimental methods are described, which were used for cross checking the accuracy of the temperature measurements done using the absolute line intensities. In order to provide further support to the experimental evaluation of temperature, it was considered appropriate to calculate the temperature of SF$_6$ arcs theoretically, using the transport properties determined in this experiment.

These calculations were performed by solving the time-dependent energy balance equation. For a wall stabilised arc the equation can be written as follows,

$$\rho c_p \frac{dT}{dt} = \sigma E^2 - u + \frac{1}{r}\frac{d}{dr}\left[rk\frac{dT}{dr}\right], \qquad (6.1)$$

where

ρ = density
c_p = specific heat
T = arc temperature
σ = electrical conductivity
E = electric field
u = net radiation emission
r = arc radius
k = thermal conductivity.

To solve the equation 6.1, a programme using the finite difference method was developed by Ramakrishnan [56]. It uses split boundary conditions that $dT/dr = 0$ at $r=0$, and $T = T_{wall}$ at $r = R$. The material properties (ρ, c_p, σ, k and u) are provided in tabular form as a function of temperature.

An arbitrary temperature profile is given as an initial input. For a given current, iterations are carried out until the solution relaxes.

The time step dt is chosen to satisfy the Von Neumann criterion [58]. This criterion ensures numerical stability from the thermal conduction term.

In order to check the validity of the programme, temperature profiles were evaluated first, by using theoretical transport properties according to Frost, Liebermann and Lowke [24,41]. These results were compared with the theoretical estimates of temperature given by Liebermann and Lowke [41], shown in figure 6.32. Calculations were then performed using the transport properties determined in this experiment and these temperatures were compared with the experimental results of this experiment, shown in figure 6.32, and few selected profiles in figures 6.33 to 6.35 at 1, 4 and 8 atmospheres pressure.

E–I Characteristic of SF$_6$ Arcs

The current range for the E-I characteristic, shown in figure 6.37, was up to 550 amperes at 1 atmosphere, 490 amperes at 4 atmospheres and 365 amperes at 8 atmospheres pressure for the 5 mm arc. Figure 6.36 shows the E–I characteristic for a 3 mm arc for the current range of up to 260 amperes at 1, 4 and 8 atmospheres pressure. The experimental values of the electric field measured by Schulz- Gulde [63], at atmospheric pressure for 5 mm arcs were higher by up to 10% with an error of ±5%. The minimum value of E,

15 V/cm, was the same as measured by Schulz Gulde, but it occurred at 100 amperes instead of 50 amperes. Waveform records for currents lower than 60 amperes had large noise. This could be indicative of spiralling of the arc core. Therefore, measurements were not reliable for arc currents below 60 amperes, and the steep rise in the field at lower currents may not be real. Liebermann and Lowke's theoretical estimate [41] of the E–I characteristic at atmospheric pressure was in good agreement with the results of this experiment, except at lower currents where the theoretical value was much lower. At atmospheric pressure the E–I characteristic for a 3 mm arc was close to the theoretical estimates [41], but was higher at lower currents by up to 20% from the theoretical estimates of Liebermann and Lowke [41]. Due to the lack of published data at 4 and 8 atmospheres pressure for 3 and 5 mm diameter arcs, the E–I characteristic at higher pressures could only be compared with the theoretical estimates of Liebermann and Lowke [41] for 3 and 5 mm diameter arcs at 10 atmospheres pressure.

6.5 Transport Properties of SF$_6$ at 1, 4 and 8 Atmospheres Pressure

Determination of the transport properties of SF$_6$ was the main object of these experiments. Electrical conductivity, thermal conductivity and net radiation emission as a function of temperature have been evaluated. All efforts were made to obtain highest possible temperatures in pure SF$_6$ plasma. Experiments were carried out for pressures of up to 16 atmospheres. But due to the highly unpredictable performance of the ignitor, only a limited number of observations could be taken at 12 and 16 atmospheres pressure. Substantial work could be done only at 4 and 8 atmospheres pressure.

Electrical Conductivity of SF$_6$ at 1, 4 and 8 Atmospheres Pressure

Electrical conductivity calculations were based upon Devoto and Mukherjee's method [16] of 'trial function' described in section 2.3.1. For determining the set of three constants A, B and C describing the function $\sigma(T)$, three temperature profiles were selected and arc conductance was calculated at three corresponding currents from the E–I characteristic. Constants A, B and C were initially given assumed trial values and the first set of approximate arc conductance was calculated from the temperature profiles. At atmospheric pressure, the assumed values for constants A, B and C were 8.00×10^{12}, 2.20 and 6.00×10^4, respectively. Using the Gauss-Siedel numerical method, these values were updated iteratively until both values of arc conductances as calculated from the E–I characteristic and as estimated here from the temperature profile, converged and the solution relaxed. If the assumed initial trial values of constants were close to the correct values, the solution relaxed quickly. The initial values of the constants A, B and C at 4 atmospheres were 7.70×10^{12}, 2.20, 6.14×10^4 and at 8 atmospheres 7.698×10^{12}, 2.2247, 5.9955×10^4, respectively. The final values of constants for the 4 atmospheres calculations were taken as the initial starting values for the 8 atmospheres calculations. Table 6.7, lists the calculated and the measured values of arc conductances and final values of the constants A, B and C for different pressures.

The electrical conductivity of SF$_6$ as a function of temperature at 1, 4 and 8 atmospheres pressure is shown in figure 6.38.

52

Pressure (atm.)	Parameters A, B and C		Arc conductance		Current (amperes)	Error %
	Initial	Final	Measured (S/cm)	Calculated (S/cm)		
1	A–8.00×10^{12}	8.50×10^{12}	33.61	33.07	99	1.6
	B–2.20	2.209	95.95	94.15	428	1.9
	C–6.00×10^4	6.80×10^4	106.59	110.43	544	3.6
4	A–7.70×10^{12}	7.698×10^{12}	42.48	43.12	180	1.5
	B–2.20	2.2247	54.91	55.14	305	0.8
	C–6.14×10^4	5.9955×10^4	61.71	62.23	345	0.8
8	A–7.698×10^{12}	7.698×10^{12}	22.77	20.53	125	9.8
	B–2.2247	2.205	42.65	44.48	261	4.3
	C–5.9955×10^4	6.088×10^4	50.04	51.00	310	1.9

Table 6.7: Parameters A, B and C for SF_6.

Thermal Conductivity of SF_6 at 1, 4 and 8 Atmospheres Pressure

Experimental evaluation of thermal conductivity, k, of SF_6 has been done using the 'form factor' technique [68], the details of which are given in section 2.3.2 . Radiation dominated flat temperature profiles did not permit an accurate determination of thermal conductivity by solving the energy balance equation due to large errors introduced in differentiating temperature profiles. On the other hand, the 'form factor' method is fairly accurate and can be applied to all types of temperature profiles [55]. As a first estimate of k, without taking radiation into account, the electrical power, P_e, was differentiated with respect to the arc centre temperature, T , and the electrical 'form factor', $2\pi F_{el}$, was assumed to be one. Using this approximate value of k, the net radiation emission coefficient, u, was calculated. Effect of the inflated values of thermal conductivity on the evaluation of u was minimal, due to the flat temperature profiles for which the value of dT/dr was very small and, therefore, thermal energy losses were insignificant.

The thermal conductivity was recalculated, once reasonably accurate estimates of u were available. From temperature profiles and the known value of u, the total radiative power, P_u, for the arc was calculated. Instead of using a constant form factor equal to one, its actual value was calculated from the known radial distribution of σ and u, using equations 2.33 and 2.37. Once $P_{el}, P_u, 2\pi F_{el}$ and $2\pi F_u$ were known, the thermal conductivity could be calculated more accurately using equation 2.38. Using the updated value of thermal conductivity the entire process was repeated until the solution relaxed. The estimated error was 20% due to 'form factor' and 10% due to the derivative of P_e, giving a combined error of 30% in the evaluation of thermal conductivity.

Figures 6.39 and 6.40 show the variation of P_{el}, P_u and 'form factors' with the arc centre temperature at 1, 4 and 8 atmospheres pressure for a 5 mm diameter arc. The variation in the values of 'form factor' was between 0.65 and 0.5 . These values were to be expected for arcs in which the whole diameter was filled with highly conductive plasma. Figure 6.41 shows the thermal conductivity of SF_6, calculated from 3 mm and 5 mm arc data, as a function of temperature at 1, 4 and 8 atmospheres pressure. These experimental values were higher than Frost and Liebermann's theoretical estimates by a factor of three at atmospheric pressure, six at 4 atmospheres and eight at 8 atmospheres pressure.

Net Radiation Emission Coefficient of SF$_6$ at 1, 4 and 8 Atmospheres Pressure

There are two radiation coefficients, the transparent radiation coefficient, u_t, and the net emission coefficient of radiation, u. The transparent radiation coefficient, u_t, can be measured by radiometric methods. In this experiment the net emission coefficient of radiation , u, has been calculated by solving the energy balance equation 2.41, since the electrical and thermal conductivities were known. At the arc centre, for a given electric field E, the net emission coefficient of radiation is equal to σE^2, and at other radial positions it is given by the difference of σE^2 and thermal losses. The net emission coefficient of radiation is not a unique function of temperature because it is dependent upon absorption which changes with the radial position. Therefore, there were different curves of u, at different arc currents. A smooth curve was drawn by tracing an upper envelope over the set of curves for u [20].

Evaluation of net radiation emission coefficient for 3 mm and 5 mm SF$_6$ arcs was done at 1, 4 and 8 atmospheres pressure. Figure 6.42 shows the value of u, for both diameters, at these pressures. Theoretical estimates of u, given by Liebermann and Lowke [41], at 1 and 10 atmospheres pressure for 3 and 5 mm diameter arcs, indicated that the present experimental values were higher by a factor of up to two at atmospheric pressure and by even a larger factor at 8 atmospheres pressure.

N_I 746.83
N_I 744.23
N_I 742.36

N_{II} 571.08
N_{II} 568.62
N_{II} 567.95
N_{II} 567.60
N_{II} 566.66

N_{II} 549.57

H_α 656.28

632.81
He-Ne Laser

N_{II} 504.51

N_{II} 510.60
N_{II} 500.73
N_{II} 500.51
N_{II} 500.15
N_{II} 499.44

N_{II} 594.02
N_{II} 593.18
N_{II} 592.78

Figure 6.1: Nitrogen arc spectrum (wavelength in nm). Arc current 371 amperes and pressure 1 atmosphere.

H_β	486.13
N_{II}	481.03
N_{II}	480.33
N_{II}	478.12
N_{II}	477.97

N_{II}	423.94
N_{II}	422.77

N_{II}	464.31
N_{II}	463.05
N_{II}	462.14
N_{II}	461.39
N_{II}	460.72
N_{II}	460.15

N_{II}	455.25
N_{II}	453.04
N_{II}	450.75
N_{II}	444.70
N_{II}	443.27
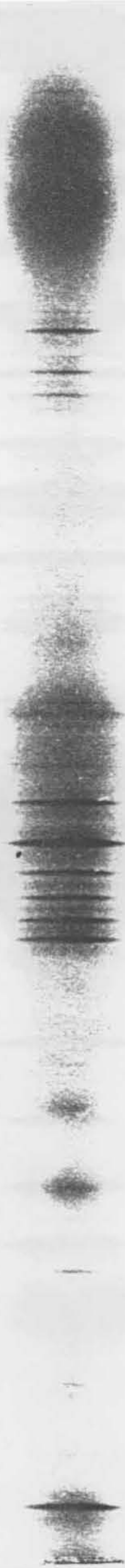
Figure 6.2: Nitrogen arc spectrum (continued).

Figure 6.3: Argon arc spectrum (wavelength in nm). Arc current 424 amperes and pressure 1 atmosphere.

H₃ 486.13

Ar_I 479.87

Ar_I 475.29

Ar_II 472.16
Ar_I 470.23

Ar_I 464.21

Ar_I 459.61

Ar_II 457.93
Ar_II 456.44

Ar_II 453.55

Ar_II 440.10

Ar_II 438.37

Ar_II 435.22
Ar_II 434.81

Ar_II 433.71
Ar_II 433.20
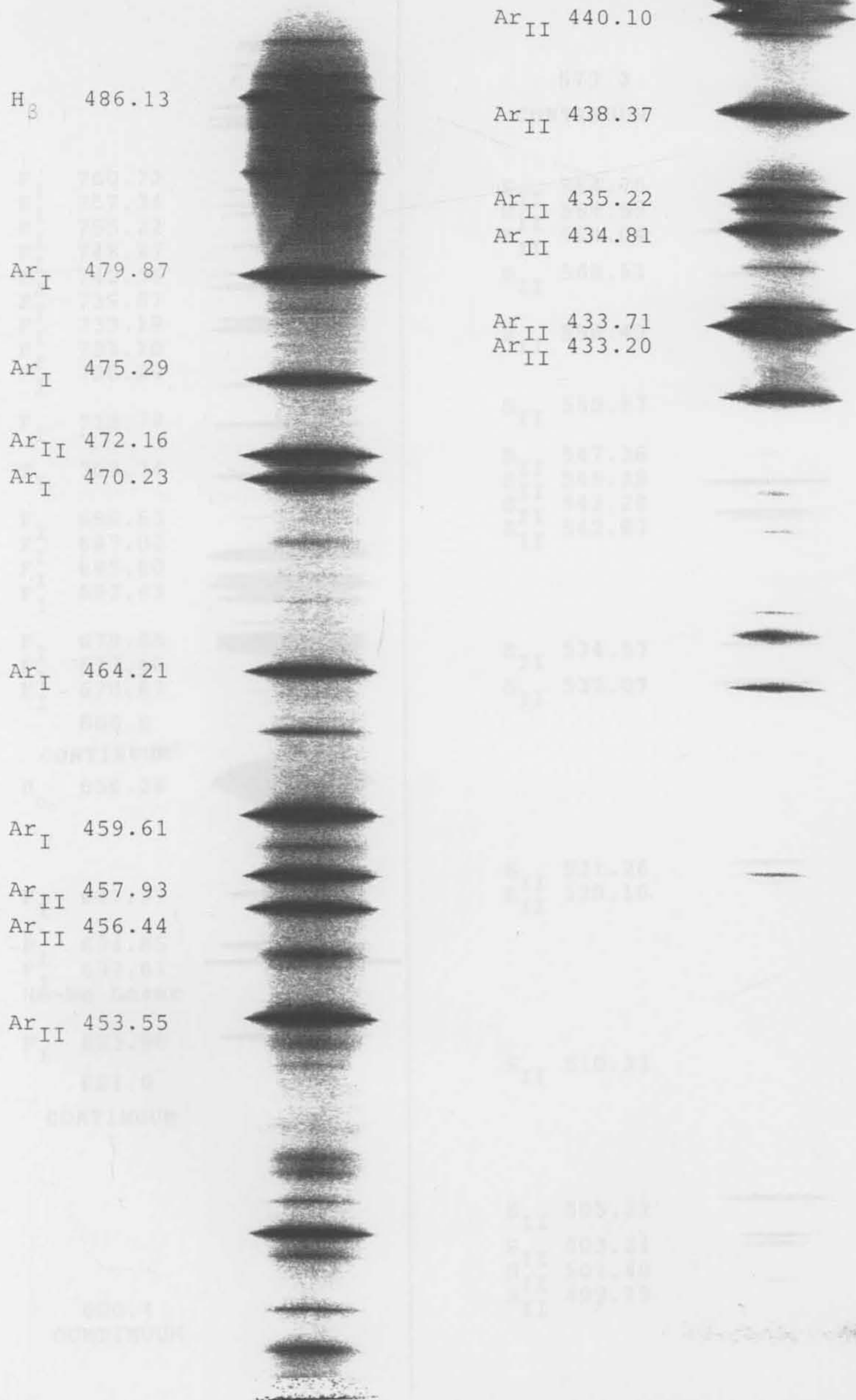
Figure 6.4: Argon arc spectrum (continued).

Figure 6.5: SF$_6$ arc spectrum (wavelength in nm). Arc current 481 amperes and pressure 1 atmosphere.

S$_{II}$ 492.53
S$_{II}$ 492.41

S$_{II}$ 443.24

H$_\beta$ 486.13

S$_{II}$ 481.55

472.3
CONTINUUM
S$_{II}$ 471.62

S$_I$ 469.54

S$_{II}$ 429.44

S$_{II}$ 465.67

S$_{II}$ 425.74

S$_{II}$ 455.24
S$_{II}$ 454.96

S$_{II}$ 452.50

S$_{II}$ 448.34

S$_{II}$ 446.36
S$_{II}$ 445.64

S$_{II}$ 415.31

F$_{II}$ 444.69

Figure 6.6: SF$_6$ arc spectrum (continued).
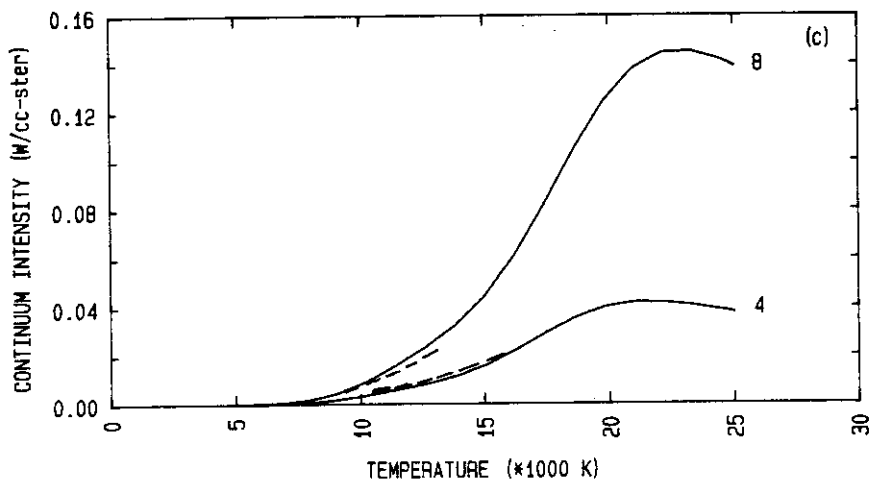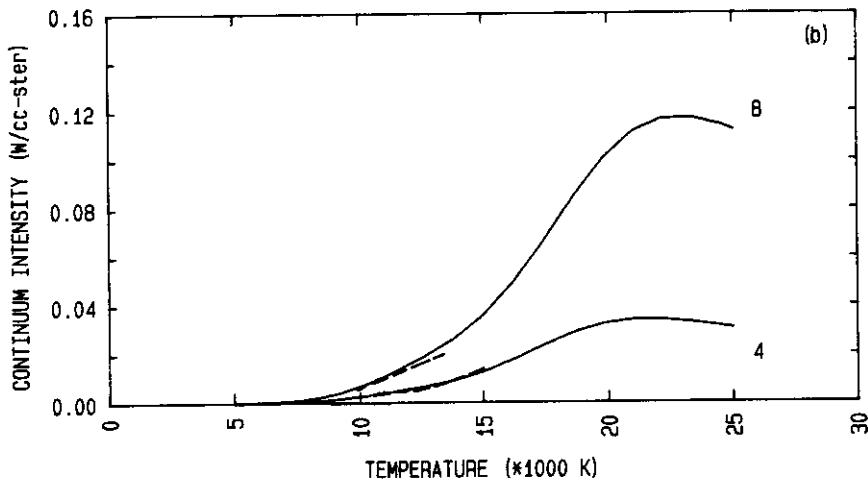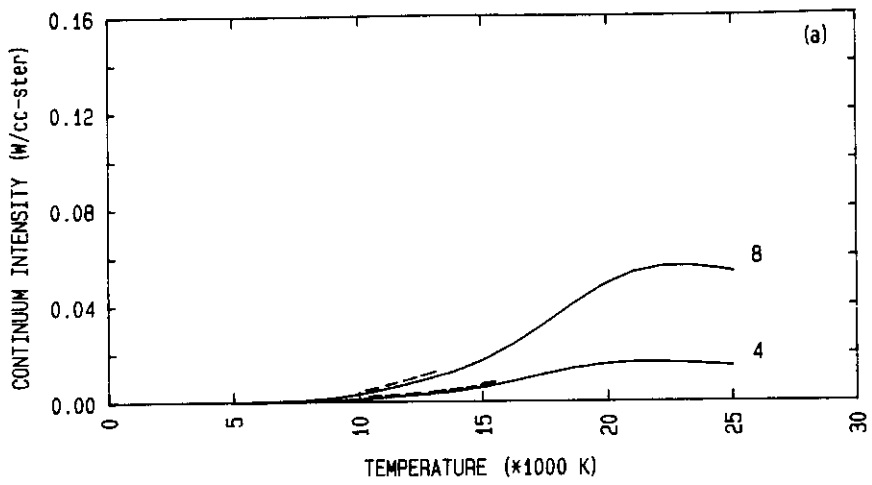
(a) 472.3 nm Continuum, C(ν) = 6.34e-42
(b) 573.3 nm Continuum, C(ν) = 13.33e-42
(c) 600.4 nm Continuum, C(ν) = 16.50e-42
———— Calculated, - - - - Measured

Figure 6.7: Calculated and measured continuum intensities at 4 and 8 atmospheres.

61
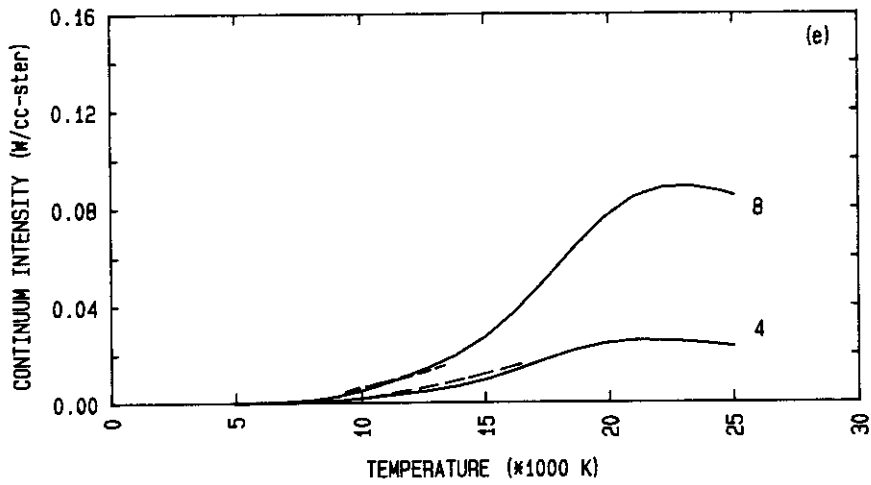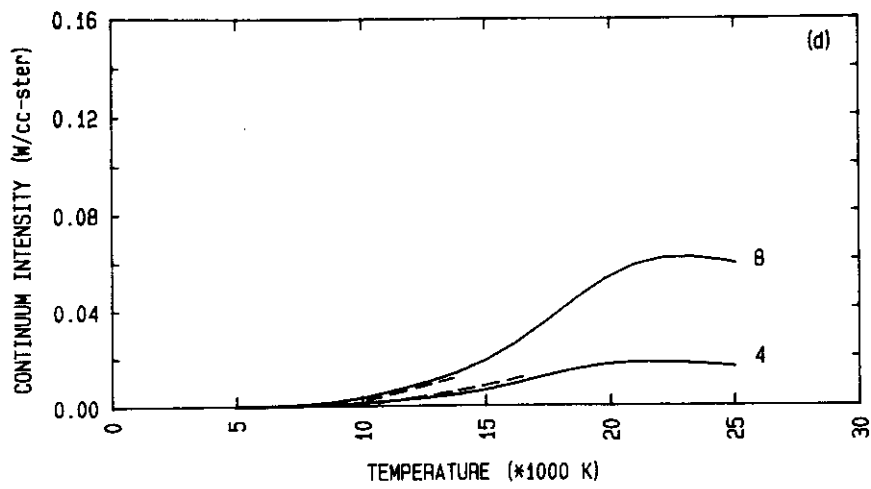
(d) 621.0 nm Continuum, $C(\nu) = 6.92e{-}42$

(e) 666.6 nm Continuum, $C(\nu) = 10.10e{-}42$

——— Calculated, - - - - Measured

Figure 6.8: Calculated and measured continuum intensities at 4 and 8 atmospheres.
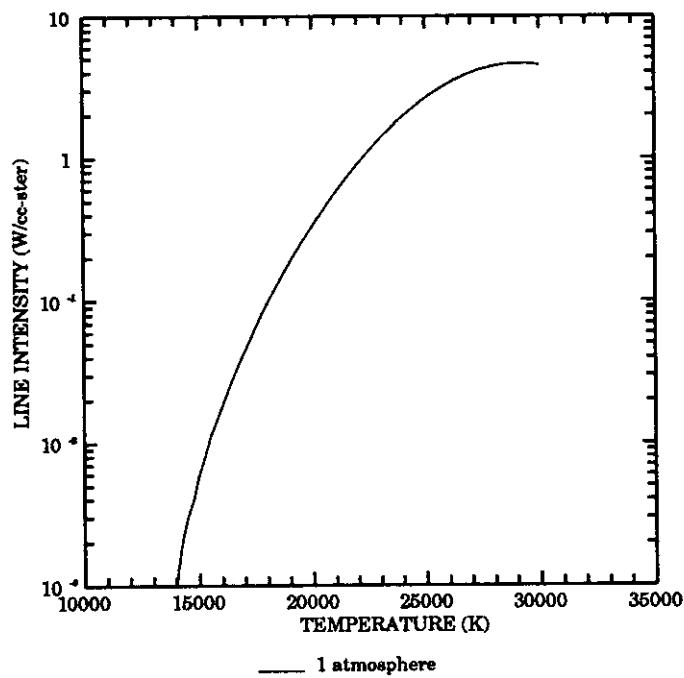
——— 1 atmosphere

Figure 6.9: Line intensity–temperature curve for 504.5 nm N_{II} line at 1 atmosphere.

62
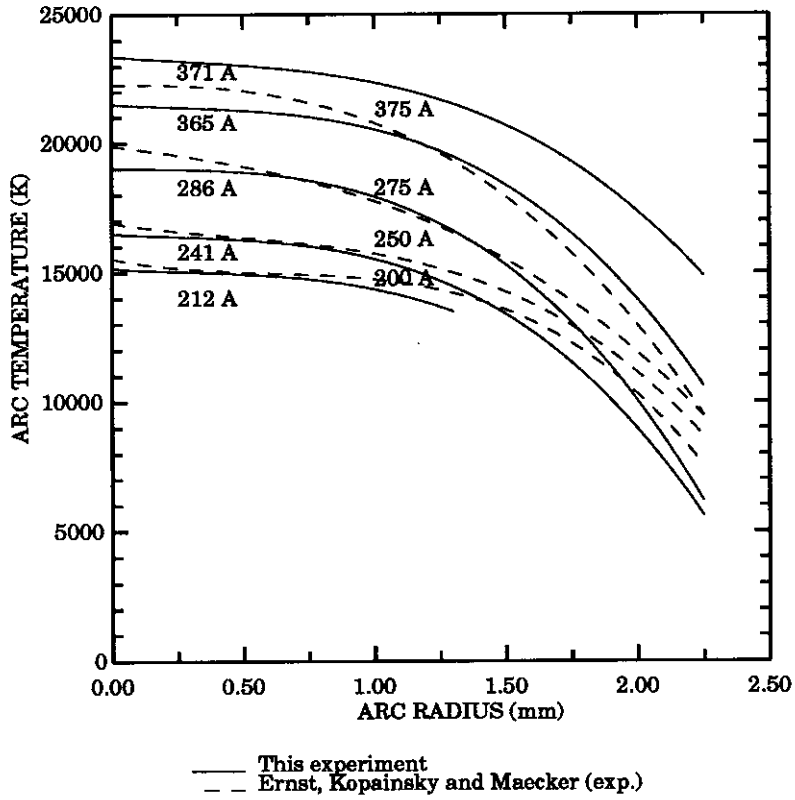
Figure 6.10: Temperature profiles for the nitrogen arcs
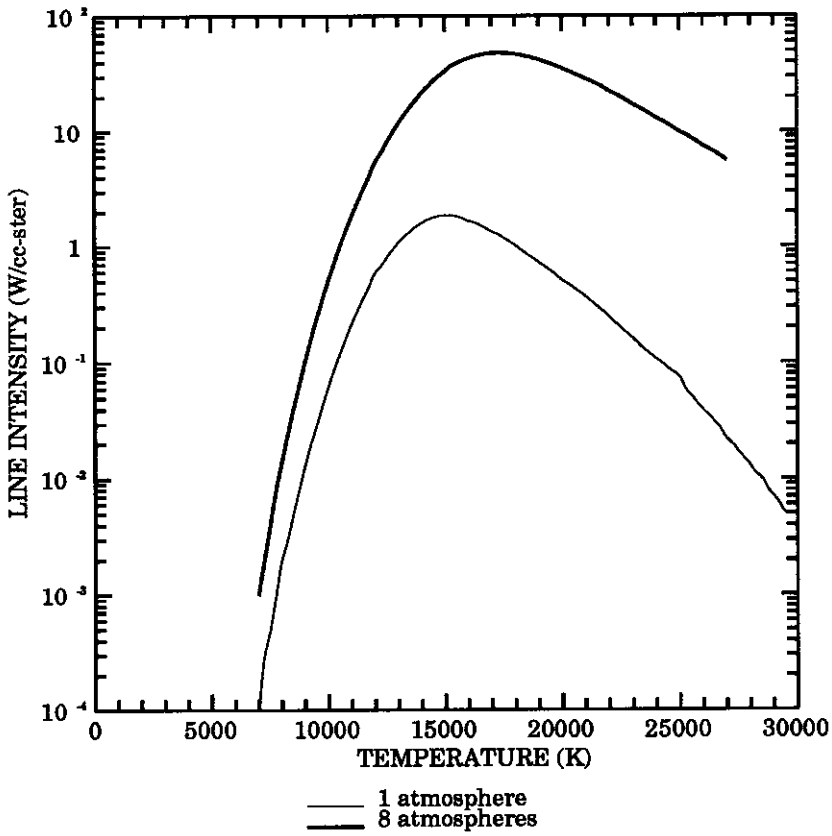
Figure 6.11: Line intensity–temperature curve for 696.5 nm Ar_I line at 1 and 8 atmospheres
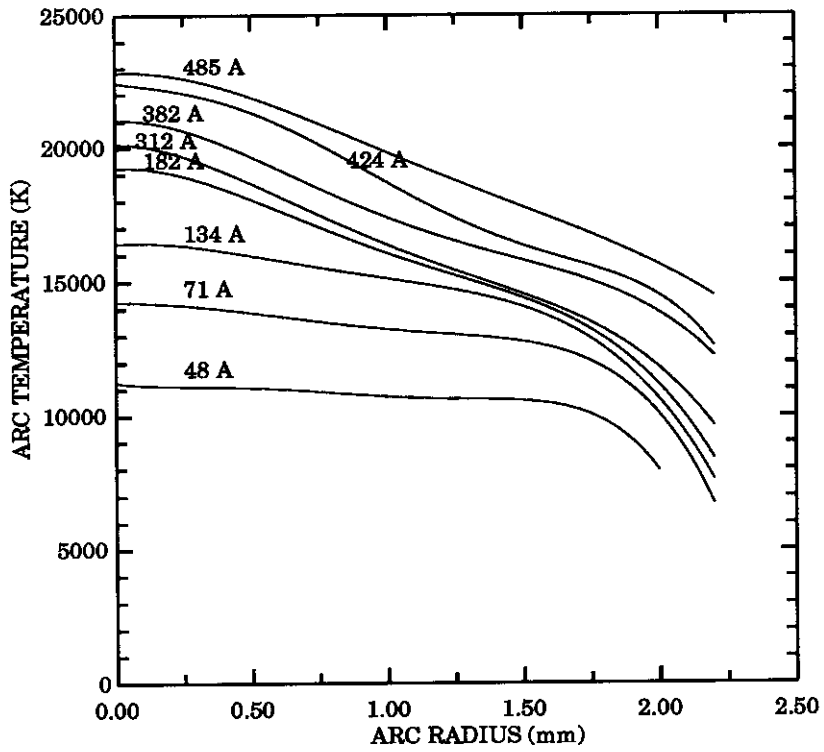
Figure 6.12: Temperature profile for 5 mm diameter argon arcs at 1 atmosphere
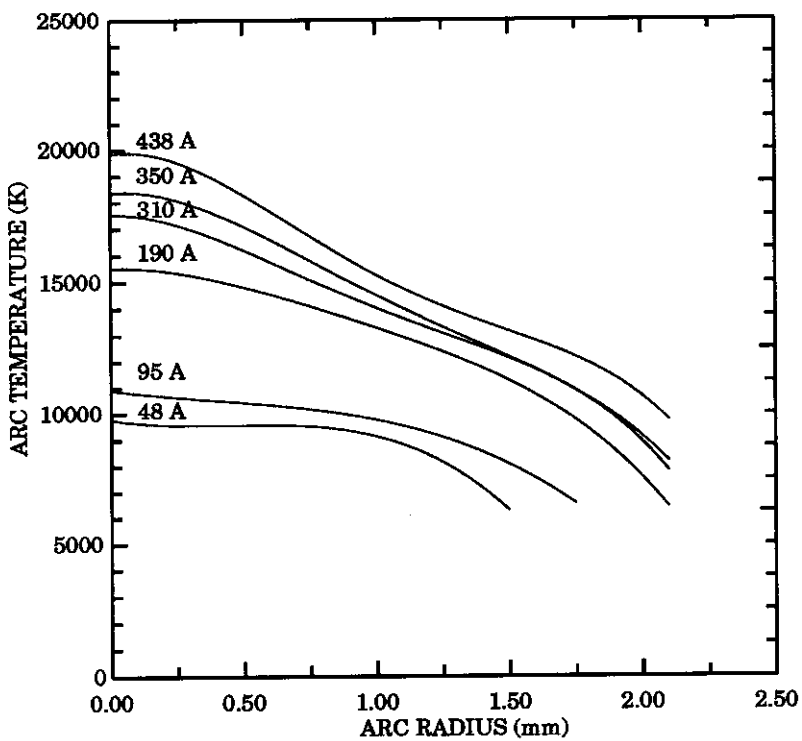
Figure 6.13: Temperature profile for 5 mm diameter argon arcs at 8 atmospheres.

64
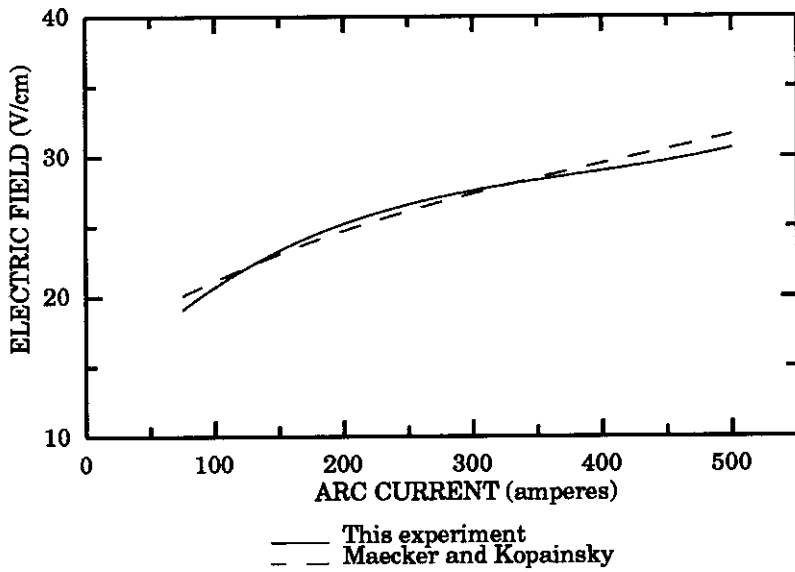
Figure 6.14: E–I characteristic, 5 mm diameter nitrogen arcs at 1 atmosphere.
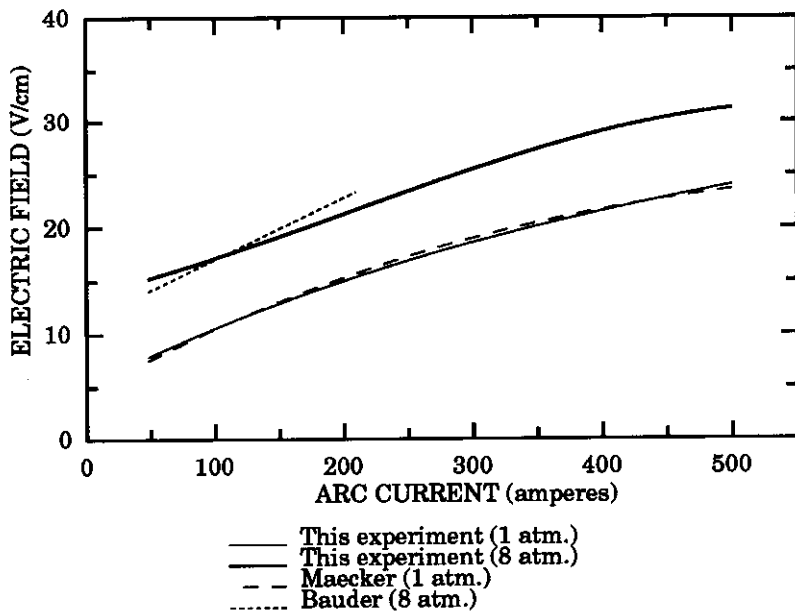
Figure 6.15: E–I characteristic, 5 mm diameter argon arcs at 1 and 8 atmospheres.
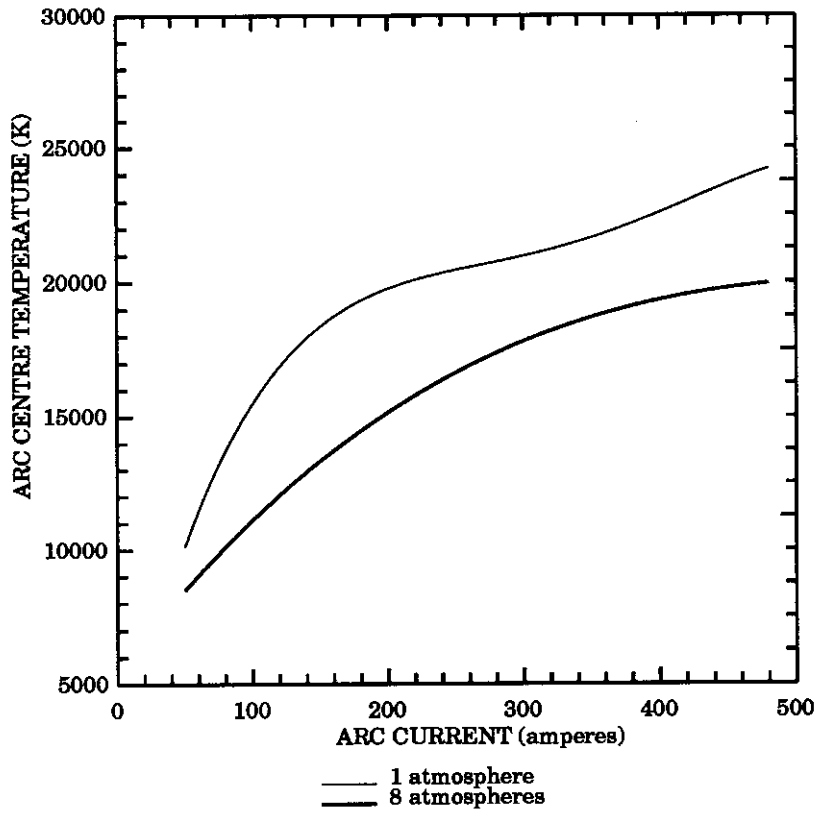
Figure 6.16: Arc centre temperature–current for argon arcs
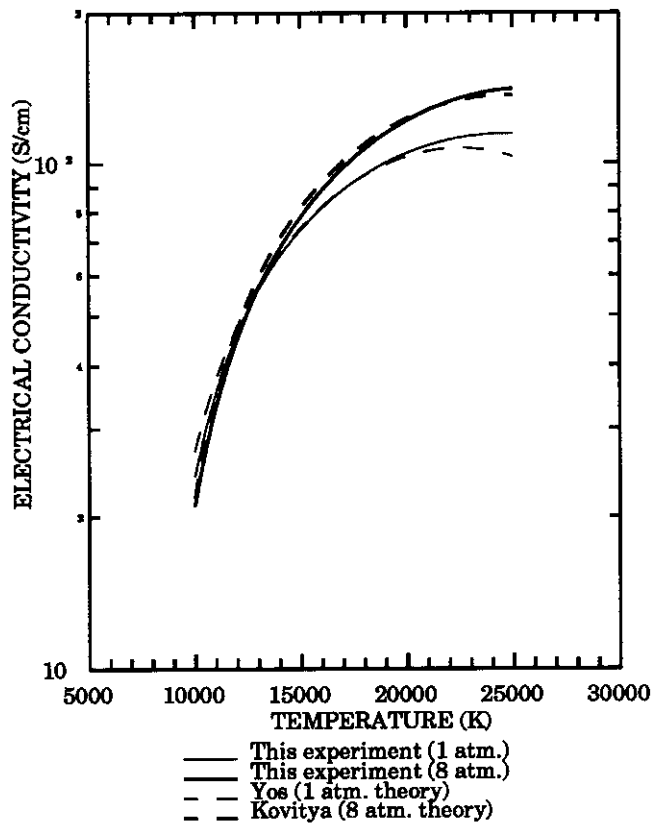
Figure 6.17: Electrical conductivity of argon at 1 and 8 atmospheres.
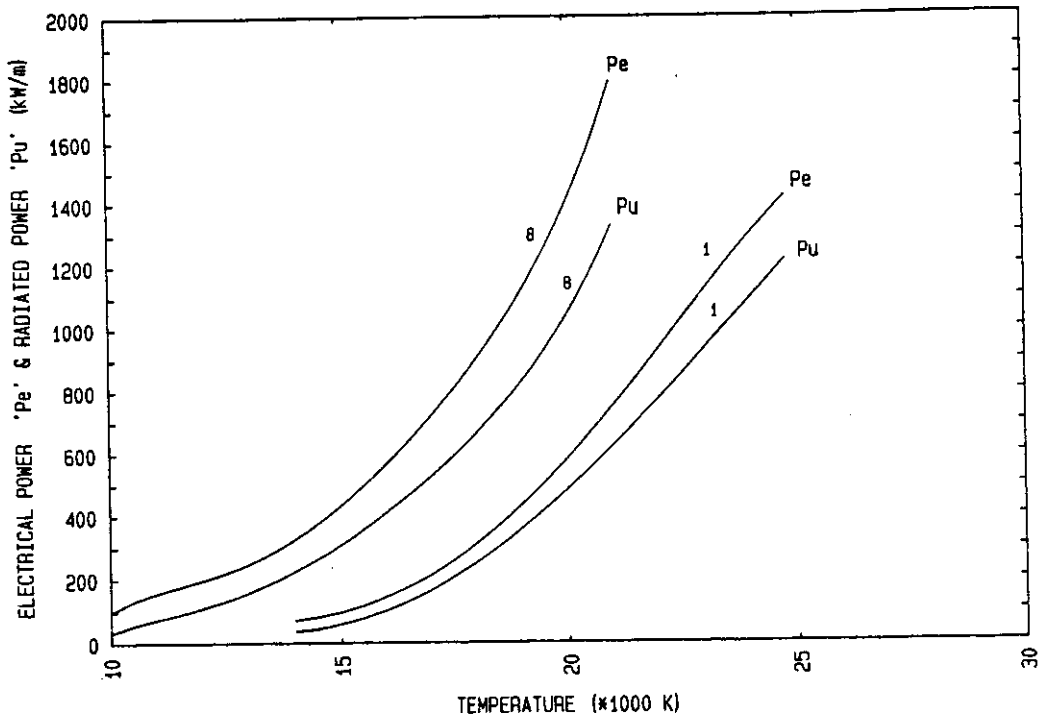
Figure 6.18: Electrical power input and radiated power - arc centre temperature, argon arcs at 1 and 8 atmospheres.
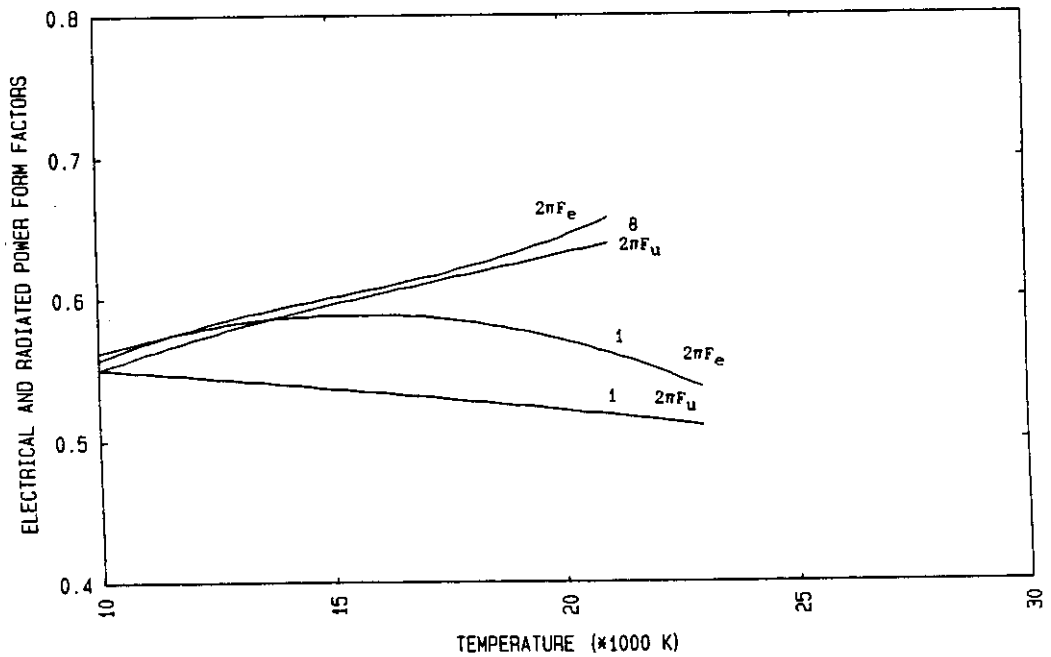
Figure 6.19: Electrical and radiated power 'form factor', argon arcs at 1 and 8 atmospheres.
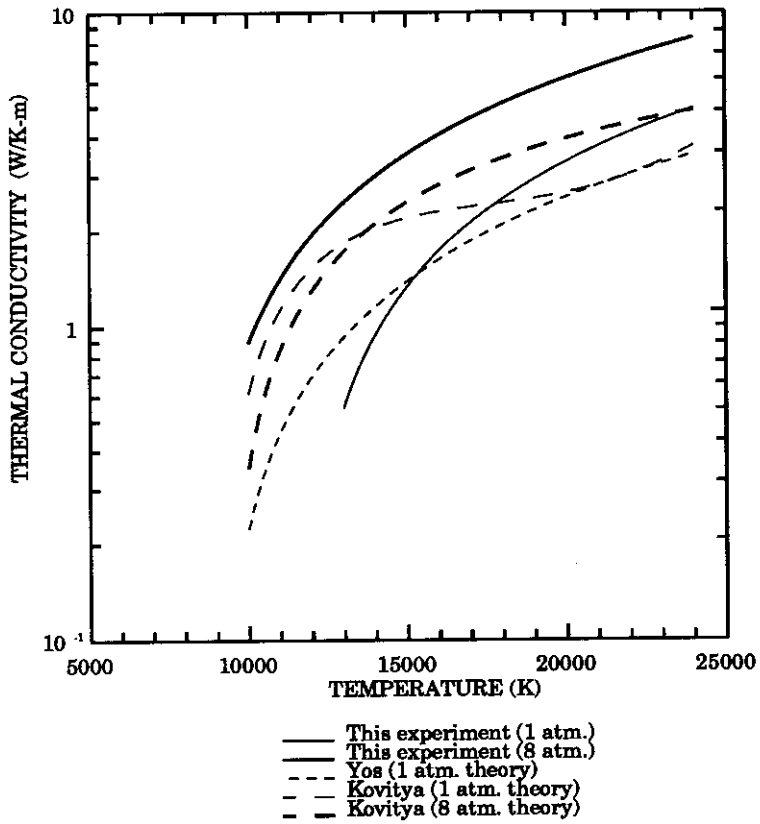
Figure 6.20: Thermal conductivity of argon at 1 and 8 atmospheres.
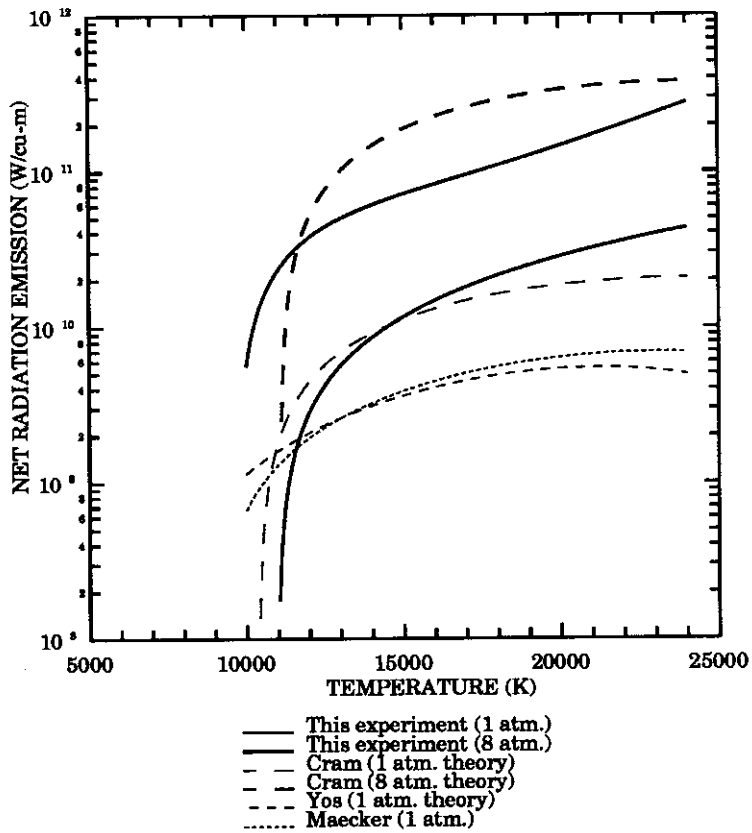
Figure 6.21: Net radiation of argon at 1 and 8 atmospheres.
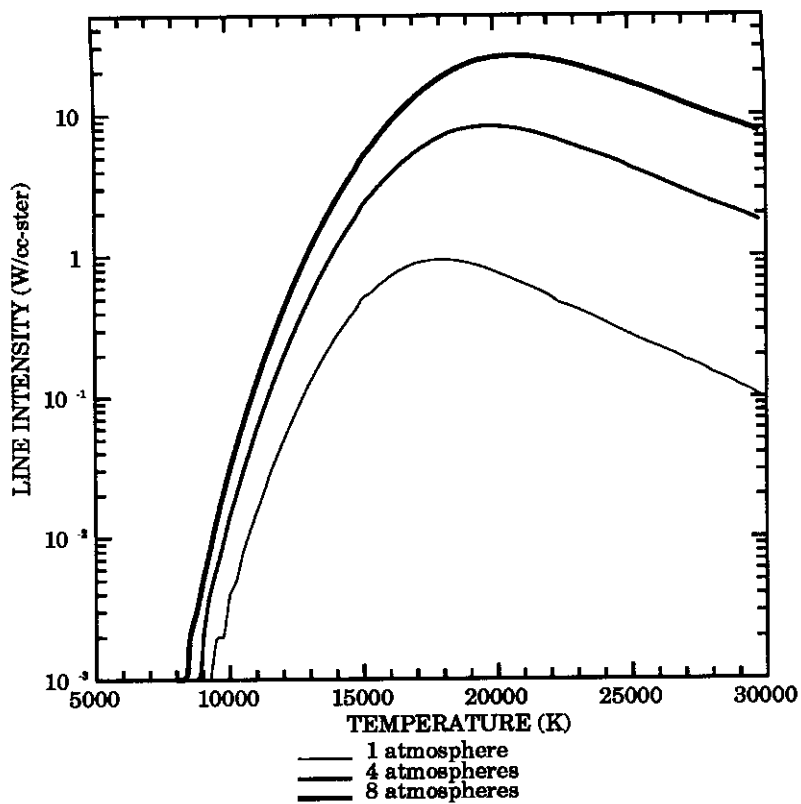
Figure 6.22: Line intensity–temperature curve for 641.4 nm F_I line at 1, 4 and 8 atmospheres.
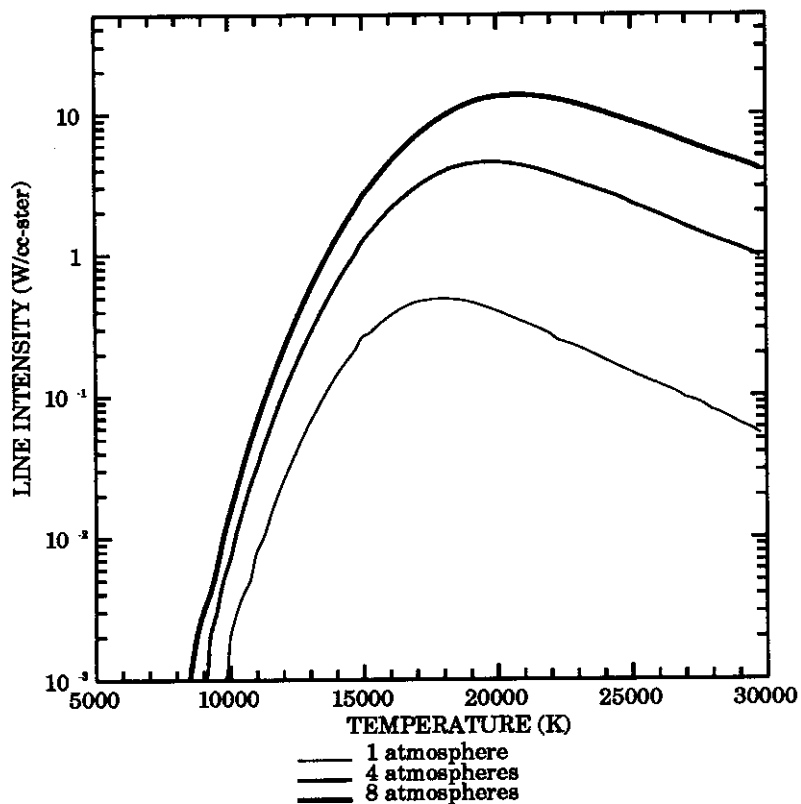
Figure 6.23: Line intensity–temperature curve for 720.2 nm F_I at 1, 4 and 8 atmospheres.

70
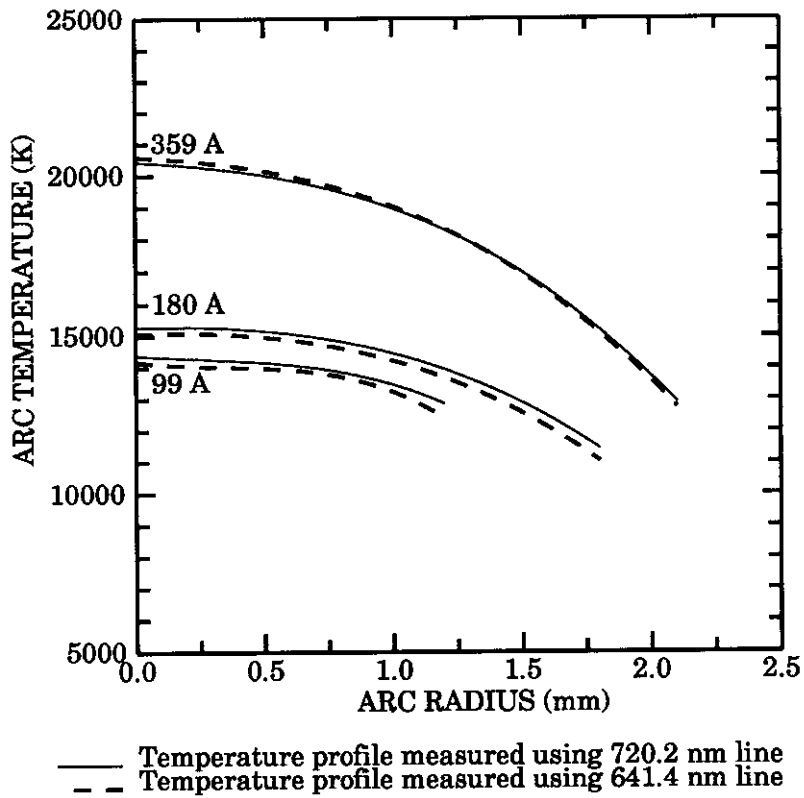
Figure 6.24: Temperature profiles of SF$_6$ arcs measured by 641.4 and 720.2 nm F$_I$ lines at 1 atmosphere pressure
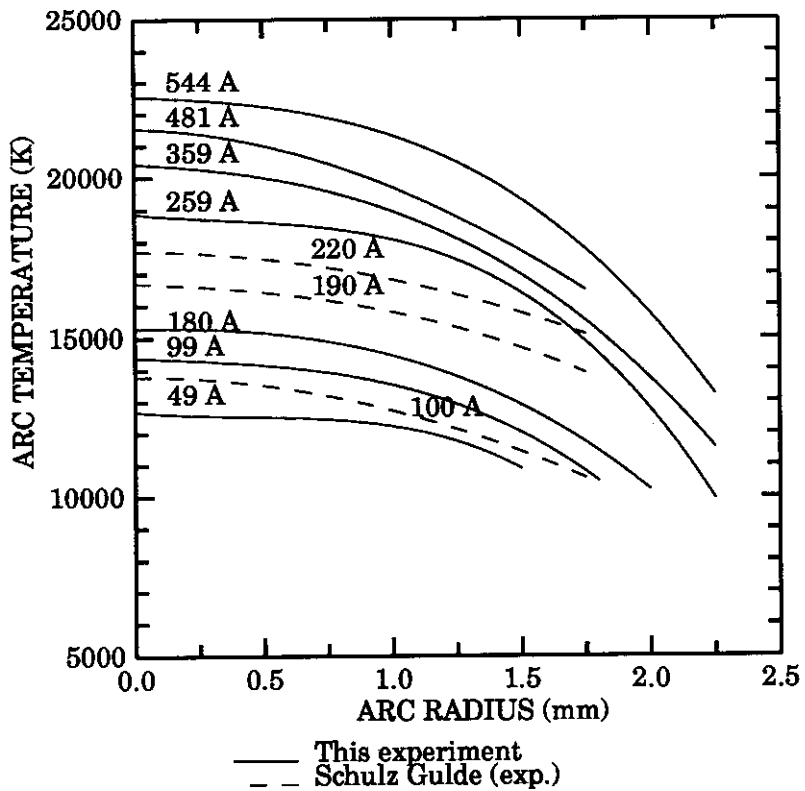
Figure 6.25: Temperature profiles of 5 mm dia. SF$_6$ arcs at one atmosphere

71
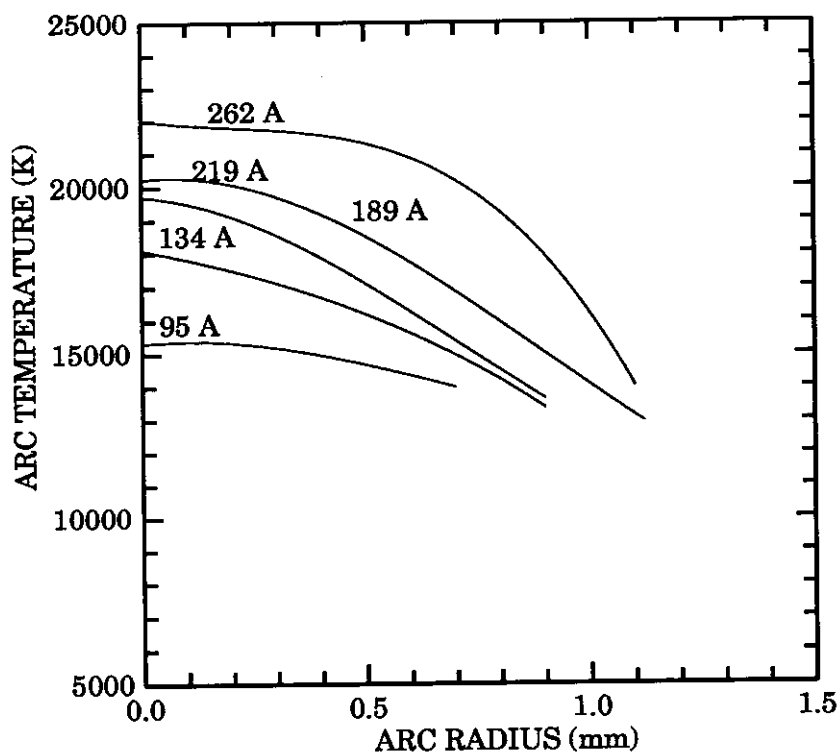
Figure 6.26: Temperature profiles of 3 mm dia. SF_6 arcs at one atmosphere
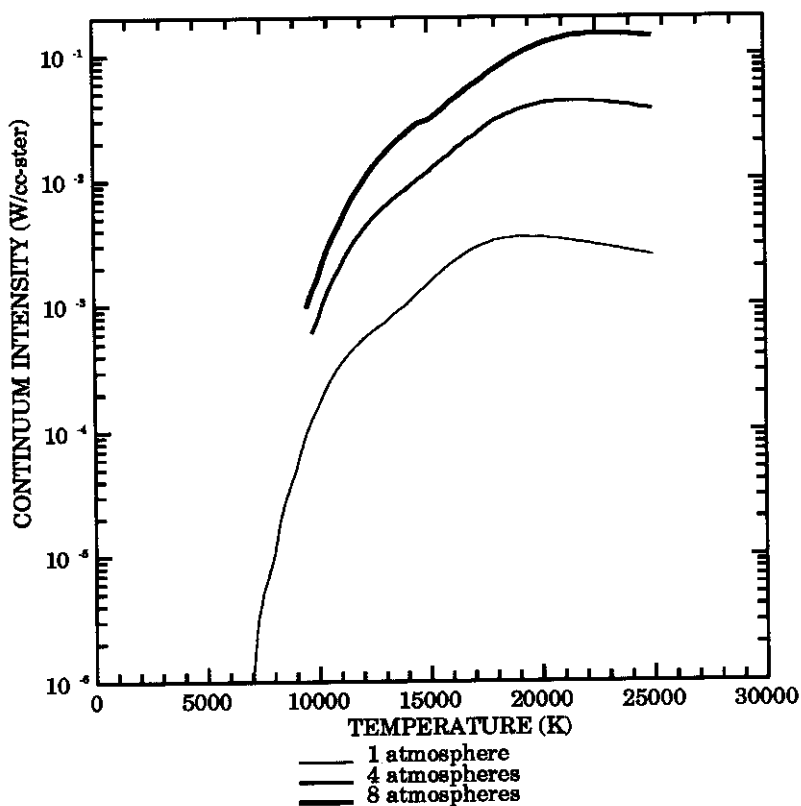
Figure 6.27: Continuum intensity–temperature curve for 600.4 nm continuum at 1, 4 and 8 atmospheres.
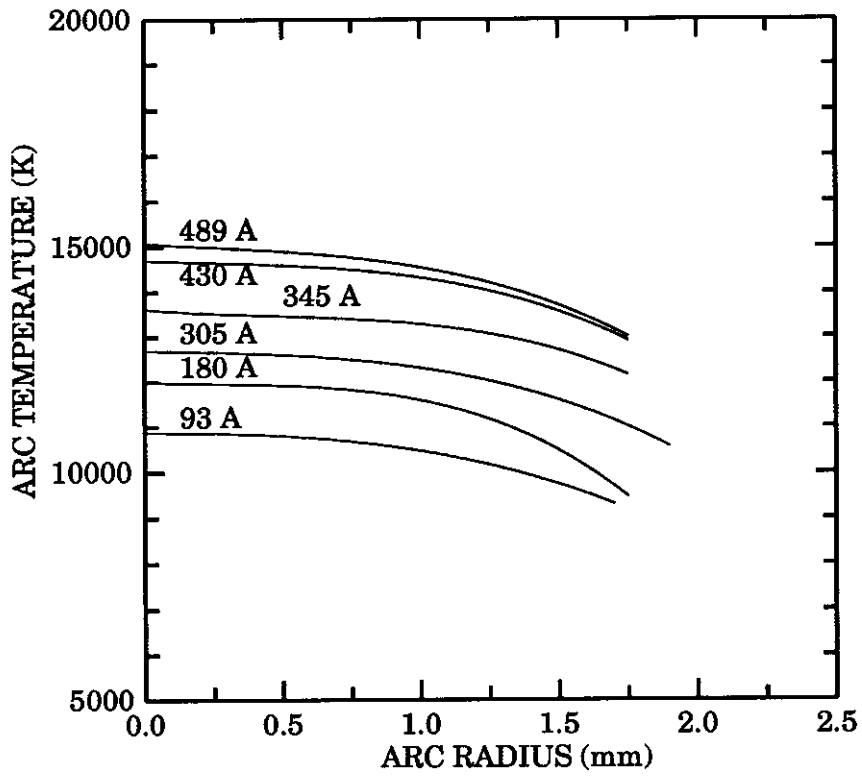
Figure 6.28: Temperature profiles of 5 mm dia. SF_6 arcs at 4 atmospheres
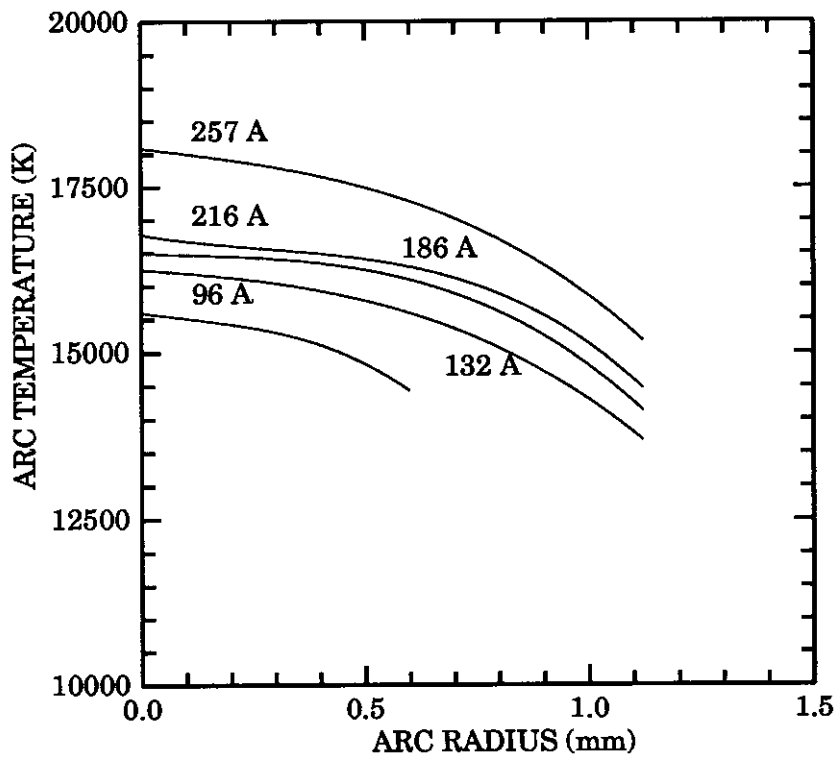
Figure 6.29: Temperature profiles of 3 mm dia. SF_6 arcs at 4 atmospheres
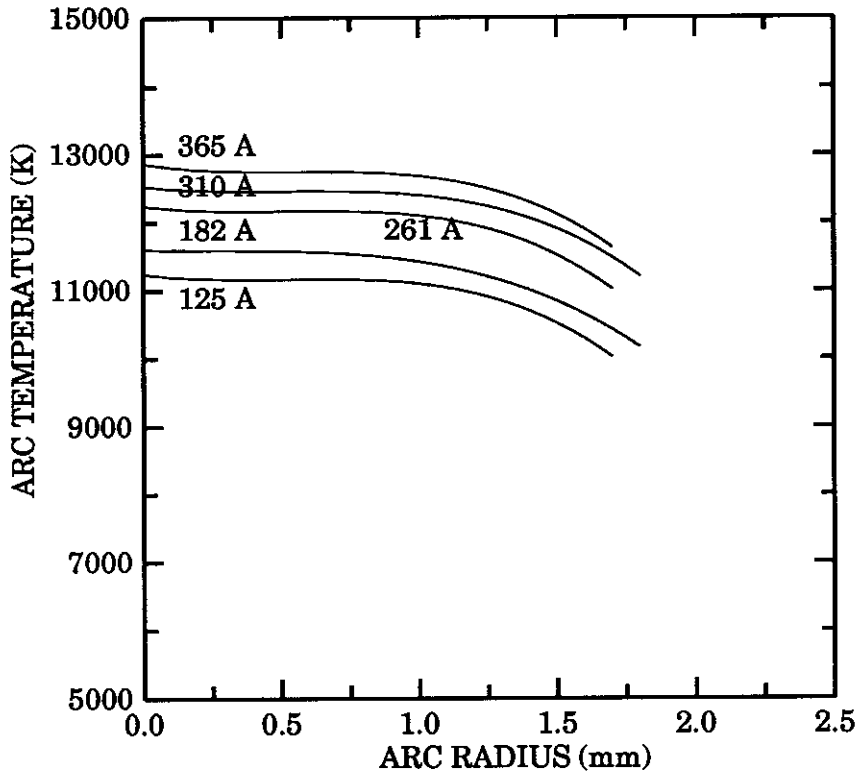
Figure 6.30: Temperature profiles of 5 mm dia. SF_6 arcs at 8 atmospheres
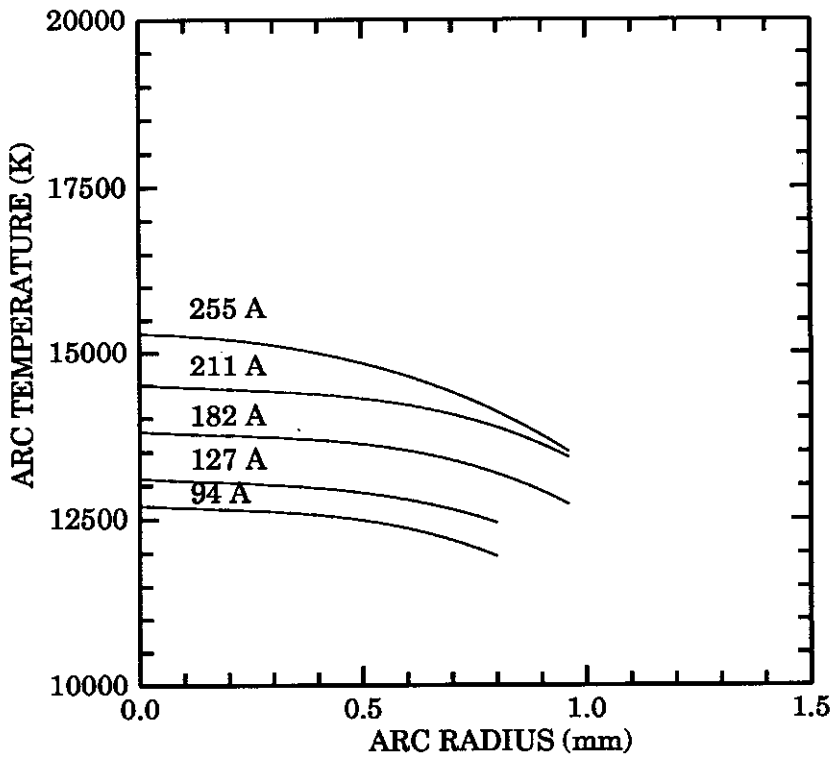
Figure 6.31: Temperature profiles of 3 mm dia. SF_6 arcs at 8 atmospheres
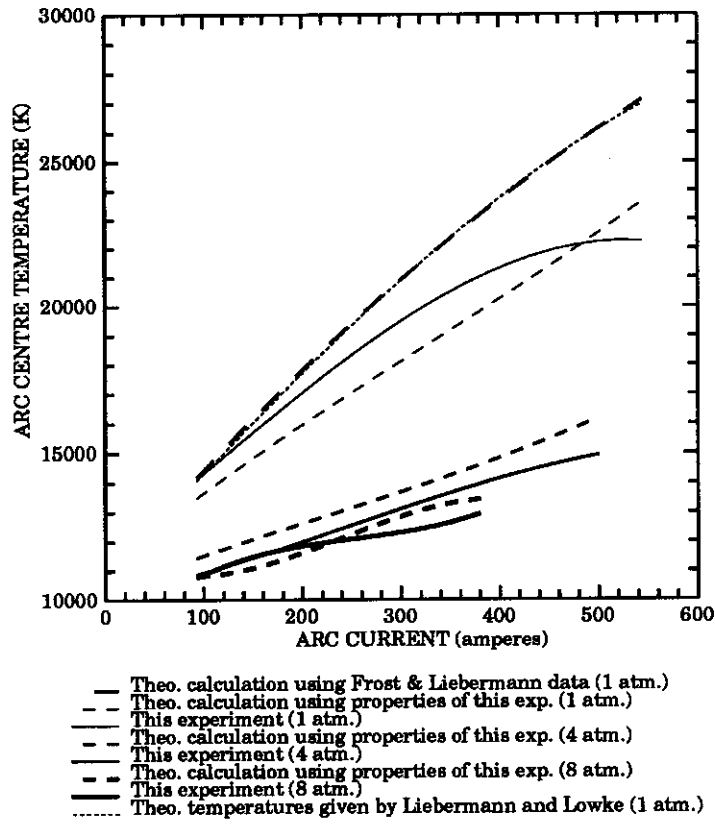
Figure 6.32: Arc centre temperature–current, 5 mm SF$_6$ arcs
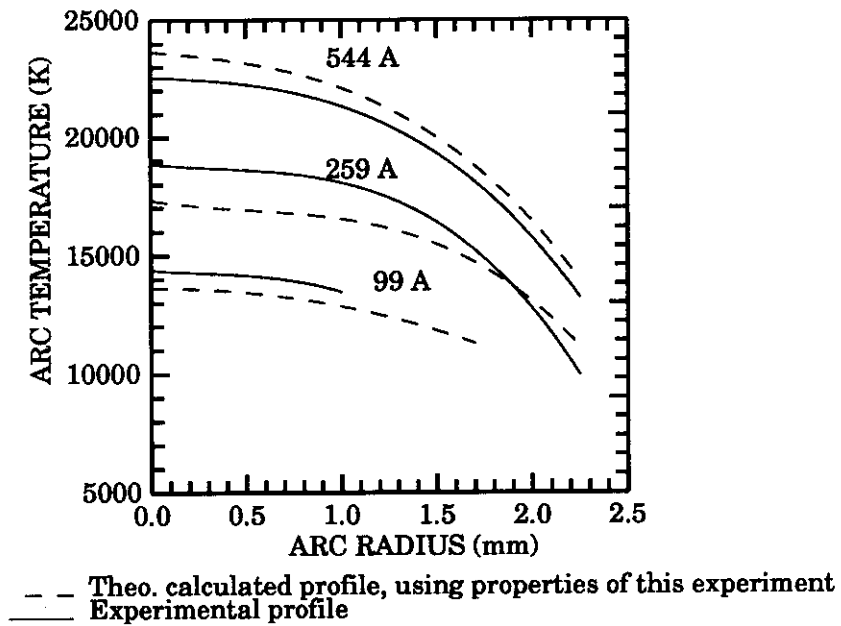
Figure 6.33: Measured and calculated temperature profiles of 5 mm dia. SF$_6$ arcs at 1 atmosphere
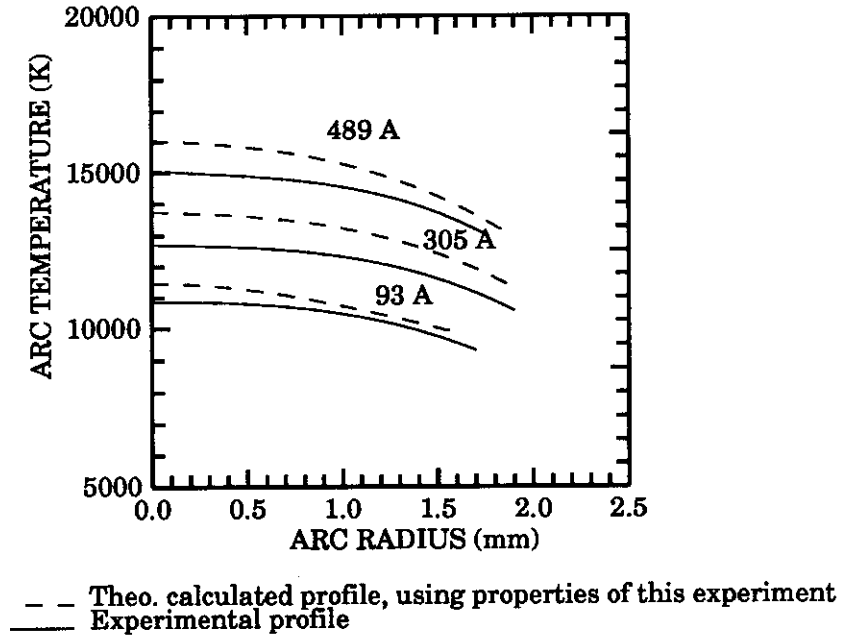
Figure 6.34: Measured and calculated temperature profiles of 5 mm dia. SF$_6$ arcs at 4 atmosphere
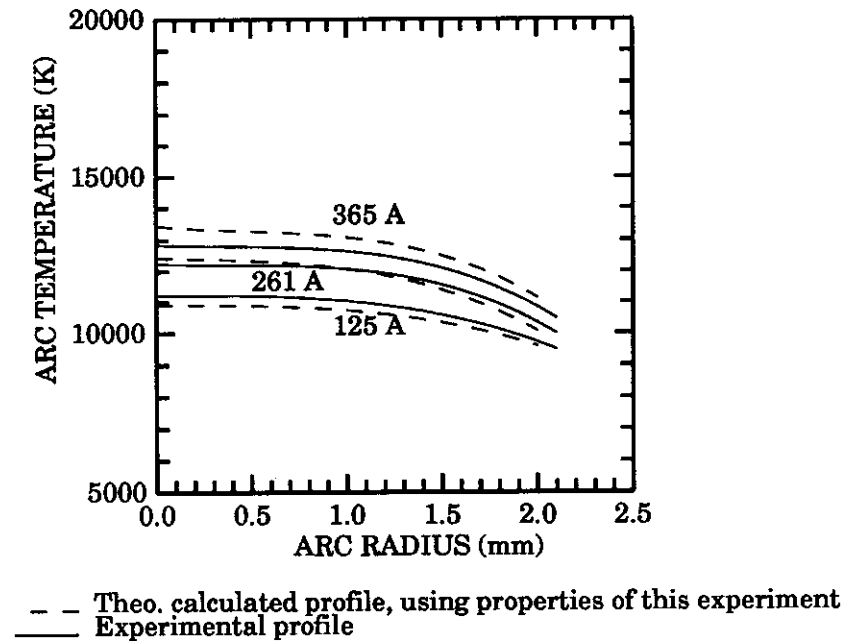
Figure 6.35: Measured and calculated temperature profiles of 5 mm dia. SF$_6$ arcs at 8 atmospheres
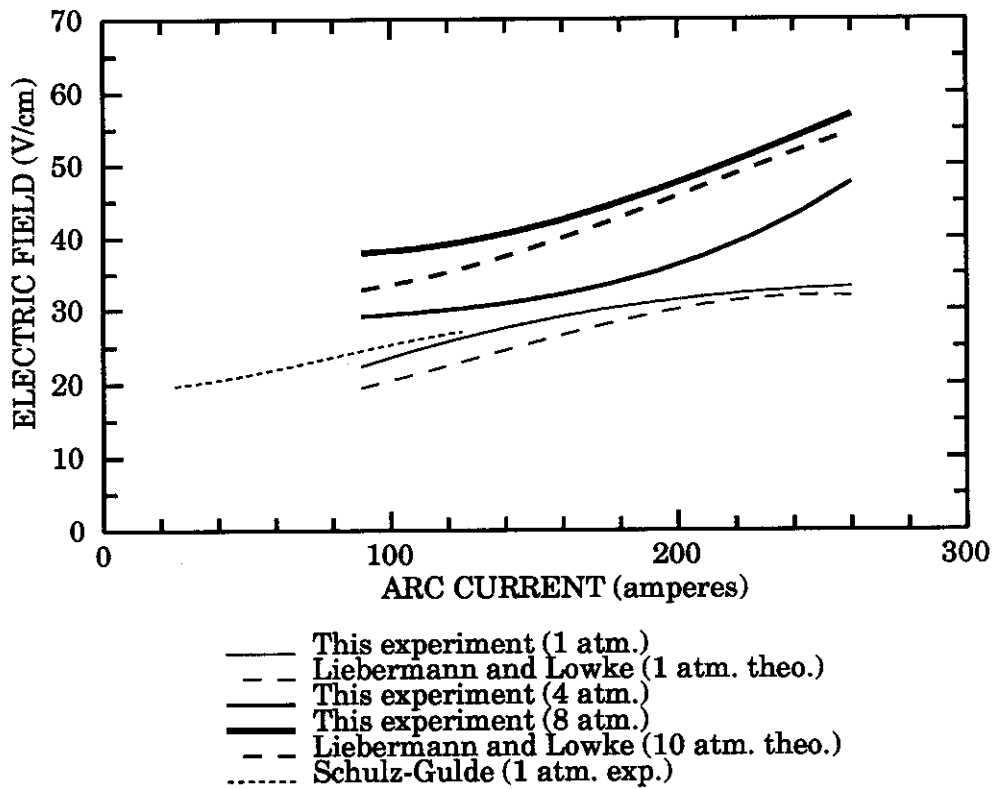
Figure 6.36: E–I characteristic, 3 mm dia. SF$_6$ arcs.
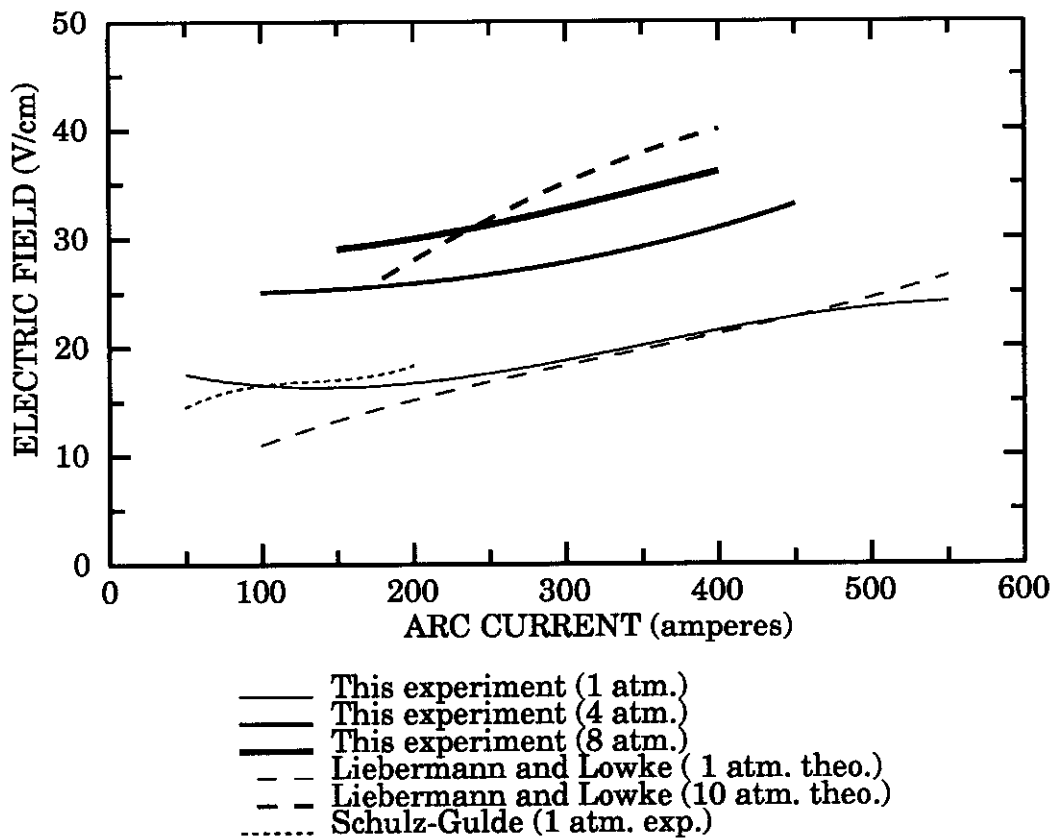
Figure 6.37: E–I characteristic, 5 mm dia. SF$_6$ arcs.

77
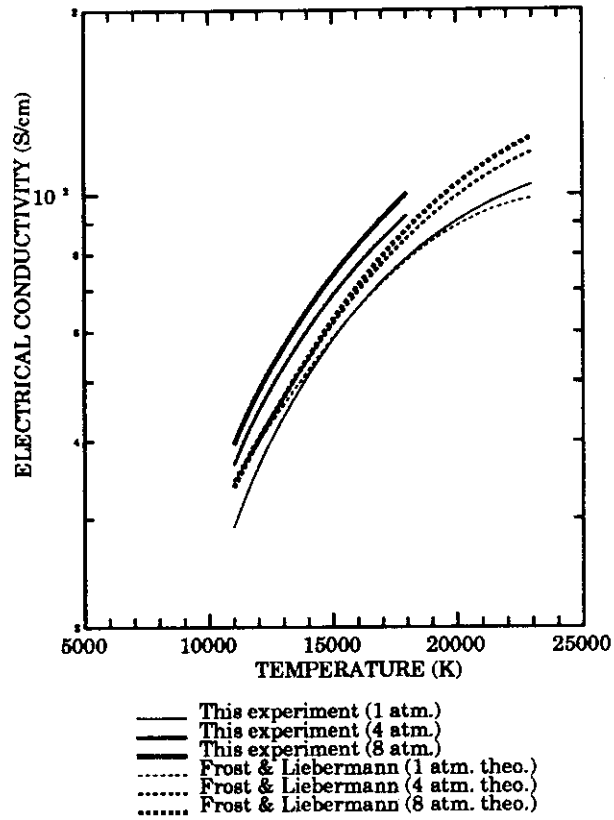
Figure 6.38: Electrical conductivity of 5 mm dia. SF$_6$ arcs
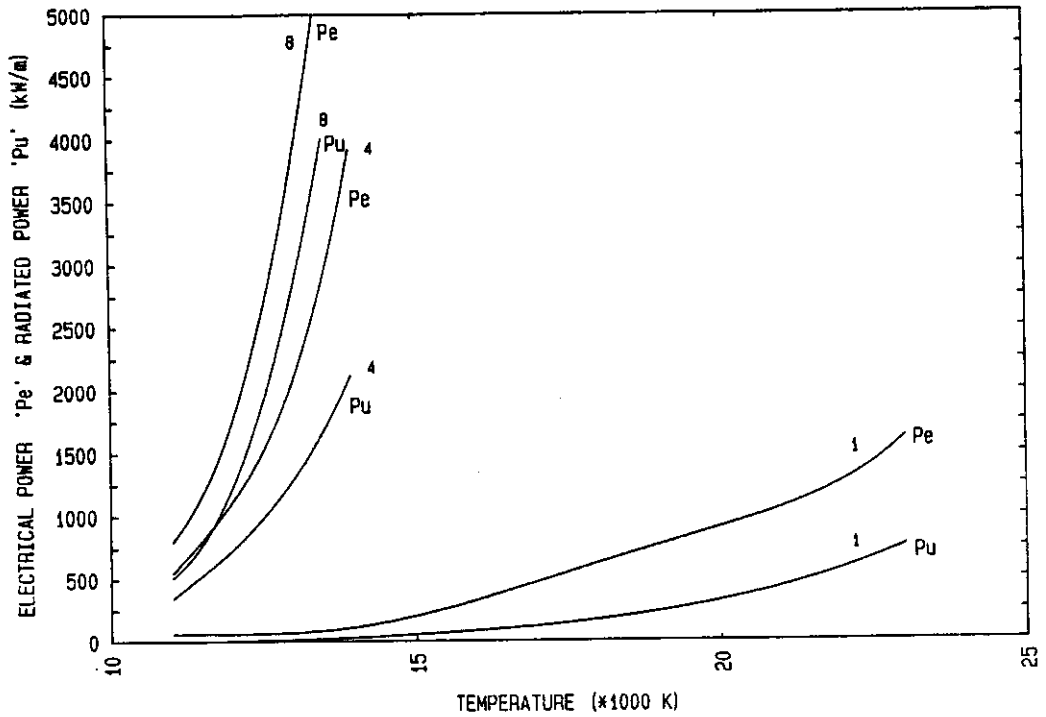
Figure 6.39: Electrical power input and radiated power - arc centre temperature, 5 mm diameter SF$_6$ arcs 1, 4 and 8 atmospheres.
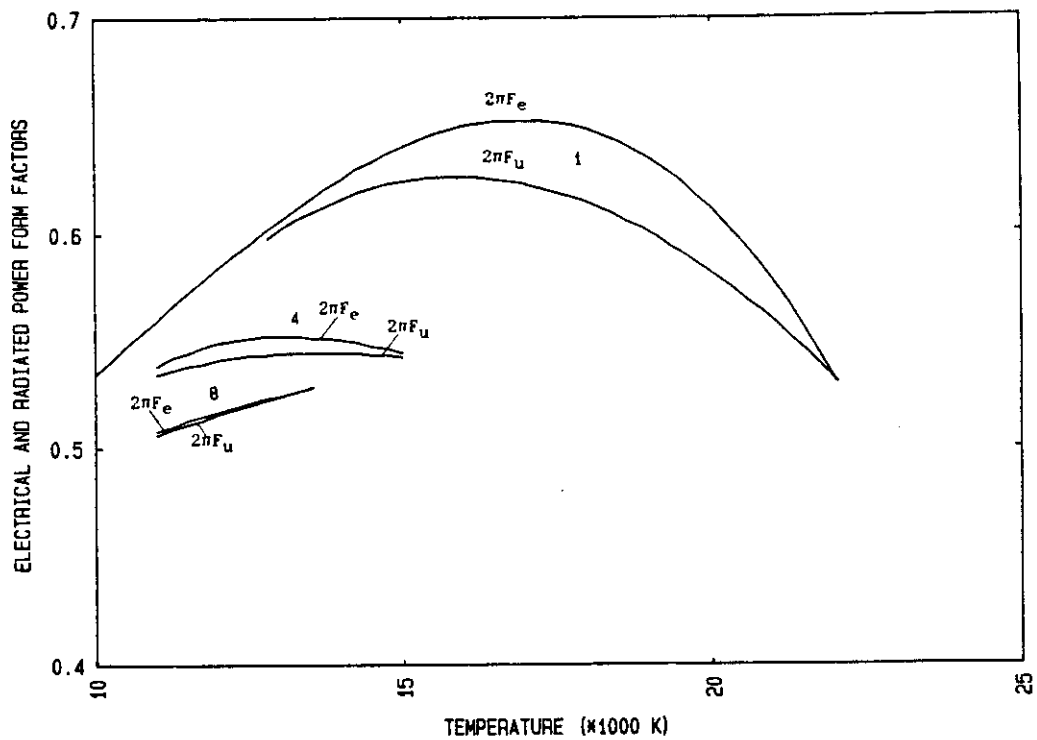
Figure 6.40: Electrical and radiated power 'form factor', 5 mm diameter SF_6 arcs at 1, 4 and 8 atmospheres.

This experiment, using data of 5 mm arc (1 atm.)
This experiment, using data of 5 mm arc (4 atm.)
This experiment, using data of 5 mm arc (8 atm.)
Frost and Liebermann (1 atm. theory)
Frost and Liebermann (8 atm. theory)
Frie (1 atm. theory)
This experiment, using data of 3 mm arc (1 atm.)
This experiment, using data of 3 mm arc (4 atm.)
This experiment, using data of 3 mm arc (8 atm.)
Motschmann (1 atm. experimental)
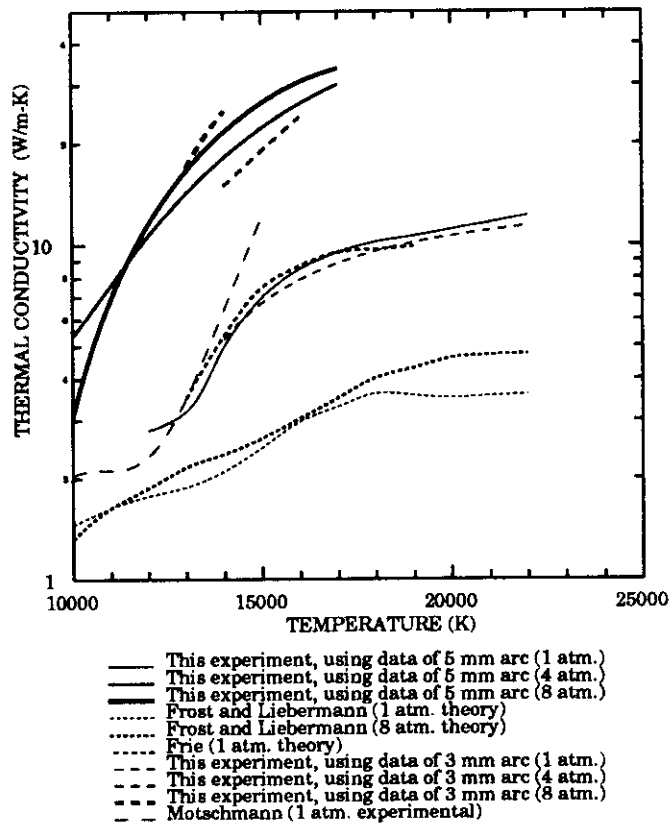
Figure 6.41: Thermal conductivity of SF_6 arc

79
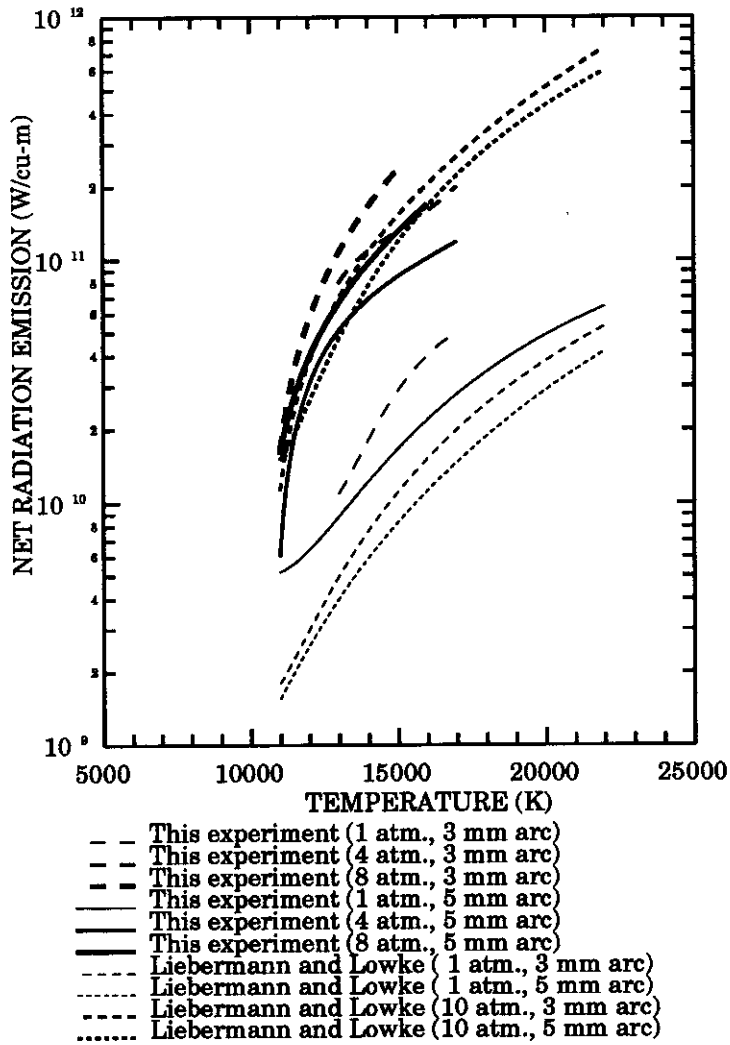
Figure 6.42: Net radiation emission of SF$_6$ arcs

Chapter 7

DISCUSSION

The major thrust of this work has been directed towards the measurement of transport properties of SF$_6$ at high pressures and temperatures. High temperatures which were achieved in this experiment ruled out the use of continuously running steady state arcs, since the thermal loading on the constricting plates would exceed the capacity of water cooled copper plates, which are limited to about 10 kw/cm^2. Theoretical calculations showed that, if the arc was operated in pulsed mode for short durations (10-20 ms), the constricting plates could withstand thermal loading of up to 20 kW/cm^2. Temperatures of up to 22,500K were achieved in this way without melting the cascade limiting plates. At this temperature, the maximum thermal loading on the cascade limiting plates was 16.5 kW/cm^2.

Spectroscopy was selected as a diagnostic tool in this investigation for a number of reasons. One, it was possible to do measurements from outside the corrosive environment of high pressure, high current SF$_6$ arcs. Two, a number of independent measurements could be made simultaneously in a short time interval (10-50 ms). Three, measurements with high spatial resolution could be made in the wavelength range of interest. Four, data could be cross correlated with other parts of the spectrum without repeating the experiment.

7.1   SF$_6$ Emission Data Calculations (Continuum Coefficient of Emission and Transition Probability)

As described in appendix B, the photographic method accumulates a massive amount of data that can be used to calculate various parameters, useful for future diagnostic work. In these experiments, the temperature measurements were at first made, using the absolute line intensity. But later on it was found that the temperatures determined, especially at higher pressure, were much lower than the theory predictions. Therefore, as a cross check, the temperatures were also calculated using absolute continuum intensities at 600.4 nm. For this purpose, the continuum coefficient of emission was evaluated from one-atmospheric data, which was then used for evaluating temperatures at 4 and 8 atmospheres pressure. It was possible to do these calculations without having to perform further experiments, since spectra were recorded for a 400 to 800 nm range.

Continuum Coefficient of Emission

Measurements of continuum coefficients of emission were made at five selected wavelengths 472.3, 573.3, 600.4, 621.0 and 666.6 nm. Values of the continuum coefficients,

81

$C(\nu)$, except at 666.6 nm, were calculated at atmospheric pressure. The continuum at 666.6 nm was affected by the strong H_α line at 656.3 nm in spectra at atmospheric pressure, inflating the value of $C(\nu)$, by a factor of four. Therefore, $C(\nu)$, at 666.6 nm, was calculated from the data at 8 atmospheres pressure where influence from the H_α line was negligible.

Continuum intensities measured at 4 and 8 atmospheres pressure were compared with the calculated intensities, using the evaluated value of $C(\nu)$ and the plasma composition. Figures 6.7 and 6.8, show that the calculated values compared well with the measured values.

Transition Probabilities

At a later stage it was decided to make use of some more data from the large accumulated bank of information recorded on the photographic plates. As a consequence, measurements have been made of the transition probability of the six most commonly used spectrum lines for the evaluation of SF_6 arc temperature. Four F_I lines at 720.2, 670.8, 641.4 and 623.9 nm, one S_I line at 469.5 nm and one S_{II} line at 545.4 nm, were considered. Transition probability for these lines was calculated using Olsen's method [53,52]. Correction for self-absorption was not necessary, since all the lines under consideration were optically thin [7]. But corrections were made to account for the demixing effect. Data for these corrections were taken from the Frie's theoretical calculations, since there was no gas flow in these arcs. The results of this experiment, given in table 6.2, were lower by up to 40% as compared to the theoretical estimates of Wiese [71,70].

7.2 Material Properties of Argon at 1 and 8 Atmospheres Pressure

Experiments were conducted to determine the E-I characteristic and the temperature profiles of nitrogen at atmospheric pressure and argon at 1 and 8 atmospheres pressure for a 5 mm diameter arc. Good agreement between these results and other experiments, as described in section 6.2, has helped in establishing the accuracy of the entire experimental procedures and calculating methods employed to determine the E-I characteristic and the temperature profile. E-I characteristic and temperature profile were the main input data from which the transport properties were extracted. Therefore, the accuracy with which the input data was measured, had a strong effect on the estimation of transport properties.

In the case of argon, experiments were conducted at 1 and 8 atmospheres pressure on 5 mm diameter arcs. Comparison of these results with the other experimental results especially at higher pressures, as described in section 6.2, established the accuracy of the high pressure measurements. Transport properties were also calculated from the measured E-I characteristic and temperature profiles.

The thermal conductivity, k, of argon, determined experimentally at atmospheric pressure had a maximum deviation of ±50%, from the theoretical values of Yos [47], shown in figure 6.20. This was quite an acceptable result considering the wide variation between the published results [40,19,47,53,13]. At 8 atmospheres pressure, the values of k were higher by up to a factor of two as compared to the theoretical estimates of Kovitya [40].

Thermal conductivity calculations of Yos [47], do not include contributions from the transfer of optically thick radiation and that may explain why his results are lower. As

shown in equation 7.4, such radiation is transferred through the plasma in a manner which is proportional to the temperature gradient and is, therefore, indistinguishable from other contributions to thermal conductivity. Due to these radiative exchanges, the net thermal conductivity measured in these experiments shows a strong pressure dependence. The effect of the radiation component on thermal conductivity becomes more clear in the case of SF_6, for which measurements were carried out for two different diameters, and it was possible to quantify the short absorption lengths in SF_6 arcs. This point is further discussed in detail in section 7.4.

The estimated values of net radiation emission for argon at 1 and 8 atmospheres pressure were also higher than those predicted by theory as described in section 6.6. As a part of the collaborative attack on this question, Cram [14], has calculated the net radiative power loss for argon arcs, which included thick radiation as well. His results were closer to the present measurements, but were higher than those of Yos [47], and Cambel [13]. It is significant, though, that both the total thermal conductivity and the radiation emission are higher than might have been predicted. Had the opposite been true, the detailed results would have been more open to question.

7.3   Temperature Profiles of SF_6 Arcs

Temperature measurements for SF_6 arcs at atmospheric pressure agreed well with the published experimental results which were limited to 17,500K [63]. In this experiment, the limit has been increased to 22,500K. At the same time, in comparison to the theoretical estimates, results of this experiment were lower by up to 15% at higher currents. This large difference in the calculated and measured temperature has been the main cause of concern and therefore, it has been investigated quite intensively.

At atmospheric pressure, the S_I line at 469.54 nm disappeared from the spectra above 18,000K and the F_{II} line at 444.69 nm appeared in the spectra recorded above 20,000K. This gave quite good rough estimates of the temperature range, and supported the measured temperatures.

At higher pressures also there was a sharp drop in the arc centre temperature. For example, at 200 amperes the temperature dropped by 4,200K from 1 to 4 atmospheres pressure and by 4,800K from 1 to 8 atmospheres pressure and the drop increased to 6,500 and 7,500K at 400 amperes for the respective pressure changes (refer to figure 6.32). In comparison to the theoretical predictions also, these results were lower by up to 15%. In view of these results, it was decided to determine the arc temperature at 4 and 8 atmospheres pressure using absolute continuum intensity at 600.4 nm. Temperatures were also measured using the H_α line profile at three points covering the entire temperature range. These measurements confirmed the accuracy of the temperatures calculated using absolute line intensities, and also showed that plasma was in LTE; the results are presented in table 6.5. In general, the results at all pressures were much lower when compared to the theoretical estimates.

Theoretical Calculation of Temperature Profiles

As pointed out earlier in chapter 6, temperature measurement was one of the most important factors in the evaluation of transport properties. For this reason, arc temperatures were measured using three different methods (absolute line intensity, absolute continuum intensity and H_α line profile method). To provide further support, the temperature was also calculated analytically, solving the time dependent energy balance

equation. The 'back' calculation for evaluating temperature profiles, using material properties determined in this experiment, provided strong support to the measured temperatures; shown in figure 6.32. At the same time, it established the credibility of the methods ('trial function' and 'form factor') used to extract material properties from the measured data.

Increase in the electric field for the pressure change from 1 to 4 atmospheres was two times higher as compared to the pressure change from 4 to 8 atmospheres. As a result there was a large increase in the electrical power input necessary to maintain the arc at higher pressures. Typically, at 360 amperes, 700 kW/m was required at 1 atmosphere as compared to 1100 and 1300 kW/m required at 4 and 8 atmospheres pressures, respectively, to maintain a 5 mm diameter arc. A large increase in the electrical power input, accompanied by a sharp reduction in the arc centre temperature, indicated a huge amount of power loss from the arc column. This meant that the energy transport mechanism in SF_6 became much more efficient as the pressure increased.

7.4 Material Properties of SF_6 at 1, 4 and 8 Atmospheres Pressure

Electrical Conductivity

Electrical conductivity is strongly dependent on the electron density in the plasma. As the temperature of the plasma increases, more atoms are ionized releasing electrons and thereby increasing the conductivity. At atmospheric pressure around 10,000K, the electrical conductivity of argon and SF_6 was significant from an arc point of view and increased rapidly up to 20,000K, because more and more electrons were stripped from the atoms due to the increase in number of collisions. As the number of electrons and ions increased, the electrical conductivity also increased. Electrons are relatively of very small mass, hence driven by a given field, they move at high speeds and are largely responsible for the current [37]. The rise in the electrical conductivity with the temperature meant that there was additional ionization up to 25,000K, where the conductivity and electron mole fraction became constant. This happened because the first ionization was complete, and the second ionization was not significant. If the temperature was increased further, the electrical conductivity would begin to increase again due to the second ionization.

The effect of increase in the plasma pressure was to increase the electrical conductivity, since at higher pressures the particle density was higher and this resulted in an increased number of energetic collisions at a given temperature, releasing more electrons.

For SF_6 at atmospheric pressure, the value of $\sigma(T)$, was in agreement with theory [24], except for temperatures around 10,000K where it was higher by up to a factor of two. This could be due to the inability of the 'trial function' to fit this type of variation in the value of $\sigma(T)$, [16]. Moreover, the minimum measured temperature was higher than 11,000 K. Therefore, values of measured $\sigma(T)$ below this temperature may not be very accurate. At 4 and 8 atmospheres pressure, values of $\sigma(T)$, were higher by up to 30%. Above 18,000K, increase in the electrical conductivity with the temperature slows down due to the completion of the first ionization process. It would increase more rapidly again beyond 25,000K when second ionization becomes appreciable. But this experiment does not extend to such higher temperatures. The estimated error associated with the evaluation of $\sigma(T)$, was ±6%, ±7% and ±9% at 1, 4 and 8 atmospheres pressure respectively.

Thermal Conductivity

The net thermal conductivity of a plasma is a complex function of temperature and depends upon different internal events which are described as follows.

Translation Component

In plasma having a certain temperature gradient, some of the faster moving heavy particles (atoms and ions) travel to the low temperature region and lose their kinetic energy in the process. Similarly, some of the slower moving heavy particles wander into the high-temperature region and absorb energy. This translation of energy associated with the temperature gradient contributes significantly towards the thermal conductivity at low plasma temperatures. But for the temperature range of this experiment, this component was small.

At the higher temperatures encountered in these experiments, electrons moving at a very high speed as compared to heavy particles contribute much more towards the thermal conductivity. The increase in this component is proportional to the growth of the electron population density with temperature [37].

Reactional Component

This component of thermal conductivity results from dissociation and ionization processes in the plasma. The plasma has a certain composition at a temperature and if there is a temperature gradient between two points in the plasma, the electrons and the ions will diffuse from the higher density region. This diffusion causes an imbalance in the equilibrium in the lower temperature region. To maintain equilibrium, some of the electrons and ions recombine by three body recombination processes, releasing the ionization energy, which appears as kinetic energy and is responsible for this contribution to the thermal conductivity. This component is significant only in the temperature range in which the equilibrium composition changes rapidly with the temperature, for example, at temperatures corresponding to strong dissociation of molecules and first and second stages of ionization. As the ionization process becomes complete, the reactional component of thermal conductivity declines.

Radiation Component

The effect of this factor on thermal conductivity is not yet fully understood and is extremely difficult to quantify. Basically, there are two kinds of radiation losses from the arc.

1. The net radiation emission, u, from the the arc which is dominated by the ultraviolet (uv) and vacuum uv regions of the spectrum. This is reabsorbed and radiated again. The process continues all along the arc radius as radiation tries to escape towards the outer edge of the arc. Finally, part of the radiation may be completely reabsorbed at the outer edge of the arc which is at a low temperature, leaving the net escaping radiation.

2. The transparent radiation emission, u_t, which, once radiated, is completely lost from the arc. It is dominated by the visible region of the spectrum and the far wings of resonance lines. u_t is generally very small as compared to u. Taking these factors into account, the energy balance equation can be written as follows [35],

$$\sigma E^2 = \nabla.k\nabla T + \int \frac{d\Omega}{4\pi} \int d\nu \left[\kappa_\nu (I_\nu - B_\nu)\right], \tag{7.1}$$

where

σ = electrical conductivity
E = electric field
k = thermal conductivity
T = temperature
ν = frequency
κ_ν = absorption coefficient
I_ν = specific intensity
B_ν = Planck function
$\overline{I}_\nu$ = mean intensity

The first term represents a thermal conduction loss and the second the radiation loss. Equation 7.1 can be rewritten [14], splitting the radiation loss into two parts, one related with the thick radiation which is reabsorbed and the other with the thin or transparent radiation which escapes the arc.

$$\sigma E^2 = \nabla.k\nabla T + \int d\nu \left[\kappa_\nu (\overline{I}_\nu - B_\nu) \right] \tag{7.2}$$

$$\sigma E^2 = \nabla.k\nabla T + \int_{thick} d\nu \left[\kappa_\nu (\overline{I}_\nu - B_\nu) \right] + \int_{thin} d\nu \left[\kappa_\nu (\overline{I}_\nu - B_\nu) \right] \tag{7.3}$$

$$\sigma E^2 = \nabla.k\nabla T + \left[\int_{thick} d\nu \left(\frac{\kappa_\nu}{3} \frac{\delta B_\nu}{\delta T} \right) \right] \frac{\delta T}{\delta r} + \int_{thin} d\nu \kappa_\nu \left[\overline{I}_\nu - B_\nu \right] \tag{7.4}$$

The second term in equation 7.4, representing the fraction of the net radiation which is reabsorbed within the arc, is a function of the temperature gradient. This contribution to the thermal conductivity is extremely difficult to estimate. There is no theory at present which can be used to estimate accurately the selfabsorption of lines which are mostly in the uv region [41]. The scope of this work does not extend to the detailed investigation of this phenomenon. Moreover, as far as the engineering development of switching arcs is concerned, it is the end result of all these processes which influence, the effective thermal conductivity that is of ultimate importance and not a detailed analysis which includes complex geometrical relationships describing the absorption process and their integrals over the full spectral range and ray paths within the arc column. Measurements of net radiation emission for 3 and 5 mm diameter arcs throw some light on this point, and will be discussed later in this section.

Experimental thermal conductivity measurements of SF_6 at atmospheric pressure were in close agreement with the theoretical results of Frie [22] and the experimental results of Motschmann [50]. But in comparison with the most recent theoretical results of Frost and Liebermann [24], which were thought to be an improvement upon their earlier work, the results of this experiment were higher by a factor of three. At 4 and 8 atmospheres pressure, the values of k measured in this experiment were higher by factors of 6 and 8 respectively. In addition to the higher values of k, the net radiation emission was also higher by up to a factor of three at 8 atmospheres pressure. This was an approximation based upon the theoretical estimate of Liebermann and Lowke [41] for a 5 mm diameter arc at 10 atmospheres pressure. There were three areas in this work which could have adversely affected the estimation of thermal conductivity. These are discussed below.

1. 'Form Factor' method

There were two parameters in this method which could affect the estimation of thermal conductivity. One, the rate of change of the electrical power input and the

radiative power output with the arc centre temperature. This could have a significant affect on k, only if the values of P_e and P_u, were progressively over or under-estimated. Two, the two form factors (electrical and radiation), which depend upon temperature profiles. It has been shown by Ter Horst [55] that, even if the form factors are assumed to be of a constant value equal to one, the maximum error of less than 23% is introduced. In the present calculations actual form factors have been determined using equations 2.34 and 2.37 and, therefore, the errors were expected to be even less.

2. Copper vapour

Presence of copper vapour in the SF_6 plasma could also introduce serious error into the evaluation of thermal conductivity, especially at higher temperatures and pressures. For this reason, the spectra were carefully scanned and no copper line was detected. Copper vapour, even in a small amount, would increase the electrical conductivity by a large amount and thereby lower electric field for a given current. E-I characteristics measured in this experiment do not show any such trend even at high currents and pressures.

Therefore, presence of copper vapour in the SF_6 plasma studied here was ruled out completely.

3. Arc geometry

The effect of arc diameter on the evaluation of transport properties was investigated by calculating transport properties using the data from two different diameter (3 and 5 mm) arc measurements. If the heat generation and loss has been properly modelled, the thermal conductivity should not change with the arc diameter; as shown in figure 6.41. This figure shows that, within the experimental errors, the thermal conductivity calculated from the two arc diameters is almost the same.

However, the results of figure 6.41 show very strong sensitivity of the thermal conductivity to arc pressure. For example at a temperature of 15,000K, the thermal conductivity at 4 atmospheres is approximately four times the thermal conductivity at one atmosphere pressure. Theoretical calculations of Frost and Liebermann, which suggest that there should be very little change, do not include the effect of optically thick radiation as part of an apparent thermal conductivity contribution. If one turns one's attention to the net radiation from arcs of different diameters having radiative absorption distances comparable with a millimetre, the 3 and 5 mm arcs should indeed show a substantial difference as indeed they do; shown in figure 6.42. This figure shows that, for an arc of 3 mm diameter as compared to 5 mm diameter, there is an increase in total radiation loss per unit volume almost exactly in proportion to the ratio of the different arc sizes, bearing in mind that the radiation is lost in all directions and at all angles to the arc axis. The overall picture suggests that there is a substantial amount of radiation in an SF_6 arc which has an absorption length of the order of one millimetre. If that is indeed the case, there may well be an explanation for the excellent performances of SF_6 as an arc quenching gas, namely that the arc diameters near current zero for the switching process are recognised to be less than a millimetre in diameter and, therefore, should provide a very considerable amount of increased radiative cooling.

These new experimental values of thermal conductivity, which are much higher than theory and at the same time are strongly pressure dependent, would provide a possible explanation for the excellent quenching capability of SF_6. High values of thermal conductivity would have a strong effect in cooling the arc at the lower temperatures encountered near current zero conditions. This influence on arc interruption would be multiplied with the increase in pressure. Since transient pressure can be very high dur-

ing the high current interruption, the pressure dependent thermal conductivities would also have a far stronger effect on it.

Net Radiation Emission

The net radiation emission was calculated by solving the energy balance equation, since $\sigma(T)$ and $k(T)$ were known. As has been pointed out earlier, the radiation emission at the arc centre dominates the absorbed radiation and the difference of the two yields a significant contribution to the energy transport. At positions away from the arc axis, absorption of radiation becomes large and finally almost all the radiation is absorbed near the arc boundary. Although there is a very small amount of radiation that escapes from the arc, the radiative heat transfer plays an important part in determining the temperature profile inside the arc column.

At atmospheric pressure for a 5 mm diameter arc, the net radiation emission was about two times higher than the theoretical estimates. At 4 and 8 atmospheres pressure results could not be compared due to the lack of published data, although a rough estimate at 8 atmospheres pressure was made on the basis of 10 atmospheres pressure results of a 5 mm diameter arc [41]. This also showed that the estimates of this experiment were higher. Because experimental thermal conductivity was also higher, especially for SF_6 at 4 and 8 atmospheres, the results obtained in these experiments were not, within themselves, in conflict.

Most puffer circuit breakers, operate at pressures of more than 4 atmospheres and, when interrupting high currents, produce much higher transient pressures. Since the present findings indicate that the effective thermal conductivity is dominated by radiative transfer for temperatures above 10,000K, it is likely that this mechanism, along with some degree of turbulance, rather than turbulence alone [33], may be responsible for the enormously high heat loss rates observed in this gas.

Chapter 8

SUMMARY AND CONCLUSION

The main objective of this work was to determine experimentally the transport properties of SF_6 at high temperatures and pressures. To date, much of the data used for circuit breaker modelling has been calculated theoretically and has not been verified experimentally. The literature does give experimental values at atmospheric pressure but it does not go up to 25,000K. In addition to the work reported here on SF_6 which extends up to 22,500K at atmospheric pressure, experiments were also conducted on nitrogen and argon. This was primarily done to compare the new results of nitrogen and argon obtained in this work with the other experimental and theoretical results. It checked the accuracy of this experiment and gave confidence for further work on SF_6. Before embarking upon the major experimental work, a preliminary investigation relating to impurities detection in SF_6 was conducted, details of which are given in appendix A. This provided a good description of SF_6 spectra and was used to locate well isolated lines which could be used for the absolute line intensity measurements. Five continuum regions were also identified for the evaluation of temperature. A computer code written for the relative intensity calculations served as a basis for further programming developments regarding absolute line and continuum intensity calculations.

The photographic method of recording the spectrum resulted in the accumulation of a massive amount of data. From the analysis of this data, transport properties were extracted and at the same time it provided a wealth of other information in the form of continuum coefficients of emission and absolute transition probabilities of selected lines. Measured values of five continuum coefficients at different wavelengths provided useful data for the spectrographic measurement of SF_6 arc temperatures, especially at the higher pressures, when the line intensities may be self-absorbed. Besides this, continuum coefficients can always be used for cross checking the temperatures measured using absolute line intensities, as has been done in this experiment.

The previous experimental evaluation of transition probabilities by Schulz-Gulde [61,62] has indicated that the theoretical estimates given by Wiese [71,70] for F_I lines of the (3p-3s) transition are inflated by up to 40%. Transition probabilities measured in these experiments have confirmed the same conclusion and were in good agreement with the previous experimental evaluations [61,62], determined by a different approach, in which demixing corrections were made using data from their own experiment which had accounted for the gas flow in the arc. In the present experiment there was no gas flow in the arc, therefore, demixing corrections were made using theoretical estimates of Frie [22], which were calculated for the arcs without the gas flow. The agreement between this experimental evaluation of transitional probabilities and those of Schulz-Gulde also indicated that Frie's estimates of demixing were correct and that a much simpler technique of determining transition probabilities as proposed by Olsen [53,52],

can be used for SF₆ arcs.

Calculation methods employed for extracting experimental transport properties have been described in chapter 2. The 'trial function' technique employed for the evaluation of the electrical conductivity permitted calculations of $\sigma(T)$, with measurements at only a few currents which need not be close together in value. Furthermore, there was no necessity to commence measurements at lower temperatures in order to construct the curve of $\sigma(T)$ at higher temperatures [19].

The actual 'form factor' method for determining thermal conductivity has been used quite successfully in this experiment. It is a simple method and the error of 30% associated with it was considered acceptable compared to the large variations between the published values of $k(T)$.

Electrical conductivity of argon at different pressures was in reasonable agreement with the other experimental and theoretical results. Thermal conductivity of argon at 1 and 8 atmospheres pressure was higher than the theoretical estimates, especially at higher pressure, and showed strong pressure dependence. Net radiation emission for argon at 1 and 8 atmospheres pressure was also higher compared to the earlier estimates of Morris, Rudis and Yos [47], but was in fair agreement with the recent theoretical estimates of Cram [14] which account for the thick radiation. Good experimental results for argon, obtained in these experiments, have also established the accuracy of the calculating methods which have been employed to extract transport properties from the measured data.

Temperature measurements of SF₆ arcs at 1, 4 and 8 atmospheres pressure were made using the absolute intensity of the F_I line at 720.2 nm. At 4 and 8 atmospheres pressure, temperature measurements were cross checked with the absolute continuum intensity and H_α line width measurements. These results confirmed the values obtained using the absolute line intensity. Temperature was also calculated analytically by solving the time dependent energy balance equation and using material properties measured in this experiment. The calculated arc temperatures were in good agreement with the experimental estimates. Therefore, strong confidence can be placed in the measurement of temperature at different pressures.

There were five factors which could have introduced serious errors in the evaluation of transport properties. One, wrong experimental procedures adopted for measuring and calculating E-I characteristic and temperature profiles. Two, presence of copper vapour in the SF₆ plasma, which could have lowered the E-I characteristic and increased the thermal conductivity values. Three, self-absorption of the line intensity, which could have lowered the arc temperatures. Four, inherent defect in the calculating methods which have been employed to extract transport properties from the measured data. Five, geometry of the arc.

These areas have been discussed in detail in the previous chapter, and it has been proved conclusively that the results of these experiments could not have been affected by any of the above mentioned factors.

Transport properties of SF₆ arcs (except for σ) were much higher so as to be in complete disagreement with the theoretical estimates of Frost and Liebermann [24]. This was especially true for the high pressure results. On the other hand, at atmospheric pressure, the thermal conductivity agreed well with the theoretical estimates of Frie [22], and existing experimental results of Motchmann [50], which were limited to 14,000K. In this experiment, the range has been extended to 22,500K. But these results were three times higher than the theoretical estimates of Frost and Liebermann [24]. Thermal conductivities at 4 and 8 atmospheres pressure were also high by a factor of six and

eight respectively. At the same time the net radiation emission at 1, 4 and 8 atmospheres pressure was higher by up to a factor of three. Since the thermal conductivity and the net radiation emission were both higher than the estimated theoretical results, it was highly unlikely that error in the measurement of one parameter was reflected in the estimate of the other.

As a consequence of measurements being carried out for 3 and 5 mm diameter arcs, over a range of pressures, for the first time in SF_6, it has been possible to demonstrate the effect of radiation absorption within the arc. Radiation measurements for two different diameter arcs have revealed that radiative exchanges of SF_6 arcs, over distances of the order of a millimeter, do produce substantial losses of cooling effect by radiation processes. This geometrical situation does in fact occur near current zero in gas blast arcs at these pressures (5 to 10 atmospheres). Although it has not been demonstrated here that the excellent quality of SF_6 as an interrupting medium are due to the radiative exchanges, the results of the experiments point to this as an area of further study. The pressure dependence of this cooling process may also help to explain the strong pressure dependence of the interrupting ability of the gas-blast, sulfur hexafluoride arc.

Bibliography

[1] *Kodak Plates and Films for Scientific Photography.* publication no. p-315 edition, 1973.

[2] W. deW. Abney. . *Photogr. J.*, 18(N.S.):302, 1894.

[3] D.R. Airey, P.H. Richards, and J.D. Swift. . *J. Phys. D: Apply. Phys.*, 8:1982, 1975. See also; Proc. of IEE Gas Discharge Conf. Swansea, 143:8, 1976.

[4] J.F. Armstrong. Private communication; School of Electrical Engineering, University of Sydney.

[5] E.I. Asinovsky, A.V. Kirillin, E.P. Pakhomov, and V.I. Shabashov. . *Proceedings of the IEEE*, 59(4):592, 1971.

[6] W.L. Bade. . *Phys. Fluids*, 5:150, 1962.

[7] G. Baruschka and E. Schulz-Gulde. . *Astron. and Astrophys.*, 44:335, 1975.

[8] U.H. Bauder. . *IEE Proc. of Gas Discharge*, 351, sep 1970.

[9] U.H. Bauder and R.S. Devoto. . *ARL Rep. 70-0135*, 115, aug 1970.

[10] U.H. Bauder and H Maecker. . *Prceedings of the IEEE*, 59(4):588, 1971.

[11] K. Behringer, W. Kollmar, and J Mentel. . *Z. Physik*, 215:127, 1968.

[12] R.D. Bengtson, M.H. Miller, D.W. Koopman, and T.D. Wilkerson. . *Phys. Rev. A*, 3:16, 1971.

[13] A.B. Cambel. *Plasma Physics and Magnetofluid-mechanics.* McGraw Hill, 1963.

[14] L. Cram. . *J. Phys. D: Appl. Phys.*, 18:401, 1985.

[15] R.S. Devoto. . *J. Plasma Phys.*, 2:617, 1968.

[16] R.S. Devoto and D. Mukherjee. . *J. Plasma Phy.*, 9(1):65, 1973.

[17] H. Dienemann. . *J. Phys. D: Apply Phys.*, 16:1651, 1983.

[18] H. Dienemann, K.P. Hinz, and H.J. Freyer. . *J. Phys. D: Apply. Phys.*, 18:2207, 1985.

[19] H.W. Emmon. . *The Phy. of Fluids*, 10(6):1125, 1967.

[20] K.A. Ernst, J.G. Kopainsky, and H.H. Maecker. . *IEEE Trans. Plasma Science*, 1:3, dec 1973.

[21] R.H. Fowler and E.A. Milne. . *Monthly Notices Roy. Astron. Soc., London*, 83:403, 1923. See also; ibid, 84:499, 1924.

[22] W. Frie. . *Z. Physik*, 201:269, 1967.

[23] R.E. Friedrich and R.N. Yeckley. . *AIEE Trans. Power App. Sys.*, 68:695, oct 1959.

[24] L.S. Frost and R.W. Liebermann. . *Proc IEEE*, 59(4):474, 1971.

[25] S. Gordon and B.J. McBride. . Technical Report SP-273, NASA special publication, 1971.

[26] H.R. Griem. *Plasma Spectroscopy*. McGraw Hill, 1964.

[27] N.T. Grier. *NASA Tech. Note*. Technical Report TN D3186, NASA, apr 1966.

[28] K. Halbach. . *Am. J. Phy.*, 32:90, 1964.

[29] J.F. Hamilton. *The Theory of the Photographic Process*. Volume Section II-A, Macmillan NY, 4 edition, 1977.

[30] C.F. Hansen, R.A. Early, F.E. Alzafon, and Witteborn F.C. *NASA Tech. Report*. Technical Report R-27, NASA, 1959.

[31] G.R. Harrison, R.C. Lord, and J. R. Loofbourow. *Practical Spectroscopy*. Prentice Hall Inc., 1959.

[32] R.A. Hartunian and P.V. Marrone. . *Phys. Fluids*, 4:535, 1961.

[33] W. Hermann, U. Kogelschatz, L. Niemeyer, K. Ragaller, and E. Schade. . *J. Phys. D: Appl. Phys.*, 7:1703, 1974.

[34] W. Hertz, H. Motschmann, and Wittel. . *Proc IEEE*, 59(4):485, 1971.

[35] J.T. Howe and Y.S. Sheaffer. . *J.Q.S.R.T.*, 7:695, 1967.

[36] R.H. Huddlestone and S.L. Leonard. *Plasma Diagnostic Techniques*. Academic Press, New York, 1965.

[37] W. Ibele. *Modern Developments in Heat Transfer*. Academic Press, 1963.

[38] D.J.G. Irwin and A.E. Livingston. . *Canadian J. Phys.*, 51:848, 1973.

[39] C.F. Knopp, R.W. Liebermann, W.L. Bade, and J.M. Yos. . *Phenomena in Ionized Gases*, 2:112, 1965.

[40] P. Kovitya. *Theoretical Determination of Material functions...* Tech. Memo. 3, CSIRO Div. of Appl. Phys., Sydney, Australia, 1982.

[41] R.W. Liebermann and J.J. Lowke. . *J.Q.S.R.T.*, 16:253, 1976.

[42] H. Maecker. . *Z. Physik*, 157:1, 1959.

[43] H. Maecker. . *Z. Naturforsch*, 11(a):457, 1956.

[44] H. Maecker. . *Ann. Physik*, 18(6):441, 1956.

[45] H.H. Maecker. . *Z. Physik*, 158:392, 1960.

[46] G.N. Minerbo and M.E. Levy. . *SIAM J. Numer. Anal.*, 6(4):598, 1969.

[47] J.C. Morris, R.P. Rudis, and J.M. Yos. . *Phys. Fluids*, 13:608, 1970.

[48] H. Motschmann. . *Z. Physik*, 214:42, 1968.

[49] H. Motschmann. . *Z. Physik*, 191:10, 1966.

[50] H. Motschmann. . *Z. Physik*, 205:235, 1967.

[51] D. Muller. . *Z. Naturforsch.*, 23(a):1707, 1968.

[52] H.N. Olsen. . *JQSRT*, 3:305, 1963.

[53] H.N. Olsen. *In Temperature, Its Measurement and Control in Science and Industry.* Volume 3, Reinhold Publ. Corp., 1962. C.M. Herzfeld, editor.

[54] T.D. Peng and W.F. Ahtye. *NASA Tech. Note D-687.* Technical Report, NASA, 1961.

[55] H.M. Pflanz and D. Th. J. TerHorst. . *Proc IEEE*, 59(4):601, 1971.

[56] S. Ramakishnan. Private communication; C.S.I.R.O., Melbourne, Australia.

[57] A. Rehnstrom. . *Jr of App. Photographic Engg.*, 3:185, 1977.

[58] R.D. Richtmyer and K.W. Morton. *Difference Methods for Initial Value Problems.* Interscience, New York, 1967.

[59] J. Scheiner. . *Bull. Comite Permanent Intern. pour l'Execution Photogr. de la Carte du Ciel*, 1:227, 1889.

[60] C.A. Schmidt-Harms. . *J. Phys E: Sci. Instrum.*, 18:705, 1985.

[61] E. Schulz-Gulde. . *Z. Physik*, 245:308, 1971.

[62] E. Schulz-Gulde and A. Wenzel. . *J. Phys. B: Atom. Molec. Phys.*, 13:3733, 1980.

[63] E. Schulz-Gulde and T. Worzyk. . *XVI Int. Conf. on Phenomena in Ionized Gases, Duesseldorf*, 500, 1983.

[64] K. Schwarzschild. . *Astrophys. J.*, 11:89, 1900.

[65] P.J. Shayler and M.T.C. Fang. . *J. Phys. D: Aplly. Phys.*, 11:1743, 1978.

[66] A.D. Stokes. . *J. Phys. D: Appl. Phys.*, 4:930, 1971.

[67] D.Th.J. Ter Horst, H. Brincmann, and J.S. Ornstein. . *Physica*, 2:652, 1935.

[68] D. Th. J. TerHorst and H.M. Pflanz. . *Z. Phys.*, 198:508, 1967.

[69] R.H. Tourin. *Spectroscopic Gas Temperature Measurement.* Elsevier Publishing Company, New York, 1966.

[70] W.L. Wiese, M.W. Smith, and B.M. Glennon. . *N.S.R.D.S.- National Bureau of Standards 4*, 1, 1966.

[71] W.L. Wiese, M.W. Smith, and B.M. Miles. . *N.S.R.D.S.- National Bureau of Standards 22*, 2, 1969.

[72] A.W. Witmer, J.A.J Jansen, G.H. VanGool, and G. Brovwer. . *Phillips Tech. Review*, 34:322, 1974.

[73] J.M. Yos. *AVCO/RAD*. Technical Report RAD-TM-3-7, Wilmington, Mass., USA, mar 1963. See also; ibid, RAD-TR-65-7, May 1965.

Appendix A

Preliminary Investigation of SF_6 Arcs

Before embarking upon the main project for the determination of the transport properties, some preliminary investigation of SF_6 arcs was conducted.

A.1 Introduction

The main aim of this preliminary exercise was to obtain a general description of the spectra by identifying all the lines and their relative intensities. At the same time the information was used to evaluate the use of the spectrographic method for assessing contamination levels in used SF_6.

A.2 Experimental Set-up and Procedure

A test cell was designed and fabricated for these studies. It consisted of two hollow electrodes made from spectrographic grade carbon. These electrodes were enclosed in a Pyrex glass tube of 50 mm diameter and 140 mm in length. It was held at both ends by two Perspex end fittings, figure A.1. One of the electrodes was fixed and the other could be moved to set the desired gap between the two electrodes. The whole unit was sealed by three 'O' rings, two for the end fittings and one for the movable electrode. The shape and size of the electrodes was selected after various designs were tried and investigated to produce stable arcs. These studies were conducted by fast photography of the arc, using an Imacon image converter camera. The trials had shown that the arc was most stable with the electrode shape shown in figure A.2 under the following conditions:

- Electrode gap 2 to 3 mm.

- Arcing current 30 to 50 amperes.

- Breakdown voltage 10 to 14 kV.

- Pressure 300 to 400 torr.

It was found that the rate of pressure drop also affected the arcing and it was most stable at pressures below atmospheric with the evacuating cylinder pressure at 500 torr.
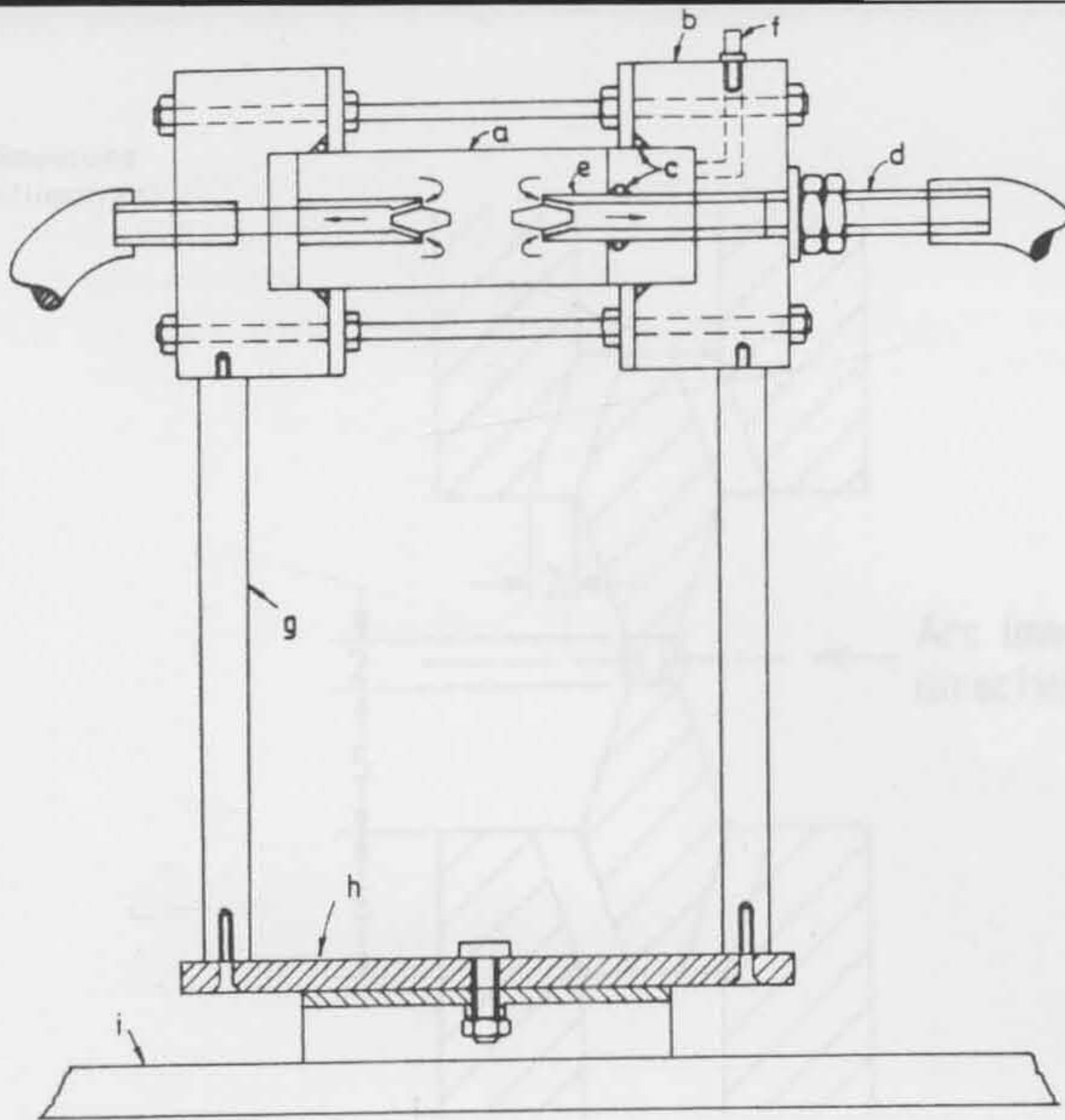
a – Pyrex glass tube
b – Perspex end fittings
c – 'O' rings
d – Electrodes
e – Graphite electrode tip

f – Pressure transducer
g – Perspex leg support
h – Base plate
i – Optical bench
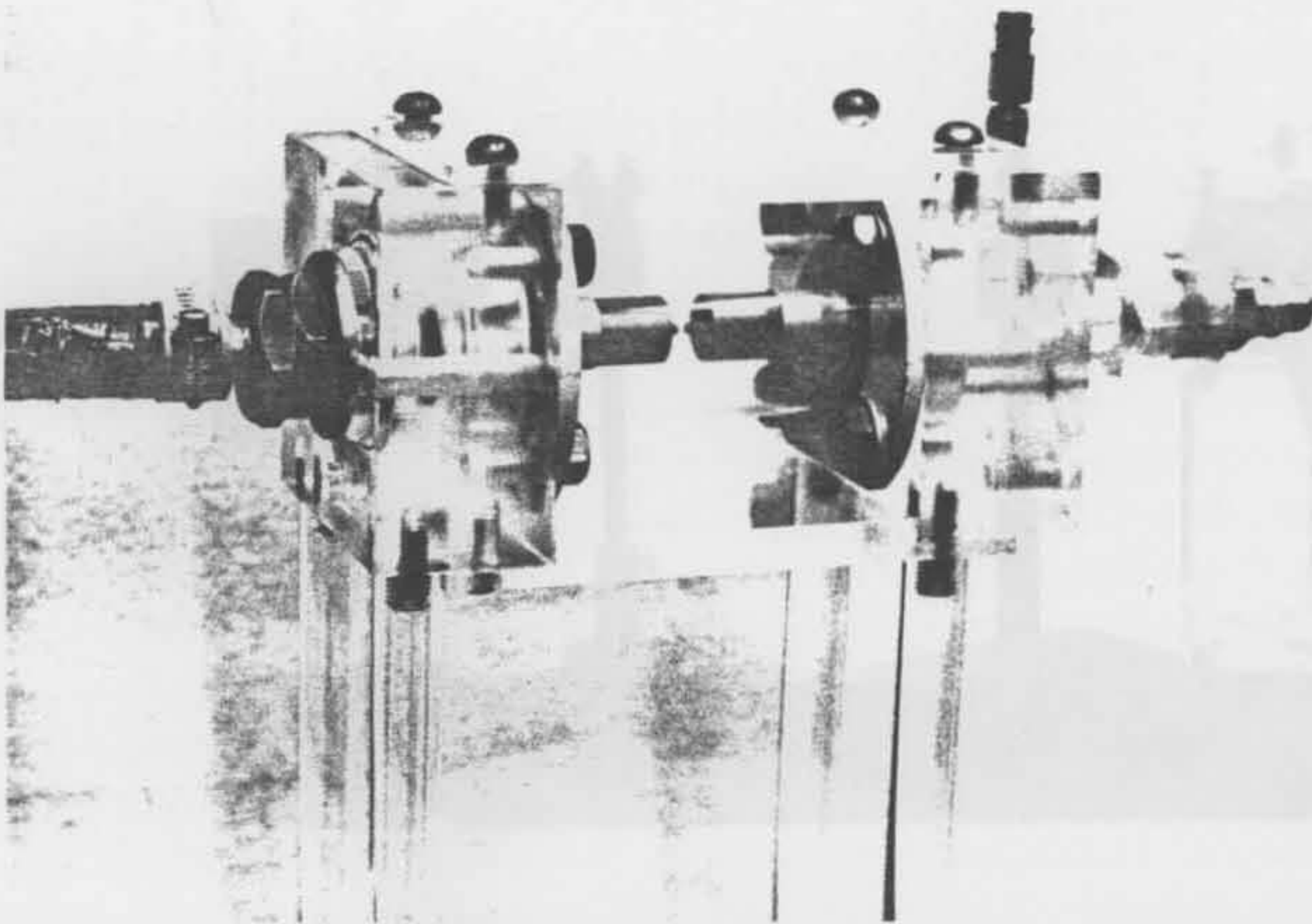
Figure A.1: The test cell
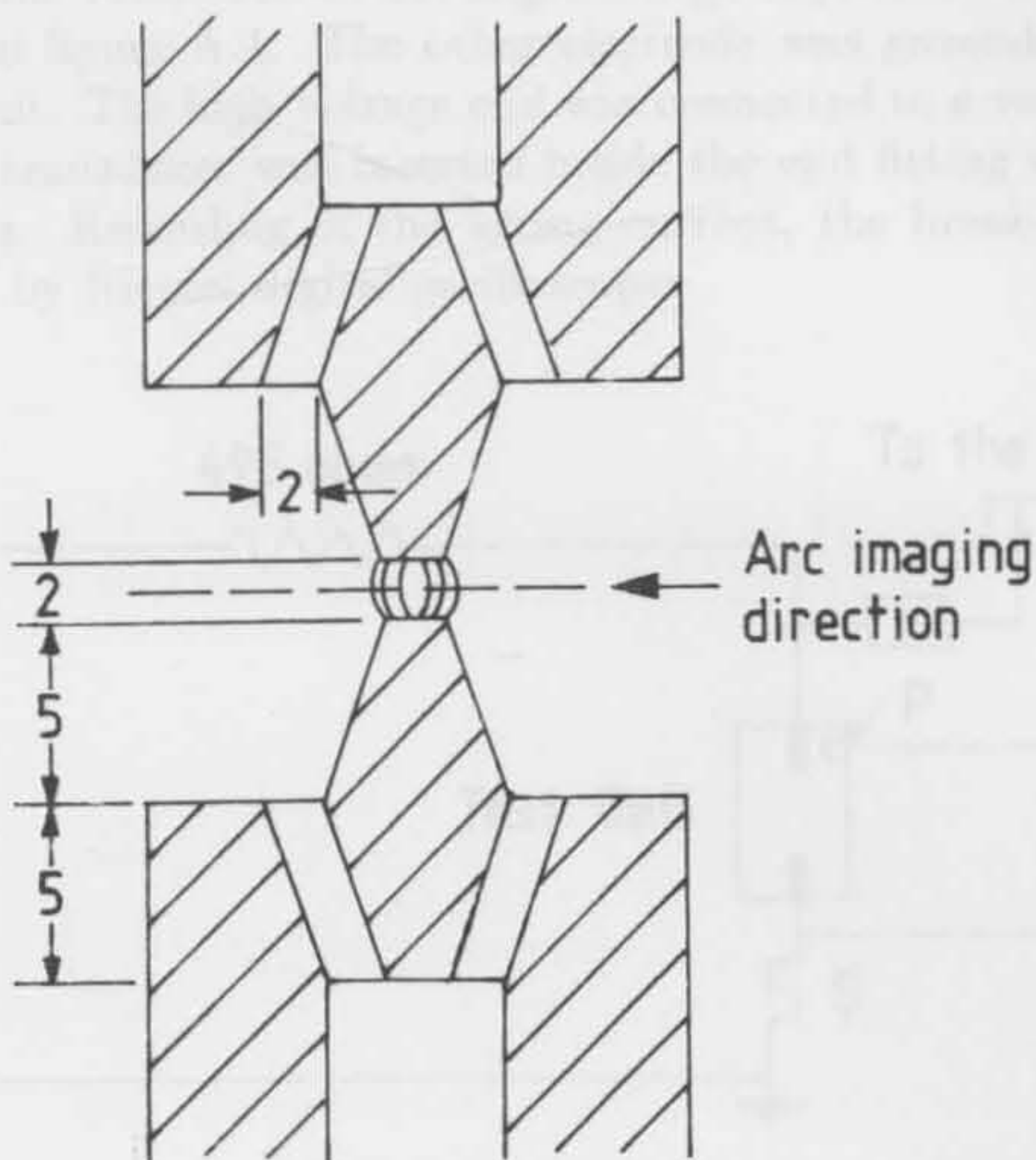
Figure A.2: Electrode shape and arc geometry
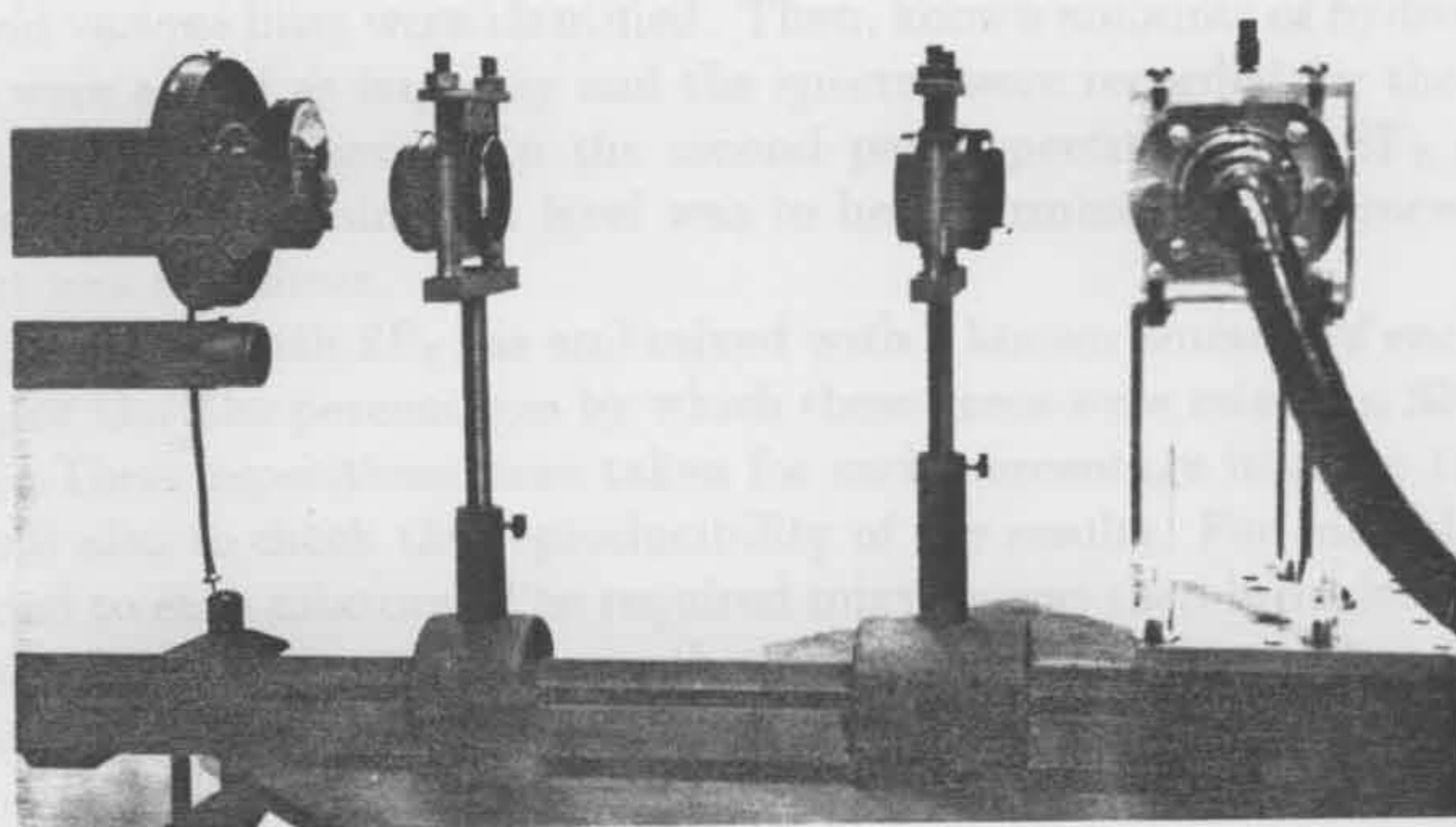
Figure A.3: Optical set-up for the test cell

One of the electrodes was connected to the high-voltage capacitor bank through a 495-Ω resistor, as shown in figure A.4. The other electrode was grounded through a shunt to measure the current. The high-voltage end was connected to a voltage divider. A capacitor-type pressure transducer was inserted inside the end fitting of the cell for the pressure measurements. Recording of the arcing current, the breakdown voltage and the pressure was done by Nicolet digital oscilloscopes.
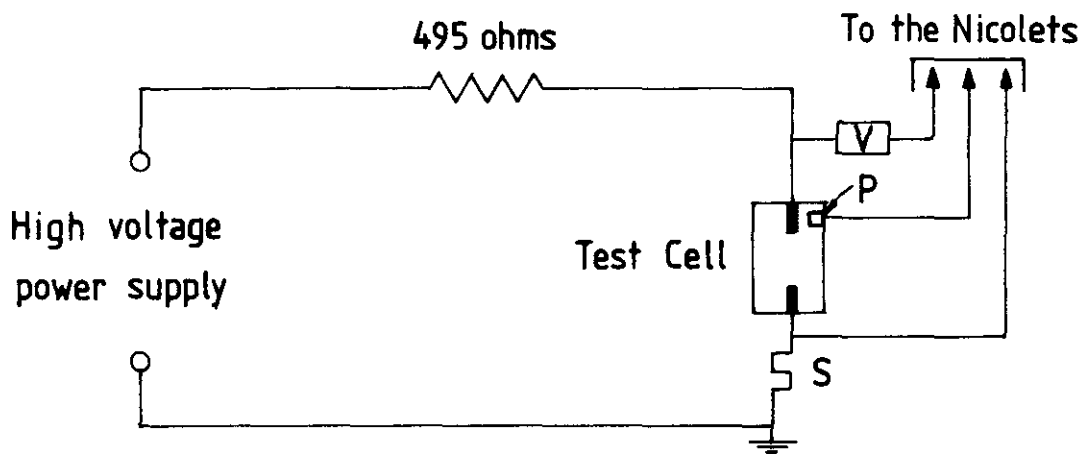
V — Voltage divider (1 volt / 1000 volts)

P — Pressure transducer

S — Current shunt (1 volt / 190 amperes)

Figure A.4: Electrical circuit for the impurity measurement

The experiment was conducted in two parts. In the first part, a pure SF$_6$ spectrum was taken and various lines were identified. Then, known amounts of hydrogen, nitrogen and oxygen were added as impurity and the spectra were recorded for the construction of impurity calibration curves. In the second part, spectra of the SF$_6$ samples were taken in which the contamination level was to be determined. The procedure followed for each part was as follows.

The cell was filled with SF$_6$ gas and mixed with a known amount of each of the three gases H$_2$, N$_2$ or O$_2$. The percentages by which these gases were mixed in SF$_6$ varied from 0.05 to 20%. Three repetitions were taken for each percentage in order to average out the errors and also to check the reproducibility of the results. For control, 2% of argon was also added to each mixture. The required mixture was then brought to atmospheric pressure and voltage was applied across the electrodes. Flashover and arcing took place as the pressure inside the cell dropped by the evacuation of the gas from the cell as an electromagnetically activated valve opened the passage to a dump cylinder.

In the second series of tests, contaminated samples of SF$_6$ were filled into the cell and mixed with 2% of argon as control. The mixture was then brought to atmospheric pressure. Arcing took place as in the first series of tests.

A Steinheil model GH universal spectrograph was used for the recording of these spectra. The details of the spectrograph and the spectrum recording procedures are

described in chapters 3 and 4, respectively. The centre of the arc was focused on the entrance slit of the spectrograph, as shown in figure A.2. On each plate, a series of unknown spectra were recorded together with a reference spectrum of a Hg-Cd lamp and one intensity calibration spectrum of a standard tungsten filament lamp. Photographic and data acquisition procedures employed in this experiment are described in section 4.3.

A.3 SF$_6$ Spectra

The Spectrograph was set to record the spectrum from 400 to 800 nm. The lines were identified using Hartmann's interpolation equation A.1:

$$\lambda = \lambda_0 + \frac{c}{d - 2d_0} \qquad (A.1)$$

where
    λ_0, c and d_0 are constants,
    d is the distance of a line from the reference position d_0,
    λ is the wavelength of the line.

The values of λ_0, d_0 and c were calculated from the wavelength of three known lines of the Hg-Cd reference spectrum in the wavelength region of the unknown lines. All the other wavelengths of the unknown lines were calculated using this equation. For better accuracy ($\pm$.05 nm), the spectrum range was split up into four sections of 100 nm each and a new set of constants was calculated for each 100 nm range. The dispersion curve for this setting of the spectrograph was determined from these calculated wavelengths of the sulfur and fluorine lines and is shown in figure A.5. The dispersion of the lines in the blue region was five times larger (1 nm/mm) than that in the red region (5 nm/mm) of the spectrum.

All the identified lines of the SF$_6$ spectrum are shown in figures 6.5 and 6.6.

A.4 Impurity Calibration Curves for Hydrogen, Nitrogen and Oxygen

For the construction of the impurity calibration curves, three lines were selected for each of the three gases. Calculations for the three lines were made because the line intensity response to the changes in the concentration varies with each line [31].

For hydrogen, the 656.3, 486.1 and 434.0 nm lines were selected for determining impurity calibration curve. The H$_\alpha$, 656.3 nm, line was the strongest line with strong continuum in its vicinity, due to which the combined density of the line and the continuum reached the saturation limits of the H-D curve. Therefore large errors were introduced in the intensity measurements.

For the H$_\beta$, 486.13 nm, line the density variation for the concentration range of 1 to 20% was in the lower half of the H-D curve. Below 1% concentration, the line was very weak and therefore for the lower concentrations, the entrance slit width of the spectrograph was increased to 60 microns. The intensities were normalized with the control argon line intensity and the logarithmic values log(I/I$_0$) were plotted against the logarithm of the percentage concentration, as shown in figure A.6. The H$_\gamma$, 434.0 nm, line was the weakest of the three and was useable only above 1% concentration as shown in figure A.6.
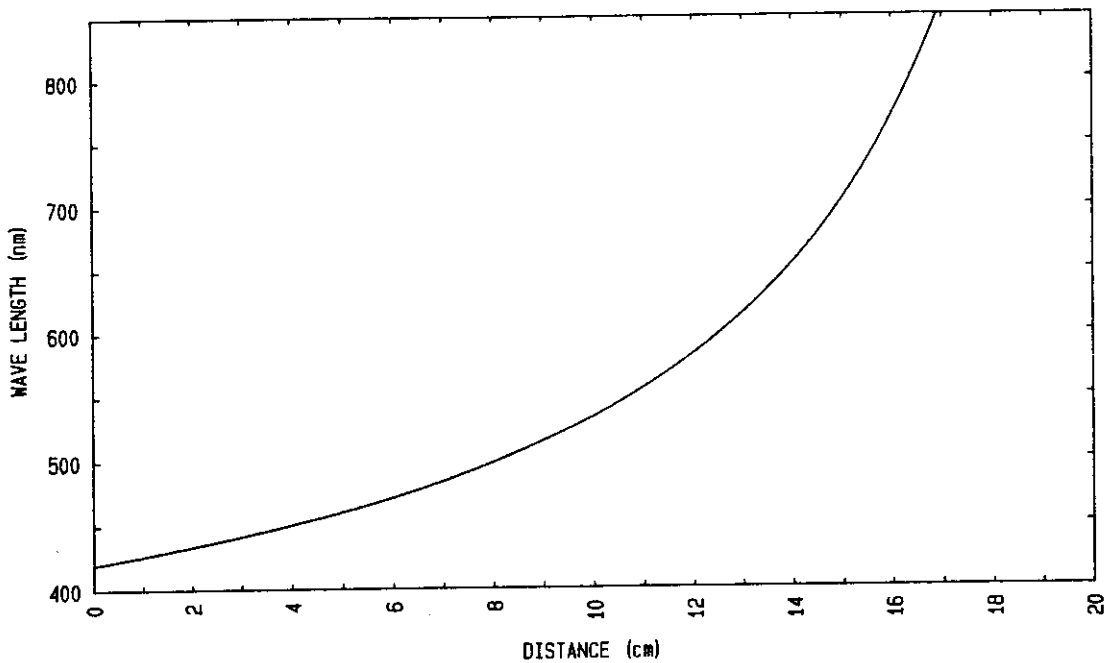
With following Spectrograph settings
Prism angle 3.2, Camera Arm angle 22 40'
Plate angle 56 42', Plate Position 157.2 mm

Figure A.5: Dispersion curve

For nitrogen, the three selected N_I lines were at 742.4, 744.2 and 746.8 nm. The intensities of all the lines were divided by the intensity of the Ar_I line at 763.5 nm, and the logarithm of the normalised intensities $\log(I/I_0)$ was plotted against the logarithm of the percentage concentration to obtain calibration curves. The change in the $\log(I/I_0)$ value for the entire concentration range was from 0.15 to 0.37 for the 742.4 nm line, 0.01 to 0.415 for the 744.2 nm line and 0.04 to 0.635 for the 746.8 nm N_I line as shown in figure A.6.

For oxygen, the three selected O_I line were 690.6, 725.4 and 777.4 nm. The intensities of the first two lines were found to be unuseable because of their low strength at the lower concentrations. But the 777.4 nm line gave better results and the variation in $\log(I/I_0)$ for the entire concentration range was from -0.5 to 1.0, as shown in figure A.6.

There were three samples of SF_6 taken from an M & G circuit breaker which had undergone endurance testing. Two samples EA0712 and EA0713 were taken out from the auxiliary circuit breaker, one of which, EA0712, had been filtered and the third sample, EA4013, was from the main test circuit breaker. The impurities of hydrogen, nitrogen and oxygen as determined from the impurity calibration curves are presented in table A.1.

A.5   Discussion and Conclusion

The relative intensity measurements were made for selected lines of hydrogen, nitrogen and oxygen. The calibration curves obtained for the different lines of each gas are
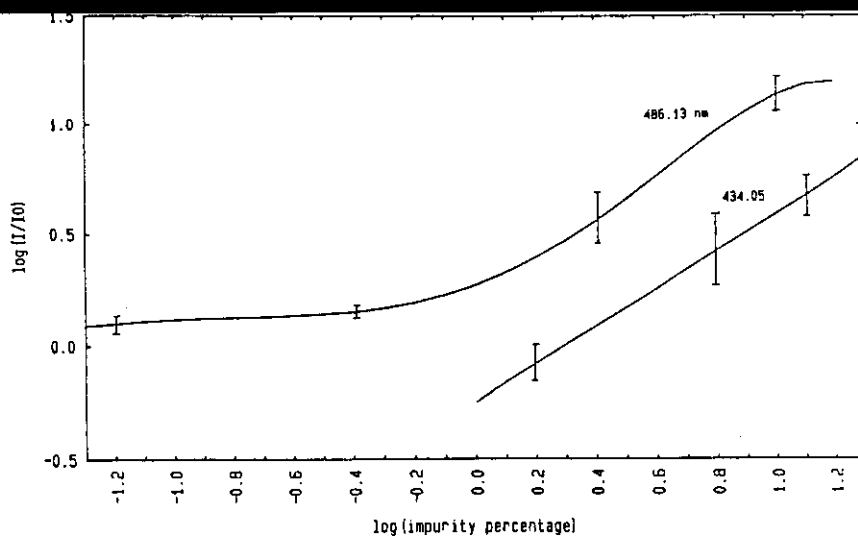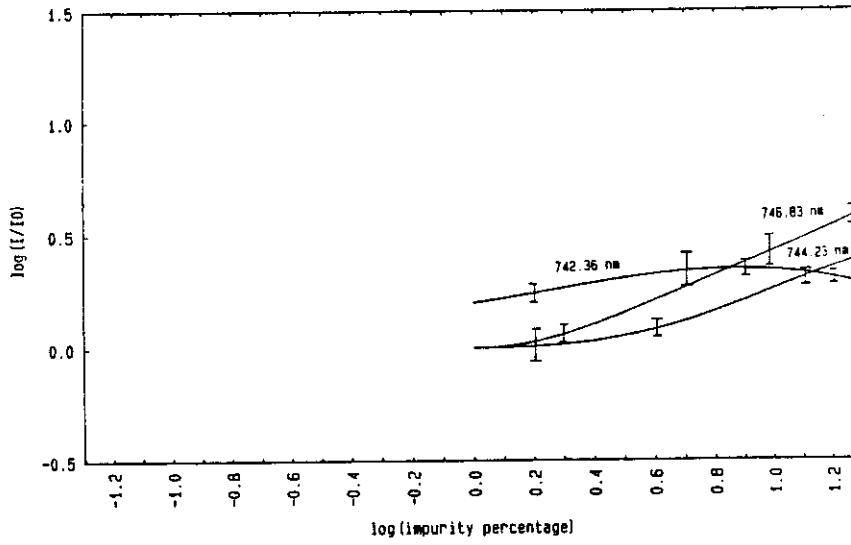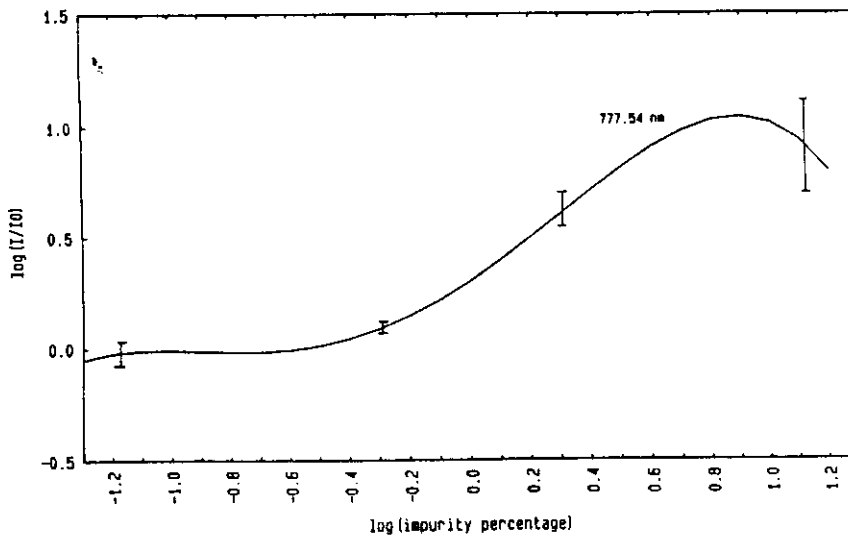
Figure A.6: Calibration curves

| | Impurity level (%) | | |
Sample no.	Hydrogen (486.1 nm)	Oxygen (777.4 nm)	Nitrogen (746.8 nm)
EA 0713 (Aux. breaker)	0.95 ± 54%	3.9 ± 35%	5.0 ± 18%
EA 4013 (Test breaker)	0.97 ± 54%	4.8 ± 31%	6.0 ± 16%
EA 0712 (Aux. breaker -) (filtered gas)	0.43 ± 64%	1.3 ± 14%	8.7 ± 30%

Table A.1: SF_6 impurity measurement by relative line intensity method.

discussed in this section. Some of the other important features of the experiment which will be used in the further investigation of SF_6 arcs have also been mentioned.

The two impurity calibration curves for the 486.1 and 434.0 nm hydrogen lines, shown in figure A.6, indicated that the H_β and H_γ lines could be used with reasonable accuracy for the concentration range of 1 to 20%, but below 1% the slope of the curve reduces and the accuracy falls by about four times. The H_α line intensities were not useable, due to the reasons described earlier and hence its calibration curve has not been shown in the figure.

Out of the three oxygen lines, the 777.4 nm un-ionised line gave the best calibration curve. The slope of the curve was promising for the concentration range of 1 to 5%, but above 5% the curve reached saturation. Below 1%, the accuracy was reduced by a large factor.

For nitrogen, the 744.2 and 746.8 nm un-ionised lines gave almost similar curves with reasonable accuracy in the concentration range of 2 to 20%. Below 2%, both the curves became almost parallel to the x-axis and therefore unuseable. The curve for the 742.4 nm line showed better accuracy for the lower concentration range of 1 to 5%.

The outcome of this exercise was not completely satisfactory. Because the impurity level of these gases which begin to affect the performance of the circuit breaker is very low. It is 5 ppm for hydrogen and water, and 0.05% for nitrogen and oxygen. These measurements have shown that the spectrographic method of detecting the impurities has low accuracy for these concentration ranges and consequently is inadequate.

The experiment has at the same time helped to develop a computer code for doing relative intensity calculations. This was further expanded for the absolute intensity calculations. The other advantage has been the establishment of the experimental procedures such as photography, data acquisition by the scanner and the spectrum imaging technique. The spectrum lines were also identified and this proved to be very useful information for the later experimental investigation.

Appendix B

Photographic Process for Recording the Spectrum

There are two methods of recording the spectrum for quantitative analysis; one, photographic, two, photo-detector.

With recent technological advances, photo-detectors have gained preference over photographic detectors.

A photo-detector, such as an optical multichannel analyzer (OMA), can be used for recording the line intensity in a short time interval as encountered in this experiment, but OMA is an expensive device and can digitise only a small area of the spectrum at a time. But it has the advantage of being a linear device, which can be easily interfaced with digital data processors to give immediate read-out of the data.

But there are some advantages in photographic recording [26,31] of the spectra, which are as follows:

1. Simultaneous recording of all the lines in broad region of the spectrum. These extra data may be useful on subsequent examination [72].

2. A compact permanent record of the spectrum which can be studied at a later time.

3. High resolution, so that fine lines can be recorded with good spatial resolution.

4. Very economical in terms of the number of measurements being carried out.

5. Most versatile detector.

However there are some drawbacks, most of which directly affect quantitative determination of the radiation by varying the relation between incident radiation and photographic blackening (density).

1. Variation of the sensitivity with wavelength.

2. Non-linear response to the incident light.

3. Sensitivity of the plate depends upon a number of factors such as, physical environment, type of development, temperature.

4. Its sensitive range is limited to the visible, near infra-red and the ultra-violet ranges of the spectrum.

5. Variation between plates of the same batch is also possible [1].

Despite these disadvantages, the photographic method was preferred in these experiments. One of the main reasons was the short duration (20-50 ms) for which the arc was run, and the photographic detection was the only medium which offered the required information density and data acquisition over the entire range of the spectrum. A second, and from the practical point of view equally important reason, was that an excellent spectrograph and microdensitometer facilities were available.

In order to make a proper selection of the photographic material and the process, it is necessary to be acquainted with some basic photographic properties.

Emulsion Response

The response of an emulsion is best described by the density versus the logarithm of the exposure (log[It]) curve, commonly called the H–D curve (after Hurter and Driffield). The x-axis of the H–D curve is logarithmic and refers to the total energy per unit area acting on the photographic material. The y-axis is linear and refers to the photographic density which is equal to log(1/T), where T is the transmittance of the developed image.

The H–D curve can be divided into four sections; figure B.1. The fog level (A) is independent of the exposure. The toe of the curve (A-B) is the non linear region in which the density increases measurably above the fog level with increase in exposure. The straight line section (B-C) is the useful region in which the density increases linearly with the logarithm of exposure. The shoulder (C-D) is where the density reaches the saturation stage and its rate of increase begins to taper off.
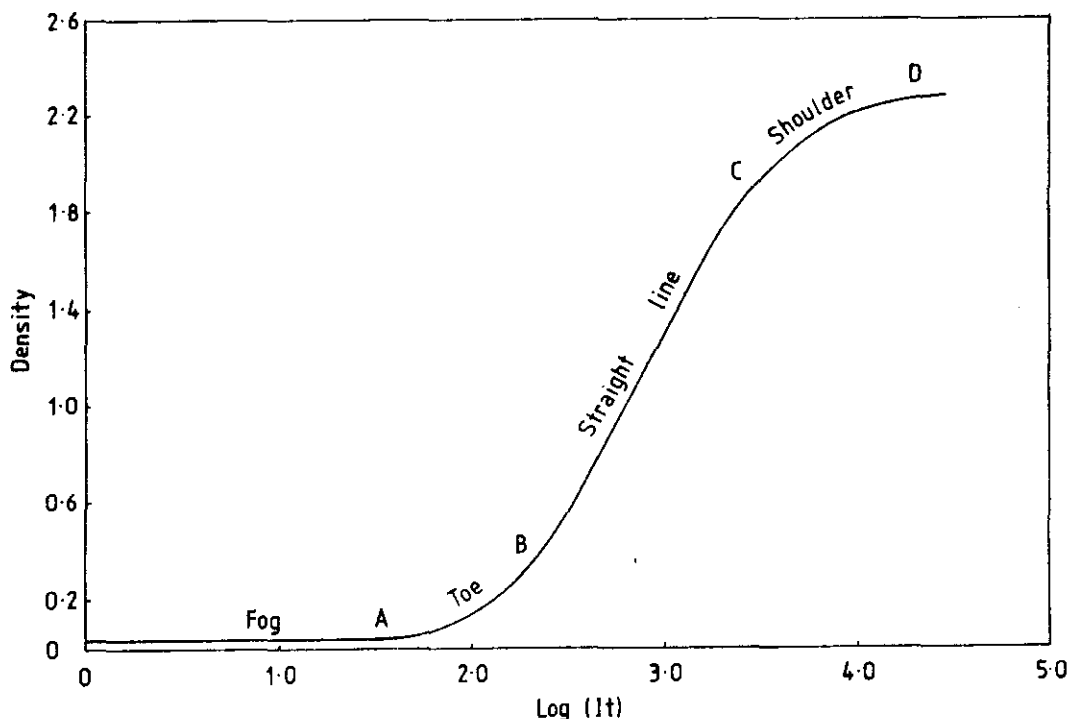
Figure B.1: H–D curve for 720.2 nm F_I line.

Three important conclusions can be drawn from the H–D curve.

- Emulsion speed

  This is defined as the reciprocal of the exposure required to produce a certain level of density, measured by standards like the ASA, DIN and ISO for defining the speed but which can mean different things for a particular emulsion. As far as quantitative spectrography is concerned, speed is only an approximate measure to determine whether the emulsion is suitable for the expected range of the exposures.

- Contrast

  This is given as the maximum slope of the straight line portion of the H–D curve. It is also referred to as gamma and is used to select the correct development time for an emulsion as given by gamma versus development time graphs [1].

- Total response range

  This is defined as the useful range of the H–D curve and usually represents the linear region of the H–D curve. This curve must be constructed by the individual user to calibrate the emulsion for the particular condition and the development technique used. It is usually done by exposing the emulsion with a series of different exposures of known radiant energy and development by a standard method. The resultant densities are then measured and related with the incoming radiation integrated over the exposure time. A rotating sector wheel with slots of different size cut around the periphery is quite commonly used for generating attenuated stepped intensities. The speed of rotation is kept above a certain level to avoid intermittency effects.

Spectral Response

The emulsion response to radiation changes with wavelength due to the sensitivity change of the silver halides present in the emulsion. The sensitivity peaks in the 380 to 480 nm range of the spectrum. To extend the range to the visible and the near infrared range, sensitizing dyes are used.

Image Properties

- Granularity

  Due to the inherent granular nature of the emulsion, any uniformly exposed and developed plate will show a small deviation in the resultant density if the scanning slit aperture is small. The noise in the recorded density can be reduced by having a larger aperture of the scanning slit.

- Resolving power

  Resolving power can be defined as the number of lines per millimetre that can be resolved on the plate. Therefore resolving power of the plate must be equal to, if not greater than, that of the spectrograph for the optimum use of the instrument.

Image Effects

There are number of effects that can occur in the image which can vary the normal D–log E relation.

- Reciprocity failure

  It has been found that the density produced by a certain exposure (It) received by the plate is not independent of the two factors taken separately [59,2,64]. Therefore, low intensity with long exposure time will not produce the same density on the photographic plate as high intensity with the corresponding short time of exposure. Thus the exposure time for the calibration and the source under investigation should not differ by a large factor.

- Intermittency effect

  A continuous exposure does not produce the same density as an intermittent one of the same energy flux below a certain level of flashes per second. Therefore, when using an intermittent exposure the flash rate must be well above the critical limit [31,29,57]. This has been overcome by keeping the speed of the attenuation wheel above a critical level; details in section 4.3.

- Brush effect

  This involves a progressive change in the latent image between its production and its development. This means that the calibrating exposure and the other source exposures must be allowed comparable time to change.

- Eberhard effect

  When an emulsion is developed, insufficient agitation produces depletion in the developer strength in any high density area, due to the build-up of the reduction products. This causes increased development in the dark area and reduced development in the light area of the plate which are adjacent to each other, due to the diffusion of the developer from the high concentration region to the low concentration region. In this experiment, developement was done by stroking the plates using a soft brush to reduce the error caused by this effect; details given in section 4.3.

Appendix C

Plasma Composition Tables for Nitrogen, Argon and SF_6

Table C.1: Nitrogen Plasma Composition and Partition Function for N_{II} Species at 1 Atmosphere Pressure

T (K)	N_e (m^{-3})	N_{II} (m^{-3})	N_{III} (m^{-3})	Q	ΔE eV
5.00e 03	6.57e 17	6.57e 17	1.90e-03	9.08e 00	6.77e-04
5.50e 03	1.48e 19	1.48e 19	1.14e 02	9.08e 00	3.06e-03
6.00e 03	2.90e 19	2.90e 19	2.28e 02	9.08e 00	4.10e-03
6.50e 03	2.06e 20	2.06e 20	4.98e 05	9.08e 00	1.05e-02
7.00e 03	3.83e 20	3.83e 20	9.96e 05	9.12e 00	1.38e-02
7.50e 03	1.27e 21	1.27e 21	2.74e 08	9.19e 00	3.07e-02
8.00e 03	2.16e 21	2.16e 21	5.48e 08	9.26e 00	4.41e-02
8.50e 03	4.74e 21	4.74e 21	3.80e 10	9.33e 00	5.32e-02
9.00e 03	7.31e 21	7.31e 21	7.54e 10	9.40e 00	6.90e-02
9.50e 03	1.30e 22	1.30e 22	2.00e 12	9.47e 00	8.06e-02
1.00e 04	1.86e 22	1.86e 22	3.93e 12	9.54e 00	9.78e-02
1.05e 04	2.88e 22	2.88e 22	5.25e 13	9.61e 00	1.11e-01
1.10e 04	3.89e 22	3.89e 22	1.01e 14	9.68e 00	1.28e-01
1.15e 04	5.40e 22	5.40e 22	8.13e 14	9.75e 00	1.42e-01
1.20e 04	6.92e 22	6.92e 22	1.52e 15	9.82e 00	1.57e-01
1.25e 04	8.79e 22	8.79e 22	8.40e 15	9.89e 00	1.69e-01
1.30e 04	1.07e 23	1.07e 23	1.53e 16	9.96e 00	1.80e-01
1.35e 04	1.25e 23	1.25e 23	6.31e 16	1.00e 01	1.89e-01
1.40e 04	1.44e 23	1.44e 23	1.11e 17	1.01e 01	1.95e-01
1.45e 04	1.59e 23	1.59e 23	3.67e 17	1.02e 01	2.01e-01
1.50e 04	1.73e 23	1.73e 23	6.23e 17	1.02e 01	2.02e-01
1.55e 04	1.81e 23	1.81e 23	1.73e 18	1.03e 01	2.03e-01
1.60e 04	1.89e 23	1.89e 23	2.83e 18	1.04e 01	2.01e-01
1.65e 04	1.92e 23	1.92e 23	6.84e 18	1.05e 01	2.00e-01
1.70e 04	1.94e 23	1.94e 23	1.08e 19	1.05e 01	1.96e-01
1.75e 04	1.93e 23	1.93e 23	2.34e 19	1.06e 01	1.93e-01
1.80e 04	1.92e 23	1.92e 23	3.59e 19	1.07e 01	1.89e-01
1.85e 04	1.90e 23	1.89e 23	7.06e 19	1.07e 01	1.85e-01
1.90e 04	1.87e 23	1.87e 23	1.05e 20	1.08e 01	1.81e-01
1.95e 04	1.83e 23	1.83e 23	1.91e 20	1.09e 01	1.77e-01
2.00e 04	1.80e 23	1.79e 23	2.78e 20	1.10e 01	1.73e-01
2.05e 04	1.76e 23	1.75e 23	4.73e 20	1.10e 01	1.70e-01
2.10e 04	1.72e 23	1.72e 23	6.69e 20	1.11e 01	1.66e-01
2.15e 04	1.69e 23	1.67e 23	1.08e 21	1.12e 01	1.63e-01
2.20e 04	1.66e 23	1.63e 23	1.48e 21	1.13e 01	1.60e-01
2.25e 04	1.63e 23	1.59e 23	2.27e 21	1.13e 01	1.57e-01
2.30e 04	1.60e 23	1.54e 23	3.05e 21	1.14e 01	1.55e-01
2.35e 04	1.58e 23	1.49e 23	4.42e 21	1.15e 01	1.53e-01
2.40e 04	1.55e 23	1.44e 23	5.80e 21	1.16e 01	1.52e-01
2.45e 04	1.53e 23	1.37e 23	7.99e 21	1.16e 01	1.50e-01
2.50e 04	1.51e 23	1.31e 23	1.02e 22	1.17e 01	1.50e-01
2.55e 04	1.50e 23	1.24e 23	1.33e 22	1.18e 01	1.49e-01
2.60e 04	1.49e 23	1.16e 23	1.64e 22	1.19e 01	1.49e-01
2.65e 04	1.48e 23	1.08e 23	2.04e 22	1.20e 01	1.49e-01
2.70e 04	1.48e 23	9.92e 22	2.44e 22	1.20e 01	1.50e-01
2.75e 04	1.48e 23	9.01e 22	2.88e 22	1.21e 01	1.50e-01
2.80e 04	1.48e 23	8.11e 22	3.32e 22	1.22e 01	1.50e-01
2.85e 04	1.47e 23	7.24e 22	3.75e 22	1.23e 01	1.51e-01
2.90e 04	1.47e 23	6.36e 22	4.19e 22	1.24e 01	1.51e-01
2.95e 04	1.47e 23	5.59e 22	4.56e 22	1.24e 01	1.51e-01
3.00e 04	1.47e 23	4.81e 22	4.94e 22	1.25e 01	

Table C.2: Argon Plasma Composition and Partition Function for Ar$_I$ Species at 1 Atmosphere Pressure

T (K)	N_e (m^{-3})	Ar$_I$ (m^{-3})	Ar$_{II}$ (m^{-3})	Ar$_{III}$ (m^{-3})	Q	ΔE eV
5.000e 03	1.419e 18	1.468e 23	1.413e 18	4.161e-01	1.000e 00	4.975e-04
5.500e 03	1.630e 19	6.848e 23	1.630e 19	1.185e 04	1.000e 00	1.608e-03
6.000e 03	3.118e 19	1.223e 24	3.118e 19	2.371e 04	1.000e 00	2.129e-03
6.500e 03	1.582e 20	1.135e 24	1.582e 20	3.082e 07	1.000e 00	4.608e-03
7.000e 03	2.852e 20	1.048e 24	2.852e 20	6.161e 07	1.000e 00	5.362e-03
7.500e 03	8.951e 20	9.809e 23	8.951e 20	1.160e 10	1.000e 00	1.020e-02
8.000e 03	1.505e 21	9.142e 23	1.505e 21	2.314e 10	1.000e 00	1.281e-02
8.500e 03	3.495e 21	8.592e 23	3.495e 21	1.204e 12	1.000e 00	1.894e-02
9.000e 03	5.486e 21	8.043e 23	5.486e 21	2.386e 12	1.000e 00	2.306e-02
9.500e 03	1.040e 22	7.537e 23	1.040e 22	5.082e 13	1.000e 00	3.091e-02
1.000e 04	1.532e 22	7.031e 23	1.532e 22	9.926e 13	1.000e 00	3.656e-02
1.050e 04	2.506e 22	6.503e 23	2.508e 22	1.115e 15	1.000e 00	4.564e-02
1.100e 04	3.480e 22	5.974e 23	3.484e 22	2.131e 15	1.001e 00	5.255e-02
1.150e 04	5.062e 22	5.380e 23	5.063e 22	1.497e 16	1.001e 00	6.197e-02
1.200e 04	6.643e 22	5.380e 23	6.643e 22	2.782e 16	1.002e 00	6.949e-02
1.250e 04	8.722e 22	4.110e 23	8.722e 22	1.376e 17	1.004e 00	7.802e-02
1.300e 04	1.080e 23	3.442e 23	1.080e 23	2.473e 17	1.006e 00	8.514e-02
1.350e 04	1.293e 23	2.811e 23	1.293e 23	9.360e 17	1.010e 00	9.142e-02
1.400e 04	1.506e 23	2.232e 23	1.506e 23	1.625e 18	1.017e 00	9.698e-02
1.450e 04	1.665e 23	1.718e 23	1.665e 23	4.999e 18	1.027e 00	1.001e-01
1.500e 04	1.824e 23	1.275e 23	1.824e 23	8.373e 18	1.040e 00	1.030e-01
1.550e 04	1.902e 23	9.091e 22	1.901e 23	2.189e 19	1.057e 00	1.035e-01
1.600e 04	1.979e 23	6.202e 22	1.978e 23	3.540e 19	1.083e 00	1.039e-01
1.650e 04	1.992e 23	4.381e 22	1.991e 23	8.122e 19	1.115e 00	1.026e-01
1.700e 04	2.005e 23	3.026e 22	2.003e 23	1.270e 20	1.159e 00	1.015e-01
1.750e 04	1.984e 23	2.168e 22	1.979e 23	2.620e 20	1.217e 00	9.952e-02
1.800e 04	1.964e 23	1.528e 22	1.956e 23	3.969e 20	1.283e 00	9.765e-02
1.850e 04	1.930e 23	1.091e 22	1.915e 23	7.483e 20	1.375e 00	9.558e-02
1.900e 04	1.896e 23	8.012e 21	1.874e 23	1.100e 21	1.475e 00	9.357e-02
1.950e 04	1.861e 23	6.039e 21	1.823e 23	1.915e 21	1.613e 00	9.171e-02
2.000e 04	1.826e 23	4.446e 21	1.771e 23	2.731e 21	1.762e 00	8.990e-02
2.050e 04	1.795e 23	3.515e 21	1.707e 23	4.412e 21	1.956e 00	8.846e-02
2.100e 04	1.764e 23	2.738e 21	1.642e 23	6.093e 21	2.164e 00	8.707e-02
2.150e 04	1.742e 23	2.123e 21	1.560e 23	9.118e 21	2.431e 00	8.625e-02
2.200e 04	1.720e 23	1.644e 21	1.477e 23	1.214e 22	2.709e 00	8.545e-02
2.250e 04	1.709e 23	1.277e 21	1.373e 23	1.678e 22	3.060e 00	8.529e-02
2.300e 04	1.697e 23	1.000e 21	1.269e 23	2.142e 22	3.427e 00	8.514e-02
2.350e 04	1.695e 23	7.944e 20	1.147e 23	2.735e 22	3.894e 00	8.547e-02
2.400e 04	1.692e 23	6.424e 20	1.020e 23	3.328e 22	4.370e 00	8.578e-02
2.450e 04	1.693e 23	5.299e 20	9.018e 22	3.956e 22	4.935e 00	8.624e-02
2.500e 04	1.695e 23	4.447e 20	7.774e 22	4.585e 22	5.554e 00	8.668e-02
2.550e 04	1.695e 23	3.062e 20	6.658e 22	5.141e 22	6.209e 00	8.692e-02
2.600e 04	1.695e 23	2.277e 20	5.543e 22	5.696e 22	7.000e 00	8.716e-02
2.650e 04	1.691e 23	1.795e 20	4.656e 22	6.110e 22	7.792e 00	8.701e-02
2.700e 04	1.686e 23	1.312e 20	3.768e 22	6.523e 22	8.720e 00	8.687e-02
2.750e 04	1.675e 23	1.027e 20	3.126e 22	6.779e 22	9.716e 00	8.634e-02
2.800e 04	1.665e 23	7.423e 19	2.484e 22	7.036e 22	1.071e 01	8.581e-02
2.850e 04	1.650e 23	5.800e 19	2.048e 22	7.155e 22	1.195e 01	8.496e-02
2.900e 04	1.635e 23	4.178e 19	1.612e 22	7.275e 22	1.319e 01	8.413e-02
2.950e 04	1.617e 23	3.269e 19	1.327e 22	7.288e 22	1.447e 01	8.305e-02
3.000e 04	1.600e 23	2.361e 19	1.042e 22	7.301e 22	1.598e 01	8.199e-02

Table C.3: Argon Plasma Composition and Partition Function for Ar_I Species at 8 Atmospheres Pressure

T (K)	N_e (m^{-3})	Ar_I (m^{-3})	Ar_{II} (m^{-3})	Ar_{III} (m^{-3})	Q	ΔE eV
5.000e 03	4.017e 18	1.174e 25	4.017e 18	4.178e-01	1.000e 00	8.371e-04
5.500e 03	5.010e 19	1.067e 25	5.010e 19	1.311e 04	1.000e 00	2.819e-03
6.000e 03	8.851e 19	9.783e 24	8.851e 19	2.404e 04	1.000e 00	3.587e-03
6.500e 03	4.789e 20	9.030e 24	4.789e 20	3.431e 07	1.000e 00	8.017e-03
7.000e 03	8.136e 20	8.384e 24	8.136e 20	6.370e 07	1.000e 00	1.007e-02
7.500e 03	2.689e 21	7.822e 24	2.689e 21	4.287e 07	1.000e 00	1.768e-02
8.000e 03	4.330e 21	7.329e 24	4.330e 21	2.465e 07	1.000e 00	2.173e-02
8.500e 03	1.050e 22	6.885e 24	1.050e 22	1.398e 12	1.000e 00	3.283e-02
9.000e 03	1.598e 22	6.490e 24	1.598e 22	2.640e 12	1.000e 00	3.936e-02
9.500e 03	3.155e 22	6.116e 24	3.155e 22	6.171e 13	1.000e 00	5.382e-02
1.000e 04	4.556e 22	5.779e 24	4.556e 22	1.149e 14	1.000e 00	6.304e-02
1.050e 04	7.773e 22	5.435e 24	7.773e 22	1.410e 15	1.000e 00	8.036e-02
1.100e 04	1.070e 23	5.123e 24	1.070e 23	2.588e 15	1.001e 00	9.211e-02
1.150e 04	1.636e 23	4.777e 24	1.636e 23	1.973e 16	1.001e 00	1.114e-01
1.200e 04	2.155e 23	4.777e 24	2.155e 23	3.544e 16	1.002e 00	1.252e-01
1.250e 04	3.015e 23	4.119e 24	3.015e 23	1.882e 17	1.003e 00	1.450e-01
1.300e 04	3.809e 23	3.755e 24	3.809e 23	3.291e 17	1.005e 00	1.599e-01
1.350e 04	4.937e 23	3.377e 24	4.937e 23	1.320e 18	1.007e 00	1.786e-01
1.400e 04	5.985e 23	2.991e 24	5.985e 23	2.240e 18	1.010e 00	1.931e-01
1.450e 04	7.245e 23	2.607e 24	7.245e 23	7.193e 18	1.014e 00	2.088e-01
1.500e 04	8.421e 23	2.232e 24	8.421e 23	1.181e 19	1.019e 00	2.213e-01
1.550e 04	9.587e 23	1.889e 24	9.586e 23	3.173e 19	1.024e 00	2.323e-01
1.600e 04	1.068e 24	1.533e 24	1.068e 24	5.041e 19	1.031e 00	2.413e-01
1.650e 04	1.155e 24	1.232e 24	1.154e 24	1.172e 20	1.039e 00	2.471e-01
1.700e 04	1.236e 24	9.788e 23	1.236e 24	1.800e 20	1.050e 00	2.519e-01
1.750e 04	1.285e 24	7.701e 23	1.284e 24	3.726e 20	1.067e 00	2.531e-01
1.800e 04	1.331e 24	6.008e 23	1.330e 24	5.545e 20	1.085e 00	2.541e-01
1.850e 04	1.349e 24	4.660e 23	1.347e 24	1.046e 21	1.113e 00	2.523e-01
1.900e 04	1.365e 24	3.609e 23	1.362e 24	1.513e 21	1.143e 00	2.505e-01
1.950e 04	1.362e 24	2.806e 23	1.356e 24	2.648e 21	1.190e 00	2.471e-01
2.000e 04	1.359e 24	2.203e 23	1.351e 24	3.726e 21	1.246e 00	2.438e-01
2.050e 04	1.345e 24	1.752e 23	1.333e 24	6.125e 21	1.324e 00	2.398e-01
2.100e 04	1.332e 24	1.404e 23	1.315e 24	8.409e 21	1.414e 00	2.359e-01
2.150e 04	1.314e 24	1.157e 23	1.288e 24	1.308e 22	1.533e 00	2.320e-01
2.200e 04	1.297e 24	9.236e 22	1.262e 24	1.754e 22	1.664e 00	2.283e-01
2.250e 04	1.279e 24	7.748e 22	1.227e 24	2.594e 22	1.833e 00	2.249e-01
2.300e 04	1.262e 24	6.324e 22	1.194e 24	3.397e 22	2.012e 00	2.217e-01
2.350e 04	1.246e 24	5.374e 22	1.150e 24	4.780e 22	2.238e 00	2.192e-01
2.400e 04	1.231e 24	4.462e 22	1.109e 24	6.106e 22	2.477e 00	2.167e-01
2.450e 04	1.220e 24	3.824e 22	1.056e 24	8.174e 22	2.747e 00	2.153e-01
2.500e 04	1.209e 24	3.211e 22	1.006e 24	1.016e 23	3.049e 00	2.138e-01
2.550e 04	1.202e 24	2.759e 22	9.432e 23	1.293e 23	3.349e 00	2.134e-01
2.600e 04	1.195e 24	2.324e 22	8.833e 23	1.560e 23	3.713e 00	2.129e-01
2.650e 04	1.192e 24	1.993e 22	8.141e 23	1.890e 23	4.056e 00	2.132e-01
2.700e 04	1.189e 24	1.673e 22	7.474e 23	2.207e 23	4.459e 00	2.134e-01
2.750e 04	1.188e 24	2.838e 24	6.765e 23	2.555e 23	4.874e 00	2.140e-01
2.800e 04	1.187e 24	5.558e 24	6.082e 23	2.891e 23	5.289e 00	2.144e-01
2.850e 04	1.186e 24	2.734e 24	5.414e 23	3.218e 23	5.806e 00	2.148e-01
2.900e 04	1.185e 24	8.213e 21	4.769e 23	3.533e 23	6.323e 00	2.151e-01
2.950e 04	1.183e 24	6.870e 21	4.187e 23	3.807e 23	6.887e 00	2.149e-01
3.000e 04	1.180e 24	5.571e 21	3.625e 23	4.072e 23	7.549e 00	2.147e-01

xvi

Table C.4: SF_6 Plasma Composition and Partition Function for F_I Species at 1 Atmosphere Pressure

T (K)	N_e (m^{-3})	F_I (m^{-3})	F_{II} (m^{-3})	F_{III} (m^{-3})	Q	ΔE eV
5.00e 03	5.87e 19	1.26e 24	1.47e 15	0.00e 00	5.77e 00	3.20e-03
5.50e 03	3.14e 20	1.14e 24	7.34e 15	0.00e 00	5.78e 00	7.05e-03
6.00e 03	5.26e 20	1.05e 24	1.22e 16	0.00e 00	5.80e 00	8.74e-03
6.50e 03	1.52e 21	9.66e 23	6.21e 16	0.00e 00	5.81e 00	1.43e-02
7.00e 03	2.38e 21	8.96e 23	1.05e 17	0.00e 00	5.82e 00	1.72e-02
7.50e 03	4.98e 21	8.34e 23	4.94e 18	0.00e 00	5.84e 00	2.41e-02
8.00e 03	7.26e 21	7.80e 23	9.17e 18	0.00e 00	5.85e 00	2.81e-02
8.50e 03	1.23e 22	7.29e 23	3.02e 19	0.00e 00	5.87e 00	3.55e-02
9.00e 03	1.67e 22	6.84e 23	4.89e 19	0.00e 00	5.88e 00	4.03e-02
9.50e 03	2.41e 22	6.41e 23	1.51e 20	0.00e 00	5.89e 00	4.71e-02
1.00e 04	3.08e 22	6.02e 23	2.42e 20	0.00e 00	5.89e 00	5.18e-02
1.05e 04	3.90e 22	5.65e 23	6.57e 20	0.00e 00	5.89e 00	5.69e-02
1.10e 04	4.64e 22	5.31e 23	1.03e 21	0.00e 00	5.90e 00	6.07e-02
1.15e 04	5.32e 22	4.99e 23	2.47e 21	0.00e 00	5.90e 00	6.36e-02
1.20e 04	5.95e 22	4.69e 23	3.79e 21	0.00e 00	5.91e 00	6.58e-02
1.25e 04	6.53e 22	4.39e 23	7.87e 21	0.00e 00	5.91e 00	6.75e-02
1.30e 04	7.07e 22	4.12e 23	1.16e 22	0.00e 00	5.91e 00	6.89e-02
1.35e 04	7.81e 22	3.79e 23	2.02e 22	0.00e 00	5.92e 00	7.10e-02
1.40e 04	8.49e 22	3.48e 23	2.81e 22	0.00e 00	5.92e 00	7.27e-02
1.45e 04	9.51e 22	3.11e 23	4.10e 22	0.00e 00	5.92e 00	7.56e-02
1.50e 04	1.05e 23	3.11e 23	5.30e 22	0.00e 00	5.93e 00	7.80e-02
1.55e 04	1.16e 23	2.38e 23	6.79e 22	0.00e 00	5.93e 00	8.10e-02
1.60e 04	1.28e 23	2.01e 23	8.19e 22	0.00e 00	5.94e 00	8.35e-02
1.65e 04	1.38e 23	1.66e 23	9.57e 22	0.00e 00	5.94e 00	8.56e-02
1.70e 04	1.48e 23	1.35e 23	1.09e 23	0.00e 00	5.95e 00	8.74e-02
1.75e 04	1.56e 23	1.05e 23	1.19e 23	0.00e 00	5.96e 00	8.84e-02
1.80e 04	1.63e 23	8.15e 22	1.28e 23	0.00e 00	5.97e 00	8.92e-02
1.85e 04	1.67e 23	6.22e 22	1.33e 23	1.98e 18	5.98e 00	8.91e-02
1.90e 04	1.70e 23	4.69e 22	1.38e 23	3.86e 18	6.00e 00	8.89e-02
1.95e 04	1.71e 23	3.50e 22	1.40e 23	5.64e 18	6.02e 00	8.82e-02
2.00e 04	1.72e 23	2.60e 22	1.41e 23	7.34e 18	6.04e 00	8.74e-02
2.05e 04	1.71e 23	1.94e 22	1.40e 23	1.61e 19	6.06e 00	8.64e-02
2.10e 04	1.70e 23	1.45e 22	1.39e 23	2.45e 19	6.10e 00	8.54e-02
2.15e 04	1.68e 23	1.10e 22	7.21e 22	4.44e 19	6.13e 00	7.48e-02
2.20e 04	1.67e 23	8.32e 21	8.23e 21	6.34e 19	6.17e 00	6.35e-02
2.25e 04	1.65e 23	6.23e 21	7.00e 22	1.08e 20	6.22e 00	7.33e-02
2.30e 04	1.63e 23	4.90e 21	1.29e 23	1.50e 20	6.27e 00	8.12e-02
2.35e 04	1.60e 23	3.83e 21	1.26e 23	2.44e 20	6.33e 00	8.01e-02
2.40e 04	1.58e 23	2.99e 21	1.23e 23	3.33e 20	6.40e 00	7.90e-02
2.45e 04	1.56e 23	2.35e 21	1.20e 23	5.20e 20	6.48e 00	7.79e-02
2.50e 04	1.54e 23	1.86e 21	1.17e 23	6.99e 20	6.57e 00	7.68e-02
2.55e 04	1.51e 23	1.49e 21	1.14e 23	1.04e 21	6.67e 00	7.56e-02
2.60e 04	1.49e 23	1.22e 21	1.11e 23	1.38e 21	6.77e 00	7.46e-02
2.65e 04	1.47e 23	1.00e 21	6.26e 22	1.99e 21	6.90e 00	6.73e-02
2.70e 04	1.45e 23	8.02e 20	1.56e 22	2.57e 21	7.03e 00	5.98e-02
2.75e 04	1.43e 23	6.71e 20	5.78e 22	3.57e 21	7.17e 00	6.56e-02
2.80e 04	1.41e 23	5.42e 20	9.84e 22	4.53e 21	7.34e 00	7.06e-02
2.85e 04	1.40e 23	4.56e 20	9.43e 22	6.05e 21	7.51e 00	6.98e-02
2.90e 04	1.38e 23	3.72e 20	9.04e 22	7.51e 21	7.70e 00	6.91e-02
2.95e 04	1.37e 23	3.12e 20	8.56e 22	9.61e 21	7.91e 00	6.85e-02

Table C.5: SF_6 Plasma Composition and Partition Function for F_I Species at 1 Atmosphere Pressure

T (K)	N_e (m^{-3})	S_{II} (m^{-3})	S_{III} (m^{-3})	Q	ΔE eV
5.00e 03	5.87e 19	8.81e 19	0.00e 00	5.77e 00	3.20e-03
5.50e 03	3.14e 20	3.47e 20	0.00e 00	5.78e 00	7.05e-03
6.00e 03	5.26e 20	5.63e 20	0.00e 00	5.80e 00	8.74e-03
6.50e 03	1.52e 21	1.56e 21	0.00e 00	5.81e 00	1.43e-02
7.00e 03	2.38e 21	2.42e 21	0.00e 00	5.82e 00	1.72e-02
7.50e 03	4.98e 21	5.02e 21	0.00e 00	5.84e 00	2.41e-02
8.00e 03	7.26e 21	7.30e 21	0.00e 00	5.85e 00	2.81e-02
8.50e 03	1.23e 22	1.23e 22	0.00e 00	5.87e 00	3.55e-02
9.00e 03	1.67e 22	1.67e 22	0.00e 00	5.88e 00	4.03e-02
9.50e 03	2.41e 22	2.40e 22	0.00e 00	5.88e 00	4.71e-02
1.00e 04	3.08e 22	3.06e 22	0.00e 00	5.89e 00	5.18e-02
1.05e 04	3.90e 22	3.83e 22	0.00e 00	5.89e 00	5.69e-02
1.10e 04	4.64e 22	4.54e 22	0.00e 00	5.90e 00	6.07e-02
1.15e 04	5.32e 22	5.08e 22	0.00e 00	5.90e 00	6.36e-02
1.20e 04	5.95e 22	5.58e 22	0.00e 00	5.91e 00	6.58e-02
1.25e 04	6.53e 22	5.75e 22	5.87e 18	5.91e 00	6.75e-02
1.30e 04	7.07e 22	5.91e 22	1.13e 19	5.91e 00	6.89e-02
1.35e 04	7.81e 22	5.79e 22	2.17e 19	5.92e 00	7.10e-02
1.40e 04	8.49e 22	5.68e 22	3.14e 19	5.92e 00	7.27e-02
1.45e 04	9.51e 22	5.40e 22	6.33e 19	5.92e 00	7.56e-02
1.50e 04	1.05e 23	5.15e 22	9.29e 19	5.93e 00	7.80e-02
1.55e 04	1.16e 23	4.82e 22	1.51e 20	5.93e 00	8.10e-02
1.60e 04	1.28e 23	4.51e 22	2.25e 20	5.94e 00	8.35e-02
1.65e 04	1.38e 23	4.19e 22	3.54e 20	5.95e 00	8.56e-02
1.70e 04	1.48e 23	3.89e 22	4.75e 20	5.96e 00	8.74e-02
1.75e 04	1.56e 23	3.60e 22	7.21e 20	5.97e 00	8.84e-02
1.80e 04	1.63e 23	3.33e 22	9.54e 20	5.98e 00	8.92e-02
1.85e 04	1.67e 23	3.09e 22	1.40e 21	6.00e 00	8.91e-02
1.90e 04	1.70e 23	2.86e 22	1.83e 21	6.02e 00	8.89e-02
1.95e 04	1.71e 23	2.64e 22	2.59e 21	6.04e 00	8.82e-02
2.00e 04	1.72e 23	2.43e 22	3.31e 21	6.06e 00	8.74e-02
2.05e 04	1.71e 23	2.21e 22	4.43e 21	6.06e 00	8.64e-02
2.10e 04	1.70e 23	2.00e 22	5.51e 21	6.10e 00	8.54e-02
2.15e 04	1.68e 23	1.77e 22	4.31e 21	6.13e 00	7.48e-02
2.20e 04	1.67e 23	1.55e 22	3.17e 21	6.17e 00	6.35e-02
2.25e 04	1.65e 23	1.34e 22	7.16e 21	6.22e 00	7.33e-02
2.30e 04	1.63e 23	1.13e 22	1.10e 22	6.27e 00	8.12e-02
2.35e 04	1.60e 23	9.51e 21	1.21e 22	6.33e 00	8.01e-02
2.40e 04	1.58e 23	7.78e 21	1.32e 22	6.40e 00	7.90e-02
2.45e 04	1.56e 23	6.44e 21	1.40e 22	6.48e 00	7.79e-02
2.50e 04	1.54e 23	5.15e 21	1.47e 22	6.57e 00	7.68e-02
2.55e 04	1.51e 23	4.22e 21	1.51e 22	6.67e 00	7.56e-02
2.60e 04	1.49e 23	3.33e 21	1.55e 22	6.77e 00	7.46e-02
2.65e 04	1.47e 23	2.72e 21	1.38e 22	6.90e 00	6.73e-02
2.70e 04	1.45e 23	2.14e 21	1.21e 22	7.03e 00	5.98e-02
2.75e 04	1.43e 23	1.75e 21	1.37e 22	7.17e 00	6.56e-02
2.80e 04	1.41e 23	1.37e 21	1.52e 22	7.34e 00	7.06e-02
2.85e 04	1.40e 23	1.12e 21	1.48e 22	7.51e 00	6.98e-02
2.90e 04	1.38e 23	8.81e 20	1.44e 22	7.70e 00	6.91e-02
2.95e 04	1.37e 23	7.20e 20	1.38e 22	7.91e 00	6.85e-02

Table C.6: SF_6 Plasma Composition and Partition Function for F_I Species at 4 Atmospheres Pressure

T (K)	N_e (m^{-3})	F_I (m^{-3})	F_{II} (m^{-3})	F_{III} (m^{-3})	Q	ΔE eV
5.00e 03	5.87e 19	5.03e 24	5.87e 15	0.00e 00	5.77e 00	5.06e-03
5.50e 03	5.60e 20	4.57e 24	2.94e 16	0.00e 00	5.78e 00	1.03e-02
6.00e 03	9.78e 20	4.19e 24	4.89e 16	0.00e 00	5.80e 00	1.27e-02
6.50e 03	2.96e 21	3.87e 24	2.48e 17	0.00e 00	5.81e 00	2.04e-02
7.00e 03	4.65e 21	3.59e 24	4.19e 17	0.00e 00	5.82e 00	2.45e-02
7.50e 03	9.96e 21	3.35e 24	2.15e 18	0.00e 00	5.84e 00	3.43e-02
8.00e 03	1.46e 22	3.13e 24	3.67e 18	0.00e 00	5.85e 00	4.02e-02
8.50e 03	2.53e 22	2.94e 24	5.35e 19	0.00e 00	5.87e 00	5.12e-02
9.00e 03	3.49e 22	2.76e 24	9.78e 19	0.00e 00	5.88e 00	5.83e-02
9.50e 03	5.23e 22	2.60e 24	2.78e 20	0.00e 00	5.88e 00	6.94e-02
1.00e 04	6.79e 22	2.46e 24	4.40e 20	0.00e 00	5.89e 00	7.71e-02
1.05e 04	9.10e 22	2.32e 24	1.13e 21	0.00e 00	5.89e 00	8.70e-02
1.10e 04	1.12e 23	2.19e 24	1.76e 21	0.00e 00	5.90e 00	9.43e-02
1.15e 04	1.37e 23	2.07e 24	3.90e 21	0.00e 00	5.90e 00	1.02e-01
1.20e 04	1.60e 23	1.95e 24	5.87e 21	0.00e 00	5.91e 00	1.08e-01
1.25e 04	1.83e 23	1.84e 24	1.17e 22	0.00e 00	5.91e 00	1.13e-01
1.30e 04	2.05e 23	1.74e 24	1.70e 22	0.00e 00	5.91e 00	1.17e-01
1.35e 04	2.26e 23	1.64e 24	3.05e 22	0.00e 00	5.92e 00	1.21e-01
1.40e 04	2.46e 23	1.54e 24	4.30e 22	0.00e 00	5.92e 00	1.24e-01
1.45e 04	2.70e 23	1.44e 24	6.80e 22	0.00e 00	5.92e 00	1.27e-01
1.50e 04	2.93e 23	1.44e 24	9.14e 22	0.00e 00	5.93e 00	1.30e-01
1.55e 04	3.24e 23	1.24e 24	1.28e 23	0.00e 00	5.93e 00	1.35e-01
1.60e 04	3.52e 23	1.11e 24	1.63e 23	0.00e 00	5.94e 00	1.39e-01
1.65e 04	3.88e 23	9.85e 23	2.07e 23	0.00e 00	5.95e 00	1.43e-01
1.70e 04	4.21e 23	8.65e 23	2.48e 23	0.00e 00	5.96e 00	1.47e-01
1.75e 04	4.57e 23	7.51e 23	2.93e 23	0.00e 00	5.97e 00	1.51e-01
1.80e 04	4.90e 23	6.43e 23	3.35e 23	0.00e 00	5.98e 00	1.54e-01
1.85e 04	5.20e 23	5.41e 23	3.73e 23	7.93e 18	5.99e 00	1.57e-01
1.90e 04	5.48e 23	4.45e 23	4.09e 23	1.54e 19	6.01e 00	1.59e-01
1.95e 04	5.69e 23	3.62e 23	4.36e 23	1.51e 19	6.03e 00	1.60e-01
2.00e 04	5.88e 23	2.92e 23	4.62e 23	1.47e 19	6.05e 00	1.60e-01
2.05e 04	5.99e 23	2.33e 23	4.77e 23	2.15e 19	6.08e 00	1.60e-01
2.10e 04	6.09e 23	1.85e 23	4.91e 23	2.80e 19	6.11e 00	1.59e-01
2.15e 04	6.12e 23	1.46e 23	4.96e 23	4.78e 19	6.14e 00	1.58e-01
2.20e 04	6.15e 23	1.14e 23	5.01e 23	6.67e 19	6.18e 00	1.56e-01
2.25e 04	6.13e 23	8.99e 22	5.00e 23	1.11e 20	6.23e 00	1.55e-01
2.30e 04	6.12e 23	7.10e 22	4.98e 23	1.53e 20	6.29e 00	1.53e-01
2.35e 04	6.07e 23	5.66e 22	4.92e 23	2.50e 20	6.35e 00	1.51e-01
2.40e 04	6.02e 23	4.55e 22	4.87e 23	3.42e 20	6.42e 00	1.49e-01
2.45e 04	5.96e 23	3.67e 22	4.78e 23	5.39e 20	6.50e 00	1.48e-01
2.50e 04	5.90e 23	2.89e 22	4.71e 23	7.28e 20	6.60e 00	1.46e-01
2.55e 04	5.84e 23	2.35e 22	4.61e 23	1.09e 21	6.69e 00	1.44e-01
2.60e 04	5.77e 23	1.91e 22	4.53e 23	1.44e 21	6.81e 00	1.43e-01
2.65e 04	5.70e 23	1.56e 22	4.43e 23	2.10e 21	6.93e 00	1.41e-01
2.70e 04	5.63e 23	1.28e 22	4.34e 23	2.73e 21	7.06e 00	1.39e-01
2.75e 04	5.56e 23	1.05e 22	4.24e 23	3.84e 21	7.22e 00	1.37e-01
2.80e 04	5.49e 23	8.81e 21	4.14e 23	4.91e 21	7.38e 00	1.36e-01
2.85e 04	5.42e 23	7.45e 21	4.04e 23	6.71e 21	7.55e 00	1.34e-01
2.90e 04	5.35e 23	6.35e 21	3.94e 23	8.46e 21	7.76e 00	1.32e-01
2.95e 04	5.29e 23	5.39e 21	3.83e 23	1.13e 22	7.96e 00	1.31e-01
3.00e 04	5.23e 23	4.44e 21	3.72e 23	1.40e 22	7.96e 00	1.31e-01

Table C.7: SF_6 Plasma Composition and Partition Function for F_I Species at 4 Atmospheres Pressure

T (K)	N_e (m^{-3})	S_{II} (m^{-3})	S_{III} (m^{-3})	Q	ΔE eV
5.00e 03	5.87e 19	2.35e 20	0.00e 00	5.77e 00	5.06e-03
5.50e 03	5.60e 20	7.74e 20	0.00e 00	5.78e 00	1.03e-02
6.00e 03	9.78e 20	1.22e 21	0.00e 00	5.80e 00	1.27e-02
6.50e 03	2.96e 21	3.25e 21	0.00e 00	5.81e 00	2.04e-02
7.00e 03	4.65e 21	4.99e 21	0.00e 00	5.82e 00	2.45e-02
7.50e 03	9.96e 21	1.03e 22	0.00e 00	5.84e 00	3.43e-02
8.00e 03	1.46e 22	1.50e 22	0.00e 00	5.85e 00	4.02e-02
8.50e 03	2.53e 22	2.57e 22	0.00e 00	5.87e 00	5.12e-02
9.00e 03	3.49e 22	3.52e 22	0.00e 00	5.88e 00	5.83e-02
9.50e 03	5.23e 22	5.24e 22	0.00e 00	5.88e 00	6.94e-02
1.00e 04	6.79e 22	6.79e 22	0.00e 00	5.89e 00	7.71e-02
1.05e 04	9.10e 22	9.02e 22	0.00e 00	5.89e 00	8.70e-02
1.10e 04	1.12e 23	1.11e 23	0.00e 00	5.90e 00	9.43e-02
1.15e 04	1.37e 23	1.34e 23	0.00e 00	5.90e 00	1.02e-01
1.20e 04	1.60e 23	1.55e 23	0.00e 00	5.91e 00	1.08e-01
1.25e 04	1.83e 23	1.72e 23	2.35e 19	5.91e 00	1.13e-01
1.30e 04	2.05e 23	1.88e 23	4.52e 19	5.91e 00	1.17e-01
1.35e 04	2.26e 23	1.96e 23	4.35e 19	5.92e 00	1.21e-01
1.40e 04	2.46e 23	2.03e 23	4.19e 19	5.92e 00	1.24e-01
1.45e 04	2.70e 23	2.02e 23	9.11e 19	5.92e 00	1.27e-01
1.50e 04	2.93e 23	2.01e 23	1.37e 20	5.93e 00	1.30e-01
1.55e 04	3.24e 23	1.95e 23	2.37e 20	5.93e 00	1.35e-01
1.60e 04	3.52e 23	1.89e 23	3.30e 20	5.94e 00	1.39e-01
1.65e 04	3.88e 23	1.80e 23	5.43e 20	5.94e 00	1.43e-01
1.70e 04	4.21e 23	1.72e 23	7.42e 20	5.95e 00	1.47e-01
1.75e 04	4.57e 23	1.62e 23	1.11e 21	5.96e 00	1.51e-01
1.80e 04	4.90e 23	1.52e 23	1.45e 21	5.97e 00	1.54e-01
1.85e 04	5.20e 23	1.43e 23	2.07e 21	5.98e 00	1.57e-01
1.90e 04	5.48e 23	1.34e 23	2.66e 21	5.99e 00	1.59e-01
1.95e 04	5.69e 23	1.25e 23	3.69e 21	6.01e 00	1.60e-01
2.00e 04	5.88e 23	1.17e 23	4.67e 21	6.03e 00	1.61e-01
2.05e 04	5.99e 23	1.10e 23	6.31e 21	6.05e 00	1.60e-01
2.10e 04	6.09e 23	1.02e 23	7.87e 21	6.08e 00	1.60e-01
2.15e 04	6.12e 23	9.51e 22	1.03e 22	6.11e 00	1.59e-01
2.20e 04	6.15e 23	8.84e 22	1.27e 22	6.14e 00	1.58e-01
2.25e 04	6.13e 23	8.13e 22	1.60e 22	6.18e 00	1.56e-01
2.30e 04	6.12e 23	7.46e 22	1.93e 22	6.23e 00	1.55e-01
2.35e 04	6.07e 23	6.76e 22	2.33e 22	6.29e 00	1.53e-01
2.40e 04	6.02e 23	6.08e 22	2.72e 22	6.35e 00	1.51e-01
2.45e 04	5.96e 23	5.40e 22	3.14e 22	6.42e 00	1.49e-01
2.50e 04	5.90e 23	4.75e 22	3.54e 22	6.50e 00	1.48e-01
2.55e 04	5.84e 23	4.14e 22	3.92e 22	6.60e 00	1.46e-01
2.60e 04	5.77e 23	3.56e 22	4.28e 22	6.69e 00	1.44e-01
2.65e 04	5.70e 23	3.07e 22	4.57e 22	6.81e 00	1.43e-01
2.70e 04	5.63e 23	2.59e 22	4.86e 22	6.93e 00	1.41e-01
2.75e 04	5.56e 23	2.20e 22	5.05e 22	7.06e 00	1.39e-01
2.80e 04	5.49e 23	1.83e 22	5.23e 22	7.22e 00	1.37e-01
2.85e 04	5.42e 23	1.55e 22	5.32e 22	7.38e 00	1.36e-01
2.90e 04	5.35e 23	1.28e 22	5.41e 22	7.55e 00	1.34e-01
2.95e 04	5.29e 23	1.09e 22	5.42e 22	7.76e 00	1.32e-01
3.00e 04	5.23e 23	8.93e 21	5.42e 22	7.95e 00	1.31e-01

Table C.8: SF_6 Plasma Composition and Partition Function for F_I Species at 8 Atmospheres Pressure

T (K)	N_e (m^{-3})	F_I (m^{-3})	F_{II} (m^{-3})	F_{III} (m^{-3})	Q	ΔE eV
5.00e 03	1.17e 20	1.01e 25	1.17e 16	0.00e 00	5.77e 00	6.40e-03
5.50e 03	6.94e 20	9.15e 24	5.87e 16	0.00e 00	5.78e 00	1.23e-02
6.00e 03	1.17e 21	8.39e 24	9.78e 16	0.00e 00	5.80e 00	1.51e-02
6.50e 03	3.97e 21	7.74e 24	4.97e 17	0.00e 00	5.81e 00	2.43e-02
7.00e 03	6.37e 21	7.18e 24	8.39e 17	0.00e 00	5.82e 00	2.92e-02
7.50e 03	1.39e 22	6.70e 24	4.30e 18	0.00e 00	5.84e 00	4.09e-02
8.00e 03	2.05e 22	6.27e 24	7.34e 18	0.00e 00	5.85e 00	4.79e-02
8.50e 03	3.59e 22	5.89e 24	7.25e 19	0.00e 00	5.87e 00	6.12e-02
9.00e 03	4.97e 22	5.55e 24	1.30e 20	0.00e 00	5.88e 00	6.98e-02
9.50e 03	7.55e 22	5.23e 24	4.02e 20	0.00e 00	5.88e 00	8.36e-02
1.00e 04	9.87e 22	4.95e 24	6.46e 20	0.00e 00	5.89e 00	9.30e-02
1.05e 04	1.35e 23	4.67e 24	1.57e 21	0.00e 00	5.89e 00	1.06e-01
1.10e 04	1.68e 23	4.43e 24	2.40e 21	0.00e 00	5.90e 00	1.15e-01
1.15e 04	2.10e 23	4.19e 24	5.13e 21	0.00e 00	5.90e 00	1.26e-01
1.20e 04	2.49e 23	3.97e 24	7.63e 21	0.00e 00	5.91e 00	1.35e-01
1.25e 04	2.93e 23	3.76e 24	1.48e 22	0.00e 00	5.91e 00	1.43e-01
1.30e 04	3.33e 23	3.56e 24	2.14e 22	0.00e 00	5.91e 00	1.50e-01
1.35e 04	3.73e 23	3.37e 24	3.78e 22	0.00e 00	5.92e 00	1.55e-01
1.40e 04	4.11e 23	3.19e 24	5.31e 22	0.00e 00	5.92e 00	1.60e-01
1.45e 04	4.52e 23	3.00e 24	8.52e 22	0.00e 00	5.92e 00	1.65e-01
1.50e 04	4.91e 23	3.00e 24	1.15e 23	0.00e 00	5.93e 00	1.69e-01
1.55e 04	5.39e 23	2.63e 24	1.67e 23	0.00e 00	5.93e 00	1.74e-01
1.60e 04	5.84e 23	2.43e 24	2.15e 23	0.00e 00	5.94e 00	1.79e-01
1.65e 04	6.42e 23	2.22e 24	2.84e 23	0.00e 00	5.95e 00	1.89e-01
1.70e 04	6.96e 23	2.01e 24	3.48e 23	0.00e 00	5.95e 00	1.89e-01
1.75e 04	7.58e 23	1.80e 24	4.26e 23	0.00e 00	5.96e 00	1.95e-01
1.80e 04	8.18e 23	1.60e 24	4.99e 23	0.00e 00	5.96e 00	1.99e-01
1.85e 04	8.78e 23	1.40e 24	5.74e 23	1.59e 19	5.97e 00	2.04e-01
1.90e 04	9.36e 23	1.20e 24	5.46e 23	3.09e 19	5.99e 00	2.08e-01
1.95e 04	9.86e 23	1.03e 24	7.10e 23	3.01e 19	6.00e 00	2.11e-01
2.00e 04	1.03e 24	8.58e 23	7.71e 23	2.94e 19	6.02e 00	2.13e-01
2.05e 04	1.07e 24	7.12e 23	8.18e 23	2.86e 19	6.04e 00	2.14e-01
2.10e 04	1.10e 24	5.86e 23	8.63e 23	2.80e 19	6.06e 00	2.15e-01
2.15e 04	1.12e 24	4.80e 23	8.91e 23	4.10e 19	6.12e 00	2.15e-01
2.20e 04	1.14e 24	3.90e 23	9.17e 23	5.34e 19	6.12e 00	2.14e-01
2.25e 04	1.15e 24	3.15e 23	9.29e 23	1.04e 20	6.15e 00	2.13e-01
2.30e 04	1.16e 24	2.54e 23	9.40e 23	1.53e 20	6.19e 00	2.12e-01
2.35e 04	1.16e 24	2.05e 23	9.40e 23	2.50e 20	6.24e 00	2.10e-01
2.40e 04	1.16e 24	1.66e 23	9.39e 23	3.42e 20	6.30e 00	2.08e-01
2.45e 04	1.15e 24	1.35e 23	9.31e 23	5.39e 20	6.36e 00	2.06e-01
2.50e 04	1.14e 24	1.10e 23	9.23e 23	7.28e 20	6.42e 00	2.04e-01
2.55e 04	1.13e 24	9.01e 22	9.10e 23	1.10e 21	6.50e 00	2.02e-01
2.60e 04	1.12e 24	7.39e 22	8.98e 23	1.47e 21	6.59e 00	1.99e-01
2.65e 04	1.11e 24	6.07e 22	8.82e 23	2.14e 21	6.69e 00	1.97e-01
2.70e 04	1.10e 24	5.01e 22	8.67e 23	2.78e 21	6.79e 00	1.95e-01
2.75e 04	1.09e 24	4.17e 22	8.50e 23	3.93e 21	6.90e 00	1.93e-01
2.80e 04	1.08e 24	3.50e 22	8.34e 23	5.03e 21	7.04e 00	1.91e-01
2.85e 04	1.06e 24	2.97e 22	8.17e 23	6.92e 21	7.18e 00	1.88e-01
2.90e 04	1.05e 24	2.54e 22	8.00e 23	8.74e 21	7.33e 00	1.86e-01
2.95e 04	1.04e 24	2.17e 22	7.81e 23	1.17e 22	7.51e 00	1.84e-01
3.00e 04	1.03e 24	1.82e 22	7.64e 23	1.46e 22	7.68e 00	1.82e-01

Table C.9: SF_6 Plasma Composition and Partition Function for F_I Species at 8 Atmospheres Pressure

T (K)	N_e (m^{-3})	S_{II} (m^{-3})	S_{III} (m^{-3})	Q	ΔE eV
5.00e 03	1.17e 20	3.52e 20	0.00e 00	5.77e 00	6.40e-03
5.50e 03	6.94e 20	1.23e 21	0.00e 00	5.78e 00	1.23e-02
6.00e 03	1.17e 21	1.96e 21	0.00e 00	5.80e 00	1.51e-02
6.50e 03	3.97e 21	4.83e 21	0.00e 00	5.81e 00	2.43e-02
7.00e 03	6.37e 21	7.30e 21	0.00e 00	5.82e 00	2.92e-02
7.50e 03	1.39e 22	1.49e 22	0.00e 00	5.84e 00	4.09e-02
8.00e 03	2.05e 22	2.16e 22	0.00e 00	5.85e 00	4.79e-02
8.50e 03	3.59e 22	3.70e 22	0.00e 00	5.87e 00	6.12e-02
9.00e 03	4.97e 22	5.07e 22	0.00e 00	5.88e 00	6.98e-02
9.50e 03	7.55e 22	7.62e 22	0.00e 00	5.88e 00	8.36e-02
1.00e 04	9.87e 22	9.91e 22	0.00e 00	5.89e 00	9.30e-02
1.05e 04	1.35e 23	1.34e 23	0.00e 00	5.89e 00	1.06e-01
1.10e 04	1.68e 23	1.66e 23	0.00e 00	5.90e 00	1.15e-01
1.15e 04	2.10e 23	2.06e 23	0.00e 00	5.90e 00	1.26e-01
1.20e 04	2.49e 23	2.43e 23	0.00e 00	5.91e 00	1.35e-01
1.25e 04	2.93e 23	2.79e 23	4.70e 19	5.91e 00	1.43e-01
1.30e 04	3.33e 23	3.12e 23	9.03e 19	5.91e 00	1.50e-01
1.35e 04	3.73e 23	3.36e 23	6.52e 19	5.92e 00	1.55e-01
1.40e 04	4.11e 23	3.58e 23	4.19e 19	5.92e 00	1.60e-01
1.45e 04	4.52e 23	3.67e 23	1.01e 20	5.92e 00	1.65e-01
1.50e 04	4.91e 23	3.76e 23	1.57e 20	5.93e 00	1.74e-01
1.55e 04	5.39e 23	3.72e 23	2.84e 20	5.93e 00	1.79e-01
1.60e 04	5.84e 23	3.68e 23	4.04e 20	5.94e 00	1.84e-01
1.65e 04	6.42e 23	3.57e 23	6.58e 20	5.94e 00	1.89e-01
1.70e 04	6.96e 23	3.46e 23	8.98e 20	5.95e 00	1.95e-01
1.75e 04	7.58e 23	3.30e 23	1.36e 21	5.96e 00	1.99e-01
1.80e 04	8.18e 23	3.16e 23	1.79e 21	5.96e 00	2.04e-01
1.85e 04	8.78e 23	2.99e 23	2.57e 21	5.97e 00	2.08e-01
1.90e 04	9.36e 23	2.83e 23	3.31e 21	6.00e 00	2.11e-01
1.95e 04	9.86e 23	2.67e 23	4.53e 21	6.02e 00	2.13e-01
2.00e 04	1.03e 24	2.51e 23	5.69e 21	6.04e 00	2.14e-01
2.05e 04	1.07e 24	2.37e 23	7.62e 21	6.06e 00	2.15e-01
2.10e 04	1.10e 24	2.22e 23	9.45e 21	6.08e 00	2.15e-01
2.15e 04	1.12e 24	2.09e 23	1.24e 22	6.12e 00	2.14e-01
2.20e 04	1.14e 24	1.96e 23	1.51e 22	6.15e 00	2.13e-01
2.25e 04	1.15e 24	1.83e 23	1.93e 22	6.19e 00	2.12e-01
2.30e 04	1.16e 24	1.71e 23	2.33e 22	6.24e 00	2.10e-01
2.35e 04	1.16e 24	1.59e 23	2.89e 22	6.30e 00	2.08e-01
2.40e 04	1.16e 24	1.47e 23	3.42e 22	6.36e 00	2.06e-01
2.45e 04	1.15e 24	1.35e 23	4.09e 22	6.42e 00	2.04e-01
2.50e 04	1.14e 24	1.23e 23	4.73e 22	6.50e 00	2.02e-01
2.55e 04	1.13e 24	1.11e 23	5.45e 22	6.59e 00	1.99e-01
2.60e 04	1.12e 24	9.93e 22	6.13e 22	6.69e 00	1.97e-01
2.65e 04	1.11e 24	8.83e 22	6.81e 22	6.79e 00	1.95e-01
2.70e 04	1.10e 24	7.77e 22	7.46e 22	6.90e 00	1.93e-01
2.75e 04	1.09e 24	6.81e 22	8.03e 22	7.04e 00	1.91e-01
2.80e 04	1.08e 24	5.90e 22	8.57e 22	7.18e 00	1.88e-01
2.85e 04	1.06e 24	5.12e 22	8.99e 22	7.33e 00	1.86e-01
2.90e 04	1.05e 24	4.37e 22	9.39e 22	7.51e 00	1.84e-01
2.95e 04	1.04e 24	3.78e 22	9.64e 22	7.68e 00	1.82e-01
3.00e 04	1.03e 24	3.20e 22	9.88e 22		

Appendix D

Programme Listings

```
0:  % ***********************************************************************
1:  % "PROGRAM    *  LAMDA  * V2.2   04.07.85"
2:  % "WAVELENGTH AND INTENSITY CALCULATION PROGRAM"
3:  % ***********************************************************************
4:  "DTRED":
5:  1=N;% ent"SCAN No.?",N;jmp not flg13 and N>=0 and N<=48
6:  if N=0;gto "ww"
7:  if N>num(P$[6]);dsp "No such scan";stp ;gto -2
8:  if itf(Q$[3,2N-1,2N])=0;dsp "Null scan";stp ;gto -3
9:  itf(Q$[3,2N-1,2N])=r4
10: itf(Q$[4,2N-1,2N])=r5
11: r5-r4+1=r1
12: "YY":enp "Start POINT:",r10;jmp not flg13
13: if r4>4096;sfg 2
14: if flg2 and H=2;r10+4096=r10
15: enp "End POINT:",r11;jmp not flg13
16: if flg2 and H=2;r11+4096=r11
17: if r11-r10<=0;gto "YY"
18: r10=r25;if r10<0;0=r25
19: r11=r26;if r11>r4-1;r4-1=r26
20: %
21: % "Curve fit for the continuum"
22: % %
23: 0=K;sfg 4;ina O,L,Q,R;cfg 5 and 6;fxd 3
24: for I=r25 to r26 by 10
25: num(A$[I+r1])=Y
26: if I=r25;I=J;Y=r73;Y-4=r74;gto +12
27: if I-J>25 and flg4;Y=r73;r73-4=r74
28: if flg4;gto +2;if r73-Y>4;cfg 4;r73-4=r74;sfg 5 and 6;gto +10
29: gto +3
30: if Y>r74;K+1=K;Y/1000=O[K];I/1000=L[K]
31: gto +7
32: if flg5 and 6;gto +6;if Y>=X;gto +3;if Y>r74;cfg 5;gto +6
33: if X>Y and flg6;gto +4
34: gto +4
35: if X>Y;gto +2;if r74-X>7;gto +3
36: gto +2
37: K+1=K;X/1000=O[K];(I-1)/1000=L[K];X=r73;X-4=r74;sfg 4;cfg 5 and 6
38: Y=X
39: next I
40: 0=J;for I=1 to K by 5
41: J+1=J;O[I]=Q[J];L[I]=R[J];next I
42: 2=M;1=r84;int(K/5)=r85;0=Z
43: gsb "POLYFIT"
44: % "Determination of line positions"
45: % %
46: 0=K;sfg 9;for I=r25 to r26 by 1
47: num(A$[I+r1])=Y
48: if I=r25;gto +6
49: if X>=Y;cfg 9;gto +5
50: if flg9;gto +4
51: 0=r80;for J=1 to M+1;r80+Z[J]*((I-1)/1000)^(J-1)=r80;next J
52: if r80*1000-X>5;K+1=K;(I-1)/1000=B[K];.255-r80+r67*X/1000=A[K];sfg 9
53: sfg 9
```

Note: In these programme listings the right arrow has been replaced by '=', because of the inability of the printer to print this character.

```
54:  Y=X
55:  "nii":next I
56:  % "Wave length and density calculation"
57:  % %
58:  gsb "CONST"
59:  for K=1 to r81
60:  r71+r72/(B[K]-2*r70)=Q[K]
61:  log(.255/A[K])=O[K]
62:  next K
63:  prtsc 701
64:  gto +9
65:  prt "                        TABLE [T4.1]"
66:  spc 2
67:  prt "             LIST OF   SF6    LINES"
68:  spc 3
69:  prt "DISTANCE","      WAVE LENGTH","       TRANSMITTANCE","      DENSITY"
70:  spc
71:  prt "   (mm)","                (nm)","                (%)"
72:  spc 2
73:  fmt 9,x,f6.0,10x,f7.2,12x,f4.1,12x,f5.3
74:  for I=1 to r81;wrt 701.9,1000*B[I],Q[I],392.16*A[I],O[I]
75:  next I
76:  sfg 4;prtsc 16
77:  stp
78:  % " CURVE FITTING PROG."
79:  "POLYFIT":
80:  M+1=Q;rdm Z[Q],S[Q,Q],P[Q]
81:  for I=2 to 2M+1;0=T[I]
82:  for L=r84 to r85
83:  T[I]+R[L]^(I-1)=T[I]
84:  next L;next I
85:  r85-r84+1=T[1]
86:  0=K;for I=1 to M+1;for J=1 to M+1
87:  T[J+K]=S[I,J]
88:  next J;K+1=K;next I
89:  for I=1 to M+1;0=P[I];for L=r84 to r85
90:  P[I]+Q[L]*R[L]^(I-1)=P[I]
91:  next L;next I
92:  % %
93:  % "MATRIX INVERSION"
94:  "MTXINV":inv S=S
95:  % " Calculation of Poly. Coeff. k0,k1,..."
96:  mat SP=Z;fxd 3
97:  ret
98:  % %
99:  % "CONSTANT r70,r71,r72 CALCULATION"
100: "CONST":
101: enp "1st Wave length",r55;enp "2nd Wave length",r56
102: enp "3rd Wave length",r57;enp "1st Line position",r60
103: enp "2nd Line position",r61;enp "3rd Line position",r62
104: (r56*r61-r55*r60)*(r62-r61)=r58
105: (r57*r62-r56*r61)*(r61-r60)=r59
106: (r62-r61)*(r56-r55)=r63
107: (r61-r60)*(r57-r56)=r64
108: (r58-r59)/(2*(r63-r64))=r70
109: (r56*r61-r55*r60-2*r70*(r56-r55))/(r61-r60)=r71
110: r55*r60+2*r71*r70-2*r55*r70-r71*r60=r72;r72/1000=r72
111: r70/1000=r70
112: fmt 8,"D0=",f13.4,"  W0=",f13.4,"  C=",f15.4
113: wrt 701.8,r70,r71,r72
114: spc 2
115: ret
116: stp
```

```
0:  % ***********************************************************************
1:  % "PROGRAM  * TEMPFI   V2.1 * 26.11.85 "
2:  % "THIS PROGRAM CALCULATES TEMPERATURE PROFILE FROM 720.2nm F(I) LINE"
3:  % ***********************************************************************
4:  "COLLECT":ent "Number of DISKS for Data Collection",r45
5:  ent "From DISK No.",r38
6:  ent "First FILE No.",r40
7:  ent "Last FILE No.",r41
8:  if r45=1;sfg 11;r38=J;r40=I;r41-r40+1=r44;gto +8
9:  ent "To DISK No.",r39
10: ent "First FILE No.",r42
11: ent "Last FILE No.",r43
12: sfg 11
13: for J=r38 to r39
14: if J>r38;dsp "Change DISK & Press CONTINUE";stp
15: r42=I;r43-r42+1=r44
16: for K=1 to r44
17: r40=I
18: dsp "Collecting Intensity FILES from","DISK No.",J,"FILE No.",I
19: I=Q;gsb "PLAYBACK"
20: A$=E$[K]
21: r40+1=r40
22: if I>r41;gto +2
23: next K
24: if r45=1;gto +3
25: r42=r40;r43=r41
26: next J
27: sfg 10
28: dsp "FILES COLLECTED"
29: % ***********************************************************************
30: "DTRED":if flg10;gto +2
31: gsb "COLLECT"
32: dsp "Change disk if necessary and press continue";stp
33: ent "No. of FILES to be Reduced",r87
34: ent "Beginning of FILE No.",r88
35: 0=U;for O=r88 to r88+r87-1;O=Q
36: dsp "FILE No.",O," is Being Processed"
37: sfg 11;gsb "PLAYBACK"
38: % %
39: "TEMP":fxd 3
40: %
41: % %
42: 1=r86;% "number of lines selected for the temperature calculation"
43: 6.937=G[1,2];7.402=G[1,1];% "Line pos. for spectrum scan"
44: 5.525=r70
45: 2757.0854=r71
46: -16251.0583=r72
47: % %
48: % " Values of wavelength increament in nm per micron 'delta-lamda'"
49: for I=1 to r86
50: (r71+r72/(G[1,I]+.001-2*r70)-(r71+r72/(G[1,I]-.001-2*r70)))/40=I[44,I
51: next I
52: %
53: 1=r95;80=r96;1=r97;9=r98;ina A,B;0=r90
54: for Z=1 to r86
55: %
56: % ***********************************************************************
```

```
57: % "Table for wavelength,statistical weight,partition function"
58: % "transition probability and upper energy level for selected lines"
59: % ****************************************************************
60: %
61: rdm I[50,10]
62: % "wavelength in nm "
63: 720.237=I[45,1]
64: 4=I[46,1];% "statis. wt.'g' "
65: 10=I[47,1];% "part. fn. 'Q' "
66: % "tansient probability 'A' "
67: 7.2e6=I[48,1]
68: % "upper state energy level 'E' in /cm "
69: 118938=I[49,1]
70: % ****************************************************************
71: %
72: for N=r95 to r96
73: itf(Q$[3,2N-1,2N])=r4
74: itf(Q$[4,2N-1,2N])=r5
75: r5-r4+1=rl
76: % "WAVELENGTH & DENSITY CALCULATION"
77: % %
78: % "Level of continuum is cal. by ave. 5 pts. on each end of scan"
79: 0=X;for I=rl to rl+4
80: num(A$[I])=Y;X+Y=X
81: next I
82: X/5=B
83: 0=X;for I=r5-4 to r5
84: num(A$[I])=Y;X+Y=X
85: next I
86: X/5=C;(B+C)/2=r80=r81
87: tn^((r80-9.765)/105.825)=X
88: log(210/X)=r80
89: % %
90: % "INTENSITY CALCULATION OF THE ENTIRE LINE PROFILE "
91: % " Density cal. of the entire line profile"
92: % ***" Densities of each scan is stored in A[*] and Inten. in B[*]"
93: ina Q;sfg 5;0=P;for I=rl+15 to r5-20
94: num(A$[I])=A
95: tn^((A-9.765)/105.825)=T
96: if A+3>=r81;P+1=P;gto +2
97: log(210/T)-r80=A[I]=Q[I];if flg5;rl+15+P=r25;cfg 5
98: next I
99: r5-rl-35-P+r25=r26;% max(Q[*])=A[N]
100: if r26=0;gto +88
101: % "cal. for eight density steps and fog level from the inten. scan"
102: if Z=r90;gto +70
103: 0=L;ina Q,R;1=rl
104: for M=r97 to r98
105: 0=X
106: for J=rl+20 to rl+39
107: num(E$[2,J])=Y;Y+X=X
108: next J
109: X/20=Y;if Y<=9.765;10=Y;prt "Y=",Y
110: tn^((Y-9.765)/105.825)=Y;Y/210=Y
111: L+1=L;if L=9;log(1/Y)=C;gto +4
112: log(1/Y)=R[L]
113: 60+rl=rl
114: next M
115: for L=1 to 8;R[L]-C=R[L];next L
116: % "Cal. of normalising factor Q[*] from temperature prof. of fil."
```

```
117: 0=L;1=r1
118: for M=r97 to r98-1
119: 0=X
120: for J=r1+20 to r1+39
121: num(E$[1,J])=Y;Y+X=X
122: next J
123: X/20=Y
124: tn^((Y-9.765)/105.825)=Y;Y/210=Y
125: L+1=L;log(1/Y)=Q[L]
126: 60+r1=r1
127: next M
128: for I=2 to 8
129: Q[I]/Q[1]=Q[I]
130: R[I]*Q[I]=R[I]
131: next I
132: % %
133: % " Spectral radiance cal. from tables given for Horn lamp"
134: 380=r6;% " lower wavelength in nm "
135: 780=r7;% " heighest wavelength in nm "
136: 10=r8;% " step size in nm "
137: (r7-r6)/r8+1=r18;% " No. of steps in the intensity table "
138: % ****************************************************************
139: % " Spectral radiance table of T242 lamp with filters"
140: % ****************************************************************
141: rdm M[45,1]
142: 1.38=M[1,1];2.186=M[2,1];3.107=M[3,1];4.02=M[4,1];4.41=M[5,1]
143: 5.19=M[6,1];5.8=M[7,1];6.42=M[8,1];6.89=M[9,1];7.34=M[10,1]
144: 7.74=M[11,1];8.17=M[12,1];8.6=M[13,1];8.95=M[14,1];9.15=M[15,1]
145: 9.1=M[16,1];9.17=M[17,1];9.69=M[18,1];10.65=M[19,1];11.1=M[20,1]
146: 10.61=M[21,1];9.45=M[22,1];9.24=M[23,1];9.3=M[24,1];9.12=M[25,1]
147: 8.66=M[26,1];8.01=M[27,1];7.67=M[28,1];7.82=M[29,1];8.4=M[30,1]
148: 9.22=M[31,1];9.87=M[32,1];10.16=M[33,1];10.18=M[34,1];10.09=M[35,1]
149: 9.96=M[36,1];9.89=M[37,1];9.86=M[38,1];9.85=M[39,1];9.93=M[40,1]
150: 9.99=M[41,1]
151: % ****************************************************************
152: (I[45,Z]-r6)/r8=X
153: int(X+1)=I
154: frc(X)=r9
155: (M[I+1,1]-M[I,1])*r9+M[I,1]=Y;prt "Y=",Y
156: % 8.985=Y
157: 1247.2=X
158: prt Y;Y*X=Y
159: for I=1 to 8
160: log(Y/2^(I-1))=Q[I]
161: next I
162: for I=1 to 8
163: Q[I]=W[9-I];R[I]=X[9-I];next I
164: for I=1 to 8
165: W[I]=Q[I];X[I]=R[I];prt R[I],Q[I];next I
166: % (Q[8]-Q[7])/2+Q[8]=Q[9];(R[8]-R[7])/2+R[8]=R[9]
167: 1=r84;7=r85;5=M
168: gsb "POLYFIT"
169: prt "values of const.";fxd 3;aprt Z;Z=r90
170: for I=1 to 8;0=E;for K=1 to M+1;E+Z[K]*R[I]^(K-1)=E;next K;E=R[I]
171: prt Q[I],R[I];next I
172: % ****************************************************************
173: for I=r25 to r26
174: if A[I]=0;gto +5;% A[I-1]=A[I]
175: 0=E;for K=1 to M+1
176: E+Z[K]*A[I]^(K-1)=E
```

```
177:  next K
178:  tn^E=B[I]
179:  next I
180:  % " Total integrated intensity of the line profile in F[4,N] "
181:  %
182:  0=S;for I=r25 to r26
183:  if I=r26;gto +4
184:  if B[I+1]=0;gto +2
185:  S+(B[I]+B[I+1])/2=S
186:  next I
187:  I[44,Z]*S=F[4,N]
188:  next N
189:  0=P;sfg 5;ina E
190:  for I=r95 to r96
191:  if F[4,I]=0;P+1=P;gto +2
192:  F[4,I]=E[I];if flg5;r95+P=r22;cfg 5
193:  next I
194:  r96-r95-P+r22=r23
195:  % gsb"FIL"
196:  % forI=r22tor23;F[4,I]=E[I];next I
197:  gsb "ABEL"
198:  % " ******** Abel inverted line profile in  F[5,N]   "
199:  for I=1 to r20
200:  Y[I,1]=F[5,r22-1+I];prt Y[I,1],I
201:  next I
202:  next Z;stp
203:  %
204:  %
205:  % ****************************************************************
206:  % " This secn. cal. Temp. by absolute inten. method of a single line"
207:  % %
208:  gto +26
209:  if O>r88;gto +25
210:  5000=r1;0=R;8.616e-5=r102;4.803e-10=r103;1*7.3377347e27=r200
211:  for N=1 to 250
212:  "ITER":
213:  gto +7;if r1>15000;gto +1;if r1>18000;gto +3;if r1>25000;gto +5
214:  2.0977e24+4.37468e20*r1-5.04649e16r1^2+1.20396e12*r1^3=r110
215:  gto +5
216:  2.42215e25-2.87743e21*r1+1.14683e17*r1^2-1.53176e12*r1^3=r110
217:  gto +3
218:  4.0735e24-4.08598e20*r1+1.37409e16*r1^2-1.54738e11*r1^3=r110
219:  if r1>34987;prt "Temperature above the range '34987' ";stp
220:  gsb "TABD"
221:  if r1>=5e3;gto +4;if r1>1.5e4;gto +3;if r1>2.5e4;gto +2
222:  prt "Temperature below 5000 K";gto -11
223:  (r106+r107+4*r108+4*r109)/r105=Z;gto +4
224:  (r106+r107+4*r108)/r105=Z;gto +3
225:  (r106+r107)/r105=Z;gto +2
226:  % 1=Z
227:  6.895e3*\(r1/(r105*(1+Z)))=r104
228:  6.2422e11*(R+1)*r103*r103/r104=E
229:  % 1.44e-7(R+1)/r104=E
230:  gsb "TABP"
231:  1.582e-17*I[46,1]*I[48,1]r110/(U*I[45,1])=X
232:  exp(-I[49,1]/(r102*8067.5*r1))=Y;X*Y=T[N];prt T[N],r1,U,E,r110
233:  r1+100=r1;next N
234:  % %
235:  % "Locating max of measured intensiteis"
236:  ina Q;for I=r22 to r21;F[5,I]=Q[I];next I
```

```
237: max(Q[*])=T;prtsc 701;prt "Max. Int.=",T,0;prtsc 16
238: for I=r22 to r21
239: if T-F[5,I]=0;I=rl21;gto +2
240: next I
241: r23-(rl21-r22)=rl22
242: if F[5,r21]=T;gto +21
243: % %
244: % "Normalising measured intensities"
245: for I=r22 to r23
246: F[5,I]/T=F[5,I]
247: next I
248: % %
249: % "Locating max. of calculated intensities"
250: ina Q;for I=1 to 250;T[I]=Q[I];next I
251: max(Q[*])=M
252: for I=1 to 250
253: if M-T[I]=0;I=rl20;gto +2
254: next I
255: 5000+100*(rl20-1)=rl25
256: % %
257: % " Normalising calculated intensities "
258: for I=1 to 250
259: T[I]/M=T[I]
260: next I
261: %
262: gto +14
263: % %
264: % "Calculating temp without offaxis peak intensity profile"
265: 1=r80;% " Intensity normalising factor    "
266: for I=r22 to r23;r80*F[5,I]=F[5,I];next I
267: for I=r22 to r23
268: for J=1 to 250
269: if F[5,I]=0;gto +5
270: T[J]-F[5,I]=X
271: if X>=0;gto +2
272: next J
273: 5000+(J-1)*100+100*X/(T[J]-T[J-1])=F[6,I]
274: next I
275: gto +25
276: % %
277: % "Calculating temp for offaxis peak intensity profile"
278: for I=r22 to rl21
279: for J=2 to rl20
280: if F[5,I]<=0;gto +5
281: T[J]-F[5,I]=X
282: if X>=0;gto +2
283: next J
284: 5000+(J-1)*100+100*X/(T[J]-T[J-1])=F[6,I]
285: next I
286: %
287: for I=rl21+1 to r21
288: 0=K;for J=rl20 to 300
289: if F[5,I]=0;gto +6
290: F[5,I]-T[J]=X
291: if X>=0;gto +3
292: K+1=K
293: next J
294: rl25+(K-1)*100+100*X/(T[J-1]-T[J])=F[6,I]
295: next I
296: for I=r22 to r21
```

```
297: F[6,I]=F[6,r23-I+r22]
298: next I
299: % %
300: % " Storing cal. temperature profile in string H$ and A$ "
301: int((100-(r23-r22+1))*.5)=K
302: % 0-r88+1=J
303: enp "SPECTRUM NO.=",J
304: for I=r22 to r23
305: F[6,I]=F[1,I-r22+1+(J-1)*100+K]
306: next I;stp
307: prtsc 701
308: spc 4
309: prt "FILE No.:",itf(R$[3,4]);prt "DISK No.:",itf(R$[1,2])
310: prt X$[1,32];if X$[33,35]#"   ";prt X$[33,48]
311: if X$[49,51]#"   ";prt X$[49,80]
312: spc 2
313: prt "  No."," TEMP"," INTEN","   RADIAL POS"
314: spc 2
315: 0=K;for I=r22 to r23
316: prt I,F[6,I],F[5,I],abs(r21-I)*.07
317: K+1=K;F[6,I]=F[0-r88+1,I]
318: if r21-I=0;1e-50=X[K];gto +2
319: ((r21-I)*.07/2.5)^2=X[K]
320: next I;prtsc 16
321: 5000=F[0-r88+1,r22]=F[0-r88+1,r23]
322: 0=K;for I=r22 to r23;K+1=K;F[0-r88+1,I]=F[0-r88+1,K];next I
323: next O
324: stp
325: % *****************************************************************
326: % " This subrtn cal. electron and particle den. of SII,SIII,FI toFIII
"
327: % " for 1 atm pressure"
328: "TABD":
329: rdm N[50,50];% " Electron den. TABLE"
330: .00004=N[1,5];.00043=N[1,6];.00227=N[1,7];.00791=N[1,8]
331: .02053=N[1,9];.04196=N[1,10];.06955=N[1,11];.09736=N[1,12]
332: .12523=N[1,13];.16199=N[1,14];.21403=N[1,15];.2781=N[1,16]
333: .3439=N[1,17];.40019=N[1,18];.44131=N[1,19];.46897=N[1,20]
334: .48685=N[1,21];.49984=N[1,22];.50973=N[1,23];.5174=N[1,24]
335: .52339=N[1,25];.52839=N[1,26];.53332=N[1,27];.53917=N[1,28]
336: .54693=N[1,29];.55731=N[1,30]
337: % *****************************************************************
338: % " Singley ionised sulfur 'SII' TABLE"
339: .00006=N[2,5];.00046=N[2,6];.00231=N[2,7];.00796=N[2,8]
340: .02054=N[2,9];.04169=N[2,10];.06805=N[2,11];.0912=N[2,12]
341: .10462=N[2,13];.1083=N[2,14];.10531=N[2,15];.09845=N[2,16]
342: .09001=N[2,17];.08172=N[2,18];.07407=N[2,19];.06625=N[2,20]
343: .05716=N[2,21];.04654=N[2,22];.03545=N[2,23];.02545=N[2,24]
344: .01753=N[2,25];.0118=N[2,26];.00787=N[2,27];.00524=N[2,28]
345: .00348=N[2,29];.00231=N[2,30]
346: % *****************************************************************
347: % " Singley ionised fluorine'FII' TABLE"
348: .00001=N[3,8];.00006=N[3,9];.00033=N[3,10];.00155=N[3,11]
349: .02061=N[3,13];.05359=N[3,14];.10835=N[3,15];.17869=N[3,16]
350: .25169=N[3,17];.31379=N[3,18];.35777=N[3,19];.38433=N[3,20]
351: .39804=N[3,21];.40354=N[3,22];.40439=N[3,23];.40281=N[3,24]
352: .39977=N[3,25];.39506=N[3,26];.3876=N[3,27];.37563=N[3,28]
353: .3572=N[3,29];.33081=N[3,30];.00619=N[3,12]
354: % *****************************************************************
355: % " Doubley ionised sulfur 'SIII' TABLE"
```

```
356: .00002=N[4,13];.00006=N[4,14];.00019=N[4,15];.00049=N[4,16];.0011=N[4
     ,17]
357: .00234=N[4,18];.00473=N[4,19];.00902=N[4,20];.01576=N[4,21]
358: .02467=N[3,22];.03441=N[4,23];.0433=N[4,24];.05021=N[4,25];.05487=N[4
     ,26]
359: .05742=N[3,27];.05803=N[4,28];.05681=N[4,29];.0538=N[4,30]
360: % ************************************************************
     **
361: % " Doubley ionised fluorine 'FIII' TABLE"
362: .00001=N[5,19];.00002=N[5,20];.00007=N[5,21]
363: .00019=N[5,22];.00047=N[5,23];.00109=N[5,24];.00238=N[5,25]
364: .00488=N[5,26];.00946=N[5,27];.01729=N[5,28];.02967=N[5,29];.0476=N[5
     ,30]
365: % ************************************************************
     **
366: % " Unionised fluorine 'FI' TABLE"
367: .85721=N[6,5];.85676=N[6,6];.85516=N[6,7];.85031=N[6,8];.83943=N[6,9]
368: .82079=N[6,10];.79593=N[6,11];.76746=N[6,12];.72916=N[6,13]
369: .66468=N[6,14];.56532=N[6,15];.44007=N[6,16];.31067=N[6,17]
370: .20032=N[6,18];.1211=N[6,19];.07107=N[6,20];.04174=N[6,21];.02498=N[6
     ,22]
371: .01537=N[6,23];.00976=N[6,24];.00638=N[6,25];.00429=N[6,26]
372: .00296=N[6,27];.00207=N[6,28];.00147=N[6,29];.00104=N[6,30]
373: % %
374: 5000=r6;% " Starting temperature "
375: 30000=r7;% " end temperature "
376: 1000=r8;% " temperature step "
377: 4+(r1-r6)/r8=X
378: int(X+1)=I
379: frc(X)=r9
380: ((N[1,I+1]-N[1,I])*r9+N[1,I])*r200/r1=r105;% " Electron density /m3"
381: ((N[2,I+1]-N[2,I])*r9+N[2,I])*r200/r1=r106;% " SII particle density"
382: ((N[3,I+1]-N[3,I])*r9+N[3,I])*r200/r1=r107;% " FII particle density"
383: ((N[4,I+1]-N[4,I])*r9+N[4,I])*r200/r1=r108;% " SIII particle density"
384: ((N[5,I+1]-N[5,I])*r9+N[5,I])*r200/r1=r109;% " FIII particle density"
385: if r1<15000;gto +2
386: if r1<27001;gto +2
387: ((N[6,I+1]-N[6,I])*r9+N[6,I])*r200/r1=r110;% "  FI particle density"
388: ret
389: stp
390: % ************************************************************
391: % " This subroutine   calculates PARTITION FUNCTION "
392: % %
393: "TABP":
394: rdm U[50,50];ina U,B
395: 4250=B[1];8500=B[2];8924=B[3];9371=B[4];9839=B[5];10331=B[6]
396: 10848=B[7];11390=B[8];11960=B[9];12558=B[10];13186=B[11];13845=B[12]
397: 14537=B[13];15264=B[14];16028=B[15];16829=B[16];17670=B[17]
398: 18554=B[18];24864=B[24];33321=B[30]
399: 19482=B[19];20456=B[20];21479=B[21];22553=B[22];23680=B[23]
400: 26107=B[25];27413=B[26];28784=B[27];30223=B[28];31734=B[29]
401: 34987=B[31]
402: 5.744=U[1,1];5.868=U[2,1];5.874=U[3,1];5.88=U[4,1];5.885=U[5,1]
403: 5.891=U[6,1];5.896=U[7,1];5.901=U[8,1];5.905=U[9,1];5.942=U[17,6]
404: 5.91=U[10,1];5.915=U[11,1];5.919=U[12,1];5.925=U[13,1];5.924=U[13,2]
405: 5.924=U[13,3];5.923=U[13,4];5.923=U[13,5];5.923=U[13,6];5.931=U[14,1]
406: 5.93=U[14,2];5.929=U[14,3];5.928=U[14,4];5.928=U[14,5];5.927=U[14,6]
407: 5.938=U[15,1];5.936=U[15,2];5.935=U[15,3];5.934=U[15,4];5.933=U[15,5]
408: 5.931=U[15,6];5.949=U[16,1];5.945=U[16,2];5.943=U[16,3];5.941=U[16,4]
409: 5.939=U[16,5];5.936=U[16,6];5.963=U[17,1];5.956=U[17,2];9.654=U[17,3]
```

```
410: 5.949=U[17,4];5.946=U[17,5];5.984=U[18,1];5.971=U[18,2];5.968=U[18,3]
411: 5.96=U[18,4];5.956=U[18,5];5.948=U[18,6];6.015=U[19,1];5.994=U[19,2]
412: 5.987=U[19,3];5.975=U[19,4];5.968=U[19,5];5.956=U[19,6];6.06=U[20,1]
413: 6.025=U[20,2];6.015=U[20,3];5.996=U[20,4];5.984=U[20,5];5.965=U[20,6]
414: 6.126=U[21,1];6.07=U[21,2];6.054=U[21,3];6.024=U[21,4];6.005=U[21,5]
415: 5.997=U[21,6];6.22=U[22,1];6.133=U[22,2];6.108=U[22,3];6.062=U[22,4]
416: 6.034=U[22,5];5.993=U[22,6];6.354=U[23,1];6.22=U[23,2];6.183=U[23,3]
417: 6.113=U[23,4];6.071=U[23,5];6.012=U[23,6];6.54=U[24,1];6.34=U[24,2]
418: 6.285=U[24,3];6.182=U[24,4];6.122=U[24,5];6.037=U[24,6];6.797=U[25,1]
419: 6.503=U[25,2];6.423=U[25,3];6.273=U[25,4];6.187=U[25,5];6.068=U[25,6]
420: 7.144=U[26,1];6.721=U[26,2];6.605=U[26,3];6.392=U[26,4];6.272=U[26,5]
421: 6.108=U[26,6];7.607=U[27,1];7.008=U[27,2];6.844=U[27,3];6.546=U[27,4]
422: 6.38=U[27,5];6.157=U[27,6];8.215=U[28,1];7.38=U[28,2];7.153=U[28,3]
423: 6.742=U[28,4];6.516=U[28,5];6.217=U[28,6];9.001=U[29,1];7.856=U[29,2]
424: 7.546=U[29,3];6.988=U[29,4];6.686=U[29,5];6.291=U[29,6];10.005=U[30,1
]
425: 8.457=U[30,2];8.04=U[30,3];7.294=U[30,4];6.895=U[30,5];6.381=U[30,6]
426: 11.269=U[31,1];9.207=U[31,2];8.654=U[31,3];7.67=U[31,4];7.149=U[31,5]
427: 6.488=U[31,6]
428: 4250=r6;% " Start temperature "
429: 34987=r7;% " End temperature "
430: 31=r18;% " No. of steps "
431: if r1>34987;r18=1;sfg 5;gto +8
432: cfg 5;for I=1 to r18
433: B[I]-r1=W
434: if W>0;gto +3;if I=1;gto +2
435: next I
436: prt "Temperature below range (4250 K) ";4=U;gto +16
437: (r1-B[I-1])/(B[I]-B[I-1])=X
438: if r1<=14537;1=J;gto +9
439: if E<=.1;1=J;gto +8
440: if E>.1;gto +2;if E>.25;gto +3;if E>.5;gto +4;if E>1;gto +5
441: if E>2;gto +5;if E>=3;6=J;gto +6
442: (E-.1)/.15=Y;1=J;gto +7
443: (E-.25)/.25=Y;2=J;gto +6
444: (E-.5)/.5=Y;3=J;gto +5
445: E-1=Y;4=J;gto +4
446: E-2=Y;5=J;gto +3
447: U[I-1,J]=B;U[I,J]=C;gto +4;if flg5;C=U;gto +5
448: if flg5;U[I,J]-(U[I,J]-U[I,J+1])*Y=U;gto +4
449: U[I-1,J]-(U[I-1,J]-U[I-1,J+1])*Y=B
450: U[I,J]-(U[I,J]-U[I,J+1])*Y=C
451: B+(C-B)*X=U
452: ret
453: stp
454: % ***********************************************************************
455: %
456: % " CURVE FITTING PROG."
457: "POLYFIT":ina Z,S,P,O
458: M+1=Q;rdm Z[Q],S[Q,Q],P[Q]
459: for I=2 to 2M+1;0=O[I]
460: for L=r84 to r85
461: O[I]+R[L]^(I-1)=O[I]
462: next L;next I
463: r85-r84+1=O[1]
464: 0=K;for I=1 to M+1;for J=1 to M+1
465: O[J+K]=S[I,J]
466: next J;K+1=K;next I
467: for I=1 to M+1;0=P[I];for L=r84 to r85
468: P[I]+Q[L]*R[L]^(I-1)=P[I]
```

```
469: next L;next I
470: % %
471: % "MATRIX INVERSION"
472: "MTXINV":inv S=S
473: % " Calculation of Poly. Coeff. k0,k1,..."
474: mat SP=Z;fxd 3
475: ret
476: stp
477: % " THIS SECTION PREPARES THE INTENSITY PROFILE for ABEL inversion"
478: %
479: "ABEL":
480: % *********************************************************************
481: % " This secn. balances no. of pts. about the max. of the int. prof."
482: % *********************************************************************
483: r23-r22+1=r20;ina B;if frc(r20/2)#.5;r20+1=r20;r23+1=r23
484: for I=r22 to r23;E[I]=B[I];next I
485: max(B[*])=Y
486: for I=r22 to r23
487: if Y-B[I]=0;I=r21=r70;gto +2
488: next I
489: if abs((r23-r22)/2+r22-r21)>=1;int((r23-r22)/2+r22)=r21=r70;prt r21
490: if B[r21]-B[r21+1]=0;r21+1=r21=r70
491: if abs(int(r20/2+r22-r21))=1;gto +9
492: if r21-r22>r23-r21;r23+1=r23;2*B[r23-1]-B[r23-2]=B[r23]
493: if r21-r22<r23-r21;r22-1=r22;2*B[r22+1]-B[r22+2]=B[r22]
494: r23-r22+1=r20
495: if abs(r21-r22-(r23-r21))>3;dsp "Line is lopsided";stp
496: cfg 5;if frc(r20/2)=.5;gto +4
497: if r21-r22<=r23-r21;sfg 5
498: if B[r22]>B[r23] and flg5;r22-1=r22;2*B[r22+1]-B[r22+2]=B[r22]
499: r23+1=r23;2*B[r23-1]-B[r23-2]=B[r23]
500: r22-1=r22;if r22=0;1=r22;0=B[r22]
501: r23+1=r23;0=B[r23]
502: r23-r22+1=r20
503: for I=r22 to r23;B[I]=E[I];next I;prt r22,r21,r23,r20
504: % *********************************************************************
505: % "This sec folds over intensity profile about the centre and ave it"
506: % *********************************************************************
507: for I=0 to r21-r22-1
508: (E[r22+I]+E[r23-I])/2=E[r22+I]
509: next I
510: % ifE[r21]>=E[r21-1];gto +3
511: % (E[r21-3]-E[r21-2]+E[r21-2]-E[r21-1])/2=X
512: % E[r21-1]+X=E[r21]
513: for I=0 to r21-r22-1
514: E[r22+I]=E[r23-I]
515: next I
516: prt r22,r21,r23,r20
517: % *********************************************************************
518: rdm K[50,50];ina K
519: for I=0 to r70-r22
520: E[r70-I]=K[I+1,1]
521: next I
522: cfg 7
523: gsb "ABL"
524: r20+1=J;rdm Y[J,1];ina B
525: for I=2 to r76
526: Y[I,1]=Y[r76-1+I,1]
527: Y[r76+2-I,1]=B[I-1]
528: next I
```

```
529:  Y[1,1]=B[r76]
530:  for I=1 to r76
531:  B[I]=Y[I,1]
532:  next I;prt r76
533:  ret
534:  stp
535:  %
536:  % "THIS SEC. PERFORMS 'ABEL INVERSION' TO CAL. RADIAL EMISSIVITY"
537:  %
538:  "ABL":r70-r22+1=r76=I;% "  No. of points from the arc centre "
539:  if flg7;gto "EMISS"
540:  4=r77;r77+1=J
541:  (r76-1)*1.0144e-3/14=r75
542:  rdm U[J,I],C[I,J]
543:  % "SETTING UP UNIFORM NET ON THE INTERVAL (1,A+1)"
544:  %
545:  for I=1 to r76
546:  (I-1)*r75/(r76-1)=W[I]
547:  W[I]=X[I]
548:  next I
549:  % "EVALUATE MATRIX U, STARTING WITH 1st ROW"
550:  %
551:  for J=1 to r76
552:  0=U[1,J]
553:  next J
554:  % "EVALUATE FIRST ROW OF U MATRIX"
555:  %
556:  for J=1 to r76
557:  1-W[J]*W[J]/(r75*r75)=O[J]
558:  \abs(O[J])*(2/3.14)=U[2,J]
559:  next J
560:  % "EVA. 2nd TO Kth ROW OF MATRIX U USING RECURRENCE RELATION"
561:  %
562:  for I=3 to r77+1
563:  (I-1)/(I-1.5)=r78
564:  for J=1 to r76
565:  r78*O[J]*U[I-1,J]=U[I,J]
566:  next J
567:  next I
568:  % "EVALUATE MATRIX C, AFTER CHANGING VARIABLE X TO V"
569:  %
570:  for I=1 to r76
571:  1-X[I]*X[I]/(r75*r75)=V[I]
572:  next I
573:  % "ASGN 1st COLUMN OF C=1 AND EVAL. J (ALPHA) & H (NI)"
574:  %
575:  0=H[1]=J[1]
576:  for I=1 to r76
577:  1=C[I,1]
578:  J[1]+V[I]=J[1]
579:  H[1]+1=H[1]
580:  next I
581:  J[1]/H[1]=J[1]
582:  % "EVALUATE 2nd COLUMN OF C AND OBTAIN J,H,G (BETA)"
583:  %
584:  0=H[2]=J[2]
585:  for I=1 to r76
586:  V[I]-J[1]=C[I,2]
587:  H[2]+C[I,2]*C[I,2]=H[2]
588:  J[2]+V[I]*C[I,2]*C[I,2]=J[2]
```

```
589: next I
590: J[2]/H[2]=J[2]
591: H[2]/H[1]=G[2,2]
592: % "EVALUATE 3rd TO Kth ROW OF C AND OBTAIN J,H,G"
593: %
594: for J=3 to r77+1
595: 0=H[J]=J[J]
596: for I=1 to r76
597: (V[I]-J[J-1])*C[I,J-1]-G[2,J-1]*C[I,J-2]=C[I,J]
598: H[J]+C[I,J]*C[I,J]=H[J]
599: J[J]+V[I]*C[I,J]*C[I,J]=J[J]
600: next I
601: J[J]/H[J]=J[J]
602: H[J]/H[J-1]=G[2,J]
603: next J
604: % "EVA. MATRIX S (C), STARTING BY RESETTING ALL ELEMENTS TO 0"
605: %
606: r77+1=I;rdm S[I,I]
607: for J=1 to r77+1
608: for I=1 to r77+1
609: 0=S[I,J]
610: next I
611: next J
612: % "COMPLETE 1st & 2nd ROW OF S AND RECURSIVELY ASSGN 1st COL."
613: %
614: 1/H[1]=S[1,1]
615: S[1,1]/G[2,2]=S[2,2]
616: -J[1]*S[1,1]/G[2,2]=S[2,1]
617: for I=3 to r77+1
618: (-J[I-1]*S[I-1,1]-S[I-2,1])/G[2,I]=S[I,1]
619: next I
620: % "CALCAULATE RECURSIVELY 1st TO Kth COLUMN OF S"
621: %
622: for J=2 to r77+1
623: for I=3 to r77+1
624: (S[I-1,J-1]-J[I-1]*S[I-1,J]-S[I-2,J])/G[2,I]=S[I,J]
625: next I
626: next J
627: % "COMPUTE TRANSFORM MATRIX N FROM C,S AND U"
628: %
629: r76=I;r77+1=J
630: ina M,N,Y,L
631: rdm L[I,J],M[I,I],N[I,I],Y[I,1],K[I,1]
632: mat C*S=L
633: mat L*U=M
634: trn M=N
635: %
636: % "OBTAIN RADIAL EMISSIVITY Y[R] FROM EQUATION Y=N*K"
637: "EMISS":
638: mat N*K=Y
639: 1/r75=D
640: smpy D*Y=Y
641: ret
642: stp
*30534
```

```
 0: % *********************************************************************
 1: % "PROGRAM  * TEMPC   V2.1 * 28.11.85 "
 2: % " THIS PROGRAM CALCULATES TEMPERATURE FROM CONTINUUM INTENSITY"
 3: % *********************************************************************
 4: "COLLECT":ent "Number of DISKS for Data Collection",r45
 5: ent "From DISK No.",r38
 6: ent "First FILE No.",r40
 7: ent "Last FILE No.",r41
 8: if r45=1;sfg 11;r38=J;r40=I;r41-r40+1=r44;gto +8
 9: ent "To DISK No.",r39
10: ent "First FILE No.",r42
11: ent "Last FILE No.",r43
12: sfg 11
13: for J=r38 to r39
14: if J>r38;dsp "Change DISK & Press CONTINUE";stp
15: r42=I;r43-r42+1=r44
16: for K=1 to r44
17: r40=I
18: dsp "Collecting Intensity FILES from","DISK No.",J,"FILE No.",I
19: I=Q;gsb "PLAYBACK"
20: A$=E$[K]
21: r40+1=r40
22: if I>r41;gto +2
23: next K
24: if r45=1;gto +3
25: r42=r40;r43=r41
26: next J
27: sfg 10
28: dsp "FILES COLLECTED"
29: ret
30: % %
31: "DTRED":if flg10;gto +2
32: gsb "COLLECT"
33: dsp "Change disk if necessary and press continue";stp
34: ent "No. of FILES to be Reduced",r87
35: ent "Beginning of FILE No.",r88
36: 0=U;for O=r88 to r88+r87-1;O=Q
37: dsp "FILE No.",O," is Being Processed"
38: sfg 11;gsb "PLAYBACK"
39: % %
40: "TEMP":fxd 3
41: %
42: 5=r86;% "number of calculations"
43: 1=r95;40=r96;1=r97;9=r98;ina A,B,F;0=r90
44: prt "FILE No.:",itf(R$[3,4]);prt "DISK No.:",itf(R$[1,2])
45: prt X$[1,32];if X$[33,35]#"   ";prt X$[33,48]
46: if X$[49,51]#"   ";prt X$[49,80]
47: spc 2
48: for Z=1 to r86
49: 3.1=G[1,1];5.85=G[1,2];6.3=G[1,3];6.6=G[1,4];7.15=G[1,5];% "Con. pos."
50: 5.6988=r70;% 5.525=r70
51: 2684.5988=r71;% 2757.0854=r71
52: -16913.5774=r72;% -16251.0583=r72
53: rdm I[50,10]
54: (r71+r72/(G[1,Z]+.001-2*r70)-(r71+r72/(G[1,Z]-.001-2*r70)))/40=I[44,Z]
55: .1(r71+r72/(G[1,Z]-2r70))=I[45,Z];prt I[45,Z],I[44,Z],Z
56: %
```

```
57: % ***************************************************************
58: %
59: % "wavelength in nm "
60: 472.3=I[45,1];573.3=I[45,2];600.4=I[45,3];621=I[45,4];666.6=I[45,5]
61: % ***************************************************************
62: %
63: for N=r95 to r96
64: itf(Q$[3,2N-1,2N])=r4
65: itf(Q$[4,2N-1,2N])=r5
66: r5-r4+1=rl
67: % "WAVELENGTH & DENSITY CALCULATION"
68: % %
69: % "Level of continueum is cal. by ave. 5 points on each end of scan"
70: if N>r95;gto +7
71: 0=X;for I=rl+5 to r5-5
72: num(A$[I])=Y;X+Y=X
73: next I
74: X/10=C=r81=r80
75: tn^((r80-9.765)/105.825)=X
76: log(210/X)=r80
77: % %
78: % "INTENSITY CALCULATION OF THE ENTIRE LINE PROFILE "
79: % " Density cal. of the entire line profile"
80: % ***" Densities of each scan is stored in A[*] and Inten. in B[*]"
81: ina Q;sfg 5;0=P;for I=rl+5 to r5-5
82: num(A$[I])=A;P+A=P
83: next I
84: P/10=A;if A+.01>=r81;gto +2
85: tn^((A-9.765)/105.825)=T;log(210/T)-r80=A[N]
86: next N
87: % r5-rl-15-P+r25=r26;% prtmax(Q[*]),N
88: % ifr26=0;gto +95
89: % %
90: % " cal. for 8 density steps and fog level from the intensity scan"
91: %
92: % ifZ=r90;gto +78
93: (r98-9)*20+1=rl
94: 0=L;ina Q,R
95: for M=r97 to r98
96: 0=X
97: for J=rl+5 to rl+14
98: num(E$[2,J])=Y;Y+X=X
99: next J
100: X/10=Y;if Y<=9.765;10=Y;prt "Y=",Y
101: tn^((Y-9.765)/105.825)=Y;Y/210=Y
102: L+1=L;if L=9;log(1/Y)=C;gto +4
103: log(1/Y)=R[L]
104: 20+rl=rl
105: next M
106: for L=1 to 8;R[L]-C=R[L];next L
107: % %
108: % " Cal. of normalising factor Q[*] from temperature prof. of fil."
109: (r98-9)*20+1=rl
110: 0=L
111: for M=r97 to r98-1
112: 0=X
113: for J=rl+5 to rl+14
114: num(E$[1,J])=Y;Y+X=X
115: next J
116: X/10=Y
```

```
117:  tn^((Y-9.765)/105.825)=Y;Y/210=Y
118:  L+1=L;log(1/Y)=Q[L]
119:  20+r1=r1
120:  next M;% prtQ[1]
121:  for I=2 to 8
122:  Q[I]/Q[1]=Q[I];% prtQ[I],I
123:  R[I]*Q[I]=R[I]
124:  next I
125:  % %
126:  % " Spectral radiance cal. from tables given for Horn lamp"
127:  380=r6;% " lower wavelength in nm "
128:  780=r7;% " heighest wavelength in nm "
129:  10=r8;% " step size in nm "
130:  (r7-r6)/r8+1=r18;% " No. of steps in the intensity table "
131:  % ***********************************************************
132:  % " Spectral radiance table of T242 lamp with filters"
133:  % ***********************************************************
134:  rdm M[45,1]
135:  1.38=M[1,1];2.186=M[2,1];3.107=M[3,1];4.02=M[4,1];4.41=M[5,1]
136:  5.19=M[6,1];5.8=M[7,1];6.42=M[8,1];6.89=M[9,1];7.34=M[10,1]
137:  7.74=M[11,1];8.17=M[12,1];8.6=M[13,1];8.95=M[14,1];9.15=M[15,1]
138:  9.1=M[16,1];9.17=M[17,1];9.69=M[18,1];10.65=M[19,1];11.1=M[20,1]
139:  10.61=M[21,1];9.45=M[22,1];9.24=M[23,1];9.3=M[24,1];9.12=M[25,1]
140:  8.66=M[26,1];8.01=M[27,1];7.67=M[28,1];7.82=M[29,1];8.4=M[30,1]
141:  9.22=M[31,1];9.87=M[32,1];10.16=M[33,1];10.18=M[34,1];10.09=M[35,1]
142:  9.96=M[36,1];9.89=M[37,1];9.86=M[38,1];9.85=M[39,1];9.93=M[40,1]
143:  9.99=M[41,1]
144:  % ***********************************************************
145:  (I[45,Z]-r6)/r8=X
146:  int(X+1)=I
147:  frc(X)=r9
148:  (M[I+1,1]-M[I,1])*r9+M[I,1]=Y;prt "Y=",Y
149:  % 8.985=Y
150:  1132.1=X
151:  prt Y;Y*X=Y
152:  for I=1 to 8
153:  log(Y/2^(I-1))=Q[I]
154:  next I
155:  for I=1 to 8
156:  Q[I]=W[9-I];R[I]=X[9-I];next I
157:  for I=1 to 8
158:  W[I]=Q[I];X[I]=R[I];% prtR[I],Q[I],I
159:  next I
160:  % (Q[8]-Q[7])/2+Q[8]=Q[9];(R[8]-R[7])/2+R[8]=R[9]
161:  % 3=r84;if Z>1;2=r84;if Z>2;1=r84;if Z>3;2=r84;if Z>4;1=r84
162:  4=M;6=r85;if Z>1;2=r84;if Z>2;1=r84;if Z>3;2=r84;if Z>4;1=r84
163:  if Z>1;gto +2
164:  3=r84;7=r85;4=M
165:  gsb "POLYFIT"
166:  prt "values of const.";fxd 3;aprt Z;Z=r90
167:  for I=1 to 8;0=E;for K=1 to M+1;E+Z[K]*R[I]^(K-1)=E;next K;E=R[I]
168:  % prtQ[I],R[I],I
169:  next I
170:  % ***********************************************************
171:  for N=r95 to r96
172:  if A[N]<=0;gto +11
173:  0=E;for K=1 to M+1
174:  E+Z[K]*A[N]^(K-1)=E
175:  next K
176:  tn^E=B[N]=S
```

```
177: % " Total integrated intensity of the profile in F[4,N] "
178: % 0=S;for I=r25 to r26
179: % ifI=r26;gto +3
180: % S+(B[I]+B[I+1])/2=S
181: % nextI
182: I[44,Z]*S=F[4,N];% prtF[4,N],N
183: next N
184: 0=P;sfg 5;ina E
185: for I=r95 to r96
186: if F[4,I]=0;P+1=P;gto +2
187: F[4,I]=E[I];if flg5;r95+P=r22;cfg 5
188: next I
189: r96-r95-P+r22=r23
190: gsb "ABEL"
191: % " ******* Abel inverted profile in  F[5,N]  "
192: % prtsc701
193: % prt"FILE No.:",itf(R$[3,4]);prt "DISK No.:",itf(R$[1,2])
194: % prtX$[1,32];if X$[33,35]#"   ";prt X$[33,48]
195: % ifX$[49,51]#"   ";prt X$[49,80]
196: % spc2
197: for I=1 to r20;% int(r20/2+2)
198: Y[I,1]=F[5,r22-1+I];prt Y[I,1],I
199: next I
200: spc 2
201: r95+40=r95;r96+40=r96;r97+9=r97;r98+9=r98
202: next Z;spc 5;next O
203: % *********************************************************************
204: % " This secn. cal. Temp. by absolute intensity method"
205: % %
206: gto +26
207: if O>r88;gto +25
208: 5000=r1;0=R;1.333e-41=r102;4.803e-10=r103;8*7.3377347e27=r200
209: for N=1 to 200
210: "ITER":
211: % " The following curve fit constants are for elect. den. at 4 atm."
212: % gto+9;if r1>15000;gto +1;if r1>18000;gto +3;if r1>25000;gto +5
213: % 2.0977e24+4.37468e20*r1-5.04649e16r1^2+1.20396e12*r1^3=r110
214: % gto+7
215: % 2.42215e25-2.87743e21*r1+1.14683e17*r1^2-1.53176e12*r1^3=r110
216: % gto+5
217: % 4.0735e24-4.08598e20*r1+1.37409e16*r1^2-1.54738e11*r1^3=r110
218: % %
219: % " The following curve fit constants are for elect. den. at 8 atm."
220: if r1>15000;gto +4;if r1>21000;gto +7;if r1>25000;gto +9
221: 2.05098e24-1.9606e20*r1+5.7626e15r1^2-4.0515e10*r1^3=r110
222: r110-3.3275e5*r1^4=r110
223: gto +6
224: 5.28236e24-7.1795e20*r1+3.605e16*r1^2-7.927e11*r1^3=r110
225: r110+6.4434e6*r1^4=r110
226: gto +3
227: 4.28455e24-5.32578e20*r1+2.21354e16*r1^2-3.07403e11*r1^3=r110
228: if r1>34987;prt "Temperature above the range '34987' ";stp
229: gsb "TABD"
230: r102*r105*r105/\r1=T[N];prt r1,T[N]
231: r1+100=r1;next N;stp
232: % %
233: % "Temperature calculation from intensity - temperature curve"
234: for I=r22 to r23
235: for J=1 to 250
236: if F[5,I]=0;gto +5
```

```
237:   T[J]-F[5,I]=X
238:   if X>=0;gto +2
239:   next J
240:   5000+(J-1)*50+50*X/(T[J]-T[J-1])=F[6,I]
241:   next I
242:   % %
243:   % " Storing cal. temperature profile in string H$ and A$ "
244:   enp "SPECTRUM NO.=",J
245:   % 0-r88+1=J
246:   int((100-(r23-r22+1))*.5)=K
247:   for I=r22 to r23
248:   F[6,I]=F[1,I-r22+1+(J-1)*100+K]
249:   next I;stp
250:   prtsc 701
251:   spc 4
252:   prt "FILE No.:",itf(R$[3,4]);prt "DISK No.:",itf(R$[1,2])
253:   prt X$[1,32];if X$[33,35]#"   ";prt X$[33,48]
254:   if X$[49,51]#"   ";prt X$[49,80]
255:   spc 2
256:   prt "  No.","    TEMP","    INTEN","    RADIAL POS"
257:   spc 2
258:   0=K;for I=r22 to r23
259:   prt I,F[6,I],F[5,I],abs(r21-I)*.065
260:   K+1=K;F[6,I]=F[0-r88+1,I]
261:   next I;prtsc 16
262:   stp
263:   % " CURVE FITTING "
264:   "POLYFIT":ina Z,S,P,O
265:   M+1=Q;rdm Z[Q],S[Q,Q],P[Q]
266:   for I=2 to 2M+1;0=O[I]
267:   for L=r84 to r85
268:   O[I]+R[L]^(I-1)=O[I]
269:   next L;next I
270:   r85-r84+1=O[1]
271:   0=K;for I=1 to M+1;for J=1 to M+1
272:   O[J+K]=S[I,J]
273:   next J;K+1=K;next I
274:   for I=1 to M+1;0=P[I];for L=r84 to r85
275:   P[I]+Q[L]*R[L]^(I-1)=P[I]
276:   next L;next I
277:   % %
278:   % "MATRIX INVERSION"
279:   "MTXINV":inv S=S
280:   % " Calculation of Poly. Coeff. k0,k1,..."
281:   mat SP=Z;fxd 3
282:   ret
283:   stp
284:   % %
285:   % " THIS SECTION PREPARES THE INTENSITY PROFILE for ABEL inversion"
286:   %
287:   "ABEL":
288:   % ****************************************************************
289:   % " This secn. balances no. of points about the max. of the profile"
290:   % ****************************************************************
291:   r23-r22+1=r20;ina B;if frc(r20/2)#.5;r20+1=r20;r23+1=r23
292:   for I=r22 to r23;E[I]=B[I];next I
293:   max(B[*])=Y
294:   for I=r22 to r23
295:   if Y-B[I]=0;I=r21=r70;gto +2
296:   next I
```

```
297:  if abs((r23-r22)/2+r22-r21)>=1;int((r23-r22)/2+r22)=r21=r70;prt r21
298:  if B[r21]-B[r21+1]=0;r21+1=r21=r70
299:  if abs(int(r20/2+r22-r21))=1;gto +9
300:  if r21-r22>r23-r21;r23+1=r23;2*B[r23-1]-B[r23-2]=B[r23]
301:  if r21-r22<r23-r21;r22-1=r22;2*B[r22+1]-B[r22+2]=B[r22]
302:  r23-r22+1=r20
303:  if abs(r21-r22-(r23-r21))>3;dsp "Line is lopsided";stp
304:  cfg 5;if frc(r20/2)=.5;gto +4
305:  if r21-r22<=r23-r21;sfg 5
306:  if B[r22]>B[r23] and flg5;r22-1=r22;2*B[r22+1]-B[r22+2]=B[r22]
307:  r23+1=r23;2*B[r23-1]-B[r23-2]=B[r23]
308:  r22-1=r22;if r22=0;1=r22;0=B[r22]
309:  r23+1=r23;0=B[r23]
310:  r23-r22+1=r20
311:  for I=r22 to r23;B[I]=E[I];next I;prt r22,r21,r23,r20
312:  % ****************************************************************
313:  % "This sec folds over intensity profile about the centre and ave it"
314:  % ****************************************************************
315:  for I=0 to r21-r22-1
316:  (E[r22+I]+E[r23-I])/2=E[r22+I]
317:  next I
318:  % ifE[r21]>=E[r21-1];gto +3
319:  % (E[r21-3]-E[r21-2]+E[r21-2]-E[r21-1])/2=X
320:  % E[r21-1]+X=E[r21]
321:  for I=0 to r21-r22-1
322:  E[r22+I]=E[r23-I]
323:  next I
324:  prt r22,r21,r23,r20;% gto"PLOT"
325:  % ****************************************************************
326:  rdm K[50,50];ina K
327:  for I=0 to r70-r22
328:  E[r70-I]=K[I+1,1]
329:  next I
330:  cfg 7
331:  gsb "ABL"
332:  r20+2=J;rdm Y[J,1];ina B
333:  for I=2 to r76
334:  Y[I,1]=Y[r76-1+I,1]
335:  Y[r76+2-I,1]=B[I-1]
336:  next I
337:  Y[1,1]=B[r76]
338:  for I=1 to r76
339:  B[I]=Y[I,1]
340:  next I;prt r76
341:  % gto"PLOT"
342:  ret
343:  stp
344:  % "THIS SECTION  PERFORMS 'ABEL INVERSION' TO CAL. RADIAL EMISSIVITY"
345:  %
346:  "ABL":r70-r22+1=r76=I;% "  No. of points from the arc centre "
347:  if flg7;gto "EMISS"
348:  4=r77;r77+1=J
349:  (r76-1)*1.0144e-3/7=r75
350:  rdm U[J,I],C[I,J]
351:  % "SETTING UP UNIFORM NET ON THE INTERVAL (1,A+1)"
352:  %
353:  for I=1 to r76
354:  (I-1)*r75/(r76-1)=W[I]
355:  W[I]=X[I]
356:  next I
```

```
357: % "EVALUATE MATRIX U, STARTING WITH 1st ROW"
358: %
359: for J=1 to r76
360: 0=U[1,J]
361: next J
362: % "EVALUATE FIRST ROW OF U MATRIX"
363: %
364: for J=1 to r76
365: 1-W[J]*W[J]/(r75*r75)=0[J]
366: \abs(0[J])*(2/3.14)=U[2,J]
367: next J
368: % "EVALUATE 2nd TO Kth ROW OF MATRIX U USING RECURRENCE RELATION"
369: %
370: for I=3 to r77+1
371: (I-1)/(I-1.5)=r78
372: for J=1 to r76
373: r78*0[J]*U[I-1,J]=U[I,J]
374: next J
375: next I
376: % "EVALUATE MATRIX C, AFTER CHANGING VARIABLE X TO V"
377: %
378: for I=1 to r76
379: 1-X[I]*X[I]/(r75*r75)=V[I]
380: next I
381: % "ASGN 1st COLUMN OF C=1 AND EVAL. J (ALPHA) & H (NI)"
382: %
383: 0=H[1]=J[1]
384: for I=1 to r76
385: 1=C[I,1]
386: J[1]+V[I]=J[1]
387: H[1]+1=H[1]
388: next I
389: J[1]/H[1]=J[1]
390: % "EVALUATE 2nd COLUMN OF C AND OBTAIN J,H,G (BETA)"
391: %
392: 0=H[2]=J[2]
393: for I=1 to r76
394: V[I]-J[1]=C[I,2]
395: H[2]+C[I,2]*C[I,2]=H[2]
396: J[2]+V[I]*C[I,2]*C[I,2]=J[2]
397: next I
398: J[2]/H[2]=J[2]
399: H[2]/H[1]=G[2,2]
400: % "EVALUATE 3rd TO Kth ROW OF C AND OBTAIN J,H,G"
401: %
402: for J=3 to r77+1
403: 0=H[J]=J[J]
404: for I=1 to r76
405: (V[I]-J[J-1])*C[I,J-1]-G[2,J-1]*C[I,J-2]=C[I,J]
406: H[J]+C[I,J]*C[I,J]=H[J]
407: J[J]+V[I]*C[I,J]*C[I,J]=J[J]
408: next I
409: J[J]/H[J]=J[J]
410: H[J]/H[J-1]=G[2,J]
411: next J
412: % "EVALUATE MATRIX S (C), STARTING BY RESETTING ALL ELEMENTS TO 0"
413: %
414: r77+1=I;rdm S[I,I]
415: for J=1 to r77+1
416: for I=1 to r77+1
```

```
417:  0=S[I,J]
418:  next I
419:  next J
420:  % "COMPLETE 1st & 2nd ROW OF S AND RECURSIVELY ASSGN 1st COLUMN"
421:  %
422:  1/H[1]=S[1,1]
423:  S[1,1]/G[2,2]=S[2,2]
424:  -J[1]*S[1,1]/G[2,2]=S[2,1]
425:  for I=3 to r77+1
426:  (-J[I-1]*S[I-1,1]-S[I-2,1])/G[2,I]=S[I,1]
427:  next I
428:  % "CALCAULATE RECURSIVELY 1st TO Kth COLUMN OF S"
429:  %
430:  for J=2 to r77+1
431:  for I=3 to r77+1
432:  (S[I-1,J-1]-J[I-1]*S[I-1,J]-S[I-2,J])/G[2,I]=S[I,J]
433:  next I
434:  next J
435:  % "COMPUTE TRANSFORM MATRIX N FROM C,S AND U"
436:  %
437:  r76=I;r77+1=J
438:  ina M,N,Y,L
439:  rdm L[I,J],M[I,I],N[I,I],Y[I,1],K[I,1]
440:  mat C*S=L
441:  mat L*U=M
442:  %
443:  trn M=N
444:  % "OBTAIN RADIAL EMISSIVITY Y[R] FROM EQUATION Y=N*K"
445:  "EMISS":
446:  mat N*K=Y
447:  1/r75=D
448:  smpy D*Y=Y
449:  ret
450:  stp
*26151
```

```
0:  % *******************************************************************
1:  % "PROGRAM  * STARK    V2.1 * 30.12.85 "
2:  % " THIS PROGRAM CALCULATES ELECTRON DENSITY FROM H-alpha LINE PROFILE"
3:  % *******************************************************************
4:  "DTRED":if flg10;gto +2
5:  gsb "COLLECT"
6:  dsp "Change disk if necessary and press continue";stp
7:  ent "No. of FILES to be Reduced",r87
8:  ent "Beginning of FILE No.",r88
9:  0=U;for O=r88 to r88+r87-1;O=Q
10: dsp "FILE No.",O," is Being Processed"
11: sfg 11;gsb "PLAYBACK"
12: % %
13: "TEMP":fxd 3
14: %
15: 1=r86;% "number of lines selected for the temperature calculation"
16: 6.786=G[1,1];% "Line pos. for spectrum scan"
17: 5.525=r70
18: 2757.0854=r71
19: -16251.0583=r72
20: for I=1 to r86
21: (r71+r72/(G[1,I]+.001-2*r70)-(r71+r72/(G[1,I]-.001-2*r70)))/40=I[44,I]
22: next I
23: 1=r95;120=r96;1=r97;9=r98;ina A,B,T;0=r90=r121=r125=r120=r130
24: for Z=1 to r86
25: %
26: % *******************************************************************
27: %
28: rdm I[50,10]
29: % "wavelength in nm "
30: 656.284=I[45,1]
31: % *******************************************************************
32: %
33: for N=r95 to r96
34: itf(Q$[3,2N-1,2N])=r4
35: itf(Q$[4,2N-1,2N])=r5
36: r5-r4+1=r1
37: % %
38: % "Level of continueum is cal. by ave. 5 points on each end of scan"
39: 0=X;for I=r1 to r1+4
40: num(A$[I])=Y;X+Y=X
41: next I
42: X/5=B
43: 0=X;for I=r5-4 to r5
44: num(A$[I])=Y;X+Y=X
45: next I
46: X/5=C;(B+C)/2=r80=r81
47: tn^((r80-9.765)/105.825)=X
48: log(210/X)=r80
49: % %
50: % "INTENSITY CALCULATION OF THE ENTIRE LINE PROFILE "
51: % " Density cal. of the entire line profile"
52: % ***" Densities of each scan is stored in A[*] and Inten. in B[*]"
53: ina Q;sfg 5;0=P;for I=r1 to r5
54: num(A$[I])=A
55: if A+4>=r81;P+1=P;gto +3
56: tn^((A-9.765)/105.825)=T
```

```
57:  log(210/T)-r80=A[I]=Q[I];if flg5;rl+P=r25;cfg 5
58:  next I
59:  r5-rl-P+r25=r26
60:  if r26=0;gto +101
61:  if r25>r26;gto +100
62:  % "                Storing the centre of the line profile in G[1,*]"
63:  max(Q[*])=Q
64:  for I=r25 to r26
65:  if Q-A[I]=0;gto +2
66:  next I
67:  I=G[1,N]
68:  % "                Storing max. half intensity point in r130 "
69:  if N>30;gto +8
70:  for I=r25 to r26
71:  if Q*.5-A[I]<=0;gto +2
72:  next I
73:  if r130=0;100=r130
74:  % ifN=7;70=r130
75:  if I-rl>r130;gto +2
76:  I-rl=r130;prt r130,N
77:  % %
78:  % " cal. for 8 density steps and fog level from the intensity scan"
79:  %
80:  if Z=r90;gto +71
81:  0=L;ina Q,R;1=rl
82:  for M=r97 to r98
83:  0=X
84:  for J=rl+70 to rl+89
85:  num(E$[2,J])=Y;Y+X=X
86:  next J
87:  X/20=Y;if Y<=9.765;10=Y;prt "Y=",Y
88:  tn^((Y-9.765)/105.825)=Y;Y/210=Y
89:  L+1=L;if L=9;log(1/Y)=C;gto +4
90:  log(1/Y)=R[L]
91:  140+rl=rl
92:  next M
93:  for L=1 to 8;R[L]-C=R[L];next L
94:  % %
95:  % " Cal. of normalising factor Q[*] from temperature profile of fil."
96:  0=L;1=rl
97:  for M=r97 to r98-1
98:  0=X
99:  for J=rl+70 to rl+89
100: num(E$[1,J])=Y;Y+X=X
101: next J
102: X/20=Y
103: tn^((Y-9.765)/105.825)=Y;Y/210=Y
104: L+1=L;log(1/Y)=Q[L]
105: 140+rl=rl
106: next M
107: for I=2 to 8
108: Q[I]/Q[1]=Q[I]
109: R[I]*Q[I]=R[I]
110: next I
111: % %
112: % " Spectral radiance cal. from tables given for Horn lamp"
113: 380=r6;% " lower wavelength in nm "
114: 780=r7;% " heighest wavelength in nm "
115: 10=r8;% " step size in nm "
116: (r7-r6)/r8+1=r18;% " No. of steps in the intensity table "
```

```
117:  % *********************************************************
118:  % " Spectral radiance table of T242 lamp with filters"
119:  % *********************************************************
120:  rdm M[45,1]
121:  1.38=M[1,1];2.186=M[2,1];3.107=M[3,1];4.02=M[4,1];4.41=M[5,1]
122:  5.19=M[6,1];5.8=M[7,1];6.42=M[8,1];6.89=M[9,1];7.34=M[10,1]
123:  7.74=M[11,1];8.17=M[12,1];8.6=M[13,1];8.95=M[14,1];9.15=M[15,1]
124:  9.1=M[16,1];9.17=M[17,1];9.69=M[18,1];10.65=M[19,1];11.1=M[20,1]
125:  10.61=M[21,1];9.45=M[22,1];9.24=M[23,1];9.3=M[24,1];9.12=M[25,1]
126:  8.66=M[26,1];8.01=M[27,1];7.67=M[28,1];7.82=M[29,1];8.4=M[30,1]
127:  9.22=M[31,1];9.87=M[32,1];10.16=M[33,1];10.18=M[34,1];10.09=M[35,1]
128:  9.96=M[36,1];9.89=M[37,1];9.86=M[38,1];9.85=M[39,1];9.93=M[40,1]
129:  9.99=M[41,1]
130:  % *********************************************************
131:  (I[45,Z]-r6)/r8=X
132:  int(X+1)=I
133:  frc(X)=r9
134:  (M[I+1,1]-M[I,1])*r9+M[I,1]=Y;prt "Y=",Y
135:  % "Slit width and exposure factor - 'X' "
136:  1118.4=X
137:  prt Y;Y*X=Y
138:  for I=1 to 8
139:  log(Y/2^(I-1))=Q[I]
140:  next I
141:  for I=1 to 8
142:  Q[I]=W[9-I];R[I]=X[9-I];next I
143:  for I=1 to 8
144:  W[I]=Q[I];X[I]=R[I];prt R[I],Q[I];next I
145:  % (Q[8]-Q[7])/2+Q[8]=Q[9];(R[8]-R[7])/2+R[8]=R[9]
146:  2=r84;8=r85;5=M
147:  gsb "POLYFIT"
148:  prt "values of const.";fxd 3;aprt Z;Z=r90
149:  for I=2 to 8;0=E;for K=1 to M+1;E+Z[K]*R[I]^(K-1)=E;next K;E=R[I]
150:  prt Q[I],R[I];next I
151:  % *********************************************************
152:  for I=r25 to r26
153:  if A[I]=0;A[I-1]=A[I]
154:  0=E;for K=1 to M+1
155:  E+Z[K]*A[I]^(K-1)=E
156:  next K
157:  tn^E=T[I]
158:  next I
159:  if r120=0;G[1,N]-(N-1)*140=r125
160:  if r120<r26-r25;(140-(r26-r25))*.5=r121;r26-r25=r120
161:  next N
162:  % " Intensity of the line profile in F[4,N] at diff. wavelengths"
163:  %
164:  r130-5=r121
165:  r125+(r125-r121)=r125
166:  "START":ina Q;r121=I;for N=r95 to r96
167:  T[I]=F[4,N]=Q[N]
168:  I+140=I
169:  next N
170:  prt max(Q[*]),r121;if max(Q[*])=0;gto +22
171:  0=P;sfg 5;ina E
172:  for I=r95 to r96
173:  if F[4,I]=0;P+1=P;gto +2
174:  F[4,I]=E[I];if flg5;r95+P=r22;cfg 5
175:  next I
176:  r96-r95-P+r22=r23
```

```
177: if r23-r22<=3;gto +15
178: gsb "ABEL"
179: % "  *******  Abel inverted line profile in  F[5,N]   "
180: for I=1 to r20
181: Y[I,1]=F[5,r22-1+I]
182: next I
183: % "This initialises T[*] and fills it with the Abel inverted inten."
184: r121=I;for N=r95 to r96
185: 0=T[I]
186: r121+140=I
187: next N
188: r121=I;for N=r22 to r23
189: F[5,N]=T[(N-1)*140+I];% prtT[(N-1)*140+I],N
190: r121+140=I
191: next N
192: r121+1=r121;if r121<=r125;gto "START"
193: r95+6=r22;r96-7=r23
194: for N=r22 to r23
195: itf(Q$[3,2N-1,2N])=r4
196: itf(Q$[4,2N-1,2N])=r5
197: r5-r4+1=r1
198: % gto+14
199: % " Line profile smoothing"
200: ina R,Q;sfg 5;0=P;for I=r1 to G[1,N]
201: if T[I]=0;P+1=P;gto +2
202: T[I]=Q[I];I=R[I];if flg5;r1+P=r25;cfg 5
203: next I
204: G[1,N]=r26
205: if max(Q[*])<=0;gto +26
206: r25=r84;r26=r85;3=M;gsb "POLYFIT"
207: for I=r25 to r26
208: 0=E;for J=1 to M+1
209: E+Z[J]*I^(J-1)=E
210: next J
211: E=T[I]
212: next I
213: % " Determination of full half-width from the smoothed profiles"
214: ina Q;for I=r1 to r5;T[I]=Q[I];next I
215: max(Q[*])/2=Q;max(Q[*])=r150
216: if Q=0;gto +15
217: for I=r1 to r5
218: if Q-T[I]<=0;gto +2
219: next I
220: I=r151
221: for I=r1 to r5
222: if r150-T[I]<=0;gto +2
223: next I
224: 2*(I-r151)=W
225: if W<=0;gto +6
226: 10*W*I[44,1]=W=F[1,N];prt "Full half-width of the line in A =",W
227: % " Calculation of the electron density"
228: % %
229: -2.6906e15+9.35181e15*W+2.38796e14*W*W=F[5,N];prt F[5,N]1e6,N
230: F[5,N]*1e6=F[5,N]
231: next N
232: stp
233: %
234: % ***********************************************************************
235: % " This secn. cal. Temp. from the full half-width of H-alpha line"
236: % %
```

```
237: % gto+32
238: if 0>r88;gto +7
239: 5000=r1;0=R;8.616e-5=r102;4.803e-10=r103;8*7.3377347e27=r200
240: for N=1 to 200
241: "ITER":
242: gsb "TABD"
243: r105=T[N];gto +1
244: r1+100=r1;next N
245: % %
246: % "Calculating temperatures from the electron density"
247: for I=r22 to r23
248: for J=1 to 200
249: if F[5,I]=0;gto +6
250: if F[5,I]<6e19;gto +5
251: T[J]-F[5,I]=X
252: if X>=0;gto +2
253: next J
254: 5000+(J-1)*100+100*X/(T[J]-T[J-1])=F[3,I]
255: next I
256: % %
257: % "Storing Temperature profils in F[1,*]"
258: enp "SPECTRUM NO.=",J
259: int((100-(r23-r22+1))*.5)=K
260: for I=r22 to r23
261: F[3,I]=F[1,I-r22+1+(J-1)*100+K]
262: next I;next O;stp
263: prtsc 701
264: spc 4
265: prt "   No."," TEMP."," ELEC. DEN."," FULL HALF-WIDTH"
266: spc 2
267: 0=K;for I=r22 to r23
268: prt I,F[3,I],F[5,I],F[1,I]
269: K+1=K;F[3,I]=F[0-r88+1,1]
270: next I
*1959
```

```
0:  % *********************************************************************
1:  % "PROGRAM    *  SIGMA  *    V2.1       03.9.85      "
2:  % " This program calculates elec. conductivity of Ar/SF6 by using "
3:  % " trial function technique - Devoto and Mukherjee"
4:  % *********************************************************************
5:  % %
6:  .25=R
7:  17.61=E[1];19.01=E[2];21.69=E[3]
8:  rdm I[50,52];165.19=I[1,52];216.09=I[2,52];259.26=I[3,52]
9:  % *********************************************************************
10: %
11: % " Initial values of the constans a, b and c for  SF6  at 1 atm."
12: %
13: rdm C[100,10],Y[100,3]
14: 8.05e11=A[1]=A
15: 2.067=B[1]=B
16: 4.918e4=C[1,10]=C;stp
17: %
18: for I=1 to 3
19: I[I,52]/(E[I]*3.14*R^2)=W[I];flt 3;prt W[I]
20: next I
21: %
22: % "This sec. cal. a,b and c iteratively using'GAUSS-SEIDEL'method"
23: "ST":1=rl=J
24: gsb "INTEG"
25: -W[1]+A[1]*1e-6+Y[rl,J]=A[1]
26: 1e6*A[1]=A[1]=A;prt "A=",A[1],Y[1,1]
27: 1=rl;2=J;gsb "INTEG"
28: -W[2]+B[1]*1000+Y[rl,J]=B[1];prt "B=",B[1]*.001,Y[1,2]
29: .001*B[1]=B[1]=B
30: 1=rl;3=J;gsb "INTEG"
31: -W[3]+C[1,10]*1e-2+Y[rl,J]=C[1,10]
32: 1e2*C[1,10]=C[1,10]=C;prt "C=",C[1,10],Y[1,3]
33: for N=2 to 10
34: N=rl;1=J;gsb "INTEG"
35: -W[1]+A[rl-1]*1e-6+Y[rl,J]=A[rl]
36: 1e6*A[rl]=A[rl]=A
37: N=rl;2=J;gsb "INTEG"
38: -W[2]+B[rl-1]*1000+Y[rl,J]=B[rl]
39: .001*B[rl]=B[rl]=B
40: N=rl;3=J;gsb "INTEG"
41: -W[3]+C[rl-1,10]*1e-2+Y[rl,J]=C[rl,10]
42: 1e2*C[rl,10]=C[rl,10]=C
43: next N
44: N-1=rl110
45: for I=1 to 10
46: prt A[I],B[I],C[I,10]
47: next I
48: % " Subroutine 'INTEG' for evaluating inegrand "
49: %
50: "INTEG":0=X
51: for I=1 to 21
52: F[J,I]=T
53: -A*B*exp(-C/T)*T^(-B-1)+A*C*T^(-B)*exp(-C/T)*(1/T^2)=Q[I]
54: ((r21-I)*.072/25)^2=X[I];if X[I]=0;1e-50=X[I];% "step=.14 or.072"
55: Q[I]*X[I]=Q[I]
56: if I=1;gto +2
```

```
57:  X+Q[I]*(F[J,I]-F[J,I-1])=X
58:  next I
59:  X=Y[r1,J]
60:  ret
61:  stp
62:  % " This secn. cal. value of sigma from final value of a,b and c"
63:  %
64:  "SIGMA":
65:  for I=5 to 26
66:  1000*I=T
67:  A[r110]*T^(-B[r110])*exp(-C[r110,10]/T)=R[I];prt R[I],T
68:  next I
69:  stp
70:  end
*26752
```

```
454: %  ****************************************************************
455: %  "PROGRAMME  *  THERMAL AND NETRAD * V2.1      15.9.85      "
456: %  ****************************************************************
457: for I=r60 to r70
458: 6.47e1-1.48e-2*F[6,I]+1.09e-6*F[6,I]^2-2.45e-11*F[6,I]^3=T[I]
459: next I
460: enp "FIELD in V/m ",E;0=D;gto "MAT"
461: next A
462: prtsc 16;cfg 11
463: "MAT":for I=r60 to r70
464: 100*(7.698e12*F[6,I]^(-2.2247)*exp(-5.9955e4/F[6,I]))=A[I]
465: if I=r60;gto +2
466: (I+1-r60)*(T[I]+T[I+1])*.5*(F[6,I+1]-F[6,I])=W[I]
467: next I
468: 2*W[r70-1]-W[r70-2]=W[r70]
469: 0=W[r60]
470: for I=r60 to r70
471: if I=r60;gto +2
472: (W[I]-W[I-1])*.5/(5.5e-5*(I-r60)*5.5e-5/(r50*r50))=X[I]
473: next I
474: 2*X[r60+1]-X[r60+2]=X[r60]
475: 0=X[r60]
476: for I=r60 to r70
477: 100*(8e12*F[6,I]^(-2.2)*exp(-6e4/F[6,I]))=A[I]
478: if I=r60;gto +2
479: (A[I]+A[I-1])*.5*E*E+X[I]=V[I]
480: next I
481: A[r60]*E*E=V[r60]
482: % %
483: %
484: prtsc 701;spc 2;prt "Elect. Field in V/m=",E;spc 2;prtsc 16
485: (r70-r60)*5.5e-5/r50=R;gsb "RAD"
486: stp
487: "RAD":0=A=B=C=S=P=Q
488: fxd 4;prtsc 701;spc 2;prt "Arc radius=",R;spc 2;prtsc 16
489: for I=r60 to r70
490: if I=r60;gto +4
491: 2*3.14*(A[I]+A[I-1])*.5*(I-r60)*5.5e-5*5.5e-5*E*E/(r50*r50)=A;Q+A=Q
492: (A[I]+A[I-1])*.5*(I-r60)*5.5e-5*5.5e-5/(r50*r50)=B;S+B=S
493: B*ln(R*r50/((I-r60)*5.5e-5))=C;C+P=P
494: next I
495: P/S=r150;prtsc 701;fxd 4;prt "Elect. Form Factor =",r150
496: % 2*3.14*(V[I]+V[I-1])*.5*(I-r60)*5.5e-5*5.5e-5/(r50*r50)=B;B+S=S
497: % 2*3.14*(F[6,I]-F[6,I-1])*(I-r60)=C;if C=0;gto +6
498: % (A-B)/C=T[I]
499: 0=A=B=C=P=S=Q;cfg 10
500: if I=r60;gto +3
501: (V[I]+V[I-1])*.5*(I-r60)*5.5e-5*5.5e-5/(r50*r50)=B;B+S=S
502: B*ln(R*r50/((I-r60)*5.5e-5))=A;P+A=P
503: next I
504: P/S=r151;prtsc 701;spc 2;prt "Rad. Form Factor =",r151
505: ret
506: stp
507: prtsc 701
508: spc 2;prt "Total Rad. Power (kW/m)=",Q/1000;spc 4
509: spc 2;prt "Total Elec. Power (kW/m)=",P/1000;spc 4
510: 2*T[r60+1]-T[r60+2]=T[r60]
```

```
511:  %  ifD=2;gto +2
512:  %  D+1=D;gto "MAT"
513:  prt "  'TEMP.'    'SIGMA'       'K'      'SP. RADIATION'"
514:  prt "   (K)       (S/m)      (W/m-K)       (W/m3)"
515:  prt " --------   ---------    ----    ----------------"
516:  spc ;flt 3;for I=r60 to r70 by r50;prt F[6,I],A[I],T[I],V[I];next I
517:  prtsc 16
518:  stp
519:  0=D;gto "MAT"
520:  %  %
*4818
```